Enhancing wave energy developments through mooring system reliability assessment
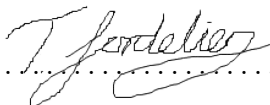
UNIVERSITY OF
EXETER

Tessa Jane Gordelier

College of Engineering, Mathematics and Physical Sciences

University of Exeter

....

A thesis submitted for the degree of

Doctor of Philosophy in Renewable Energy

July 2016

Abstract

Wave energy generation is a promising renewable energy source but it faces certain challenges before it can become commercially viable. In comparison to conventional energy generation it is expensive, furthermore it has been plagued by reliability challenges due to the harsh operating demands of the marine environment.

This Thesis investigates the reliability of wave energy devices, and specifically focuses on mooring system reliability. Two major themes are developed: Firstly, an assessment is conducted on a conventional mooring component, reviewing safety factors suggested in mooring system design guidelines and investigating whether there is a potential to reduce these safety factors (and in so doing, reduce system costs). Numerical modelling, laboratory testing and field testing demonstrate that excessively large safety factors are published in design guidance for static loading scenarios. However, when considering fatigue loading regimes (a critical aspect of wave energy generation), the proposed safety factors are found to be appropriate. In fatigue design, the importance of selecting an appropriate stress concentration factor for use with generic S-N curves is highlighted. These findings indicate the publication of additional stress concentration factors and a standard approach for mean stress adjustment would be a valuable addition to mooring system design guidance for fatigue.

The second theme introduces a novel mooring component, The Exeter Tether, designed to reduce mooring loads and thus reduce system costs. The introduction of any novel technology brings new reliability considerations, and a reliability assessment of the tether and sub-components is

presented in this Thesis. Following a failure modes and effects analysis, a bespoke range of physical tests is developed to investigate reliability concerns unique to this novel component. Laboratory testing of the tether assembly shows promising fatigue performance, however field trials highlight concerns regarding bio-fouling and marine debris ingress. Sub-component testing of the EPDM[1] polymer core suggests an increase in material stiffness with both marine ageing and repeated compression cycles. This finding supports results from assembly trials in the laboratory and at sea, where tether assembly dynamic axial stiffness is observed to increase over time. The overarching design philosophy behind the Exeter Tether is to reduce mooring system loads, so establishing the 'worked' operating profile of the tether is crucial for the design intentions to be realised without compromising the reliability of the overall mooring system. Trials on the anti-friction membrane establish optimum performance when using two layers of UHMWPE[2] tape. Further areas requiring research are highlighted, and suggestions are made to improve the reliability of future design iterations of The Exeter Tether.

The two reliability approaches presented demonstrate the potential for cost reduction in mooring system design and highlight the importance of physical component testing, both in the field and in laboratory conditions, to optimise component design whilst ensuring overall system reliability.

---

[1]Ethylene propylene diene monomer
[2]Ultra high molecular weight polyethylene

Acknowledgements

Contents

5   Reliability assessment of a novel mooring component: The Exeter Tether   233

List of Figures

17

List of Tables

Chapter 1

Introduction

Contents

1.1 Research context

Over recent decades international understanding of global warming has developed; the earth is unequivocally warming and few now question the contribution of anthropogenic carbon dioxide emissions to this (Pachauri *et al.*, 2014). The potential implications of global warming are severe, and are already being felt in some parts of the world (Holpuch, 2015). Alongside this, the global population is increasing with a shift to ever more energy intensive lifestyles (Petrecca, 2014). Conventional fossil fuel combustion is the main contributor to global carbon dioxide emissions (Friedlingstein *et al.*, 2014), thus the search for new, low carbon forms of energy is essential to enable the necessary transition to a sustainable, low carbon world. Marine renewable energy is one of the low carbon forms of energy generation offering part of the solution through an array of options including wave energy, tidal energy, offshore wind and more recently the use of temperature or salinity gradient to generate electricity. Wave energy is the focus for

the work described in this Thesis, although some of the presented work is also relevant to floating wind and some tidal energy systems.

Wave energy has the potential to make a significant contribution to global electricity generation. There are various estimates of the global potential of wave energy (as will be explored in Section 2.1.1, Page 32), the potential economically exploitable resource estimate is 2,000TWh/year (Thorpe, 2010). This is approaching 9% of global electricity generation based on 2012 figures (International Energy Agency, 2014). Estimates specifically for the UK suggest a potential contribution of 23% to the UK's total electricity consumption (Boud, 2012; Department of Energy and Climate Change, UK, 2015a).

However, it is not only the contribution to low carbon energy generation that makes the whole marine energy sector so attractive. In a turbulent global energy market (Choi & Hammoudeh, 2010; Nandha & Faff, 2008), marine energy could provide the UK with a level of energy security not offered by many conventional fossil fuels. In addition, estimates suggest that by 2035 the sector could employ 19,500 individuals and be worth £6.1bn to the UK economy (RenewableUK, 2010).

Marine energy, specifically wave energy, looks an attractive proposition, but so far it has not achieved market penetration. As with any novel technology making wave energy cost competitive with existing technologies is a key challenge and has, to date, prevented it from becoming a commercial reality. Estimates from 2012 suggest wave energy has a levelised cost of energy (LCOE) of £250 - £400/MWh (Low Carbon Innovation Coordination Group, 2012). The report demonstrates this is high even in comparison to offshore wind which, at £140 - £180/MWh, is still comparatively expensive in relation to fossil fuel generation. Priority areas for cost reduction will be further discussed in Section 2.4, Page 77.

Alongside the need to drive down costs, it is also necessary for the industry to prove devices can reliably deliver to specification. The harsh operating environment required of wave energy devices has proved a considerable challenge and contributed to the failure of some of the leading players in the industry (BBC, 2015; Danko, 2014).

The common understanding of the overall *Risk* of a component failure is the result of the *Probability* of the failure multiplied by the *Consequence* of the failure (Hamedni & Bittencourt Ferreira, 2014). Given that much of the guidance for mooring system design has evolved from the oil and gas industry (Det Norske Veritas, 2010a, 2011),

where the consequence of a mooring line failure is severe, it is suggested in this Thesis that a review of safety factors is necessary, given the reduced consequence of a mooring line failure for a wave energy converter (WEC) [1].

Current practice in the wave energy sector involves the application of large safety factors to designs to guarantee reliability (Weller *et al.*, 2015b). Safety factors are applied to allow for the inherent variability present in both material and manufacturing processes (intrinsic variability) and the variability in operating conditions such as wave climate (extrinsic variability). These safety factors increase device costs at a time when reducing the cost of energy is critical. This careful balance between reliability and cost of energy is of central importance to this Thesis.

In this Thesis, two main themes are considered for reliable, cost-effective mooring system development:

1. The use of existing components but with reduced safety factors applied to designs reflecting the reduced consequence of a wave energy converter (WEC) mooring line failure.

2. The introduction of a novel component to reduce mooring system loads (and costs), whilst ensuring the novel component does not compromise the overall system reliability.

This Thesis aims to develop these two approaches. The pertinent literature and related work for this Thesis is reviewed and discussed in Chapter 2. An overview of the research approach and test facilities used is provided in Chapter 3. Following this overview, in order to develop the first approach discussed above, a detailed analysis will be conducted on a standard mooring component in relation to existing guidance on safety factors in Chapter 4. The second approach will be addressed in Chapter 5 through the introduction of a novel mooring component which aims to improve system reliability and reduce cost. Any novel component creates new reliability challenges and the reliability assessment of this component is conducted and presented in this chapter. Broad discussions relating to both approaches and addressing the potential benefits of

---

[1]WECs currently under development are unmanned so a failure is unlikely to lead to loss of life. Additionally, the environmental impact of a mooring line failure is minimal in comparison to the potential damage caused by an oil spill for example. Further discussion of consequence is provided in Sections 2.3.2.1 and 2.5.5.2 where 'Consequence Class' is explained and quantified numerically.

the novel component to overall system reliability will be addressed in Chapter 6 before drawing general conclusions and outlining next steps to progress this work in Chapter 7.

1.2 Research questions

Given the competing demands of cost and reliability discussed in Section 1.1 the overarching question for this Thesis is:

How can reliable mooring solutions for wave energy devices be developed?

To address this overarching question several areas of work are developed. Specifically, this Thesis seeks to answer the following questions:

1. **Is there industry consensus on priority areas for development to facilitate commercial wave energy generation?**

2. **Given the reduced consequence of a wave energy converter (WEC) mooring line failure, should the safety factors applied to mooring system design be reduced when using standard mooring components?**

3. **During the development of a novel mooring component how should reliability be assessed to ensure overall mooring system integrity is maintained?**

4. **What are the potential implications of novel mooring components on system reliability?**

1.3 Aims and objectives

In order to address the research questions set out, the aim of this work is to assess the reliability associated with both a standard and a novel component for wave energy devices. The importance of component reliability in the development of new technologies is assessed through these two reliability approaches. One will focus on an existing,

commonly used component and review the reliability of this component within the context of design safety factors. The second will focus on the reliability assessment of a completely novel component. Key objectives for this work are:

- Conduct a full review of current literature to establish a firm definition of reliability in the context of this work.

- Through the literature review, assess priority areas for development within the wave energy sector with a focus on improved device reliability.

- Conduct numerical modelling, laboratory experimentation and field testing on a standard mooring component to establish the safety factors present within the component design. Relate this to specified safety factors within design standards.

- Conduct a review of reliability considerations for a novel mooring component, identifying those reliability aspects unique to the novel component.

- Establish a suitable test schedule to assess the critical reliability considerations, focusing on items with limited or no existing data.

- Conduct physical testing as identified in the test schedule to explore these reliability considerations for the novel component.

- Identify key recommendations for reliability improvements of the novel component and identify further areas for development.

- Discuss the findings from both case studies in the wider context of cost effective reliable mooring solutions for wave energy devices.

1.4 Research approach and Thesis structure

In this section Figure 1.1 provides a schematic representation of the Thesis structure, before a brief description of each Chapter is outlined with reference to the research questions presented in Section 1.2.
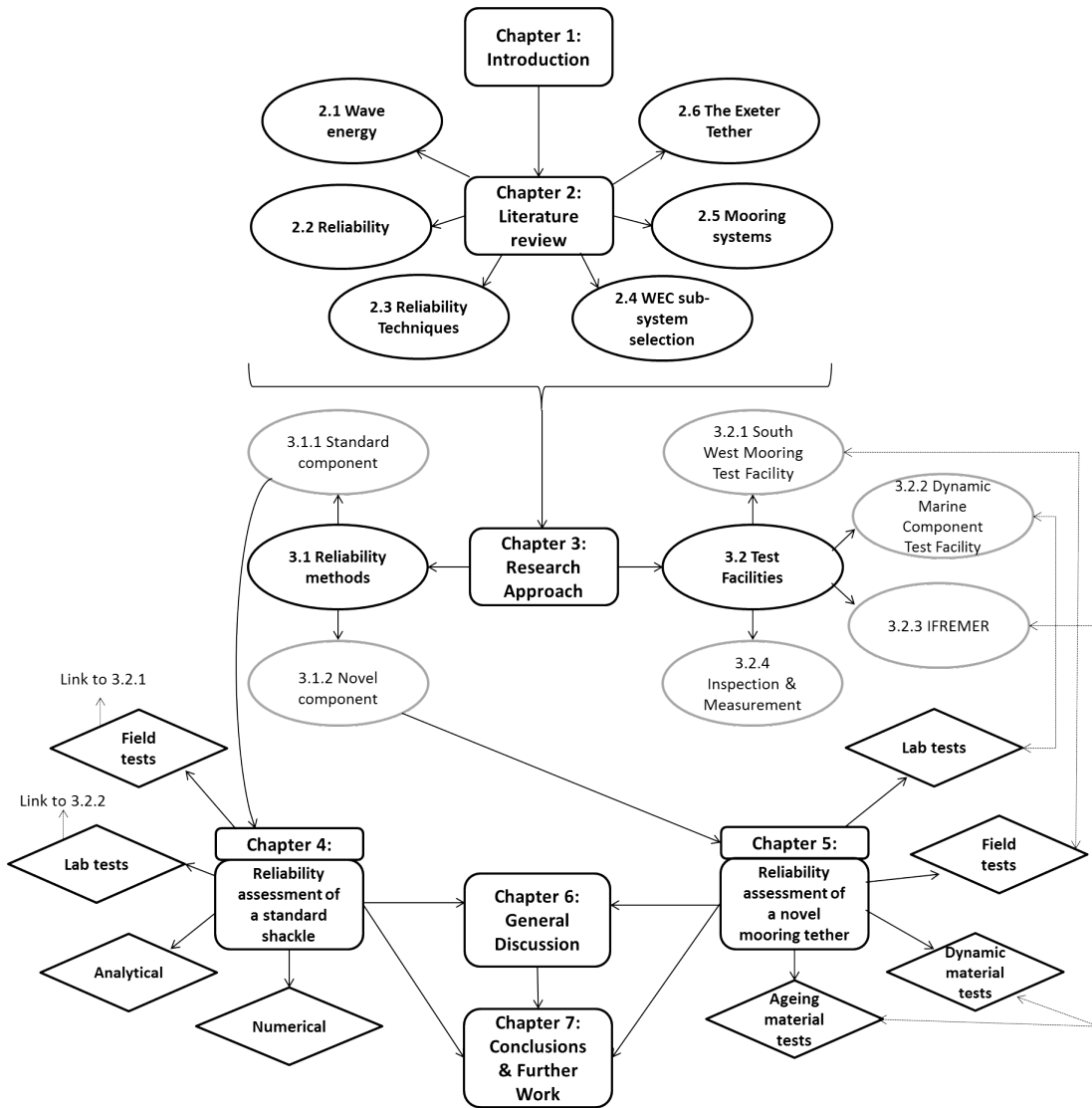
Figure 1.1: Flow diagram outlining Thesis structure

Chapter 2 addresses question one, through a literature review of current guidance

relating to wave energy development. Priority areas for development will be discussed, identifying the generic or specific nature of the sub-system in relation to the industry as a whole. This review establishes the mooring system as a key area for development and the focus for the work presented in this Thesis.

Chapter 4 presents a case study looking at a standard component used in a mooring system in order to address question two. Computer modelling, laboratory experiments and field deployment are used to investigate the safety factors present in a steel shackle and relate this to current guidance.

Chapter 5 introduces a novel mooring component with unique reliability challenges. Question three will be addressed through a thorough review of the reliability considerations of the Exeter Tether. Component tests both in the field and in controlled laboratory conditions are reported as well as material tests establishing the durability of the tether materials in a marine environment. Key areas for further development are highlighted.

Finally, Chapter 6 will address question four through an over arching Discussion. The implications of the introduction of the Exeter Tether will be discussed with reference to mooring system reliability.

1.5 Contribution to knowledge

- The review and synthesis of key guidance relating to priority areas for WEC device development provides an original contribution to knowledge. The approach taken to review the guidance in relation to the novel or generic aspect of the sub-system provides an evidenced and informative overview of priority areas for development.

- The investigation of a standard shackle in relation to mooring system guidelines to assess the appropriateness of safety factors given the revised operating requirements[1] of WECs is a novel contribution to knowledge.

---

[1]The majority of mooring guidance has been developed for the oil and gas industry, where large platforms are designed to be held relatively statically. WECs are small in comparison, and are generally designed to be highly dynamic. Section 2.5.3 provides further information. Furthermore, as previously

- The Exeter Tether is a novel component under development, many aspects of this work therefore form an original contribution to knowledge. Specific novel aspects of this work include:

  1. Polymer marine ageing tests: Prior to this work there was no published data on the effect of marine ageing on the properties of the ethylene propylene diene monomer (EPDM) polymer used in the Exeter Tether core.

  2. The novel use of the polymer core within the tether to resist radial compression required a range of bespoke tests to be developed. These include 'radial compression modulus tests' observing the affect of marine ageing and fatigue cycles on the modulus of the polymer.

  3. Results from the above material tests suggest EPDM polymer may not be the most suitable material for the Tether core; further work should be done to validate these findings, and it is suggested that alternative materials are also investigated.

  4. To facilitate the testing of tether screens without the need to re-splice the end termination of each tether a novel collet arrangement was designed and manufactured.

  5. Durability assessment of the anti-friction screen of the tether identified the original screen as inadequate and revised screen materials have been proposed.

  6. Results from fatigue testing of the Exeter Tether identified a critical failure mechanism and informed the proposal of a revised Tether design.

1.6 Author's Declaration

In order to clearly demonstrate the scientific contribution from the Author of this Thesis this declaration has been included. Whilst the author wrote this Thesis and conducted all aspects of data processing and analysis independently, many of the practical aspects

---

discussed, the consequence of a WEC mooring line failure is less critical than a failure in the oil and gas industry.

of the work presented required a team of people. This section will detail how the Author coordinated this practical work, and the contribution of others.

For the reliability assessment conducted on a standard mooring component (Chapter 4), test work conducted at the DMaC[1] test facility was led by the Author with the assistance of Dr. Andrew Vickers. The field testing of the shackles at the SWMTF[2] test site required the deployment and recovery of a mooring limb from the SWMTF. The Author worked with a team from the University of Exeter and Marine and Towage Services (MTS) to complete these deployments.

For the reliability assessment conducted on a novel mooring component, the Exeter Tether (Chapter 5), the Author led on all aspects of work relating to tether reliability. The original development of the Exeter Tether and the performance characterisation of the P1 Tether Series (reported in the Literature Review Chapter 2, Section 2.6, Page 112) was led by Dr. David Parish, with the Author providing assistance with much of the DMaC test work. Developing from Parish's work, the research presented in Chapter 5 of this Thesis and led by the Author, relates to the reliability assessment of the Exeter Tether. A joint publication by the Author and Parish (Gordelier *et al.*, 2015) brings both aspects of work together and reports on both the performance characterisation and the reliability assessment of the Exeter Tether.

The reliability assessment test work conducted on the tether assembly and the anti-friction membrane at the DMaC test facility was led by the Author with assistance from Dr. David Parish. The novel collet arrangement used for these tests was designed by they Author and manufactured by James Yule. The field testing deployment and retrieval were conducted during the same marine operations as detailed above for the standard mooring component. Again, the Author worked with a team from the University of Exeter and MTS to conduct these deployments.

The reliability assessment of the polymer core was funded by the EU's MARINET programme, which supported a two week testing programme at the IFREMER Materials in a Marine Environment Research Laboratories in Brest, France. The test plan for the work conducted during this visit was developed by the Author with assistance

---

[1]Dynamic Marine Component Test Facility, detailed in Chapter 3, Section 3.2.2, Page 139
[2]South West Mooring Test Facility, detailed in Chapter 3, Section 3.2.1, Page 136

provided from the IFREMER team. Some longer term aspects of this work were initiated by the IFREMER team in advance of the author's visit (such as the ageing of the polymer material). Following induction by the IFREMER team, the majority of the test work conducted at IFREMER was led by the Author with assistance from the IFREMER team and Dr. David Parish. The exception to this was the tensile fatigue testing (Chapter 5, Section 5.3.2.2, Page 257) and the dynamic mechanical analysis (DMA) testing (Chapter 5, Section 5.3.2.5, Page 270); these tests were set up and conducted by experts from IFREMER with assistance from the Author. Due to the length of time required to age the Ø25mm sections of EPDM polymer (Chapter 5, Section 5.3.2.1, Page 253), the compression tests were conducted on these samples by experts at IFREMER following the Author's visit. The author provided a detailed methodology for this work to ensure the results were comparable to the virgin material compression tests (Chapter 5, Section 5.3.2.4, Page 268).

Chapter 2

Literature Review

Contents

2.1   Wave energy

2.1.1   Scale of potential

As the global demand for electricity grows, so the search for low carbon and renewable energy sources is becoming increasingly important. Marine energy offers a potential

solution and has many benefits, particularly to the UK. Not only can it provide low carbon energy, it also delivers a level of energy security to the island nation not always available from conventional fossil fuel energy sources. As well as the provision of electricity, the marine energy sector has the potential to provide jobs and income for the country. By 2035 estimates suggest the sector could employ 19,500 individuals and have an annual value of £6.1bn to the UK economy (RenewableUK, 2010).

Looking specifically at wave energy, estimates vary for the national and global potential. It is important to be clear regarding the terminology of wave energy potential; unhelpfully, many estimations fail to be specific. Clear definitions of the terminology are provided in (Boud, 2012) and detailed here:

- *"Total resource: The total resource arriving in UK waters. It is the total resource flowing over a single frontage (or group of frontages) that are arranged to give the highest overall energy availability to the UK. These frontages do not take into account potential location constraints such as water depth and distance to shore.*

- *Theoretical resource: The maximum energy available from a set of frontages positioned in realistic locations based on areas likely to have the most competitive low cost of energy.*

- *Technical resource: The energy available from the theoretical frontages using envisaged technology options.*

- *Practical resource: The proportion of the technical resource that can be extracted taking into account location constraints such as sea uses and environmental impacts."*

Total resource values will generally be calculated from publications such as the *Atlas of UK Marine Renewable Energy Sources* (Department for Business Enterprise and Regulatory Reform, 2008) that details the kW/m of an incoming wave crest. In 1999 a review produced for the DTI estimated the UK's theoretical wave resource potential as 700-842TWh/year, and an unspecified global resource of over 2,000TWh/year (Thorpe, 1999). These estimates have been refined over recent years to provide an estimate of the practical wave resource for the UK of 50TWh/year (Carbon Trust, 2011) and to confirm the technical global resource as approximately 2,000TWh/year

(Thorpe, 2010). A recent report by the Carbon Trust however, reviews several previous reports and revises the figure for UK practical resource up to 70 TWh/year (Boud, 2012). To put this into context, in 2014 the final consumption of electricity in the UK was 303TWh (Department of Energy and Climate Change, UK, 2015a). 70TWh/year therefore represents over 23% of total electricity consumption in the UK. To compare this figure to other renewable energy sources in the UK, in 2014 total renewable energy sources accounted for 19.1% of electricity generated, a total of 64.7TWh (Department of Energy and Climate Change, UK, 2015b).

Boud (2012) also provides a useful summary of previous resource estimates and the methods behind them. A further more detailed study was conducted by Gunn & Stock-Williams (2012) which updated the global resource estimate by combining NOAA[1] WaveWatch III data over a six year period with an illustrative WEC. Although the authors do not categorise the estimate using the above definitions, it is essentially a technical resource assessment, locating Pelamis WEC devices at a density of 5 devices per km. Given this device type the global extractable wave power is calculated to be 96.6 ± 1.3GW.

Despite the various approaches discussed to calculate the wave energy resource, one thing is clear; there is a large potential for wave energy. The next section will give a brief overview of WECs currently under development or in use to harness this resource.

2.1.2 Wave energy generic device type

Wave energy is not a new concept; Clement et al provide an interesting summary of early developments (Clément *et al.*, 2002), including a French patent filed by Girard & Son in 1799 and the first British patent filed in 1855. Early designs used the motion of waves to drive simple mechanical systems such as pumps or mills. Evolution to modern systems has seen the direct generation of electricity, with the potential pairing of wave energy electricity generation with desalination plants an obvious opportunity. Significant progress has been made in the last 30 years due to R&D efforts both in Europe and globally. One of the challenges for WECs at the time of writing is the lack of convergence on device operating principal.

A European review paper written in 2002 identified over 1,000 patents for wave energy conversion techniques in Japan, North America and Europe alone (Clément

---

[1]National Oceanic and Atmospheric Administration

et al., 2002), and a summary of devices in January 2010 lists over 100 different WECs currently under development (Thorpe, 2010). A further source of information is the Marine and Hydrokinetic Technology Database, which keeps current records of marine and hydrokinetic renewable energy projects and also categorises these with regard to level of development (US Department of Energy, 2013). A search for wave energy devices results in 193 different project entries currently under development. Magagna & Uihlein (2015) further highlight the range in development across the sector, amongst others citing the European Marine Energy Centre who maintain a record of current wave energy developers with a total of 254 entries (Eurpoean Marine Energy Centre, 2015).

Despite the broad range of devices, WECs can be categorised based on their operating principles as cited throughout much of the literature (Day *et al.*, 2015; Drew *et al.*, 2009; Falcao, 2010; RenewableUK, 2011; Thorpe, 2010; Wolfram, 2006)

- **Oscillating water columns (OWCs)** A chamber of air is alternately compressed and depressurised by the rise and fall of waves. The rise of a wave compresses air and forces it through the turbine. As the wave falls, air is drawn back through the turbine to fill the chamber. A Wells turbine is commonly used as this allows generation of electricity on both the rise and fall of the wave. The PICO Power Plant, OE Buoy and Limpet are all examples of OWC devices.

- **Overtopping devices (OTDs)** OTDs capture sea water from the crests of waves in a reservoir above sea level. The potential energy of the water is recovered by releasing the water back to sea level through turbine(s). The Wave Dragon is an OTD.

- **Wave activated bodies (WABs)** The motion of waves cause oscillatory movement between different parts of the device or between the device and a fixed reference. Heave, pitch or roll motion can be used and typically hydraulic systems with generators are used to extract the energy. A well-known example of this type of WEC is Pelamis, other examples include the Anaconda.

- **Surge devices or oscillating wave surge converter** These are located in shallower water and are often based on a pivoted flap creating a pendulum that is activated by the horizontal to-and-fro movement of water particles in the surge

region. The Oyster is a surge device. (In some device definitions this type of device falls under WAB.)

A further classification can be used, based on how the device interacts with an incoming wave:

- **Attenuator** These devices lie parallel to the incoming wave direction and 'ride' the wave, generating energy from the relative motion of different parts of the device. Pelamis falls under the category of attenuator as well as WAB.

- **Point absorbers** These have small dimensions relative to the wave front and can be floating on the wave surface, or submerged below the surface with motion induced by the differential pressure created by a passing wave. OPT's PowerBouy is an example of a point absorber.

- **Terminators** These are large devices, with their principal dimension parallel to the wave front to intercept ('terminate') the wave. The Wavedragon falls under this category, as well as being an OTD.

A final classification is based on the location of the device:

- Shoreline

- Near-shore

- Offshore

(Harris *et al.*, 2004) developed two very useful tables to identify the relationships between the device operating principals, location, and directional characteristics. These tables are detailed in Figure 2.1 and Figure 2.2 and will be used as a basis for defining operating principals throughout this work.

In 2010 the World Energy Council conducted their annual survey of resources (Thorpe, 2010). Included is an interesting chart detailing the breakdown of wave energy devices under development by type. This has been included in Figure 2.3 and demonstrates that although over 50% of devices are point absorbers, the remaining device development is extremely broad. Research focusing on the reliability issues affecting
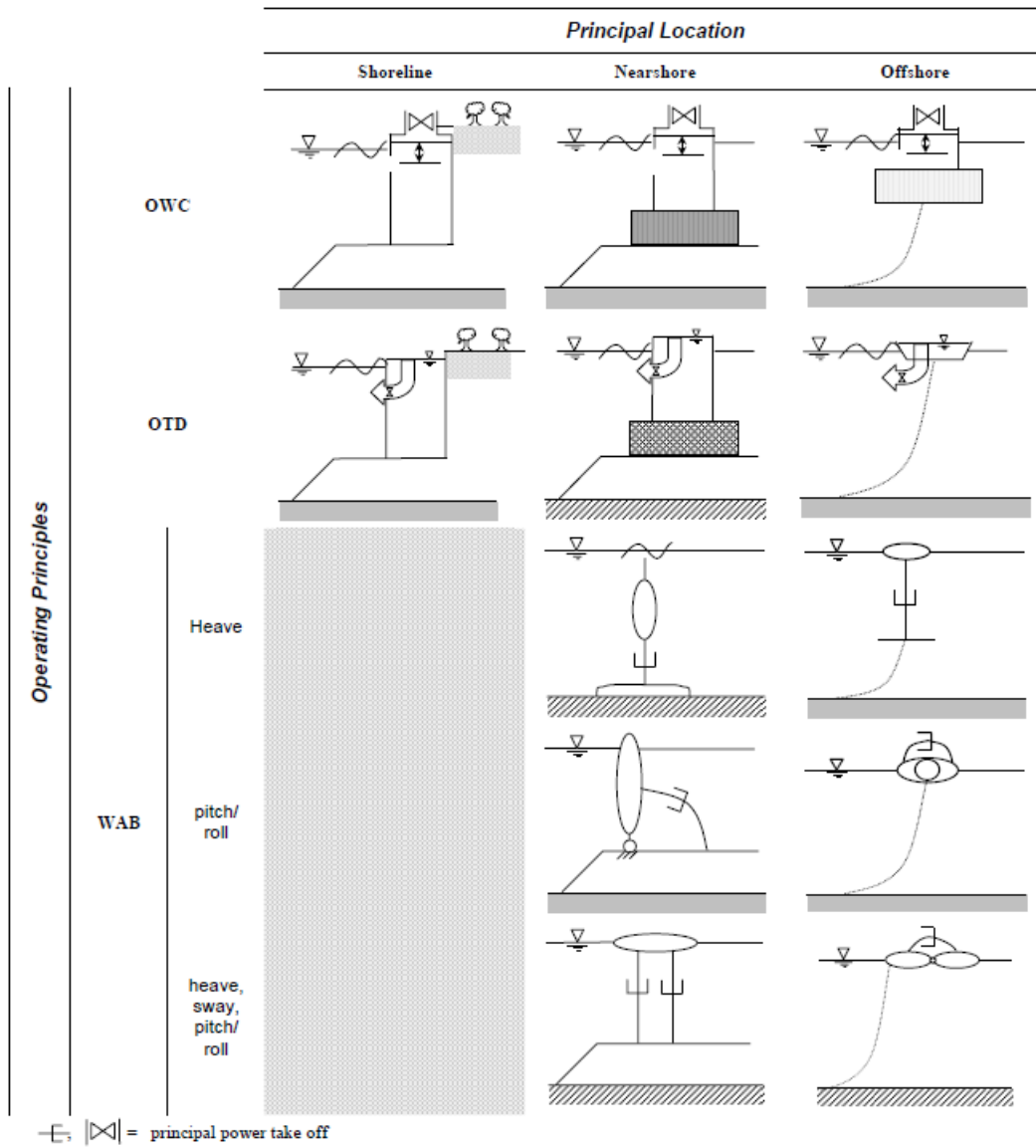
Figure 2.1: *"Schematic drawings of WEC devices for operating principles and principal locations"* (Harris *et al.*, 2004).

	Directional Characteristic		
Principal Location	**Point Absorber**	**Terminator**	**Attenuator**
Shoreline		OWC, OTD	
Nearshore	WAB	OWC, OTD, WAB	WAB
Offshore	WAB	OWC, OTD, WAB	WAB

Figure 2.2: *"Possible operating principles for the principal locations and directional characteristic"*(Harris *et al.*, 2004).

point absorber technology (which also falls within the WAB categorisation) may therefore prove the most valuable and this will be explored further in Section 2.4.1, WEC subsystem selection.

Having provided an overview of device classification, the next section will explore current work in WEC device development.

2.1.3 Current developments

Before detailing those devices currently leading the market, at the start of this section it seems appropriate to mention one of the very first wave energy devices to be proposed; the Edinburgh Duck. Designed by Stephen Salter in 1975, the terminator type wave energy system utilised a gyroscope together with a hydraulic power take off system designed around a 'duck' shaped nodding body, as detailed in the schematic in Figure 2.4 (Boud, 2002). Full details of the design and development of the device over the years can be found in Thorpe (1999).

The example of the Edinburgh Duck demonstrates that wave energy is not a new concept. Since 1975 there have been many years of development and numerous devices have been proposed. The rest of this section details a selection of these wave energy devices but before exploring this in detail, it is helpful to define the various stages of development. A thorough definition of these is given by the U.S. Department of Energy through their Marine and Hydrokinetic Technology Database in the form of Technology Readiness Levels (TRLs) (US Department of Energy, 2013), summarised in Table 2.1.
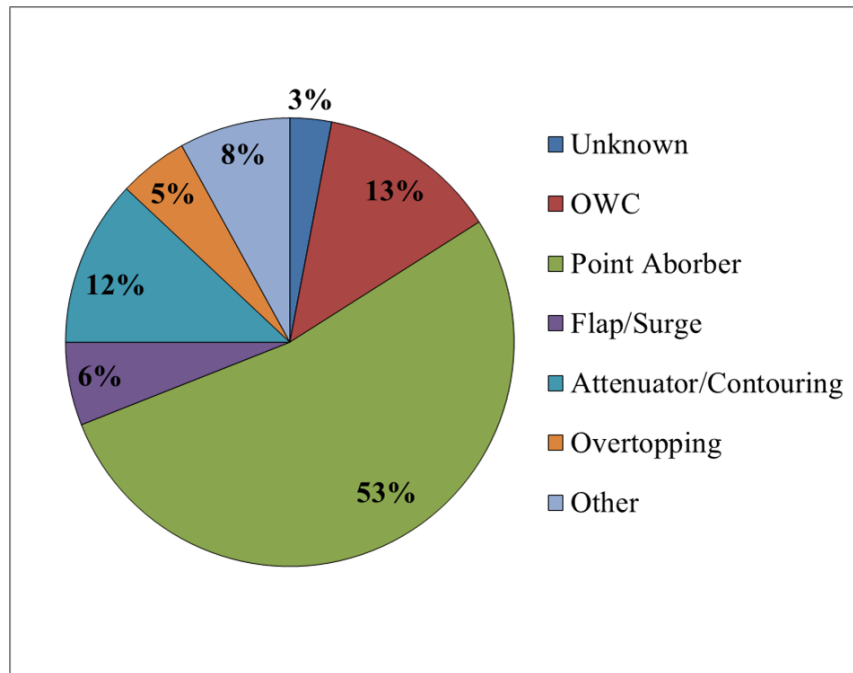
Figure 2.3: Breakdown of wave energy devices by device type. Graph replicated from data presented in (Thorpe, 2010). % figures are approximate.
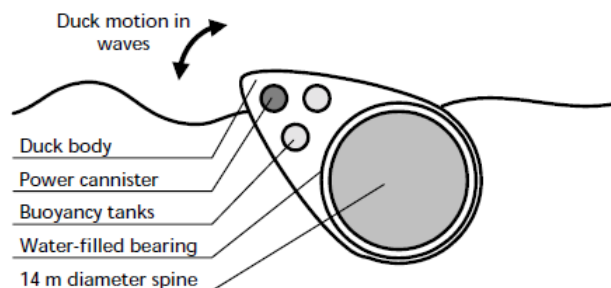
Figure 2.4: Schematic of the Edinburgh Duck wave energy converter. Replicated from (Boud, 2002).

2. LITERATURE REVIEW

Table 2.1: *Technology Readiness Level definitions as set out in* (US Department of Energy, 2013)

Technology readiness level (TRL)	Summary	Description
TRL 1 - 3	**Discovery / concept definition / early stage development, design and engineering.** (Purpose to evaluate scientific or technical merit and feasibility of ideas that appear to have commercial potential)	**TRL 1/2:** Scientific research begins to be translated into applied research and development where basic principles are observed and reported. Technology concepts and applications are formulated and investigated through analytic studies and in-depth investigations of principal design considerations. This level is characterized by paper studies, concept exploration, and planning.
		TRL 3: Active research is initiated, including engineering studies and laboratory studies to physically validate analytical predictions of separate elements of the technology.
TRL 4	**Proof of concept** (Concept validation, development of critical technology elements and testing in laboratory with scale models)	Basic technological components of a subscale model are integrated to validate design predictions and system-level functionality. The models, or critical subsystems, are tested in a laboratory environment.
TRL 5/6	**System integration and technology laboratory demonstration** (Device, system, subsystem level interfacing/integration testing must be demonstrated. Relevant scale models with realistic environmental testing conditions and monitoring. Foundation concept should be demonstrated)	**TRL 5:** Basic technological components are fabricated at a scale relevant to full-scale and integrated to establish and verify subsystem and system-level functionality and preparation for testing in a simulated environment.
		TRL 6: A representative model or prototype system at a scale relevant to full-scale, which is beyond that of TRL 5, is tested in a relevant environment. This level represents a major step up in a technology's demonstrated readiness and risk mitigation leading to open water testing.
TRL 7/8	**Open water system testing, demonstration and operation.** (At or near full scale. Initial testing may be in benign environments with the expectation that fully exposed, representative testing will follow. Foundations/moorings incorporated into model testing)	**TRL 7:** The prototype scale components and subsystems are fabricated and integrated to establish and verify subsystem and system level functionality and preparation for testing in an open water operational environment to verify expected operation and fine tune the design prior to deployment in an operational demonstration project.
		TRL 8: The prototype in its final form (at or near full scale) is to be tested and qualified in an open water environment under all expected operating conditions to demonstrate readiness for commercial deployment in a demonstration project. Testing should include extreme conditions.
TRL 9	**Commercial scale production/application** (In service application of technology in its final form under mission condition)	The actual, commercial-scale system is proven through successful mission operations, whereby it is fielded and being used in commercial application
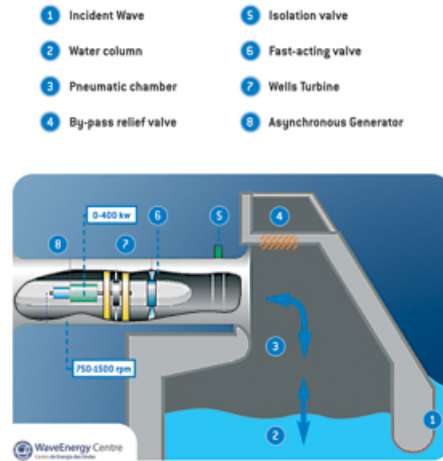
Figure 2.5: PICO Power Plant operating principles (Wave Energy Centre, 2006).

As discussed in Section 2.1.2, the sheer number of devices currently under development does not permit lengthy descriptions of each device. Published in 2015, (Magagna & Uihlein, 2015) identify 46 devices approaching or at open sea deployment stage (TRL 7 or above). To give an overview of the variety of technology types leading the market a selection of devices at this TRL will be presented:

OWC - shoreline: PICO Power Plant, Wave Energy Centre. This device is based around a shoreline reinforced concrete structure housing a pneumatic chamber. Incident waves cause water to oscillate vertically in the chamber, forcing air to and from the atmosphere through a Wells turbine with symmetric blades (Figure 2.5). The turbine is connected to a generator for electricity generation. Constructed in 1999, the 400kW full scale system installed on the Azores has faced some technical difficulties but the plant has been operating intermittently since 2005 (Wave Energy Centre, 2006).

OWC - offshore: OE Buoy, Ocean Energy. The OE Buoy works on the same operating principal as the PICO plant; however instead of housing the pneumatic chamber within a concrete structure on the shoreline, the pneumatic chamber is housed within a floating structure, tethered to the sea bed, with sub-merged openings to the sea. Again, the rise and fall of waves within the chamber forces air through a Wells turbine connected to a generator on the floating structure, Figure 2.6. A ¼ scale model has been tested over a three year period in Galway Bay, Ireland and Ocean Energy are preparing to deploy a 1MW full-scale device for grid connection at Wave Hub in
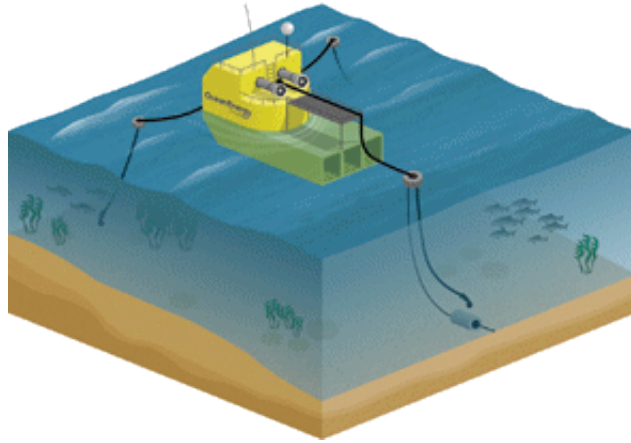
Figure 2.6: Artist's impression of OE Buoy (Ocean Energy, 2013).
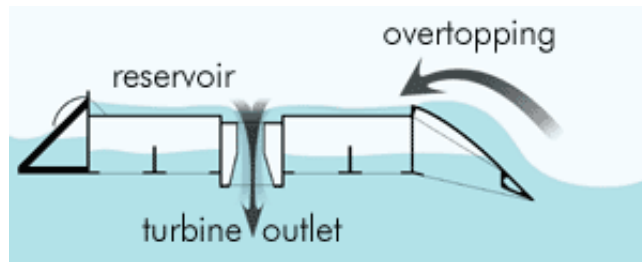
Figure 2.7: Operating principles of the Wave Dragon (Dragon, 2005).

Cornwall (Ocean Energy, 2013; Wave Hub, 2013b, 2015)

OTD - terminator: Wave Dragon. Wave Dragon is a floating offshore platform, moored to the seabed that works on the same principle as land based hydro power plants. The overtopping device elevates waves into a reservoir where they are held above sea level. From here the water is released back out to sea through a number of low-head hydro turbines to generate electricity, enabling control over when electricity production occurs (Figure 2.7). A ¼ scale device was tested in a Danish inlet in 2003 and work is on-going to deploy a full scale device in Denmark, Wales and Portugal. The initial ¼ scale prototype was designed for a more benign environment than envisaged for the full scale model, and as such was rated at 20kW ((MacDonald, 2014; Thorpe, 2010).

WAB - offshore - attenuator: Pelamis. The best known of all WECs, the operating principle behind Pelamis is based on a series of cylinders, connected by joints housing hydraulic power take off units (PTOs). As a wave travels down the length
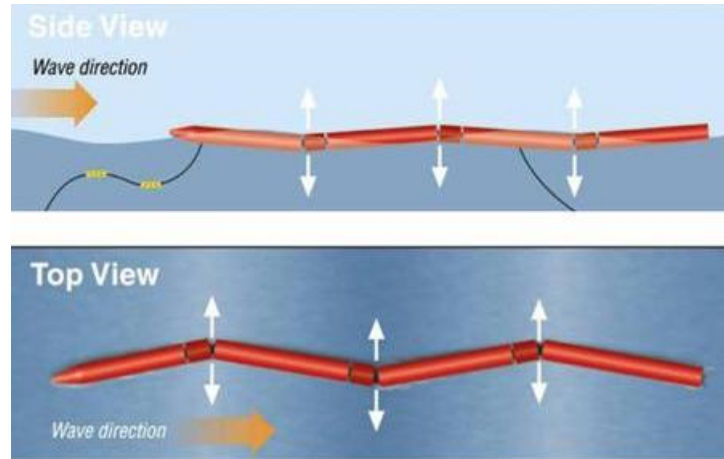
Figure 2.8: Operating principles of Pelamis (Parsons, 2013).

of the device, the cylinders move independently from one another (Figure 2.8). The relative motion between adjacent cylinders is converted to electricity via a hydraulic PTO within each joint. The whole system is attached to the sea bed via flexible moorings. This device has gone through a well published development route with both scale component and scale model tests. The first full scale model, rated at 750kW, was tested in European Marine Energy Centre (EMEC), Scotland from 2002 to 2004. Two full scale second generation P2 devices, consisting of 5 cylinders connected with 4 PTO joints, were deployed at EMEC (Pelamis Wave Power, 2013).

In 2014 Pelamis Wave Power, unable to secure the funding necessary to continue development, called in the administrators (BBC, 2014c). The assets of the company were acquired by Highlands and Islands Enterprise, through the Wave Energy Scotland project funded by the Scottish Government in 2014 (BBC, 2014a) and as yet no further developments have been announced.

WAB - offshore - point absorber: PowerBuoy, Ocean Power Technologies. The PowerBuoy generates electricity via the vertical motion of a floating buoy in relation to the fixed spar, attached to the sea bed (Figure 2.9). This relative motion drives a mechanical system which is coupled to generators that produce electricity. Several PowerBuoy prototypes have been tested including projects in Scotland, Hawaii and the USA, with peak generation of over 400kW achieved. PowerBuoy wave parks are planned in Spain, Australia and the USA (Ocean Power Technologies, 2013).
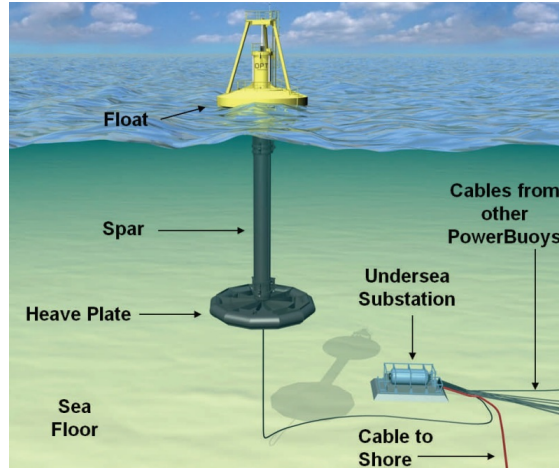
Figure 2.9: OPT PowerBuoy System (note mooring system not shown) (Ocean Power Technologies, 2013).

WAB - nearshore - surge device: Oyster, Aquamarine. The Oyster device is designed for location around 0.5km from the shore, in depths of 10 to 15 metres. The device is an underwater hinged flap, attached to the sea bed. The top flap is buoyant, and pitches backwards and forwards in the nearshore waves, driving two hydraulic pistons which pump high pressure water to shore via sub-sea pipelines. At shore this high pressure water is used in a conventional hydro-electric turbine to generate electricity (Figure 2.10). Oyster 1, rated at 315kW and the first full-scale prototype, was successfully tested from 2009-11 at EMEC. Testing has commenced on Oyster 800, rated at 800kW, also being tested in EMEC. Consent has been granted for two further devices in Scotland (Aquamarine Power, 2013).

Aquamarine Power significantly downsized in 2014 following a strategic review (BBC, 2014b) but the firm was boosted in 2015 through the award of an £580,000 EU Horizon 2020 grant to continue the development of the Oyster in collaboration with National University of Ireland, Maynooth (BBC, 2015a). Disappointingly, only a month and a half following this announcement Aquamarine Power called in the administrators, citing *"cash flow strain"* as a major issue for the company (BBC, 2015b).
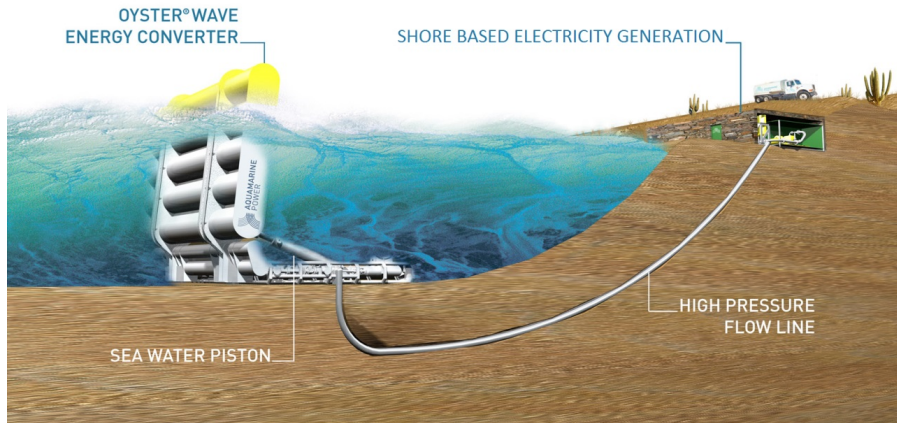
Figure 2.10: Operating principle of Aquamarine Power's Oyster (Gadgets, 2009)

2.1.4 Costs of wave energy

Despite the identified resource available and numerous devices under development, reducing the cost of wave energy is essential in order to be competitive with other forms of electricity generation. The Low Carbon Innovation Coordination Group (2012) suggests a cost saving of 50-75% must be achieved by 2025 for wave energy to become a commercial reality. A breakdown of device cost contributions from major component technologies is detailed in both (Carbon Trust, 2007) and (Low Carbon Innovation Coordination Group, 2012). The values from each are replicated in Figure 2.11.

Cost of energy is often referred to as 'levelised cost of energy' which accounts for capital costs, operating costs and annual energy production. A schematic published by SI Ocean (2013) and replicated in Figure 2.12 details the different cost components accounted for within the LCOE term.

It is helpful to consider the costs of wave energy in relation to offshore wind, which has faced many of the same challenges but is much further along the development path. The Low Carbon Innovation Coordination Group (2012) states that offshore wind is capable of delivering power at £140/MWh currently and £180/MWh for sites further offshore. Leading players in the UK market have established a potential path to offshore wind arrays generating at £100/MWh with further innovation bringing this as low as £65/MWh by 2050 making it cost competitive with other forms of conventional generation. In comparison the report states that in 2012 wave energy costs

(a) (Carbon Trust, 2007)

(b) (Low Carbon Innovation Coordination Group, 2012)
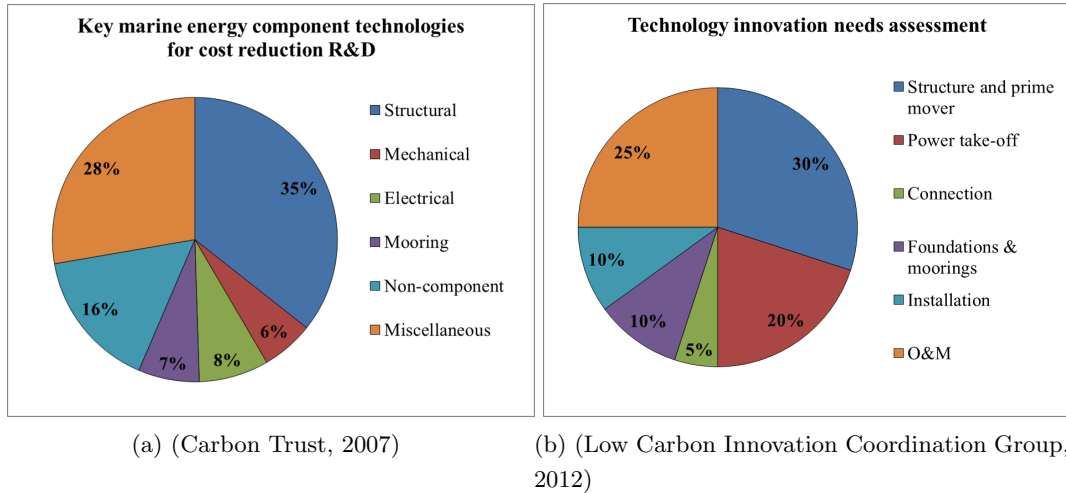
Figure 2.11: Wave device capital cost breakdown estimates for major component technologies, comparing two reports.
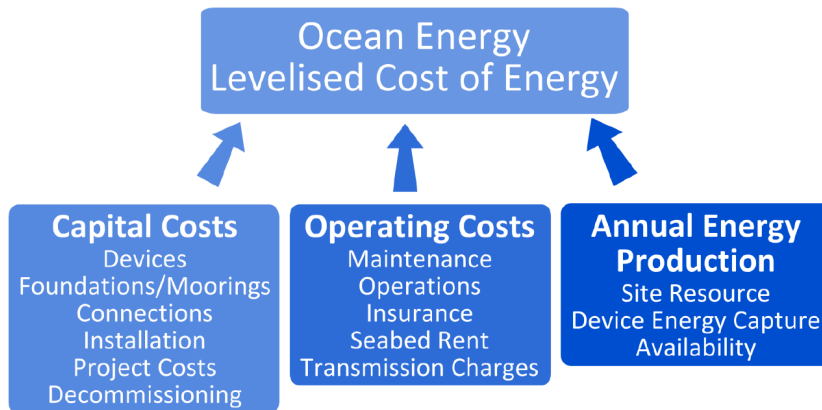
Figure 2.12: Levelised cost of energy factors as detailed in SI Ocean (2013)

are estimated in the order of £250-400/MWh. Reducing these costs to be competitive with offshore wind will be a challenge, and a clear cost reduction pathway must be established.

Further estimates of the cost of wave energy are provided by Allan *et al.* (2011), Carbon Trust (2011), SI Ocean (2013) and Krohn *et al.* (2013). Allan et al. conducted a detailed assessment considering all costs that *"would be paid by the owner of the electricity generation technology"* and refer to this as 'private levelised cost of energy'. The result of this paper is significantly lower than previous estimates, with a point estimate at 2006 prices of £189.68/MWh. The range of estimates is shown in Figure 2.13 alongside other electricity generating technologies that have been subject to the same assessment process.

The report issued from the Carbon Trust (2011) makes a cost estimate based on actual costs obtained from leading developers at the time and assumes costs based on the development of the first wave farms of approximately 10MW. This report suggests a higher figure at £380 - £480/MWh, however based on the implementation of an accelerated innovation scenario leading to 0.3GW of installed wave capacity, the report forecasts potential costs of £150/MWh - £200/MWh by 2020.

LCOE estimates reported in Krohn *et al.* (2013) broadly support those values detailed in Low Carbon Innovation Coordination Group (2012). Written in 2013, Krohn et al. detail how the cost of energy is anticipated to fall over time as second generation arrays are installed (Figure 2.14).

The most recent cost estimates for wave energy are summarised in graphical form by Magagna & Uihlein (2015) and are calculated based on Corsatea & Magagna (2013). The figures presented by Magagna & Uihlein (2015) show a LCOE for wave energy ranging from €50 - €65/kWh. This value appears to be a factor of 100 larger than other published figures and it must be assumed that the scale on the published graph is incorrect. At an exchange rate of €1 = £0.70 this is the equivalent of £35 - £45/kWh or £35,000 - £45,000/MWh. Assuming there is a unit error in the presented graph, the correct price is in the region of £350 - £450/MWh, which corresponds much better with the estimated figures in Low Carbon Innovation Coordination Group (2012) and Krohn *et al.* (2013).

The estimates for LCOE of wave energy clearly vary in the different reports discussed, but broadly estimates fall within the range of £250 - £450/MWh. What is
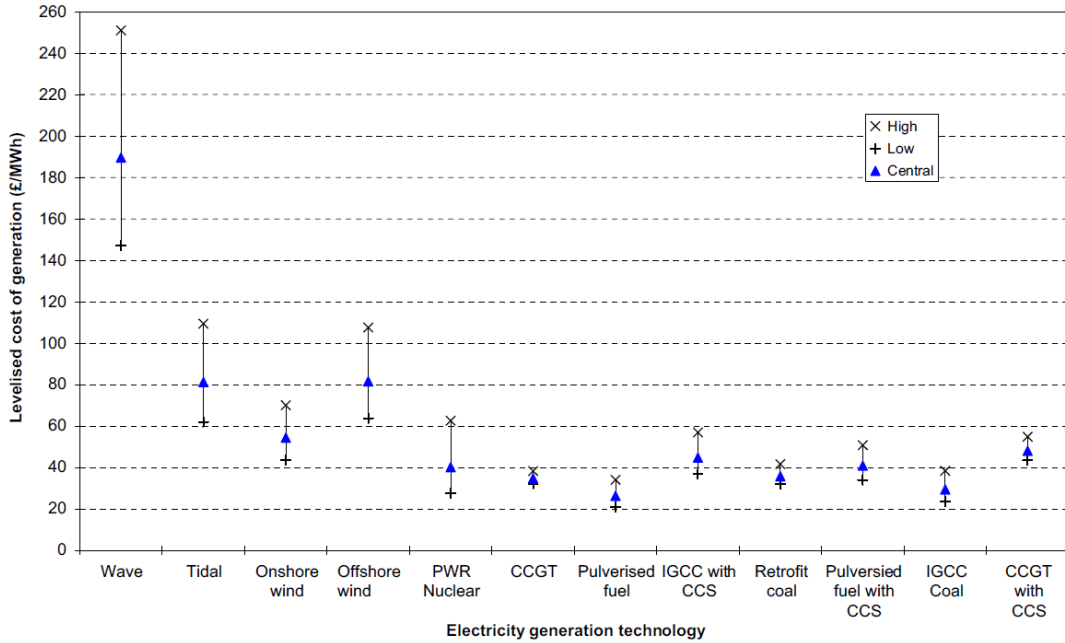
Figure 2.13: Levelised cost of energy ranges for twelve different technologies with high and low estimates of capital costs(Allan *et al.*, 2011)
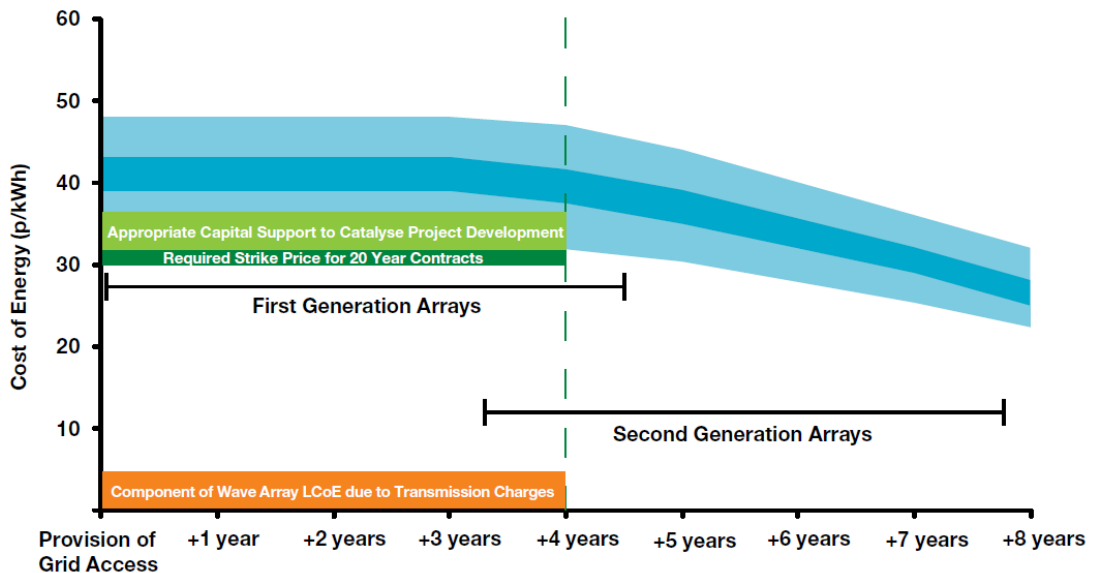
Figure 2.14: Anticipated levelised cost of energy ranges (Krohn *et al.*, 2013)

consistent across all these reports is that currently, the LCOE of wave energy is significantly higher than other electricity generation techniques, particularly conventional fossil fuels. It is clear that substantial cost savings are required from the wave energy industry if it is to become cost competitive with other forms of electricity generation. How these cost savings might be achieved and the anticipated cost savings through research and development of major components will be further explored in Section 2.4, Page 77.

2.2 Reliability

The significance of reliability changes over the development stages of a new device. At concept and early development stages (TRL 1-4), devices are often substantially over-engineered. These stages are about proving the device can generate electricity as the design intended; developers do not want embarrassing early failures, and want to ensure investor confidence. Large safety factors are applied to early designs and prototypes to ensure a robust performance.

These large safety factors have an associated cost, both in terms of device build and device deployment. Once a new device has been successfully demonstrated in concept stage, these safety factors must be reduced so that the device can be built, deployed and operated economically for TRLs 7-9. Understanding device reliability is crucial to achieving this.

With many devices now coming out of concept stage and preparing for large scale production and deployment, the need for accurate reliability methods is increasingly important. In this section a brief literature review into the reliability of wave energy converters is conducted.

2.2.1 Defining reliability

There have been various attempts to define reliability across many industries, but until recently there were very few definitions specific to wave energy. At the most basic level the dictionary definition of reliable is *"able to be trusted; predictable or dependable"* (Sinclair, 1998). This is a good starting point for a definition but to look more specifically at engineering and materials design, the ASM Materials Selection and Design Handbook provides the following definition of reliability: *"Reliability is a*

measure of the capacity of equipment or systems to operate without failure in the service environment" (Dieter, 1997). Refining the definition further to look at renewable energy systems, the offshore wind sector has recently gone through significant development and should provide some guidance to the emerging wave energy industry. A paper published in 2001 defines the reliability of a system as: *"Reliability of a system is the probability that the system will perform its tasks. This probability is usually determined as a percentage of time. For a wind turbine this indicates percentage of time it is producing power that corresponds to the acting wind according to its nominal power curve."* (Van Bussel & Zaaijer, 2001).

A new, equivalent definition could be established for a wave energy converter:

Reliability of a wave energy system is the probability that the system will perform its tasks. This probability is usually determined as a percentage of time. For a wave energy converter this indicates percentage of time it is producing power that corresponds to the wave climate according to its nominal power output at a given wave climate.

Reliability in relation to wave energy converters specifically is addressed in a limited number of papers. In 2009 Brown discusses the importance of definitions and describes some examples in a series of papers submitted as part of his Thesis (Brown, 2009). As well as discussing various definitions, he endeavours to define the relationship between reliability, maintainability and survivability and draws important distinctions. Reliability, he argues, defines the operation of the device when working within its design parameters. Survivability on the other hand, deals with extreme events; during these periods a device may go into 'shut-down' mode and stop generating, but it still must survive the extreme event intact. He uses the example of a wind turbine, summarised below, to demonstrate this:

- During high winds the blades of a wind turbine will rotate into the wind to alleviate the loads on the system and force the turbine into shut-down. It is during this 'survival mode' that the survivability of the system should be defined.

- The reliability of the system on the other hand, should be defined when the system is generating within normal operating conditions.

He believes this distinction between reliability and survivability is particularly pertinent to renewable energy devices operating in more volatile environments than conventional energy production methods e.g. a gas turbine has a very predictable operating

environment. As this Thesis develops, it will be important that I clearly define whether I am analysing a system for reliability or survivability.

Another publication specific to marine energy, written for the European Marine Energy Centre and published at a similar time to Brown's paper quotes a definition of reliability from the international standard IEC 600050 definition as: *"The probability that an item can perform a required function under given conditions for a given time interval"* (Starling, 2009). The guidelines also state reliability can be specified as Mean Time Between Failure (MTBF). Survivability is also discussed in the guidelines, and is separated into two aspects:

- *"Safety survivability: the probability that the converter will stay on station over the stated operational life."*

- *"Functional survivability: the probability that the converter will produce its rated energy (or an allowed degraded energy rating) without damage leading to the need for major unplanned removal or repair over the stated operational life."*

When discussing aspects to consider in relation to survivability, some long term conditions are included in these guidelines such as corrosion and fatigue. Arguably these should also be considered in relation to reliability; these are known factors of the design environment that a device should be designed to tolerate within its working parameters. Having reviewed the various definitions discussed in the literature, a new definition of reliability has been formulated that will be considered as a reference throughout this Thesis:

The ability of a device to successfully perform its purpose, without failure and within its design parameters. In relation to a wave energy converter this will be to produce electricity, as predicted for the given wave climate, for the duration of its design life.

Within this Thesis fatigue and corrosion will be considered to fall within this definition of reliability. They are part of the design parameters of a WEC and should therefore be considered as part of the system reliability.

Although the focus of this PhD is reliability, it is also important to have an understanding of availability and maintainability as these three matters are inextricably linked and have significant effects on one another. The following definitions will be used

for these terms; taken from the IEC 600050 definition as referenced in the Guidelines on Reliability, Maintainability and Survivability of Marine Systems written for the EMEC as previously discussed (Starling, 2009)):

Maintainability: *"The probability that a given maintenance action, for an item under given conditions of use, can be carried out within a stated time interval, when the maintenance is performed under stated conditions and using stated procedures and resources."*

Availability: *"The ability of an item to be in a state to perform a required function under given conditions at a given instant of time or over a given time interval, assuming that the required external resources are provided."*

The guidelines also describe this in a simplified format for continuously running equipment:

$$Availability = \frac{uptime}{uptime + downtime} \qquad (2.1)$$

Additionally, the guidelines bring together the relationship between reliability (specified as Mean Time Between Failures - MTBF), maintainability (specified as Mean Time to Repair - MTTR) and availability, for continuously running equipment:

$$Availability = \frac{MTBF}{MTBF + MTTR} \qquad (2.2)$$

Another definition of interest is raised in Brown's collection of papers (Brown, 2009); the concept of RISKEX. This is further detailed by the Carbon Trust in the publication Guidelines on design and operation of wave energy converters (Carbon Trust, 2005). RISKEX is defined as reliability expenditure and calculated by multiplying the estimated cost of failure by the estimated likelihood of occurrence. This is a useful term as it allows a price tag to be added to the reliability of a system by clearly defining profit as:

$$Profit = Revenue - CAPEX - OPEX - RISKEX \qquad (2.3)$$

(Where CAPEX is capital expenditure and OPEX is operational expenditure.)

A final definition that is relevant to the work presented here is for **durability**. Weller *et al.* (2014b) discuss durability in relation to wave energy mooring and foundation design and state *"the term durability accommodates both holding capacity and*

reliability". The definition includes overloading and fatigue damage, in addition to allowance for wear, corrosion and other changes to material properties.

2.2.2 Reliability and WECs

The concepts of reliability and the overall viability of WECs are closely linked. A review of the literature immediately identifies the importance of reliability to the development of the industry. In this section, the most important references to reliability in the literature will be discussed.

From an initial review of the various roadmaps and action plans issued from UK government regarding marine energy, it is clear that they regard reliability as a key challenge to the sector. One of the earlier government reports looking specifically at wave energy was conducted in 2002. The DTI contracted Arup Energy to conduct a report into the current status of the technology for various purposes including the development of a set of recommendations for future research and development priorities. Within this study, 11 key technology issues are identified, 6 out of the 11 technology areas identified include reliability as a key challenge (Ove Arup Energy, 2002). From the paper a series of recommendations are made. These include the development of a reliability database (for sharing of information between developers), and further research and development priorities that will be discussed within Section 2.4, WEC sub-system selection.

In 2010 the Department of Energy and Climate Change (DECC) issued a Marine Energy Action Plan specifically written to address barriers to development and to promote and stimulate the marine sector in the UK. The first point in the summary of recommendations states: *"At the highest level, technology development and deployment will require measures to address the underpinning generic technical challenges. These can be summarized as: predictability, manufacturability, installability, operability, scalability, survivability, reliability and affordability."* (Department of Energy and Climate Change, UK, 2010). The report highlights the need to advance reliability and survivability at a component level by funding developments of 'enabling components'. This sentiment was repeated in a more generic report, the 2011 UK Renewable Energy Roadmap from DECC; priority actions to progress marine energy are highlighted. To manage the risks and costs of research and development, the report suggests that following demonstration projects *"further innovation will often be required, so that the*

reliability, performance and durability of devices can be improved, before companies can move to commercial deployment." (Department of Energy and Climate Change, UK, 2011).

To summarise the Marine Energy Accelerator programme, run by the Carbon Trust from 2007-2010 an insight report was written in 2011. This detailed the outcomes from the programme, which aimed to reduce the costs of wave and tidal energy by developing new device concepts, improving specific device components, and working on installation, operation and maintenance strategies. This insight report states *"Both wave and tidal stream technologies will place increased emphasis on proving reliability and on risk reduction as the resource is harnessed from inherently more difficult environments."* (Carbon Trust, 2011). The issue of improving reliability, the report suggests, will not reduce as the industry develops but become increasingly important as developers strive to extract energy from increasingly hostile environments.

Following from these reports, The Energy and Climate Change Committee commissioned a report for the House of Commons in 2012 entitled The Future of Marine Renewables in the UK (House of Commons, 2012). The report addresses how the marine sector should be supported by the UK Government, and recognises the current costs for wave and tidal energy need to be brought down. In a section detailing methods for doing this, improving reliability is cited as one of the priorities for reducing costs.

Written evidence to this report supplied by several parties is detailed, this includes a submission by DECC detailing reliability as a key non-financial barrier to development. Further evidence from the energy company E.ON, when asked how the government should support marine technologies, acknowledges that the marine sector could make a useful contribution to the UK's energy mix but *"enabling the potential contribution to be realised will require improvements in the reliability of wave and tidal technologies coupled with reductions in costs associated with construction and deployment."*

Memorandums submitted by other companies also reference the need for improved reliability to reduce costs. The Energy Technologies Institute related reliability to investment and suggested proven reliability is required to acquire investment for a project. They also highlighted that the demonstration of reliability is a key challenge for most SMEs developing marine technology.

Looking more globally at issues impacting the development of WECs; a detailed, multinational and multi discipline review into wave energy status in Europe, conducted in 2001, highlights the potential of wave energy but suggests that to achieve its full potential *"survivability and reliability of many devices... has still to be demonstrated"*(Clément *et al.*, 2002). Finance of projects is another reason the reliability of devices is so important. An International Energy Agency report in 2003 stated *"The priority for wave energy is to demonstrate the survivability and reliability of the first devices in order to overcome the credibility problems resulting from the early days of development. Concepts need to be proved and devices verified and certified. This is imperative if the devices are to attract investment in the technology..."* (Boud, 2002). In a more recent report the World Energy Council, in their 2010 review of energy resources, listed the key challenges to a successful WEC device (Thorpe, 2010). Reliability remains one of the five key challenges listed; the report details the difficulty and expense of access for repair of WECs as one of the key reasons reliability of devices must be high.

Further confirming the importance of reliability to progress the wave energy industry, it is specifically addressed in the Horizon 2020 Work Programme 2016-2017. Horizion 2020 is an EU Research and Innovation funding programme with a budget of €79bn. The Work Programme 2016-2017 Section 10 focuses on *"Secure, Clean and Efficient Energy"*. In relation to Ocean Energy the document specifically cites reliability as a key priority: *"Increased performance and reliability of ocean energy subsystems: The priority for the ocean energy sector is to increase significantly the performance, reliability and survivability (15-20 years target) of ocean-energy devices developing solutions based on alternative approaches, sub-systems and materials."* The document continues *"The challenge resides in an improved understanding of component failure and low reliability in current ocean-energy devices, and in the development of improved performance, contributing to reduce the cost of ocean-energy."* (European Commission, 2015). It is interesting to note the dates of these publications; 2001, 2003, 2010 and 2015 respectively. Survivability and reliability of devices, despite being a priority for many years, still remains to be proven.

From this literature review it emerges that at a policy level, both in the UK and globally, reliability is regarded as a key challenge to the marine energy sector. How do these high level strategies relate to the design of systems, and the research and

development being conducted? The Guidelines on Reliability, Maintainability and Survivability of Marine Energy Conversion Systems (Starling, 2009), mentioned previously in relation to definitions, are intended to act as guidance to the WEC industry. These guidelines state *"Reliability, maintainability and survivability are crucial to the economic and environmental case for a marine energy converter. They affect:*

- *Capital expenditure*

- *Revenue*

- *Operational expenditure*

- *Risk expenditure."* (Starling, 2009).

These effects are discussed in further detail in the paper which also raises an interesting discussion on the balance between reliability and maintainability. Ideally, of course, a system should be highly reliable and maintainable; however the paper suggests that there is a balance between these two that should be maximised to obtain a high level of availability and ultimately minimise the lifetime cost of energy from the device. A system should either have *"high reliability and poor maintainability or good maintainability and low reliability"*. Similarly the level of redundancy can be put in a balance with reliability and a choice made on where investment should be focused *"high component reliability and low redundancy or high redundancy and low component reliability"*.

Clearly with infinite finances a system will have high reliability, good maintainability and multiple redundancy; however finances are never infinite, and this paper raises an interesting (and realistic) perspective on balancing these issues. For a large proportion of WECs, particularly those in nearshore and offshore environments, access for maintenance and component replacement is limited. Weather windows over the summer months provide some opportunity for maintenance tasks, but for failures occurring outside of weather windows, accessing the device for repair can be challenging and expensive. Consequently, applying these guidelines to the majority of WEC devices suggests that high system and component reliability should be the focus, in favour of high maintainability or multiple redundancy.

Those that are working to develop testing facilities are clear why the need for reliability is so important. *"The viability and success of these projects is strongly dependant*

on the reliability of devices as this determines the amount of generated electricity and the cost for operation and maintenance." (Thies & Johanning, 2010). Effective reliability, availability and maintainability assessment (RAM), Thies et al argue, *"provides vital information for decisions on project investment, design alternatives, operation and maintenance strategies and the identification of components and subsystems for further improvements, (it is a tool to) ensure the viability of marine energy projects.''* (Thies & Johanning, 2010).

A recent article by a Scottish WEC developer, Aquamarine, refers to component reliability hindering the development of the Oyster device. *"One of Scotland's leading pioneers of wave power has reaffirmed confidence in the nascent marine power technology, after revealing that component failures had set the company back by at least two years."* The article goes onto discuss the difficulty of developing survivable equipment, with McAdam (Chief Executive of Aquamarine) stating that *"There is no doubt there is strong investor interest in the wave sector. What we must do as an industry is deliver reliable power production from our devices and investment will follow."* (Donald, 2013). McAdam's refreshingly open attitude to discussing failures continues in (Bayar, 2013) where he discusses the unexpected failure of all the cables and connectors tested with the Oyster device in 2011. Despite utilising suppliers to the offshore oil and gas industry, the highly aggressive operating conditions of the Oyster truly tested the reliability of these components, which could not survive these conditions. Survivability of key components of another well known WEC, Pelamis, was cited as one of the developer's main challenges in an article published following the announcement of the company going into administration (Danko, 2014).

It can be useful to compare to best practice from other industries and Thies et al refer to the OREDA data base developed by the offshore oil and gas industry (Thies *et al.*, 2009). This reliability database provides a platform for companies to collate and exchange reliability and maintenance data obtained from their offshore operations. This database can then be drawn upon for developers so that industry learns by the shared experience of others. A similar data base is suggested for the marine renewables sector, with a focus on more generic components, not specific to any one device. The inclusion of existing reliability data from other industries, modified to be relevant to WECs is also recommended.

Although progress has been slow for the offshore renewable energy industry in this area, in 2015 a pioneering data platform was launched for offshore wind farm owners and operators. The 'System Performance, Availability and Reliability Trend Analysis' (SPARTA) was launched in July 2015 and all 10 of the UK's wind farm owner/operators have committed to sharing this data with the aim of improving the sector overall (The Crown Estate, 2015). Other countries have been quick to introduce their own databases for such information sharing, including the Wind Energy Information Data Pool (WIND-POOL) database created by Fraunhofer for German offshore windfarms (Fraunhofer, 2015). Despite these developments for offshore wind, there is still no such knowledge exchange database for the wave or tidal energy sectors.

2.3 Reliability techniques

2.3.1 Introduction to reliability techniques

Many different approaches are used to estimate the reliability of a given component or system. Over the years different industries have refined these approaches for their specific application. Currently, there is no standard method of reliability analysis for WECs. In this section, the most common approaches used in the wave energy industry will be reviewed from the literature. These have been broken down into three key areas: Analytical techniques; computer modelling; and physical tests.

Within Section 2.3.2, *Analytical Techniques*, a specific approach for accumulated fatigue damage calculations is introduced in Section 2.3.2.6. Although this is not generic in nature, as the other approaches are, this is an important technique for calculating accumulated fatigue damage to inform the more generic approaches detailed. It has been included here as it forms an important part of the estimation techniques used in this research.

Following a review of how the different approaches have been used within existing literature, the final section will provide a comparison of the advantages and disadvantages of the different approaches. The approaches used in this research will then be outlined.

Item	Failure Mode	Probability	Failure Effect (Local)	Failure Effect (End)	Detection	Compensating Provisions	Consequence	Risk	Remarks

Figure 2.15: Failure modes and effects criticality analysis (Starling, 2009)

2.3.2 Analytical techniques

It is not uncommon for a combination of different analytical approaches to be used for reliability assessment. For clarity some of the more common approaches will be explained separately, however in practice they may be used in combination.

2.3.2.1 Failure modes and effects criticality analysis (FMECA)

This can be referred to by its constituent parts; Failure Modes and Effects Analysis (FMEA) and Criticality Analysis (CA) or the combined FMECA. FMEA is a qualitative process to analyse each component in a system for potential failures and review the impacts of these failures on the system as a whole. The CA extends the analysis by quantifying the FMEA and often ranking failure modes in terms of probability or consequence. The analysis is often constructed as a series of worksheets; in the *Guidelines on reliability, maintainability and survivability of marine energy conversion systems* (Starling, 2009), an example worksheet is included, this is detailed in Figure 2.15. Depending on the project, different criteria can be included in the FMEA analysis and this table provides one example.

FMECA are referenced throughout the literature and guidance (Bittencourt, 2007; Brown, 2009; Carbon Trust, 2005; Starling, 2009; Wolfram, 2006). Wolfram et al suggest a particularly effective use for this approach when taking existing component reliability data from another sector, and analysing the new and different failure modes possible in a new (marine) environment.

Guidance published by DNV for the certification of tidal turbines and arrays presents an adapted approach, Failure Mode Identification and Risk Ranking (FMIRR) (Det Norske Veritas, 2015). This process involves the development of a certification plan to control the identified high risks. The guidance provides some useful look up tables with

typical failure rates for each probability class (Figure 2.16a) and example descriptions of each consequence class based on the impact of a failure on safety, environment, operation, assets and project finance (Figure 2.16b). These look up tables are detailed on page 61. It should be noted that these are examples and the consequence class will be project dependant. Different consequence classes are required depending upon whether the risk matrix being developed is for a project involving an array of turbines or a single turbine. In each case the boundaries of the assessment must be clearly defined so that appropriate consequences can be specified. For example a cost consequence class 5 for a turbine array project is defined at £100m whereas for a single turbine project this consequence class would be £10m. Once the probability and consequence classes are defined a 'Risk matrix' is used to define each item as Low, Medium or High risk. Mitigation actions are then required to reduce any Medium or High risks to Low.

A common criticism of the FMEA approach is its subjectivity. Look up tables such as those published by DNV detailed in Figure 2.16 should help limit this subjectivity. However, to create a useful and accurate FMEA remains a labour intensive process, requiring an experienced, multi-disciplinary team to make correct judgements (Brown, 2009).

2.3.2.2 Reliability block diagrams

Also known as dependence diagrams (DDs); Reliability Block Diagrams (RBDs) are used to display a system's reliability diagrammatically, and to understand the contribution of sub-system or component reliability to the overall system reliability. A given system is broken down into logical blocks that represent sub-systems or components. These are joined in series or, if there is redundancy in the system, they are joined in parallel. Generally a RBD is used to represent the success of a specific function of the system; for multiple functions, each should have a separate RBD. Probabilistic success rates can be applied to each block and the success rate of the complete system can then be calculated. Several marine energy papers refer to RBDs (Carbon Trust, 2005; Thies & Johanning, 2010; Thies *et al.*, 2009, 2012c); an interesting case study of a generic WEC is conducted by Thies *et al.* (2009) and is detailed in Figure 2.17.

A RBD is a useful diagrammatic representation of a system, and provides a sound basis for understanding the impacts of component reliability on whole system reliability. The main drawback of a RBD remains the calculation of the total system reliability;

Class	Name	Description	Indicative annual failure rate (up to)	Reference
1	Very low	Negligible event frequency	1.00E-04	Accidental (event not failure)
2	Low	Event unlikely to occur	1.00E-03	Strength / ULS
3	Medium	Event rarely expected to occur	1.00E-02	Fatigue / FLS
4	High	One or several events expected to occur during the lifetime	1.00E-01	Operation low frequency
5	Very high	One or several events expected to occur during each year	1.00E+00	Operation high frequency

(a) Probability classes

Class	Description of consequence (impact on)				
	Safety	Environment	Operation	Assets	Cost (GBP)
1	Negligible injury or health effects	Negligible pollution or no effect on environment	Negligible effect on production (hours)	Negligible	1k
2	Minor injuries or health effects	Minor pollution / slight effect on environment (minimum disruption on marine life)	Partial loss of performance (retrieval not required outside maintenance interval)	Repairable within maintenance interval	10k
3	Moderate injuries and / or health effects	Limited level of pollution, manageable / moderate effect on environment	Loss of performance requiring retrieval outside maintenance interval	Repairable outside maintenance interval	100k
4	Significant injuries	Moderate pollution, with some clean-up costs / serious effect on environment	Total loss of production up to 1m (GBP)	Significant but repairable outside maintenance interval	1m
5	A fatality	Major pollution event, with significant clean-up costs / disastrous effects on the environment	Total loss of production greater than 1m (GBP)	Loss of device, major repair needed by removal of device and exchange of major components	10m

(b) Consequence classes

Figure 2.16: Example probability and consequence classes for defining the risk matrix used in a FMIRR as suggested by DNV (Det Norske Veritas, 2015).
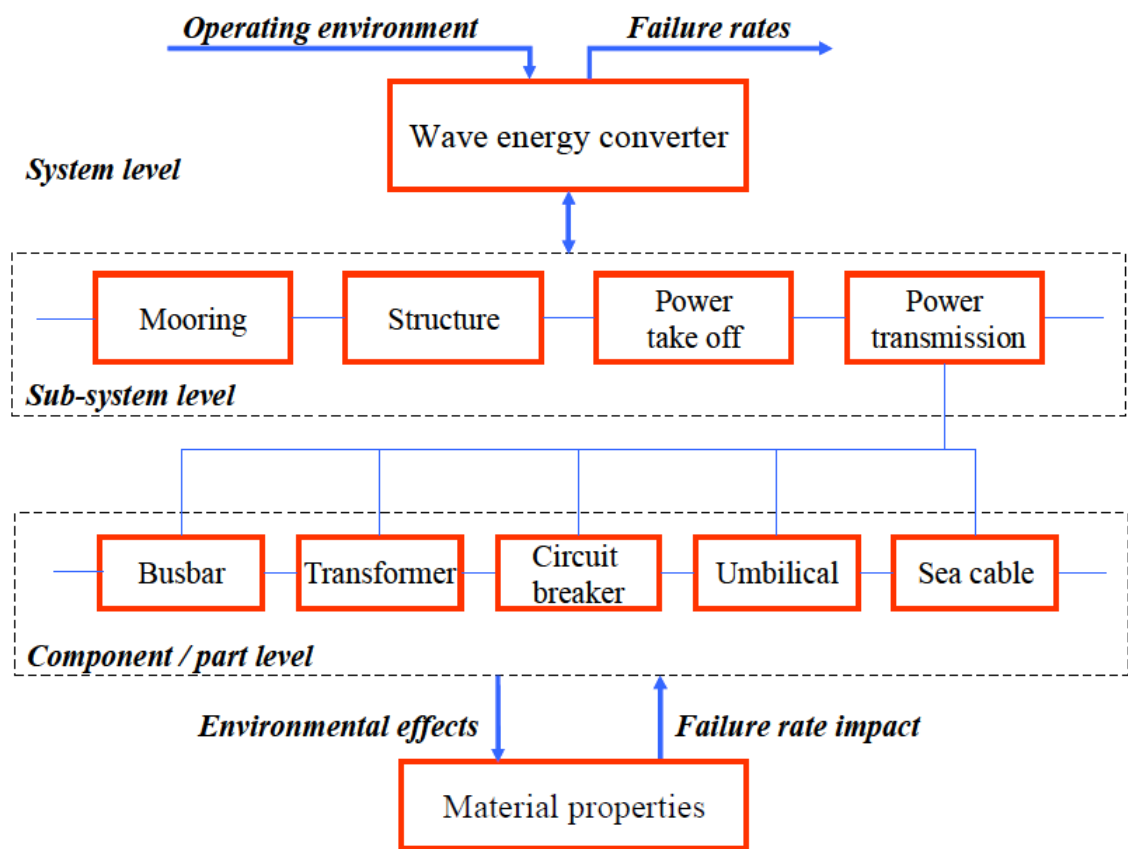
Figure 2.17: Generic Reliability block diagram for a wave energy converter (Thies *et al.*, 2009)

this will only ever be as thorough as the data for each of the sub-systems or components. Collecting accurate data to feed into a RBD remains a key challenge and will be addressed in Sections 2.3.2.4 and 2.3.2.5.

2.3.2.3 Fault tree analysis (FTA)

FTA is used to analyse a specific undesired event and to understand the contributing factors to that event. In this respect it is a top down approach as it starts with the 'top event' and attempts to define what factors could lead to it. Again, probabilities can be applied to each event to enable a calculation of the probability of the top event occurring, and to understand the significance of the different contributing events. References to FTA can also be found in the literature (Brown, 2009; Carbon Trust, 2005; Thies *et al.*, 2009).

A FTA is helpful to understand a system's resilience to a specific fault however it will not identify all possible faults. Again, its weakness lies in the accuracy of the data that informs the analysis.

The key difference between a FTA and a RBD is that a FTA focuses on failure events, whilst a RBD focuses on success events. In many situations however, a FTA can be converted into a RBD and vice-versa.

2.3.2.4 Use of existing data

The accuracy of the data that is fed into the selected analysis method is critical. One of the issues with an emerging technology like wave energy is that there is a lack of component data to inform these processes. There is however, abundant data from other fields that can be used to inform component reliability but it must be used with caution, as the operating environment will be significantly different.

One approach for dealing with this is discussed by Wolfram (2006) and is taken from the US department of Defence (1991). The approach takes the existing failure rate (the base rate) λ_B and multiplies it by a series of influence factors π_i to account for the altered operating environment to calculate a new predicted failure rate λ_P. This is further discussed in (Johanning *et al.*, 2010), where Equation 2.4 is detailed and typical influence factors are given:

$$\lambda_P = \lambda_B . \pi_Q . \pi_E . \pi_A ... \tag{2.4}$$

Where:

λ_P =predicted failure rate

λ_B =baseline failure rate

π_Q =quality factor

π_E =environmental factor

π_A =application stress factor

This approach will allow the calculation of an informed starting estimate for the failure rate of a given component, which can then be refined as necessary. The final results will obviously be dependent on the accuracy of the influence factors used.

Many different approaches can be used to refine an estimate, from further analytical methods, to physical testing. The following section will detail a statistical approach that can be used to update an initial probability distribution.

2.3.2.5 Statistical approaches

Different statistical approaches inform the reliability estimation techniques already discussed. There are a large number of different statistical approaches used across many different industries and it would be impossible to document them all here. There is one statistical approach of particular interest due to its contribution to the accuracy of the existing framework of reliability estimation techniques for WECs already discussed. Previously the weakness of some of the reliability approaches (such as FMEA and RBD) has been cited as the reliability of the input data for the analysis. Bayesian Inference is a statistical approach that allows an initial probability estimate to be updated when additional evidence becomes available. Both (Thies *et al.*, 2012c) and (Skjong & Torhaug, 1991) detail this method and provide good examples of its use in reliability estimation techniques. The case study provided in (Thies *et al.*, 2012c) uses the Bayesian updating methodology to refine a failure rate estimate for a marine power cable under dynamic loading, and is briefly described here to explain the method:

- Prior probability distribution: This is the initial probability distribution for the anticipated failure rate. In this case it is established from the OREDA[1] database, which collects information from oil and gas production units. The failure rate of

---

[1] Offshore and onshore reliability data

a marine power cable on an oil or gas unit is a good starting point for the analysis but is unlikely to account for the loads a power cable will be subject to on a WEC so will need some refining.

- Likelihood probability distribution: This is a new data set that will provide further information to add to the prior distribution. Data used for the likelihood distribution could be collected from field trials or component testing; in this example it is modelled by a two-parameter Weibull distribution.

- Posterior distribution: Bayes' theorem is then used to calculate a more refined distribution, the posterior distribution. This is essentially an update of the prior distribution with the new information derived from the likelihood distribution.

Other statistical approaches can be used in reliability estimations techniques but this technique has been included due to the advantages the method offers with updating and refining a known data set with further evidence. This approach seems to lend itself particularly well to the WEC industry where established data from other offshore industries such as oil and gas can be used, but will need refining to allow for the altered operational and environmental conditions a WEC will be subject to.

2.3.2.6 Palmgren-Miner damage model (for fatigue)

The approaches that have been introduced so far are generic approaches that can be utilised for reliability estimation. The Palgrem-Miner damage model is more specific in nature but of particular interest to the work presented in this Thesis due to the fatigue loading of mooring systems from the loads induced by wave action on a floating WEC. It has been included in this chapter due to its particular relevance to the fatigue aspects of this work and its importance in informing the previous techniques. The method is used for estimating the accumulated damage caused to a system or component from fatigue loading.

The Palmgren-Miner rule, sometimes referred to as the Miner rule or the linear cumulative damage rule, specifically looks at fatigue accumulation and can be used to estimate the fatigue life of a component under variable amplitude loading (such as the loads imposed by a sea state). The rule relies on having an accurate S-N curve[1] for

---

[1]An S-N curve characterises the fatigue properties of a material or a component in terms of S (applied cyclic stress amplitude) against N (number of cycles to failure)

the component. S-N curves will be further explored in Chapter 4, in relation to the fatigue performance of a shackle. The Palmgren-Miner model states if failure occurs at N cycles for a given stress amplitude, cycling to n cycles at the same stress amplitude will cause relative damage D of:

$$D = \frac{n}{N} \qquad (2.5)$$

$D =$ Damage

$n =$ Number of stress cycles conducted at given stress amplitude

$N =$ Number of stress cycles to cause failure at given stress amplitude, obtained from the S-N curve for the given material or specimen.

When $D = 1$ complete failure occurs e.g. $n = N$.

This rule operates cumulatively over a series of different stress amplitudes. The cumulative damage can be summated from the above giving:

$$D = \Sigma \frac{n_1}{N_1} + \frac{n_2}{N_2} + \frac{n_3}{N_3} + \frac{n_4}{N_4}....etc \qquad (2.6)$$

Or to present this in a generic form, for k number of different stress ranges:

$$D = \Sigma_{i=1}^{k} \frac{n_i}{N_i} \qquad (2.7)$$

Incorporating the equation for N from the S-N curve e.g.

$$logN = log\bar{a} - mlog\Delta\sigma \qquad (2.8)$$

Where:

$N =$ Number of cycles to failure

$\bar{a} =$ Intercept of x axis

$m =$ Slope of the S-N curve

$\Delta\sigma =$ Stress range

Combining equations 2.7 and 2.8, and rearranging gives:

$$D = \frac{1}{a}\Sigma_{i=1}^{k} n_i (\Delta\sigma_i)^m \qquad (2.9)$$

Equation 2.9 provides us with an equation relating total damage D to the number of cycles n at a given stress range σ, with constants $\bar{a}$ and m taken from the S-N curve for a given component or system.

This rule allows a very simple approach to calculating the accumulated fatigue damage to a given component and hence a prediction of component lifetime that can be fed into the reliability approaches previously discussed. Some, such as Langer, have criticised the simplicity of the approach, arguing it would be more accurate to apply the approach separately to the two distinct phases of fatigue life; crack initiation and crack propagation (Schijve, 2009). Despite these misgivings, much of the guidance recommends the use of the Palmgren-Miner rule to estimate fatigue life, recommended in The Carbon Trust's *Guidelines for design and operation of wave energy converters* (Carbon Trust, 2005) and again in DNV's *DNV-OS-C101 Fatigue design of offshore steel structures* (Det Norske Veritas, 2011). As well as recommendations in the guidance, this approach has been widely adopted by those conducting research into the reliability of WECs (Guoyang & Torgeir, 1992; Jing *et al.*, 2012; Schijve, 2003; Skjong & Torhaug, 1991; Thies *et al.*, 2012b). It should be noted however, that large safety factors are still employed when designing for fatigue loads. Det Norske Veritas (2010a) suggests using a minimum safety factor of 5 in the fatigue design of position mooring systems. The use of such large safety factors suggests confidence in S-N curves and the use of the Palmgren-Miner rule to accurately calculate accumulated fatigue damage remains to be proven. S-N curves are also generated from an often scattered data set, this scatter burdens fatigue prediction and is another reason large safety factors are employed when designing for fatigue loads. These ideas will be further explored in Chapter 4.

A common method for distilling a complex load history into a more manageable data set to use for fatigue prediction with the Palmgren-Miner rule is the Rainflow Cycle Method. The application of this rule and its use with the Palmgren-Miner rule is detailed in (Thies *et al.*, 2012b).

2.3.2.7 Computer modelling

Once the environmental conditions are established, loads, stresses and strains within components and systems can be estimated by various software packages. This can be at a device scale (typically referred to as a *global* analysis), using packages such as

OrcaFlex$^{\circledR}$ or MOSES to analyse the dynamic response of a system to a set of given environmental conditions. Alternatively analysis can be conducted at component scale (typically referred to as a *local* analysis), looking specifically at component response to applied loadings and boundary conditions.

A detailed analysis of various software packages available is beyond the scope of this Thesis, but a brief review of some case studies and guidance provided in the literature will be discussed.

Global analysis

Typically global analysis involves the modelling of a whole system with external parameters imposed upon the model. Results will include loads and displacements of different components of the model. In the wave energy industry global analysis will be conducted using software such as OrcaFlex$^{\circledR}$ which is used to model the response of cables or mooring systems to a surface vessel. Mooring lines and cables are modelled using finite elements to create an idealised system of mass components (nodes) connected to visco-elastic elements, with each component having specified properties such as mass, stiffness and damping (Masciola *et al.*, 2011). Numerous sea states can then be imposed upon the model set up, with detailed results including motion and load information for each mooring line or cable.

An example of a global analysis is provided by Jing *et al.* (2012) where the fatigue life of mooring chains for a floating tidal current power station is assessed using MOSES software. The paper states MOSES software has the ability to combine the simulation of the system response to the given sea states and the stress analysis into one program. This analysis is conducted for a new mooring chain system and the paper concludes that the mooring system meets the design requirements. An interesting progression from this study would be to physically test the mooring system to verify the results from the simulation.

This approach is taken by Johanning *et al.* (2010), in a paper comparing tank tests results to an OrcaFlex$^{\circledR}$ model of the South West Mooring Test Facility to better understand peak tensions in the mooring limbs. This paper finds the data from the tank test and OrcaFlex$^{\circledR}$ model compare well, however a quantitative assessment is not detailed.

This work is further developed by Harnois *et al.* (2015) who seek to fully validate the numerical model with the tank test data. Various sea states are analysed and the study finds mooring loads are underestimated by the numerical model with maximum loads being 5-17% less than those observed in tank tests. In addition the paper finds a large discrepancy in mean drift, which is particularly poorly represented by the model in the highest wave frequencies.

In a similar approach the analysis of marine cable dynamics was conducted by Thies *et al.* (2012a) using an OrcaFlex® model. A detailed description of the model is provided in the paper. In this case, following an assessment of the wave resource, tank tests were conducted to determine device motions under the given wave climate. Motion results from these tank tests (in 6 degrees of freedom) informed a numerical model using OrcaFlex® that was used to calculate the loading in the cable and inform a reliability assessment.

Local analysis

Looking at a smaller scale, much of the guidance relates to component scale finite element analysis (FEA). The Finite Element Technique is a numerical method employing the use of 'elements' to subdivide larger components into more manageable sections (finite elements) for which an approximate solution can be calculated from the imposed load profile and boundary conditions. The solution calculated for the finite elements is accumulated over the component to provide a total component solution. Computer packages widely available perform the assessment based on parameters applied by the user (such as material properties and load profile), and can perform static, dynamic and fluid flow assessments. Various software packages are available for this, and it is often used as a critical part of component design. Modelling the component response to a given loading regime and boundary conditions allows the identification of high stress and critical areas in the component. The component design can then be altered to mitigate this. Looking to a different industry with many similarities to the wave energy industry, the design of ship structures utilises FEA throughout the development process as detailed in DNV guidelines for the fatigue assessment of ship structures (Det Norske Veritas, 2010b). The use of FEA is again recommended in the DNV guidelines for Fatigue design of offshore steel structures (Det Norske Veritas, 2011).

Looking specifically at WECs the *Guidelines on design and operation of wave energy converters* developed by the Carbon Trust with DNV bring together much of the relevant documentation in the field, and also detail the use of FEA for structural design criteria (Carbon Trust, 2005). This guidance however, highlights a weakness with FEA in analysing composite materials due to the complex relationships that occur between laminate lay ups within composite structures.

Although not specific to WECs, in 2006 HSE produced a report into floating production system (FPS) mooring integrity (Noble Denton Euorpe Limited, 2006); this has considerable information relevant to WEC mooring system integrity. The report details FEA as a key part of the assessment process throughout the life of the mooring components, from the strength assessment in connector design, to understanding the fracture mechanics of chains and connectors, and (towards the end of the mooring life) understanding the remaining strength of worn mooring components. FEA is used as a crucial tool throughout. Interestingly the report suggests that to fully understand the remaining strength of a worn mooring component, a break test may be cheaper and more reliable. Despite all the benefits of FEA, if minute cracks are present in the component and these aren't modelled in the FE model, then it will produce overly confident results of the strength of the mooring. The report suggests a simple break test of a sample of the mooring system is likely to be quicker and more accurate in this particular application.

It is likely that most device developers will use Finite Element Analysis (FEA) for some aspects of component validation, however examples of this are not widely published in the literature. A typical application of FEA in device development was conducted by Rhinefrank *et al.* (2006), when looking at a WEC using a novel permanent magnet linear generator. A 2D finite element model was created to analyse the linear generator and act as a 'sanity check' for initial analytical calculations. The model was then verified using laboratory tests and good correlation was found.

The above examples use generic software packages to analyse a specific system response however, some organisations choose to develop their own software packages to model aspects of their technology. Pelamis Wave Power did just that to model the power take off system for the well-known WEC Pelamis (Henderson, 2006). Although the focus of this software is not device reliability, it never-the-less shows a good application of software for device development. The computer simulation is verified in this paper,

first with a 1/7th scale test rig, and secondly with a full-scale test rig. Successfully verifying a computer simulation with physical testing allows it to be used with much more certainty for further work and makes it a more valuable tool in device development.

A further example software developed for a specific field is a piece of software developed by Tension Technology International called Fibre Rope Modeller (Banfield *et al.*, 2001; TTI, 2015). This software has particular relevance to the mooring work presented in this Thesis as it has been specifically designed to inform the development or selection of synthetic fibre rope. It has several modules including the calculation of load/extension properties of rope in addition to the prediction of cyclical load performance and splice behaviour. The focus for the reliability work presented on the Exeter Tether in Chapter 5 is physical testing (as detailed in Chapter 3 this is often more appropriate at such an early stage of development (Det Norske Veritas, 2008)). However further development work in the future may benefit from using this software to optimise the rope selected for the tether.

There clearly is a place for computer modelling in device and component development; amongst other things it provides an understanding of system responses, estimates of system strength and an understanding of failure mechanisms. Once a computer model has been adjusted to optimise the model outputs the next obvious step is to verify that model with physical tests.

2.3.3 Physical tests

It is widely accepted that lab based tests form a crucial part of device and component development. An eloquent explanation of the need for tank testing is provided by Mueller et al who argue there is still a significant need for tank testing models at a range of scales prior to full scale testing at sea: *"Tank testing is much faster and more repeatable than at sea and can emulate extreme events, at scale, again and again to allow understanding and mitigation of their effects with improved concepts and designs."*(Mueller & Wallace, 2008). In a similar vein, the laboratory test approach is equally supported by Salter who regards lab tests of components and sub-assemblies as the most economical way to develop a WEC: *"The cheapest and quickest way to achieve reliability for internal parts of a wave energy system is to use laboratory test rigs to develop and prove new sub-assemblies under conditions where controlled loads can be progressively increased under careful observation with comprehensive instrumentation"*

(Salter, 2003b). Laboratory physical testing has many benefits over sea trials; these will be discussed later in Section 2.3.4, when comparing different approaches.

Although not specific to WECs (Santhamma *et al.*, 1988) discuss the need for reliability testing and demonstration in terms of statistical confidence levels. To have a statistically confident result, tests must be repeated numerous times, and this is only possible in a perfectly controlled environment such as in a tank test or laboratory testing environment.

When listing research and development priorities for wave energy (Boud, 2002) is clear in the generic recommendations that *"Devices need to be tested at part and full scale in repeatable and predictable environments"*. It is also suggested that independent test facilities should be developed and shared between device developers, perhaps even providing a level of certification for components or devices. It is these kinds of recommendations that may have led to the launch of MARINET[1] in 2011 (MARINET, 2013). The MARINET network is a consortium of research centres including universities, government agencies and industry, mostly from Europe, that offer a range of research facilities to device developers. At the time of writing there are 45 different facility offers from the network aimed at supporting the development of wave energy, tidal energy, offshore wind, environmental data and cross-cutting areas like power take off. Facilities for testing at different scales are available, from component scale tests to tank tests and sea trials.

There is now a large number and variety of test facilities, and a wealth of literature to draw from detailing different testing conducted. A selection of different facilities from the literature will be discussed below.

2.3.3.1 Component tests

As highlighted in Section 2.2.2 the Horizon 2020 Work Programme (European Commission, 2015) specifically addresses failure at a component level as a key priority. Various test facilities have been set up to conduct research at a component level. The development of the Pelamis wave energy converter has been widely documented, and the stepped approach from simulation (as discussed previously) through component testing to scale model trials is a sound basis for any device development; in the words of Ross Henderson, Technical Director, a staged development is used to *"maximise learning and*

---

[1]Marine Renewables Infrastructure Network: www.fp7-marinet.eu

minimise risk" Henderson (2006). In the case of Pelamis, developers chose to design specific component test rigs. One such rig was developed to test a full scale joint system and another built to verify and optimise the operation and control of a scaled hydraulic PTO system. A similar approach was taken at Oregan State University during the development of a permanent magnet linear generator buoy. Here a reciprocating device was used to simulate the motion of waves and test the linear generator performance (Rhinefrank *et al.*, 2006). Another PTO testing facility has been developed recently by the National Renewable Energy Centre (NAREC) in the form of the Nautilus test rig which has a 3MW shaft input power rotary test system, for the evaluation of PTOs. This system will allow for the accelerated lifetime testing of systems and components of a PTO system, in a monitored environment to allow verification in advance of expensive offshore deployments. The effects of fatigue loads and extreme load cases on components such as gearboxes, generators, bearings etc. can be assessed at this facility (MARINET, 2013).

Two early papers looking specially at the verification of mooring systems presented in (Halliwell & Harris, 1988; Sundaravadivelu *et al.*, 1991), detail some early approaches for evaluating mooring response to different wave conditions by monitoring induced mooring forces. These were predominantly conducted in wave tanks; Heriot-Watt University and HR Wallingford wave tanks were used in (Halliwell & Harris, 1988), and a wave flume at the Ocean Engineering Centre in the Indian Institute of Technology was used in (Sundaravadivelu *et al.*, 1991). Since these early studies test facilities have become more advanced and component specific.

The Renewable Energy Group at the University of Exeter operates two component test facilities; one lab based and one sea based. The Dynamic Marine Component Test Facility (DMaC) has been designed to replicate motion characteristics experienced by WECs at a component level and verify component reliability. A description of the facility and typical research conducted is provided by Johanning *et al.* (2010); Thies & Johanning (2010) and Thies *et al.* (2012a) and further detailed in Chapter 3, Methodology, Page 139. A relevant example of research conducted on DMaC is an investigation of marine power cables, looking at mechanical loading regimes and fatigue damage (Thies *et al.*, 2012a). The second component test facility is the South West Mooring Test Facility (SWMTF) located in Falmouth bay. This takes component testing into the marine environment and provides a comprehensive monitoring system

to evaluate sea trials of mooring and anchor components. Further specification of the SWMTF is also provided in Chapter 3, Page 136.

Despite the obvious benefits, in two reports written in 2003 (Salter, 2003a,b) Salter discusses the weaknesses of laboratory based test rigs. He argues that despite being *"quick, safe and comfortable"*, they are not sufficient to fully test components that are *"exposed to the external influences of the chemistry and biology of sea water"* Salter (2003b). He proposes a floating test platform that could be utilised to test a variety of components under real sea conditions exposing them to corrosion, fatigue and bio-fouling and allowing the collection of statistically significant reliability data. At the time of writing such a platform has yet to be developed.

2.3.3.2 Scale model and tank tests

As well as testing at a component level, many device developers choose to test scale models of devices, in controlled tank tests, prior to sea deployments. The need for this is highlighted by Mueller & Wallace: *"At present, numerical modelling doesn't provide reliable enough results to prevent the need for tank testing, and there is still much merit in and need for physical modelling in tanks from 1/100 scale to 1/10 scale (perhaps even at 1/3 scale)"* (Mueller & Wallace, 2008). The many advantages of tank testing are also highlighted in Salter (2003a) and will be discussed in Section 2.3.4, Page 76. Again, Pelamis Wave Power demonstrates the effective use of scale modelling with their development of Pelamis which included several intermediate scale demonstrators. The development of the 1:7 scale machine is well documented in (Yemm, 2003) and having a working scale prototype was regarded as an extremely important step for the device development, and one that encouraged the continuation of financial support from investors.

The majority of device developers will use scale models at some point during the development process. It is interesting to note from the literature there is no consensus on a standard scale and various examples detail the broad range of scales utilised. The University of Lancaster during the development of a point-absorber WEC , the PS Frog Mk 5, utilised a 1:1000 scale model to evaluate the WEC performance and verify early simulations (McCabe *et al.*, 2006). During the development of the oscillating water column device, the LIMPET, 1:40 scale tests were conducted at tank trials in the Wavegen test facility in Inverness (Boake *et al.*, 2002). A further device, the

Wave Dragon, an overtopping WEC, initially used a 1:50 scale device in wave tanks in Aalborg University and University College Cork. Following this a 1:4.5 scale prototype was developed and tested in a Danish inlet that resembled a scale version of the North Sea Climate to match the prototype scale (Kofoed *et al.*, 2006). Further examples of scale models can be seen in Washio *et al.* (2000) and Rhinefrank *et al.* (2006).

2.3.3.3 Full scale prototypes

The ultimate step in device development is a full scale working prototype. In their *Guidelines on the design and operation of WECs*, the Carbon Trust discuss the difficulties of predicting the response of particular WEC geometries; this is where computer modelling and scale models can fall short. The guidance suggests that full scale measurements should always be used to support calculations and scale models. The guidance also highlights the importance of detailed instrumentation and data logging of the system response and environmental data when conducting full scale trials. This will ensure the trial results can be accurately utilised to fully understand the system performance (Carbon Trust, 2005). Although Salter (2003b) mostly focuses on the benefits of tank tests, he does concede that at the time of writing tank tests cannot reproduce the effects of currents and current-wave combinations. This has begun to be addressed by new testing facilities such as the FloWave TT Facility developed by The University of Edinburgh which combines both wave and current simulation for assessment of scale models (The University of Edinburgh, 2013). A further drawback of tank tests is the inability to replicate the corrosive effects of the marine environment and biofouling caused by the growth of marine organisms accumulating on a WEC structure, both of which require testing at sea to fully understand the severity of the processes and the impacts on components and devices. Both corrosion and biofouling are time dependant processes, and would therefore prove difficult to 'accelerate' in the way a lifetime loading regime can be accelerated under laboratory testing conditions.

Sea trial location can be selected to provide an appropriate wave environment for the level of development of a device; not all prototype devices will be installed directly into an extreme wave environment. As detailed in (Starling, 2009) sea testing can be conducted at a sheltered (nursery) site, a specific test site or at the proposed installation location. Over the last decade there has been considerable progress in creating suitable test sites to trial new and developing WECs. The UK in particular has seen much

progress in this area. In Scotland the development of the European Marine Energy Centre has created a network of wave and tidal test sites around Orkney. Incorporating both full scale and nursery sites, EMEC also provide a device verification service (Eurpoean Marine Energy Centre, 2013).

Cornwall has also been developing test sites. The Wave Hub, located 16km off the north coast of Cornwall, provides four grid connected test berths for WEC developers to trial devices (Wave Hub, 2013a). To complement the Wave Hub, the University of Exeter in collaboration with Falmouth Harbour Commissioners have developed a pre-consented nursery site, on the more sheltered south coast of Cornwall. Situated within Falmouth harbour, this is known as the FaB Test Site (Renewable Energy Research Group - University of Exeter, 2013b). Although not grid connected, this pre-consented site provides developers with a more protected site, with good access and existing monitoring systems, where early prototypes can be trialled.

All device developers will at some point trial a full scale prototype, although not all developers will be willing to share the results of these trials. At this point in the development process, many undetected issues with the system may become apparent for the first time, and developers are rarely prepared to publicise such things. Although limited, examples where papers have been published following sea trials include the sea trials conducted on the Mighty Whale (Washio *et al.*, 2000), a detailed overview of the initial findings from sea trials conducted on the full scale LIMPET (Boake *et al.*, 2002), and test results from sea trials on the Archimedes Wave Spring (AWS) permanent magnet generator (Polinder *et al.*, 2005).

Although a full scale working prototype is the ultimate way a device developer can test and prove a device, it has been recently suggested that the policy push for MW scale devices has been detrimental to the marine industry causing both the wave and tidal energy sectors to *'bypass a formative phase of technological development'* (MacGillivray *et al.*, 2015). This paper suggests the need for 'technology push' focused policy, supporting technology development and optimisation at an affordable scale, as opposed to incentivising up-scaling before the technology is ready.

2.3.4 Comparison of approaches

As demonstrated, there are many approaches used in the marine industry to verify components and devices and ensure they are fit for purpose, robust and reliable. Table

2.2 brings together what has been discussed and compares the different approaches and the pros and cons of each approach. It is clear that each of the different approaches informs the design process in a different way, and they can be thought of as a series of increasingly in depth assessments.

2.4 WEC sub-system selection

2.4.1 WEC sub-systems

Section 2.2, introduced definitions of reliability and the need for reliability in WEC development. This section will review the literature to identify particular sub-systems of WECs that require attention with regard to development and reliability.

Before going into detail about where sub-system research should be focused, it is useful to define the main components of a WEC. Although written in 1980, Hudson et al thoroughly defined the various components of a WEC in a review of the materials aspects of wave energy converters (Hudson *et al.*, 1980). Those main components are listed in the following, along with a short discussion on key areas of consideration for reliable system design:

- **Main hull:** The main body of a WEC. Generally device specific but similar design approaches within each WEC category. Reliability issues arising will also be device dependant; particularly in relation to materials employed. Reliability issues include fatigue from wave loading, extreme loading from storm states, corrosion and biofouling effects.

- **Mooring system:** This facilitates the station keeping of a WEC by keeping the floating body connected to the seabed. This is most relevant to nearshore and offshore WAB and OTD devices (non-floating devices will have foundations as opposed to moorings). Overall design requirements are device neutral with minor adjustments for a particular device / location. Key reliability issues include fatigue loading, extreme loading, corrosion and biofouling.

- **Primary power take-off (PTO):** The system converting wave energy to usable energy, often a combination of varied components. Device specific but again similar design requirements within WEC categories. Reliability issues arising will

77

Table 2.2: Comparing different development approaches

General approach	Examples	Positives	Negatives
Analytical	- FMECA - RBD - FTA	- Relatively cheap and quick to apply - Good starting point to assess design - Compare a range of design iterations on equal basis	- Simplifications required for methods can lead to inaccuracies - Only as accurate/reliable as input data - how to verify this? - Will not test against all loading regimes the sea will impose - Limited or no account of corrosion or biofouling
Computational	- FEA of components e.g. ANSYS. - FEA of mooring system e.g. ORCALFEX. - Bespoke simulation packages for generation.	- Relatively cheap and quick method to apply - Simulate a large range of operating conditions, not always possible in a tank / at sea - Extract detailed stress profile from components (including internally) - Alter component specification and quickly assess impacts - Compare a range of design iterations on equal basis - Test at component level and build up models to device level	- Can be limited in complexity of loading regimes, requiring a simplified profile which may lead to inaccuracies - Complex models can be computationally demanding and take time - Easily mis-used by under qualified staff, leading to poor results - May not test against all loading regimes the sea will impose - Limited or no account of corrosion or biofouling
Component testing	- Lab testing with generic equipment. - Lab testing with bespoke equipment.	- Emulate extreme events (e.g. one in 100 yr storm) - Repeatability to understand specific events - Statistical certainty due to repeatability - Instrumentation to monitor response - Observation / documentation (video / photo etc) - Compare different design iterations on equal basis	- Can be expensive, particularly if bespoke equipment required - Time consuming - May not test against all loading regimes the sea will impose - May not test crucial interactions between components - No account of corrosion or biofouling
Scale models & tank tests	- Lab testing - Tank testing	- Emulate extreme events (e.g. one in 100 yr storm) - Repeatability to understand specific events - Statistical certainty due to repeatability - Instrumentation - Observation / documentation (video / photo etc.) - For wave energy Froude scaling rules work well - Less public than at sea (mistakes aren't publicised) - Easy repairs to damaged equipment so testing can continue - Compare different design iterations on equal basis	- Quite expensive and time consuming - Some environmental factors neglected e.g. corrosion from salt water, marine growth - Certain geometries / motions may not scale accurately and lead to inaccurate results - May not test against all loading regimes the sea will impose - No account of corrosion or biofouling
At sea trails	- Sheltered site - Test site - Installation site	- Ultimate test of a device - Expose device to complex current wave combinations (can't model in tanks) - Understand impacts of biofouling - Understand impacts of corrosion	- Very expensive and time consuming - Cannot control environmental loads, so may not expose equipment to loads required to fully test - Cannot repeat particular events - limited statistical certainty - Due to above, cannot compare different design iterations on an equal basis. - Wave environment can be difficult to accurately monitor / record. - Limited weather windows makes deployment and repairs difficult - Very public, difficult to deal with problems privately

be those common to such systems in conventional application (such as fatigue), with the added concern of corrosion and biofouling to exposed components.

- **Hinges and bearings:** Generic components used throughout WEC design. Reliability issues arising from complex load paths created by variable sea states and sealing issues to prevent ingress of sea-water and retain lubrication. Limited maintenance access also restricts preventative maintenance and inspections. Corrosive environment also a concern.

- **Seals:** As above, generic component used in some WEC designs. Similar reliability considerations.

- **Valves and flap gates:** As above.

- **Generators and turbines:** Generators and turbines (often a sub-component of the PTO system) will be specific to the WEC device type and mode of operation. There will be some commonality within device types. Reliability issues similar to those found in conventional applications, with the additional concerns of complex load paths, corrosion and biofouling.

- **Flexible power cables:** Common across many device types, with particular reliability concerns around peak load mitigation, fatigue, corrosion and biofouling.

2.4.2   Review of guidance

Many of the roadmaps and government documents already discussed provide much guidance on where research efforts should be focused. This section will provide a brief review of the most recent guidance to establish a framework for sub-system selection in this research. Working chronologically, the Ove Arup report written in 2002 for the DTI lists key research recommended to develop the industry. Of these recommendations, those relating to component research are detailed below (DTI and OVE ARUP, 2002):

- Power conditioning modules

- Mooring studies (generic and device specific, looking at long term fatigue, connection points and standard connector designs)

- Turbine trials

- Development of hydraulic systems (based on water or other environmentally acceptable fluids)

- Development of hydraulic machines

- Standardized electrical connectors

- Storage of energy

The international community faces the same challenges as UK industry and shortly after the above report the DTI collaborated with the International Energy Agency, to focus on research and development priorities for the international marine industry (Boud, 2002). Although there are cross-overs between device types, this report attempts to classify research priorities based on WEC type.

The following details the recommended areas of research for each device type. Recommendations relating to policy/standards have been omitted.

Overtopping devices: Impoundment/superstructure material and construction, power take off (crossover with more established small scale hydro industry).

Oscillating water columns: Improvements to pneumatic PTOs.

Offshore devices: control systems, array configuration, mooring, electrical cabling, hydraulics.

Following these early reports, in 2007 the Carbon Trust commissioned Black and Veatch to assess and prioritise component technologies to focus research (Carbon Trust, 2007). They were asked to base their recommendations on three criteria: contribution to device costs, across many device types; potential for significant cost reduction; cost reduction unlikely to occur through other industries. A Venn diagram was used to consider the selection criteria and is detailed in Figure 2.18.

The report also published Figure 2.11a which was shown previously in Section 2.1.4, Page 46. This provides a useful breakdown of capital cost by major component for an average wave farm. It is interesting to consider these figures alongside the generality of components e.g. moorings account for 7% of device costs however appear in almost all

Wave Components

1 – Commonality

2 – Cost Reducibility

- Tethers/Anchors
- AC/DC/AC Converter
  ~15%

- Offshore Platform
  ~10%

- Floats & Device body
  30–40%

- Generator
  3–5%

- e.g. Concrete formwork

- e.g. Turbines

3 – Lack of Industry Cross-over
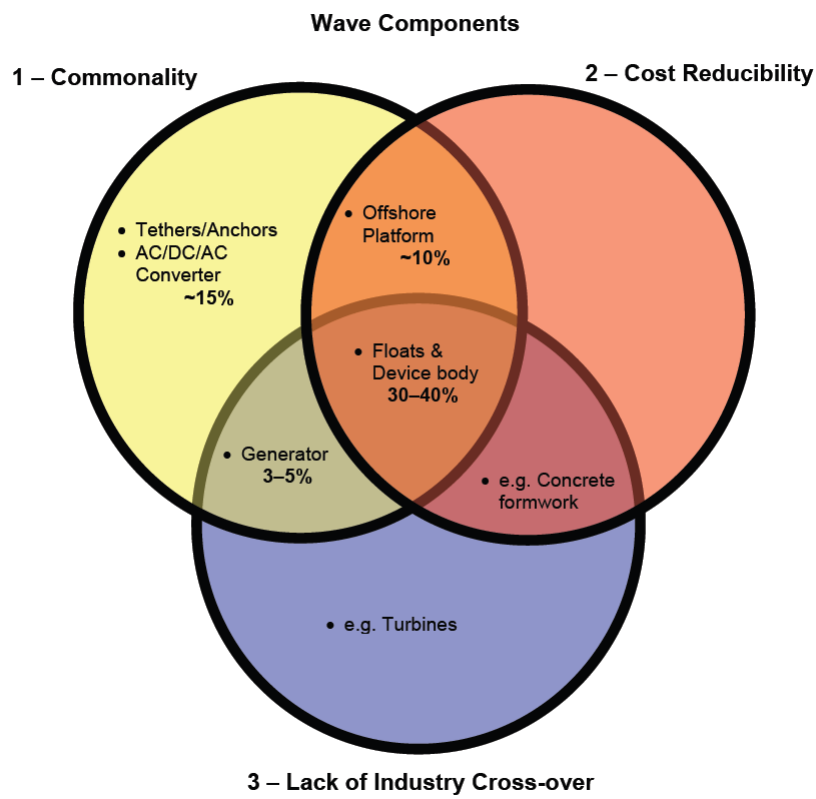
Figure 2.18: Wave component technology classifications (% figures reflect contribution to total cost) (Carbon Trust, 2007)

device types. Structural components on the other hand, account for 35% of the costs but are likely to be more device specific.

Following a thorough assessment of the selection criteria, the report identified three priority categories for both tidal and wave energy. The sub-systems listed as the three priority areas for wave energy were:

- Structural materials (including floats, device body, platforms)

- Powertrains (generator, AC/DC/AC power converter)

- Moorings (tethers, anchors, WEC connection)

Another different set of criteria was used to prioritise work streams in the 2010 report published when the UK Energy Research Centre worked with the Energy Technologies Institute (a UK consortium with industrial and government partners) to jointly write a Marine Energy Technology Roadmap (ETI and UKERC, 2010). The roadmap aimed to identify *"key technologies and deployment issues faced by the marine energy sector in the UK"* and to prioritise work streams to overcome these issues. Five key themes were identified:

- Device and system demonstrators

- Sub-components

- Guidelines and standards

- Tool development

- Infrastructure and enablers.

Within these themes, each activity was ranked based on a set of weighted assessment criteria, industry need and fit with the Energy Technology Institute's objectives. A priority category A, B or C was then calculated according to these criteria. Of the Sub-component theme, the following items were identified as Priority A:

- Energy conversion systems e.g. PTO

- Foundations and mooring systems

- New device and component development (step change)

- Offshore umbilical / wet HV connectors

It is also interesting to note that within the Tool Development theme of this work 'Reliability modelling tools' was listed as a 'priority A activity'.

In the same year as this report, DECC released a Marine Energy Action Plan (Department of Energy and Climate Change, UK, 2010) which also gave several recommendations for technology development. As well as addressing system demonstrators, the recommendations include some device components for particular attention. They are referred to as 'enabling components', and the action plan suggested reliability and survivability of projects as a whole can be advanced by developing these specific components. Examples given include foundations, moorings, power take off technology and wet-mateable connecters.

A more recent report is the Technology Innovation Needs Assessment (TINA) report, issued by the Low Carbon Innovation Coordination Group in 2012. This report reviewed the marine energy industry and provided recommendations for public sector funding prioritisation based on the value of, and need for, specific innovations. Various system sub-areas were reviewed against multiple criteria, including potential cost saving achievable, the value of meeting targets and the benefits of public sector investment. Full details of the categories and assessment process is detailed in the TINA report (Low Carbon Innovation Coordination Group, 2012).

In the context of this Thesis only the sub-system assessment is relevant. Within that category, the sub-area 'structure and prime mover' achieves the highest score, accounting for a high proportion of devices costs, with a good potential for cost savings from innovation both in terms of meeting emissions targets and business creation. 'Foundations and moorings' are rated medium, as although there is a large potential for % cost savings, the sub-area accounts for 10% of device costs so large % cost savings does not translate to high savings in £bn. 'Power take-off' despite having a lower potential % saving, has a higher monetary value in savings due to accounting for 20% of device costs and also the potential for business creation. Connections scores poorly in all categories of the review.

2.4.3 Synthesis of guidance

Following a review of the above reports, a table was generated summarising the purpose of each report and the sub-system research priority recommendations detailed in each report; this is shown in Figures 2.19 (a) and (b). Although the terminology in the table reflects that used in each individual report, recommendations that have similarities across reports are aligned along rows in the table. The sub-systems are highlighted to signify if they are device neutral, device specific or have both neutral and specific aspects. To compliment this table the information has been summarised in a chart detailed in Figure 2.20.

From this synthesis, three key component areas stand out:

- Power take off systems: Referred to using slightly different terminology across the reports, the PTO came up in every report as a priority area. Some aspects of PTO research (such as Wells turbine development for OWCs) will be device neutral, while other aspects will be more device specific.

- Mooring systems: Mooring systems were recommended as a priority in all six reports. Mooring systems are relatively device neutral; certain devices will however require specific mooring systems.

- Electrical connectors/cabling: Recommended in five of the six reports, wet mateable connectors were highlighted as a key recommendation. Out of all components, this is the most device neutral component considered, and is a necessary component for the majority of WECs.

Other sub-systems that came up in more than one report are detailed below:

- Hydraulic systems: Both the development of the system and the use of an alternative hydraulic fluid came up. This is only relevant to those devices that involve hydraulic components so was regarded as having both neutral and specific aspects.

- Impoundment / superstructure: The main hull of a WEC was listed in three reports as a recommendation; the device body is very device specific although materials research could have some generic applications in the marine environment.

- Device demonstrators: Recommended in two reports, this is inherently device specific.

2.4.4   Selected sub-system

This review of WEC sub-systems recommended by various governmental and professional bodies for further development is a useful guide to understanding where reliability research should be focused. Due to the numerous recommendations throughout the literature, and the broad nature of applicability, mooring systems will be the focus of reliability assessment for this Thesis.

To add further support to this, a more recent report by SI Ocean looking at the gaps and barriers to ocean energy (MacGillivray *et al.*, 2013) provides additional insight. Following consultation with key stakeholders including Government, supply chain, researchers, developers and funders, a technology prioritisation matrix was developed, assigning technologies an 'Attention Area' defining suitability for intervention (with A being the most suitable). A review was conducted analysing the level of engagement required from different stakeholders in order to progress development. The assessment conducted specifically on subsystems concluded foundations and moorings fitted into Priority Area A for both research and industry, and a high Priority Area B score for Government intervention. The findings from this report further support the need for research focused on mooring systems.

In addition to the guidance documents presented here, the review of different WEC device types under development in Section 2.1.2, also suggests moorings are an appropriate focus for this research. Primarily this is due to the fact that point absorber devices account for over 50% of devices under development and rely heavily on compliant and reliable mooring systems for their mode of operation. Other device types such as attenuators, overtopping devices and some oscillating water column designs also require reliable, compliant mooring systems. Due to this, mooring system reliability assessment has the potential to be applicable for a large proportion of the wave energy devices currently under development.

	Sustainable Energy Technology Route Maps		Status and Research and Development Priorities - Wave and Marine Current Energy	Key Marine Energy Component Technologies for Cost Reduction R&D	
Title	Sustainable Energy Technology Route Maps		Status and Research and Development Priorities - Wave and Marine Current Energy	Key Marine Energy Component Technologies for Cost Reduction R&D	
Date	2002		2002	2007	
Organisation	Ove Arup on behalf of DTI		Future Energy Solutions on behalf of DTI and IEA	Black & Veatch on behalf of Carbon Trust	
Purpose	Review status and define rationale / priorities for DTI programme		To review the status of technology and address R&D priorities	Assessment and prioritisation of component technologies for cost reduction	
Component specific recommendations	Turbine trials (testing various turbines)		Power take off (OTD)	Powertrain	Electrical generator. AC/DC/AC power converter.
	Mooring studies	Generic & device specific. Long term fatigue. Connection points. Standard connector designs.	Moorings (Offshore)	Moorings	Mooring tethers. Anchors. WEC connection.
	Standardised electrical connectors		Electrical cabling (Offshore)		
	Hydraulics	Hydraulic systems (based on water or alternative). Development of hydraulics machines.	Hydraulics (Offshore)		
			Impoundment / superstructure (OTD)	Structural materials	Floats and device body. Offshore substation platform.
	Power conditioning modules				
	Storage of energy				
			Control system (Offshore)		
			Array configuration (Offshore)		
			Improvements to pneumatic PTOs (OWC)		
Notes			Component recommendations are listed by device type, included in (brackets) following each component.		

(a)

Title	Marine energy technology roadmap	Marine Energy Action Plan	Technology Innovation Needs Assessment
Date	2010	2010	2012
Organisation	UK ERC & ETI	DECC	Low Carbon Innovation Group
Purpose	To detail marine technology development and identify priorities for ETI project intervention	To set out vision to 2030, outlining actions required from private and public sectors to facilitate development/deployment	To identify and value the innovation priorities of marine energy industry to inform public sector investment.
Component specific recommendations	Energy conversion systems e.g. PTO	Power take off	Power take off
	Foundations and mooring systems	Foundations and moorings	Foundations and moorings
	Offshore umbilical / wet HV connectors	Wet mateable connectors	Connection
			Structure and prime mover
	New device and component development (step change)	Device and system demonstrators	
Notes	The above are all priority A; this means there is an industry need and objectives are aligned with ETI purpose. Priorities B and C not included.	Listed components are given in the action plan as examples of 'enabling components' recommended for technology development.	All above components listed in report and reviewed against various criteria - board categories listed.

(b)

Figure 2.19: Literature review, summary of report recommendations for sub-system research priorities. Priorities obtained from six reports and grouped in rows with similar recommendations. Colour coding: Green denotes device neutral sub-systems; yellow denotes sub-systems with neutral and specific aspects; red denotes device specific sub-systems. (a) Summarises DTI and Ove Arup (2002), Boud (2002) and Carbon Trust (2007); (b) summarises Mueller & Jeffrey (2008), Department of Energy and Climate Change, UK (2010) and Low Carbon Innovation Coordination Group (2012).
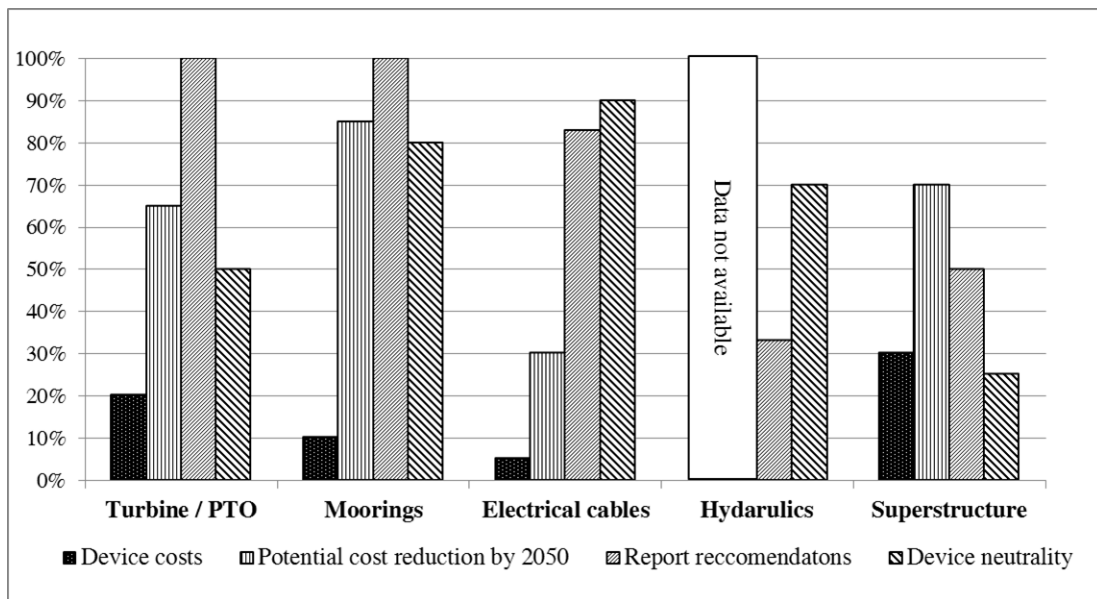
Figure 2.20: Graphical summary of recommendations for sub-system research priorities. Priorities summarised from six reports (Boud, 2002; Carbon Trust, 2007; Department of Energy and Climate Change, UK, 2010; DTI and Ove Arup, 2002; Low Carbon Innovation Coordination Group, 2012; Mueller & Jeffrey, 2008). Report recommendation figure based on % of the reports recommending sub-component research; device neutrality figure based on the perceived device neutrality of a subsystem where 100% is completely device neutral and 0% is completely device specific.

2.5 Mooring systems

2.5.1 Overview of a mooring system

Mooring systems are a critical part of a WEC device, ensuring the system remains safely on location throughout a deployment. An excellent review of mooring system requirements and options is provided by Harris *et al.* (2004) and a further review conducted through the DTOcean project by Weller *et al.* (2014b) also details options for mooring and foundation technologies for marine renewable devices. The following draws mainly on these reviews to discuss the most relevant points for this research.

The primary requirement of a mooring system is the station keeping of a floating body; to achieve this, the system components must have adequate strength to withstand the loads and the environmental effects of the operating environment. This includes the effects of extreme storm loads and fatigue cycling of normal operating loads, as well as corrosion and bio-fouling occurring from the marine environment. Once this primary purpose has been met, secondary requirements should be considered, such as the excursion of the device; this must be limited to protect electrical cables and avoid contact with adjacent devices. The mooring system should also be designed to reduce peak loads on the device and anchor points by introducing compliance into the system and to cope with the changing operational environment such as tidal variation. Further requirements include PTO interaction, redundancy options, ease of inspection and maintenance, design life (Harris *et al.* (2004) states up to 30 years) and, importantly, cost effectiveness. This is not an exhaustive list of considerations for mooring design but presents a picture of the complexities involved in the design process.

Although a mooring system design will be specific to a particular device and location, the components of a mooring system are generic. The primary mooring components are:

Mooring line
Mooring line options include chain, wire rope, synthetic rope or a combination of these.

Anchor
Anchor options include gravity anchor, drag-embedment anchor, driven pile/suction anchor, vertical load anchor or a drilled and grouted anchor.

Secondary components
As well as the primary components of a mooring line detailed above, connecting com-

ponents such as shackles and swivels may be used, as well as floats or weights to provide buoyancy to certain parts of the mooring if required (Harris *et al.*, 2004; Hudson *et al.*, 1980). Connecting shackles will be used to connect different sections of a mooring system together for example to connect a riser chain to a ground chain or a ground chain to an anchor. Swivels are introduced into a mooring system to avoid torsion. Floats will be utilised to give buoyancy to certain parts of the mooring line in order to achieve specific multi-catenary mooring configurations, such as a catenary with a lazy wave configuration.

The price per m of mooring line is closely associated with the specified minimum breaking load (MBL) as evidenced by Harris *et al.* (2004) in Figure 2.21. When designing a mooring system it is therefore important to ensure components are specified to survive the mooring loads but not over specified, as this will lead to unnecessary cost and unnecessary weight. This careful balance is critical to the investigation into a standard mooring component presented in Chapter 4.

Much of the evolution of mooring design has come from the offshore oil and gas industries. WECs however, introduce a different requirement to these industries in that many devices, particularly WABs, are located in areas of high energy density and are specifically designed to oscillate with incoming waves. Harris *et al.* (2004) introduce various mooring configurations and discuss their suitability to WEC applications. Weller *et al.* (2014b) provide a useful schematic detailing various configuration options (detailed in Figure 2.22) and a useful summary table listing advantages and disadvantages of each (Table 2.3).

The choice of a mooring system for any particular project will be dependant on many factors. The load case for a specific device in a particular location will determine the strength requirements, and conventionally this will in turn dictate the compliance of the main mooring system components. Compliance can be introduced into a system through system architecture (such as through a multi-catenary mooring system) or through mooring components with high extension properties. Weller *et al.* (2014b) provide a summary of the material properties of common mooring components and show that although steel has high strength (2600MPa) it has very low compliance (2% extension at yield point). In contrast polyester has a strength of 1130MPa but
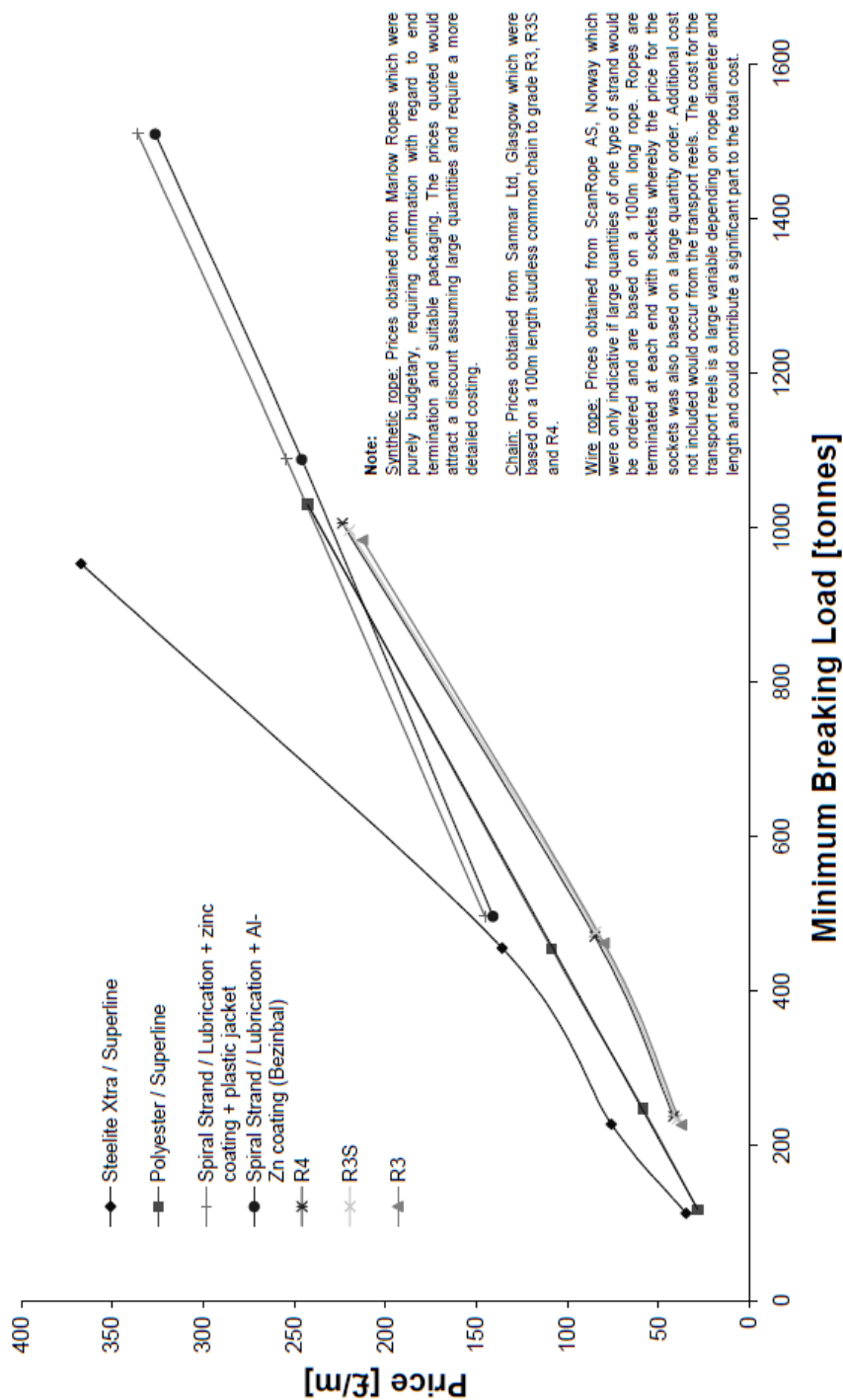
Figure 2.21: £/m of standard mooring materials in relation to MBL as detailed by Harris *et al.* (2004).

Table 2.3: The advantages and disadvantages of common mooring arrangements taken from (Weller *et al.*, 2014b). Schematic detailing each arrangement detailed in Figure 2.22.

Type	Configuration	Advantages	Disadvantages
Taut	Single line	1) Can provide a direct link between the floating part and PTO system 2) Few components (cost and reliability implications)	1) No redundancy is provided in the case of line failure 2) Not suitable for large tidal ranges (unless the floating part can be submerged) 3) Anchors and foundations that can be loaded vertically are required
	Multiple lines	1) Redundancy is provided 2) Allows the specification of lower capacity components than a single taut line system as tensions are shared 3) Mooring system footprint is usually smaller than for catenary systems 4) Horizontal restoring forces tend to be higher than for catenary systems	1) A significant tidal range may necessitate a large mooring footprint (unless the floating part can be submerged) 2) Anchors and foundations that can be loaded vertically are required 3) More components (cost and reliability implications)
Catenary	Single line	1) The compliance that is provided the by mooring geometry may mean lower peak loads than a taught system 2) Suitable for large tidal range sites 3) A wider range of anchor and foundation options are suitable 4) Few components (cost and reliability implications)	1) No redundancy is provided in the case of line failure 2) The floating part of the device may be capable of large horizontal motions which could have clearance implications for device arrays
	Multiple lines	1) Redundancy is provided 2) Allows the specification of lower capacity components than a single taut line system as tensions are shared	1) More components (cost and reliability implications) 2) Risk of line entanglement with adjacent devices in arrays
	With surface buoy	1) Horizontal peak loads lower than normal catenary and taut-mooring systems	1) More components (cost and reliability implications) 2) Surface buoy will be subjected to wind and current loading
	Lazy-wave	1) Horizontal peak loads lower than normal catenary and taut-mooring systems	1) More components (cost and reliability implications) 2) Surface buoy will be subjected to wind and current loading
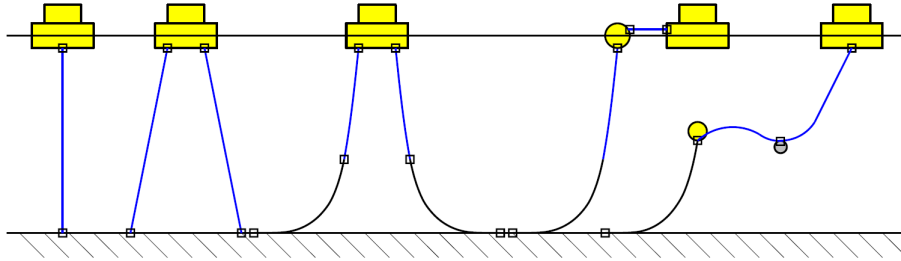
Figure 2.22: Schematic of mooring arrangements for marine renewable energy (MRE) devices taken from Weller *et al.* (2014b). From left: Taut-moored system, single line; taut-moored system, multiple lines; simple catenary system; catenary system with surface buoy; lazy-wave system with subsea floater and sinker. Options for using a combination of synthetic rope (blue lines) and chains (black lines) are highlighted.

will extend by 12% before failing (rope does not show a clear yield point to enable a direct comparison to the steel extension). The tensile strength value of 2600MPa assigned to steel in this paper seems high and although some particular grade steels may achieve this strength, a general tensile strength figure for steel would be much lower. For comparison, the tensile strength of a high tensile steel alloy (Type 4340) is still considerably lower than this figure at 1480 MPa (Young & Budynas, 2002). However, the important point remains that both the ultimate tensile strength and compliance of the specified mooring material are very important factors in mooring specification, and it is necessary to strike the correct balance in these material properties.

The choice of mooring arrangement will also have an impact on the power-take-off (PTO) of a wave energy device. An interesting paper (Vicente *et al.*, 2011) seeks to numerically quantify the effects a given mooring arrangement can have on the power absorbed by a floating point absorber WEC device, reviewing the differences between a single mooring line and a mooring line with a submerged floater. For the single mooring line, power absorbed was found to be linearly related to the mooring parameters investigated, with a negative correlation between average power and both distance from the device to anchor point and cable submerged weight, over a range of depths. The relationships for the mooring line with submerged floater were more complex and it should be noted that the results are only presented for regular waves with the authors suggesting a further analysis using irregular waves would be beneficial.

Further mooring considerations include system costs and Johanning & Smith (2009) provide a useful overview of relative costs of different mooring configurations. Mooring footprint is another consideration and will become more critical as the industry moves from single prototype devices to farms of devices, with designers attempting to minimise mooring footprint spread. Finally, the weight of different mooring options is a significant consideration, which not only affects the system dynamics but will dictate the deployment strategy for each system.

2.5.2 Mooring system reliability considerations

To understand the reliability issues affecting mooring systems, a list of key factors that control the life of a mooring rope or chain as detailed in Hudson *et al.* (1980) are replicated below. The significance of these factors will differ with regard to the mooring type selected:

- *"Effects of prolonged steady forces (mooring force)*

- *Effects of snatch forces (due to wave motion)*

- *Fatigue cycling*

- *Environmental attack: corrosion, stress corrosion, corrosion fatigue, fish bite, marine animal attack, UV degradation*

- *Abrasive wear*

- *Damage tolerance."*

Currently, there is limited data available on the reliability of mooring systems for WECs. Developers regard information on reliability of devices or components as a competitive advantage and as discussed in Section 2.3.2 they are not forthcoming in sharing this information. In an attempt to address this limited information, Thies *et al.* (2013b) highlight reliability issues typical for specific WEC components across a range of device types within the wave energy sector.

No comprehensive database of failures is recorded, but occasional cases of failures are discussed by developers or in the news. One such mooring incident is reported by (Christensen *et al.*, 2005) when discussing the development of The Wave Dragon wave

energy device (described in Section 2.1.3). During a severe storm the main mooring connection is reported to have broken resulting in the device stranding close to a beach nearby. The mooring failure is reported to have occurred due to a force transducer in the mooring system failing below the specified break-load. This failure is also reported by (Thies *et al.*, 2013b).

In addition, a news article referring to Mk3PC, the Oceanlinx wave enregy system, reported the device, located 150m offshore, broke free of its moorings. Limited details are provided in the article however it does state that the unit had *"more than double the required mooring lines in place to ensure its safe operation"* before adding there had been historical issues with the device mooring system (although the company felt these issues had been addressed) (Arnold, 2010).

These reports suggest that mooring failures are occurring in the wave energy industry even if they are rarely publicised. The more established offshore oil and gas industries have built up a detailed picture of reliability issues for moored floating production systems (FPS). Having many more years' experience and numerous operators, the wealth of knowledge on mooring failures is considerable (Bureau of Ocean Energy Management, 2011; Choi *et al.*, 2006; Gallagher & Ku, 2013; Kvitrud, 2014; Low & Cheung, 2012; Ma *et al.*, 2013; Syvertsen, 1997; Washington *et al.*, 2014). These reports suggest that failures can occur in all parts of a mooring system, including chains, shackles and ropes. As discussed previously, there are some significant differences between the requirements of a mooring system for a WEC, however, reviewing the offshore oil and gas literature will provide a good baseline understanding of the key reliability issues.

A full review of all these publications is out of the scope of this literature review, but some relevant publications will be discussed. The UK Health and Safety Executive (HSE) published a thorough review of mooring system integrity for FPS (Noble Denton Euorpe Limited, 2006) which covered data on North Sea Unit mooring line failure over the period 1980 - 2001. The HSE have statutory reporting requirements for incidents in the North Sea so these figures can be considered fairly accurate. Over the 1980 - 2001 period the report quotes one failure for every 5.4 operating years or a failure rate of 0.186 per unit operating year. This failure rate seems high however an 'incident' is defined as *"Problems with anchor/anchor lines, mooring devices, winching equipment*

or fairleads (e.g. anchor dragging, breaking of mooring lines, loss of anchors(s), winch failures.)", which is a broad definition, likely to capture many incidents.

A significantly reduced figure of failure rate is given by Ma *et al.* (2013) in a report which reviews incidents between 2001-2011. The annual probability of a mooring system failure here is estimated as 3.0×10^{-3}. However, there are some significant differences in the definition of failure. Namely *"Failure is defined as any incident involving (A) breakage of 2 or more lines, or (B) riser damage. With this definition, an incident would not be counted as a failure if there is only a single break"*. In addition to this alternative definition of failure, the report is not specific in its scope, though it appears to cover failures across the world. It therefore cannot be assumed the same compulsory reporting requirements apply globally as they do for the HSE discussed in the North Sea report above (Noble Denton Euorpe Limited, 2006). In summary, the failure rates cannot be considered directly comparable and an improvement in failures across the period certainly cannot be assumed.

The most recent failure rates to be published cover the Norwegian Continental shelf over the period 2010-2014 (Kvitrud, 2014). This report suggests that following the period 1996-2005 where a high number of cases were observed the industry reacted to reduce incidents but since 2010 there has been a gradual increase. Two failure rates are provided in this report:

- Single line failures: 9.2×10^{-3} per line year

- Double line failures: 1.2×10^{-3} per line year

It should be noted that these failure rates refer to per line year in comparison to the previous rates that were per operating unit year (Noble Denton Euorpe Limited, 2006) and per mooring system year, which is assumed to be the entire mooring system of a unit (Ma *et al.*, 2013). Again, the figures are therefore not directly comparable with the previous reports discussed.

Ma *et al.* (2013) provide a useful analysis of the different failures, reviewing both the mooring system component and length of deployment before the failure. Figure 2.23 details the range of component failures recorded. Data from (Kvitrud, 2014) broadly supports this distribution of component failure; of 15 incidents discussed 47% were chain failures, 20% steel wire failures and 13% connector failures. The major difference between the reports is an increase of fibre rope failures from 5 % to 20%, this may be
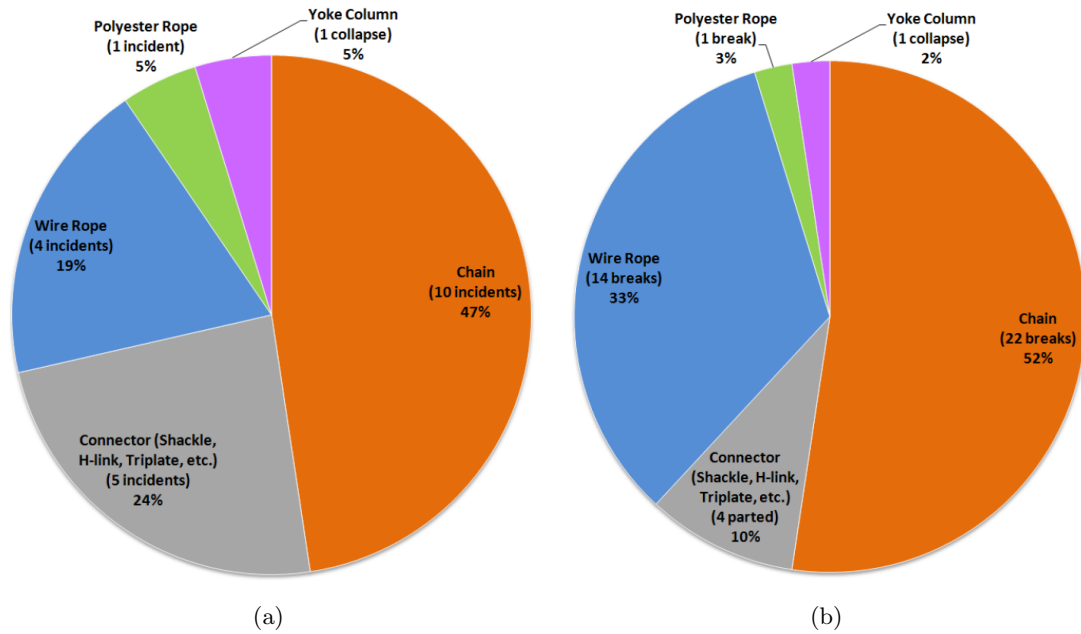
Figure 2.23: Distribution of mooring component failure type based on: (a) 21 incidents or (b) 42 breaks (Ma *et al.*, 2013).

interpreted as a reflection of the increased use of fibre ropes in mooring systems over the reporting periods of the two reports with Ma *et al.* (2013) covering 2001-2011 and Kvitrud (2014) covering 2010-2014. However, given the limited number of incidents making up these % values, strong conclusions cannot be drawn.

It might be assumed that many of the failures are due to equipment coming to the end of its safe operational life, however this is not the case. In the 2010-2014 review of anchor line failures on the Norwegian Continental Shelf (Kvitrud, 2014) 9 of the 15 failures occurred on equipment with just 0-5 years service life. This finding is supported by (Ma *et al.*, 2013) where 12 of the 21 failures discussed occurred within 1-5 years of deployment (6 of these being within the very first year of deployment).

These early life failures need to be further investigated and better understood by the industry. Kvitrud (2014) suggests that following many of the failures analysed in the report, material tests proved that the failed materials were actually within specification. Among other recommendations the report suggests that instead of just increasing the strength of lines, the number of lines should be evaluated (increased redundancy) due to these findings.

Others suggest fabrication of larger components is an issue with (Andreassen, 2012) suggesting the failure of a D-shackle after just three months installation was due to defective heat treatment causing temper embrittlement (a decrease in impact toughness). The affect of manufacturing on key material properties of mooring chain steel is further investigated by Cheng *et al.* (2015), who found that an increase in the tempering temperature of the steel led to a decrease in tensile strength (within the range tested from 560°C - 640°C).

There is common consensus from the reports that the majority of failures occur at connecting points, interfaces and discontinuities in the mooring systems and that further research in these areas is required. The need for frequent monitoring of moorings and improved design codes were also highlighted.

Given the sparse level of detail available regarding WEC mooring system reliability, findings from these reports provide some insight into potential issues. Although some of these topics will be specific to FPS, many of these findings can be related to mooring systems for WECs and prove a useful reference for this work. Key items of relevance for this Thesis include the concerns raised regarding connection points of mooring systems, which is of direct relevance to the work presented in Chapter 4, particularly the concerns raised regarding fatigue endurance (Noble Denton Euorpe Limited, 2006). This should also be considered with reference to the termination approach used for the novel mooring tether detailed in Chapter 5.

2.5.3 Relevant guidance in mooring system design

Much of the guidance applied to mooring system design for wave energy mooring systems has evolved through the offshore oil and gas industry. Paredes *et al.* (2013) discuss over 303 relevant standards to this industry with 37 devoted to anchoring, mooring and foundations. It is unnecessary to go into all these standards in detail so the most salient standards will be discussed here. Det Norske Veritas provide a whole range of guidance documents including the commonly used *DNV-OS-E301: Position mooring* (Det Norske Veritas, 2010a) and *DNV-RP-C203: Fatigue design of offshore steel structures* (Det Norske Veritas, 2011). In addition to the DNV publications, there was a specific B.S standard *BS 6349-6: Maritime structures - Design of inshore mooring and floating structures* (BSI, 1989) although this has now been withdrawn. In the U.S. different guidance has evolved, including *Recommended practice 2SK: Design and analysis of*

stationkeeping systems for floating structures(American Petroleum Institue, 2005) and *SP-2209-OCN Handbook for marine geotechnical engineering* (Thompson & Beasley, 2012).

Gradually guidance is catching up with the needs of the evolving offshore renewable energy sector with the publication of guidance documents such as *DNV-OS-J103: Design of floating wind turbine structures* (Det Norske Veritas, 2013b), which due to the scale and location of offshore floating wind turbines is perhaps more relevant to wave energy than guidance relating to FPS mooring systems. Despite the publication of DNV's *Certification of tidal and wave energy converters* (Det Norske Veritas, 2008) there is no specific guidance relating to mooring systems for either of these sectors. In an attempt to fill the gap in the literature the Carbon Trust (2005) provided a useful summary, *Guidelines on the design and operation of wave energy converters*, bringing together all the relevant documentation for wave energy converters, including mooring systems. This document however, does not meaningfully add to the guidance but just refers to existing documentation. The most useful contribution of this document is to introduce a new reduced consequence safety level *'Safety level low'* which the industry has been suggesting for some time. However no revised safety factors are provided for this new safety level, to reflect the reduced consequence of a failure. The document continues to reference existing guidance (Det Norske Veritas, 2010a) for safety factor specification. The result of this, argue Paredes *et al.* (2013), is that there is no relaxation in the design requirements and the need for specific guidance remains.

Some recent additions go the guidance have offered specific guidance on mooring system design that is more appropriate for offshore renewable energy installations. Bureau Veritas' *Classification of mooring system for permanent and mobile offshore units* (Bureau Veritas, 2015) provides detailed design guidance for mooring systems including design for fatigue, methods for calculating safety factors for mooring line components and minimum safety factor values. In addition to this, the IEC recently released a guidance documented aimed directly at marine energy, entitled *Marine energy - Wave, tidal and other water current converters - Part 10: Assessment of mooring system for marine energy converters* International Electrochemical Commision (2015). This document has many similarities with the DNV guidance document *DNV-OS-E301: Position mooring* (Det Norske Veritas, 2010a), however it adds an additional design consider-

ation, 'Serviceability limit state (SLS)' providing mooring guidance for the 'service mode' of the WEC for situations such as installation, commissioning and maintenance.

Weller *et al.* (2014b) provide a useful comparison between some of the guidance documents. The suggested safety factors in Det Norske Veritas (2010a) and American Petroleum Institue (2005) are compared in detail and for the specific case addressed it is concluded that the safety factor in the DNV guidance is 10% lower than the equivalent specified by the API guidance. A further comparison between these two documents is also conducted by Paredes *et al.* (2013) who also compare a third guidance document Standard Norge (2009), which focuses on the design requirements for Norwegian fish farms. This Norwegian document is utilised as it is argued that the characteristics of a fish farm are more closely related to a wave energy device than an offshore oil or gas platform (Paredes *et al.*, 2013). The paper does however concede that this is not entirely suitable due to the fact wave energy devices are often designed to resonate at particular wave periods, unlike fish farms. It is therefore argued that specific guidance documents are necessary for the WEC industry.

Having reviewed the range of guidance documents available, Det Norske Veritas (2010a) provides comprehensive guidance relating to mooring system design, and will be the main standard referred to during this work. Additional standards will be referenced when applicable.

2.5.4 New versus proven technology

Although not specific to mooring systems, DNV provide an overview of the differing requirements for the certification of new and proven technologies, which is a useful reference for the mooring component case studies presented in this Thesis. The approach is detailed in two DNV documents, DNV-OSS-312 *Certification of tidal and wave energy converters* (Det Norske Veritas, 2008), and DNVGL-SE-0163 *Certification of tidal turbines and arrays* (Det Norske Veritas, 2015). These documents both outline the framework for the certification approach that sets out the different requirements for new and proven technologies. With reference to DNV-OSS-312 (Det Norske Veritas, 2008), firstly, the definition of new and proven technology is detailed, taking into account both the *Application Area* and the *Technology Status*, as detailed in the matrix in Figure 2.24.

Application area	Technology status		
	1 **Proven**	**2** **Limited field history**	**3** **New or unproven**
1. Known	1	2	3
2. New	2	3	4

1: Proven technology
2 - 4: New technology

Figure 2.24: Technology assessment according to (Det Norske Veritas, 2008). The classifications detailed imply: *(1) No new technical uncertainties; (2) New technical uncertainties; (3) New technical challenges; (4) Demanding new technical challenges.*

The certification process is then detailed with reference to these definitions, as described by Figure 2.25. This process sets out the additional demands on the certification of any technology classified as 'new' (technology class 2 - 4) which require 'qualification' in addition to the traditional certification processes required for technology class 1.

2.5.5 Safety factors for mooring systems

Safety factors applied to mooring system designs are dependent on the limit state, the consequence class and the type of analysis conducted. These categories will now be defined as described in Det Norske Veritas (2010a):

2.5.5.1 Limit state

The limit state is a classification introduced into the standard to account for the specific type of failure that the safety factors applied to the mooring system design intend to avoid. The definitions are provided on Page 12 - 13 of the standard as follows:

Ultimate limit state (ULS): *"to ensure that the individual mooring lines have adequate strength to withstand the load effects imposed by extreme environmental actions."*
Accidental limit state (ALS): *"to ensure that the mooring system has adequate capacity to withstand the failure of one mooring line or one thruster or thruster system failure for unknown reasons."*
Fatigue limit state (FLS): *"to ensure that the individual mooring lines have adequate capacity to withstand cyclic loading."*
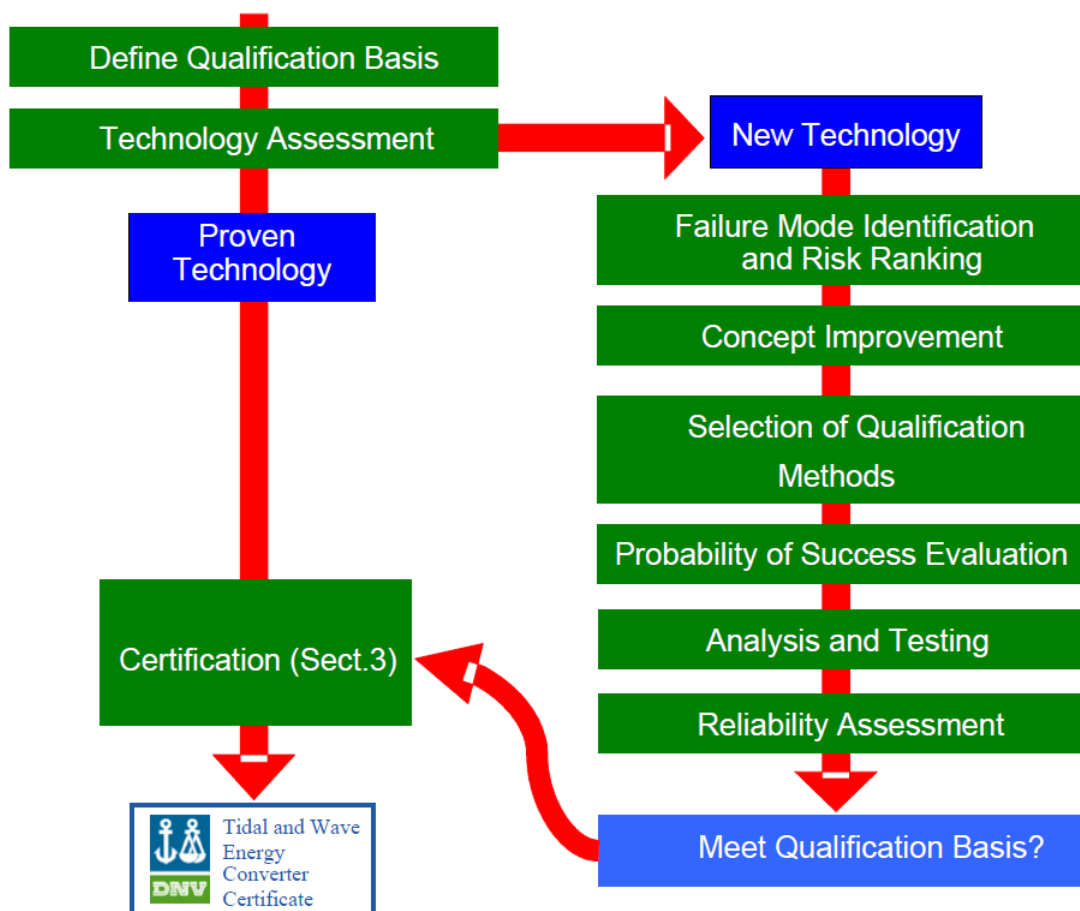
Figure 2.25: Certification approach for tidal and wave energy converters (Det Norske Veritas, 2008).

2.5.5.2   Consequence class

The consequence class classification is important as it accounts for the severity of the potential failure; the more severe the consequence, the higher the required safety factor applied to the design. The definitions of consequence class are provided on page 45 of the standard and are summarised below:

Class 1: The lower consequence class, relating to mooring failures <u>unlikely</u> to lead to severe consequences such as loss of life, major oil spill, collision or sinking.

Class 2: The higher consequence class, relating to mooring failures <u>likely</u> to lead to unacceptable consequences as detailed above.

2.5.5.3   Analysis type

The type of mooring line response analysis also affects the choice of safety factors applied, with a more in depth dynamic analysis requiring the use of lower safety factors within the standard. The analysis types are defined on page 41 of the standard:

Quasi-static analysis: *"to determine the mooring line response to mean and low frequency platform displacements"*. This type of analysis should take account of:

- *the displacement of the upper terminal point of the mooring line or yoke arms due to the unit's motions*

- *the weight and buoyancy of the mooring line components*

- *the elasticity of the mooring line components*

- *reaction and friction forces from the seabed."*

Dynamic analysis: *"mooring line response to wave-frequency displacement of the platform."* In addition to the considerations for a quasi-static analysis, a dynamic analysis must also account for:

- *"hydrodynamic drag forces acting on the mooring line components*

- *inertia forces acting on the mooring line components, including any buoyancy elements."*

2. LITERATURE REVIEW

2.5.5.4 Safety factors

With the above categories clearly defined, it is now possible to define the safety factors for both ULS and ALS based on the following design equation:

$$S_c - T_{c-mean}.\gamma_{mean} - T_{c-dyn}.\gamma_{dyn} \geq 0 \tag{2.10}$$

Where:

S_c = Characteristic strength of the mooring line segment

T_{c-mean} = Characteristic mean line tension, due to pretension and mean environmental actions in the environmental state.

T_{c-dyn} = Characteristic dynamic line tension induced by low-frequency and wave-frequency loads in the environmental state.

γ_{mean} and γ_{dyn} are specified in Tables 2.4 and 2.5.

The design equation and applied safety factors for the Fatigue Limit State are defined differently and the figures quoted here are based on mooring lines which are not regularly inspected ashore. The design equation is:

$$1 - d_c.\gamma_F \geq 0 \tag{2.11}$$

Where:

d_c = the characteristic fatigue damage accumulated as a result of cyclic loading during the design life time (different approaches are provided in the guidance for calculating this value).

γ_F = is the single safety factor for the fatigue limit state defined in Equation 2.12 by:

$$\gamma_F = 5 \ \ \text{when } d_F \leq 0.8 \tag{2.12}$$

$$\gamma_F = 5 + 3(\frac{d_F - 0.8}{0.2}) \ \ \text{when } d_F > 0.8 \tag{2.13}$$

Where:

d_F = adjacent fatigue damage ratio. This is the ratio between the characteristic fatigue damage d_c in two adjacent lines taken as the lesser damage divided by the greater damage. d_F cannot be larger than one.

Table 2.4: Safety factor ultimate limit state (Det Norske Veritas, 2010a).

Consequence Class	Type of analysis of wave freqency tension	Partial safety factor on mean tension (γ_{mean})	Partial safety factor on dynamic tension ($\gamma_{dynamic}$)
1	Dynamic	1.10	1.50
2	Dynamic	1.40	2.10
1	Quasi-static	1.70	
2	Quasi-static	2.50	

Table 2.5: Safety factor accidental limit state (Det Norske Veritas, 2010a).

Consequence Class	Type of analysis of wave freqency tension	Partial safety factor on mean tension (γ_{mean})	Partial safety factor on dynamic tension ($\gamma_{dynamic}$)
1	Dynamic	1.00	1.10
2	Dynamic	1.00	1.25
1	Quasi-static	1.10	
2	Quasi-static	1.35	

From Equations 2.12 and 2.13 the calculated safety factor applied to the design equation for fatigue limit state (Equation 2.11) can range from 5 - 8, which appears to be a very high figure. As discussed in Section 2.5.3 much of the guidance stems from the oil and gas industry where mooring failures have severe consequences. Given the reduced consequence of a mooring line failure in an unmanned WEC there is an argument for a further reduced consequence class with lower safety factors for WEC moorings. Chapter 4 seeks to investigate the use of safety factors in relation to a standard mooring component, a steel shackle. This case study is intended to explore the trade off for component specification in wave energy applications ensuring a component is fit for purpose whilst not imposing excessive safety factors onto a system which will lead to unnecessary costs.

2.5.6 Requirements for WEC mooring systems

As discussed in Section 2.5.1, mooring systems for wave energy converters have particular requirements that are different to the requirements of conventional mooring systems developed for the offshore oil and gas industries. The most significant difference lies in the compliance required by the mooring system to allow a wave energy device the motion required to generate energy without creating excessive mooring loads. This challenge is extensively described by (Gordelier *et al.*, 2015). It should be noted that not all wave energy devices require high compliance from the mooring system; systems such as the OTD Wavedragon do not require large device motion to generate energy. However, as discussed in Section 2.1.3 and detailed in Figure 2.3, Page 39, 53% of devices under development fall under the 'Point absorber' definition and 12% are of the 'Attenuator' type. Both these device types are very likely to require compliant mooring systems to operate. Development in this area will therefore be of interest to the majority of wave energy device developers.

Increased compliance in a mooring system is necessary to allow the motion required for energy generation and should also result in reduced mooring loads. This not only has a benefit to the survivability and long term reliability of a device but also reduces costs as discussed by Harris *et al.* (2004) where the cost of conventional mooring line material is shown to be directly proportional to minimum breaking load (MBL). A further potential benefit of reduced mooring loads lies in the down-rating of a mooring system to match these lower loads. The reduced weight of the revised mooring system

may allow for a reduction in the size and weight of the main hull of the floating body, which in turn may further reduce mooring loads. Thus there is a potential downwards design spiral of reducing loads and system costs, as discussed by Parish (2015). In addition to the potential for reduced capital costs, with lighter and more manageable mooring systems deployment costs should also be reduced due to revised vessel and crane sizes required to manage the reduced system (Davies *et al.*, 2014).

Compliance can be introduced into a mooring system through two main routes:

- System architecture: Floats and weights can be used to create a 'multi-catenary' mooring system as described in Section 2.5.1. Whilst increasing system compliance, this approach comes at the expense of the mooring footprint, which will be significantly increased to accommodate the more complex mooring architecture. Minimising the mooring footprint will be a key priority when developing wave farms if developers are to maximise devices deployed for a given area, so an increased mooring footprint is not desirable.

- Compliant mooring elements: Sections of mooring line with increased compliance can be introduced into the mooring system to increase the compliance of the overall system. It is this second option that will be further explored in Section 2.5.7.

2.5.7 Innovations in mooring systems

As discussed by Weller *et al.* (2014b) synthetic fibre ropes have many advantages over traditional steel chain, with larger extensions achievable (extension at break of Nylon is 20%), favourable cost and ease of manoeuvring. To support exploration in deeper waters, the offshore oil and gas industry have become aware of these potential advantages and begun replacing steel chain or wire rope with synthetic fibre rope (Bugg *et al.*, 2004). Despite some concerns on the fatigue performance of synthetic ropes, early research by Banfield *et al.* (1999) concluded polyester ropes are suitable for deepwater moorings for lifetimes of 20 years with fatigue performance *'at least as good as'* spiral strand steel wire rope. Polyester ropes have now been widely used in offshore platforms for over 15 years (Davies *et al.*, 2014).
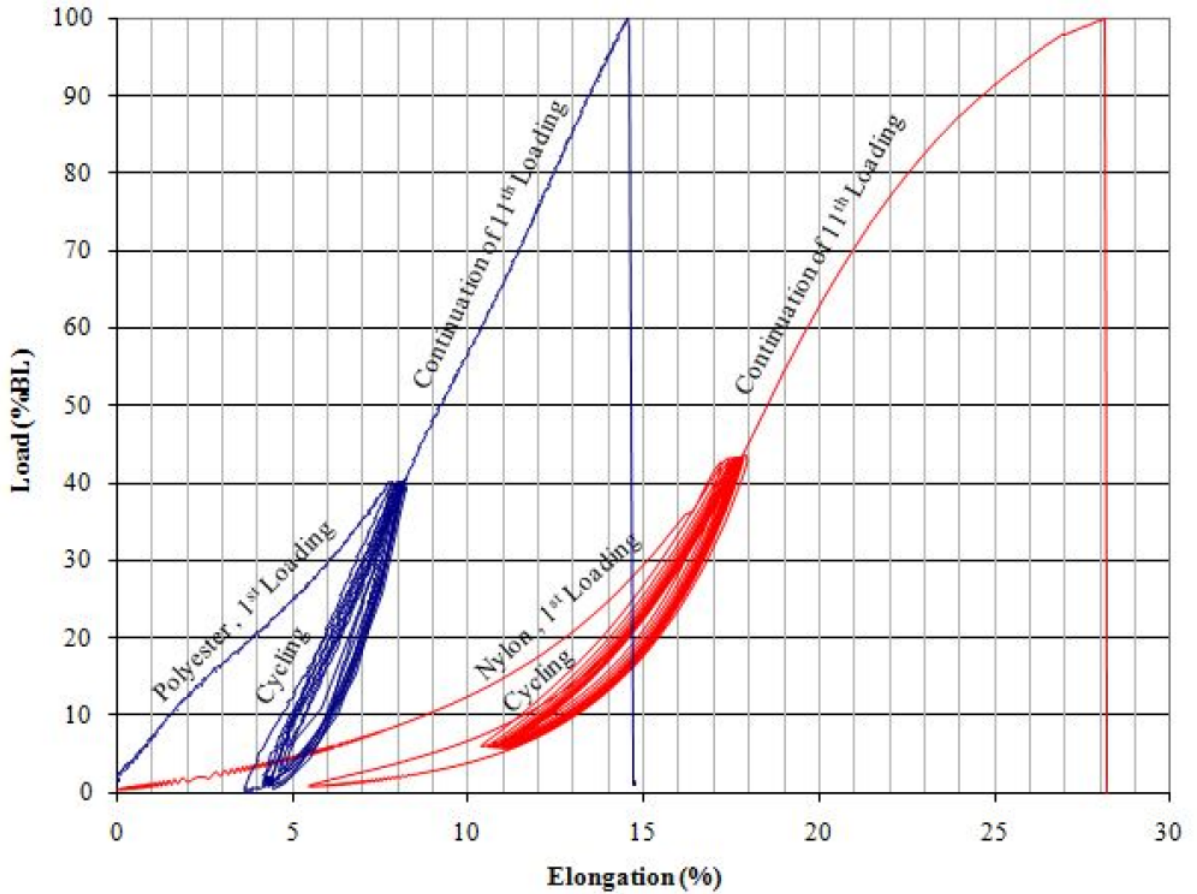
Figure 2.26: Comparison of the load-elongation characteristics of nylon and polyester fibre ropes from (Ridge *et al.*, 2010). Load (%BL) refers to breaking load.

There is a large potential for synthetic fibre moorings for marine energy deployments and a recent review paper discusses current applications (Davies *et al.*, 2014). Whilst the use of polyester ropes is more established, ongoing research by Tension Technology International funded by the Carbon Trust has been looking to develop the use of nylon fibre ropes moorings for wave energy converters (Ridge *et al.*, 2010). The main advantage of nylon over polyester is increased compliance as shown in Figure 2.26. However, there have been concerns about the fatigue performance of nylon. Ridge *et al.* (2010) conclude that although the fatigue performance of nylon subrope is inferior to the polyester subrope under review, it is sufficient for the needs of WEC mooring applications, with a service life of 20-30 years.

Figure 2.27: Seaflex Buoy Mooring as detailed in Bengtsson & Ekstrm (2010).

Synthetic fibre ropes provide a degree of customisation through the selection of material and rope construction however, further, more advanced properties could provide advantages over these conventional solutions. Mooring systems that provide increased compliance and different phases of operation to respond to the particular operational needs of a device have been suggested. Several innovative mooring solutions have been proposed as discussed by Gordelier *et al.* (2015):

- Seaflex Buoy Mooring System, which incorporates a number of rubber cords (2 to 10 depending on design) and a 'by-pass' which prevents over extension in extreme conditions (Bengtsson & Ekstrm, 2010). This system is detailed in Figure 2.27.

- Combined Mooring Tether developed by Technology From Ideas incorporates a combination of elastomeric and thermoplastic elements to deliver *"low stiffness response in normal load scenarios and high stiffness response in extreme weather scenarios"* (McEvoy, 2012; Thies *et al.*, 2014b). This system is detailed in Figure 2.28.

- The Exeter Tether is constructed with a polyester outer load carrying rope and an elastomeric inner core which controls the stiffness of the tether, providing two distinct phases of stiffness as described in Gordelier *et al.* (2015) and detailed in Figure 2.29. This final solution will be further discussed in Chapter 5, where the reliability assessment of this novel component will be reported.

Recent studies have indicated that these novel systems do have the potential to reduce loads. To assess the feasibility of a representative non-linear mooring arrangement Thies *et al.* (2015) develop a spar buoy model in OrcaFlex$^{®}$. Sections of chain are replaced with a representative non-linear load response curve within the mooring system. Results from a representative case with $H_S = 7m$ and $T = 10s$[1] show that the

---

[1]H_S represents significant wave height, and T is wave period.
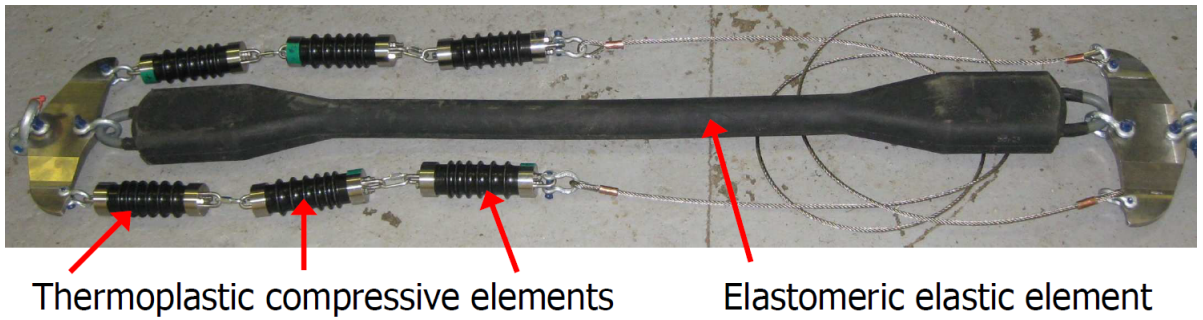
Figure 2.28: TFI's Combined Mooring Tether as detailed in Thies *et al.* (2014b).
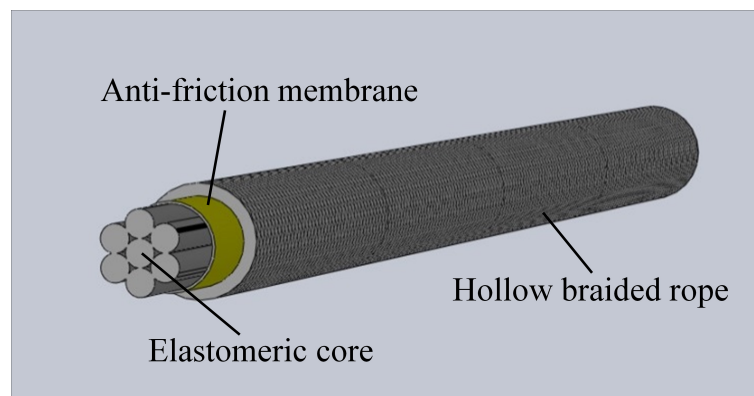
Figure 2.29: The Exeter Tether with key components identified as detailed in Gordelier *et al.* (2015).

(a) Maximum tension

(b) Mean and standard deviation tension
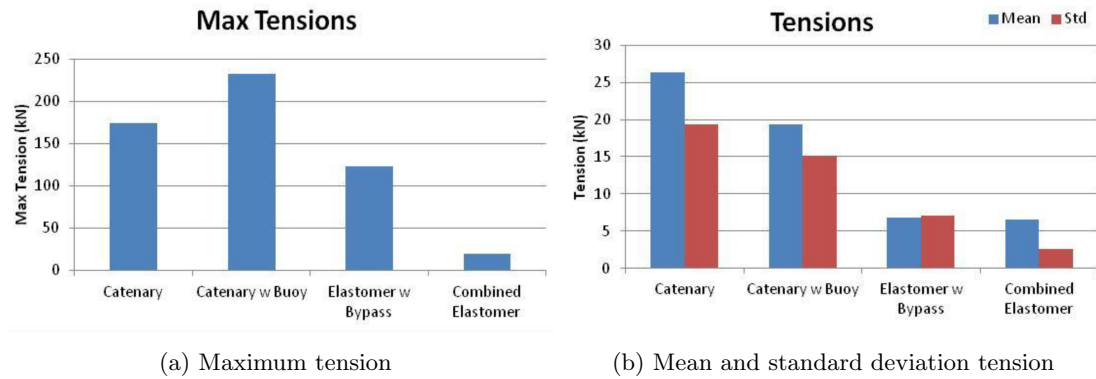
Figure 2.30: TFI Tether load summary from an Orcaflex® model of a storm scenario (McEvoy, 2012).

novel mooring tether reduces the maximum mooring line tension by 20% and the mean tension along the line is reduced by approximately 10%.

The potential load reduction provided by TFI's Combined Mooring Tether is investigated in McEvoy (2012). This study also uses OrcaFlex® to model a broad range of device types with different mooring configurations through a full range of sea states including 100 year storm scenarios. Mooring configurations reviewed include catenary, catenary with buoy (multi-catenary), elastomer with bypass and combined elastomer (representing the TFI novel tether arrangement). Results from a storm scenario are shown in Figure 2.30 and the paper claims 80-90% load reduction from the combined elastomeric tether.

Parish (2015) uses OrcaFlex® to develop a numerical model of the SWMTF buoy (described in Section 3.2.1). A reference case is established in high energy wave conditions and a mooring system incorporating the Exeter Tether is compared directly to a conventional nylon rope mooring system. It is found that the peak tension observed in the mooring line is reduced by a factor of three when replacing the nylon rope with the Exeter Tether. It should be noted that nylon rope was used as the comparator in this study having the greatest compliance achievable of all synthetic ropes currently available (as discussed at the start of this chapter).

It is clear from these studies that innovations in mooring system technology certainly have the potential to reduce the tension loads observed in a mooring system. As described previously, this holds the potential to lead to a downward design spiral of

reducing loads and reducing weight, leading to an overall reduced system cost. However, the introduction of any novel component brings with it new reliability challenges and in the wave energy industry these challenges are two fold. Not only are the components completely new, but they are being used in a relatively novel load scenario given the highly dynamic nature of wave energy devices. If these novel systems are to improve system reliability, a thorough assessment of the component reliability is vital to prove they are fit for purpose. Chapter 5 will provide such an assessment for the Exeter Tether.

To put this reliability assessment into context, an overview of the background behind the Exeter Tether, and literature to date is provided in the next section.

2.6 The Exeter Tether

Given the novel component utilised for the reliability assessment presented in Chapter 5 will not be familiar to the reader, it is necessary to outline the Exeter Tether to allow the reliability assessment to be reported in the context of the operating principles of this component. This section will therefore outline the rational behind this novel component, and detail the operating principles and sub-components of the system, to provide some background for the reliability assessment presented in Chapter 5.

2.6.1 Rationale behind the Tether

The Exeter Tether was conceived in direct response to the specific mooring needs of floating wave energy devices which are required to operate in highly dynamic wave environments. The original design idea came to the University of Exeter's Offshore Renewable Energy Team, when designing the mooring system for the SWMTF (detailed in Chapter 3, Page 136). Through the design process, it became apparent that when using conventional fibre rope mooring systems, the compliance afforded to the mooring system is significantly compromised by the required minimum breaking load of the fibre rope, with these two properties being inextricably linked. When specifying rope for the mooring system that had an adequate MBL (that accounted for both the expected operational loads and a suitable factor of safety) Lead Design Engineer, David Parish, observed he was forced to compromise on compliance. Despite manufacturers of some of the more compliant rope designs quoting extensions up to 30%, this is only achievable

at 100 % MBL (see Figure 2.31). Clearly a system should not be designed at 100% MBL and accounting for the reduction in MBL caused by the eye splices, water absorption, ageing and fatigue, and applying an adequate factor of safety, a 47t (460.9kN) rope was eventually specified for a 68.9kN maximum load (estimated through an OrcaFlex® Model). During operation, the rope was unlikely to see loads higher than 15% MBL and therefore only extend up to approximately 10%.

As detailed by Parish (2015), an upwards design spiral was observed, resulting from the high peak loads in the mooring system (due to low compliance) which required an increase in mooring system strength. The additional weight from the strengthened mooring necessitated an increase in floating body mass, which then further increased the mooring system loads and so on through several iterations. The result of this design spiral was to reach a design solution where both the mooring system and floating body were significantly increased from the original design, ultimately resulting in higher costs. Parish felt that an ability to specify rope compliance independently from the MBL of the tether would have allowed for a design solution to be achieved at a much earlier design iteration.

Given these observations, Parish set out to design a new type of mooring tether, with the following principal aims:

- To de-couple axial stiffness from minimum breaking load.

- To increase compliance in the mooring system via reduced axial stiffness.

- To achieve the above without introducing complex system architecture.

Since the conception of these aims, considerable development work has been undertaken which resulted in the design for the Exeter Tether. During the development process, the following patents have been filed for the tether:

- United Kingdom Patent Publication Number: GB 2476986 A (Parish, 2011).

- International Patent Publication Number: WO 2011/089545 A1 (Parish & Johanning, 2011).

- United States Patent Grant Number: US 8,807,060 B2 (Parish & Johanning, 2014).
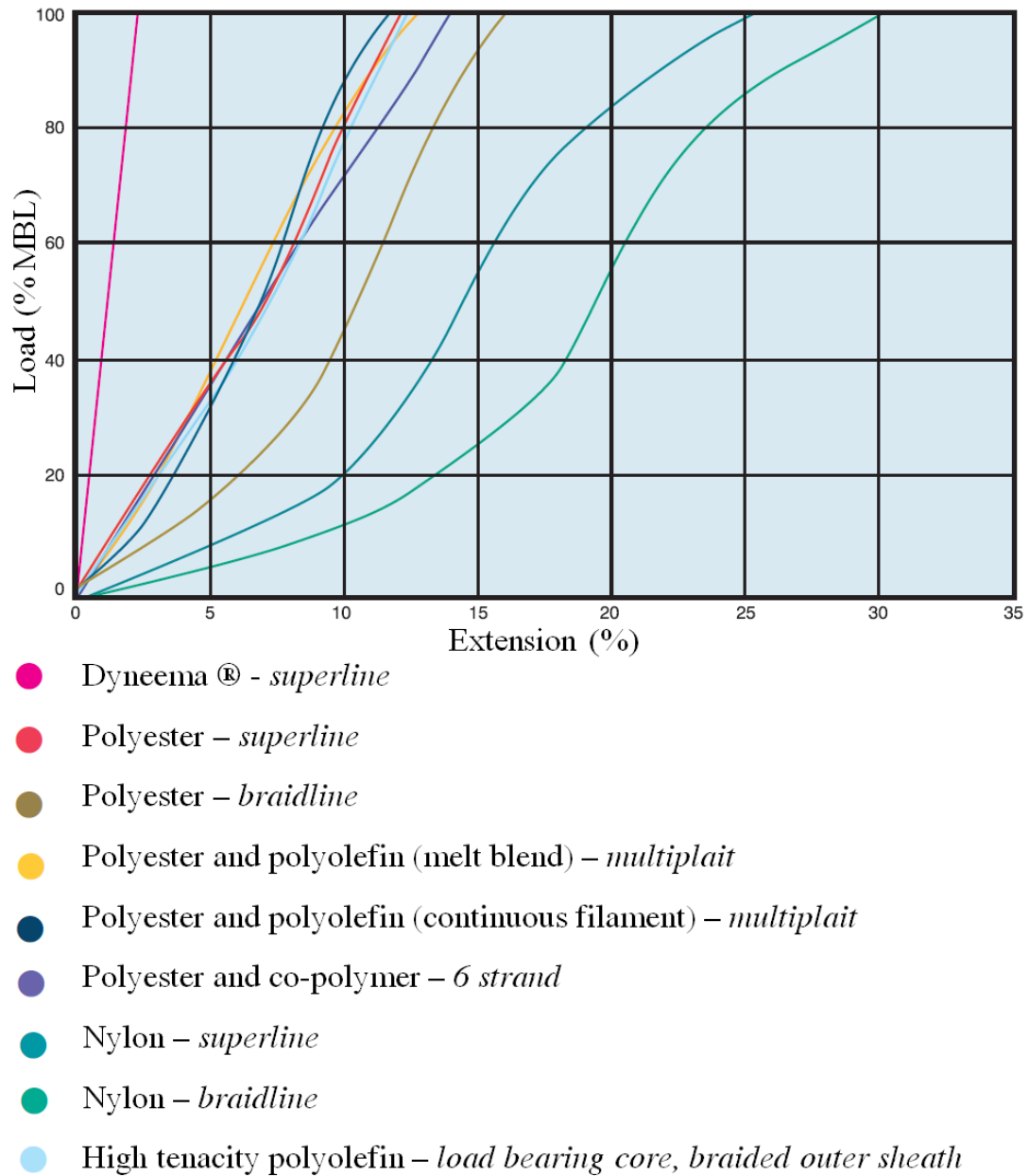
Figure 2.31: Load - Extension characteristics of a variety of worked ropes from rope manufacturer Bridon (Bridon, 2015b). Key details material alongside construction type in italics. Graph highlights the limited extension available in the likely operating load range of commercially available ropes and also demonstrates the load extension variation available from selected materials and construction types.

Since the filing of these patent applications the tether has gone through several further stages of development. Following initial assessments using small scale prototypes a collaboration was established with Lankhorst Ropes to develop the 'Proof of Concept Prototype' series of tethers, the P1 Series. This series of tethers were developed at a scale suitable for testing at the DMaC[1] and SWMTF[2] and will be the focus for the reliability assessment detailed in Chapter 5 of this Thesis.

2.6.2 Operating principles

The operating principles behind the Exeter Tether are detailed by Parish (2015) and Gordelier *et al.* (2015) and will be summarised here in relation to the three main components of the tether as detailed in Figure 2.29, Page 110.

The hollow braided rope acts as the predominant load carrier for the Tether and is terminated at either end with an eye splice. The principles of operation to appreciate are:

- When the tether is under load, the rope extends along its length (axially) and simultaneously contracts across its diameter (diametrically). The pitch angle of the braid of the rope controls the relationship between axial extension and diametric contraction. Figure 2.32 details the relationship between braid angle and diametric compression for one of the P1 Series Tethers.

- As the rope contracts diametrically, the elastomeric core resists this contraction and therefore limits the axial extension. The 'compressibility' of the elastomeric core controls the level of resistance to diametric contraction (and hence axial extension) and this 'compressibility' is determined by both the cross-sectional form of the core and the material selection.

The critical aspect of these operating principles is that the cross sectional form and material choice of the elastomer core control the axial extension (e.g. compliance of the tether) **completely independently** of the breaking load of the hollow braided rope. Thus a series of tethers with the same breaking load can be designed with a range of compliance values selected specifically for a particular device or location.

---

[1]Dynamic Marine Component Test Facility, Section 3.2.2, Page 139.
[2]South West Mooring Test Facility, Section 3.2.1, Page 136.

(a) P1-2 tether at zero extension (b) P1-2 tether at 30% extension
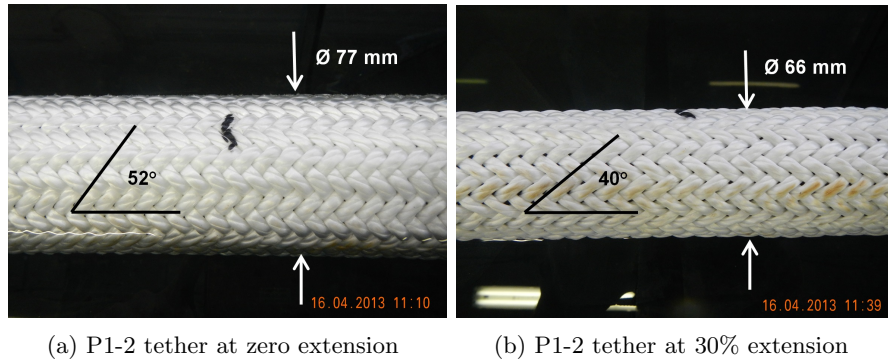
Figure 2.32: The relationship between braid angle and diametric contraction of the P1-2 Tether. Replicated from Gordelier *et al.* (2015).

Further to this de-coupling of the breaking load from the axial extension of the tether, an additional design feature provided by the tether construction facilitates two different stages of axial extension. This is achieved via two stages of operation:

- During the first phase the core assembly deforms becoming a more solid cross section. This compression of the core is achieved relatively easily hence the tether has a soft axial extension response initially.

- During the second phase, once the core has deformed to a solid cross section, further extension is controlled via the Poisson's ratio of the elastomer material (as the elastomer is compressed radially it extends axially). In addition to this, there will be some extension of the rope strands and some embedment of the rope strands into the polymer core which will also provide some extension at this stage (Parish, 2015). The overall affect is a much stiffer axial extension phase.

In addition to the processes described above, during the initial extension phase the high braid angle of the rope (Figure 2.32a) means it has a 'mechanical advantage' in compressing the core. However, as the tether extends, and the braid angle reduces, this mechanical advantage over the core decreases. This reinforces the two phases of axial extension discussed above (Gordelier *et al.*, 2015).

The P1 Tether Series, manufactured in collaboration with Lankhorst Ropes, was created to explore these operating principles with a range of design variants as described in the next section.

2.6.3 The P1 Tether Series defined

The design and functionality testing of the P1 Tether Series was conceived and led by Parish and is fully described in his Thesis entitled *'A novel mooring tether for highly dynamic offshore applications'* (Parish, 2015). To understand the reliability assessment of the Exeter Tether presented in Chapter 5, it is necessary to outline the construction of the tether, and the key operating principles. This section and the next section *The Proof of Concept Study*, Section 2.6.4, will therefore summarise these aspects to enable the reliability assessment (Chapter 5) to be presented within the context of the operating principles of the tether.

As described by Parish (2015) and Gordelier *et al.* (2015) the P1 Tether series included 12 tether variants. The elastomer core and anti-friction membrane components were assembled by the University of Exeter (UoE). The hollow braided rope was manufactured by Lankhorst ropes directly onto the core assembly. The following sections will outline the different variants within the P1 Tether Series.

2.6.3.1 Geometry

Two different geometric options were employed both designed to have similar cross-sectional solidity:

1. Seven Ø25mm continuous rubber cords, assembled in a hexagonal pack as detailed in Figure 2.29 Page 110, with a cross sectional solidity of 86%.

2. A series of moulded rubber articulated sections comprising female double hemispheres fitting into male double hemispheres along the length of the tether, terminated with a female double hemisphere at either end (Figure 2.33). The cross-sectional solidity of this assembly was 83% and a further variant with 78% solidity was also manufactured. These moulded components engage into one another but are not connected, so no axial load will be taken through the core and it was anticipated that this design iteration would have a lower axial stiffness than the seven strand hexagonal pack.

Figure 2.33: Articulated Core construction detailing moulded female and male double hemisphere components assembled (top) and exploded (bottom).

2.6.3.2 Material selection

Different material suppliers were used for the different core geometries introduced above:

1. The Ø25mm rubber cords were supplied by Ley Rubber Ltd. They were specified as ethylene propylene diene monomer (EPDM) with a range of Shore A hardness values of 50, 60, 70 , 80 and 90. Additionally, for direct comparison to the P0 Tether Series (the original, reduced scale prototype), Polymax Ltd also supplied rubber cords at 70 Shore A hardness and a further set of foam EPDM 70 Shore A hardness cords. This was used as the central core for one tether variant, with 6 non-foam cores surrounding it (resulting in a reduced cross sectional solidity of 80%).

2. The articulated sections were moulded by The Harboro Rubber Company in EPDM rubber at 70 Shore A hardness.

Despite specifying the above Shore A hardness values from Ley Rubber, the supplied polymer cords and hence the final tethers were manufactured with different values to those specified, this became evident during test work. Whilst at IFREMER[1] the difference between the specified material and supplied material was measured and is detailed in Table 2.6.

---

[1]L'Institut Français de Recherche pour l'Expoloitation de la Mer. Further information detailed in Chapter 3, Page 146

Table 2.6: EPDM polymer hardness values as specified by Ley Rubber Ltd and as measured (Gordelier *et al.*, 2015; Parish, 2015).

Specified Hardness (Shore A)	Measured Hardness (Shore A)			Mean Hardness (Shore A)
50	54	54	54	54.0
60	59	59	59	59.0
70	70	71	71	70.7
80	70	70	70	70.0
90	81	80	81	80.7

Through the rest of this Thesis, the **mean** supplied EPDM values from Ley Rubber Ltd will be referred to as opposed to those specified in the original design.

2.6.3.3 Anti-friction screen

The anti-friction screen serves several purposes. Most significantly, it creates a low friction surface for the rope to move freely over the core assembly, but in addition it holds the core assembly together to ease manufacturing of the rope jacket around the assembly. Further to this, it was anticipated it may give some protection to the core construction from bio-fouling. Two options of anti-friction screen were employed for the P1 Series:

1. PVC tape, manufactured by Advance Tapes International Ltd.

2. Dacron sailcloth, from Penrose Sailmakers of Falmouth, this was selected as it had lower friction than the PVC tape.

2.6.3.4 Hollow braided rope

Once the core assembly was assembled by the University of Exeter, it was taken to Lankhorst Ropes' manufacturing facility in Portugal where polyester rope was braided onto the core assembly. The rope was then terminated at either end, by hand, using a form of Lankhorst Rope's A3 soft eye splice (Parish, 2015). Manufacturing of an eye splice is a highly skilled process as, once completed, the load must be evenly distributed between the load bearing components of the rope (Weller *et al.*, 2013). If the splice is

Figure 2.34: Exeter Tether dimensions detailing core length. Note total length has some variation but maximum length of 4500mm (image not to scale). Replicated from Gordelier *et al.* (2015).

not accurately manufactured, the uneven distribution of the load will cause premature failure. The rope making process was identical for all the original tethers of the P1-Series, with the exception of the first tether, P1-1, which was manufactured with slightly higher tension in the braiding.

2.6.3.5 Full Tether Assemblies

A summary of the different tether variations in the P1 test series is detailed in Table 2.7. In addition to the 12 originally manufactured tethers, throughout the testing process various tethers were subsequently manufactured to suit specific testing needs. This includes reduced length tethers to enable testing to failure to occur within the maximum 1m stroke length of the DMaC linear actuator. The details for these additional tethers are shown in Table 2.8, along with their heritage i.e. if they are remade from previous tethers. It should be noted that for some of these additional tethers, the eye splicing was done in house by Exeter University. Although the same procedure for eye splicing was followed for these tethers, it is a highly skilled practice and it is likely that these eye splices were not made to the same standard as the original tether eye splices, which were manufactured by expert rope makers with many years practice.

Following the manufacture of the P1 Series, a 'Proof of Concept' study was conducted to establish the performance of the different tether variants; this is reported in the next section.

Table 2.7: P1 Tether Series prototype construction. Working length of all original tethers 2.5m (as detailed in Figure 2.34). Note. There is no P1-11, also P1-13 and 14 are hollow ropes with no core.

Prototype	Core type	Core material	Core sheathing
P1-1	7 x Ø 25mm profiles	EPDM - 70A (Polymax)	Helically wound PVC adhesive tape
P1-2	7 x Ø 25mm profiles	EPDM - 54A (Ley)	Helically wound PVC adhesive tape
P1-3	7 x Ø 25mm profiles	EPDM - 59A (Ley)	Helically wound PVC adhesive tape
P1-4	7 x Ø 25mm profiles	EPDM - 70.7A (Ley)	Helically wound PVC adhesive tape
P1-5	7 x Ø 25mm profiles	EPDM - 70A (Ley)	Helically wound PVC adhesive tape
P1-6	7 x Ø 25mm profiles	EPDM - 80.7A (Ley)	Helically wound PVC adhesive tape
P1-7	6 x Ø 25mm profiles + 1 x EPDM foam Ø 25mm (reduced solidity)	EPDM - 70A (Polymax)	Helically wound PVC adhesive tape
P1-8	7 x Ø 25mm profiles	EPDM - 70A (Polymax)	Helically wound Dacron sailcloth tape
P1-9	Articulated	EPDM - 70A (Haboro)	Helically wound PVC adhesive tape
P1-10	Articulated	EPDM - 70A (Haboro)	Helically wound PVC adhesive tape
P1-12	Articulated	EPDM - 70A (Haboro)	Helically wound Dacron sailcloth tape
P1-13	No core	-	-
P1-14	No core	-	-

Table 2.8: P1 Tether Series - additional tether constructions. Working length of all tethers in table 2m except P1-2* which had a working length of 2.5m.

Prototype	Core type	Core material	Core sheathing	Heritage
P1-16	7 x Ø 20mm profiles (new)	EPDM - 70A (Polymax)	Helically wound PVC adhesive tape	P1-14
P1-17	7 x Ø 25mm profiles	EPDM - 70.7A (Ley)	Helically wound PVC adhesive tape	P1-4
P1-20	6 x Ø 25mm profiles + 1 x EPDM foam Ø 25mm (reduced solidity)	EPDM - 70A (Polymax)	Helically wound PVC adhesive tape	P1-7
P1-16*	7 x Ø 20mm profiles (new)	EPDM - 70A (Polymax)	Helically wound mixed tape	P1-14 / P1-16
P1-17*	7 x Ø 20mm profiles (new)	EPDM - 70A (Polymax)	Helically wound mixed tape	P1-4 / P1-17
P1-2*	7 x Ø 25mm profiles	EPDM - 54A (Ley)	Helically wound PVC adhesive tape	P1-2

2.6.4 The Proof of Concept Study

The Proof of Concept Study is summarised in Gordelier *et al.* (2015) and fully detailed in Parish (2015). The study focused on 5 tether variants P1-2, P1-3, P1-4, P1-5 and P1-6. These 5 variants covered the full range of EPDM hardness values supplied by Ley Rubber (as detailed in Table 2.6) and therefore allowed the Proof of Concept study to fully investigate the effect of core hardness. These five tethers are all of solid Ø25mm type with no articulation.

The first step of the study was to establish the minimum breaking load (MBL) of a typical P1 Tether Series. P1-17 (with a reduced working length of 2m) was used to establish the MBL of the tether series as a full length tether could not be parted within the 1m working stroke of the DMaC linear actuator. The tether was not submerged in this test, but a hose was used to thoroughly wet the tether assembly during the test set up. The break test found the MBL of P1-17 to be 222kN and this load was used to inform further test work. Once the MBL of the tether was established, it was possible to calculate the tether load-extension properties as a % of MBL. This is beneficial as it allows comparison of the tether performance to other available ropes.

Table 2.9: Ranked tether stiffness in relation to Shore A hardness as reported by Gordelier *et al.* (2015).

Hardness (Shore A)	Tether	Gradient	Stiffness
54	P1-2	3.1534	1
59	P1-3	2.7741	2
70	P1-5	2.2655	3
71	P1-4	2.0097	4
81	P1-6	1.7261	5

Relating back to Section 2.6.1, one of the principal aims of the tether design was to de-couple the axial stiffness from the minimum breaking load of the tether. Figure 2.35 details the load extension properties of several of the P1-Series Tethers, and demonstrates a selection of tethers with identical MBLs showing markedly distinct axial stiffness behaviour. The gradient of the line of best fit detailed in Figure 2.35 represents the tether axial stiffness and this can be shown to be related to the hardness of the material as detailed in Table 2.9

In addition to de-coupling of the axial stiffness from the MBL of the tether, the Exeter Tether also aimed to provide increased compliance with distinct phases of axial stiffness. Figure 2.36 details the improved compliance of the tether available with extensions in excess of 30% achievable at just 30% MBL (Gordelier *et al.*, 2015); this represents nearly 10 times the extension available in a 'reference' polyester rope. This 'reference' rope was selected for comparison as it represents one of the more compliant mooring ropes commercially available. Further to the increased compliance, two distinct phases of stiffness can be seen. The initial phase below 25% extension provides a low stiffness phase with loads remaining below 5% MBL. Following this initial stage, the tether response becomes markedly stiffer with further extension requiring a large increase in tension.

With the background of the Tether explained, and the key operating parameters detailed, the reliability assessment of the Exeter Tether can be presented within this operational context. The reliability assessment is addressed in Chapter 5.
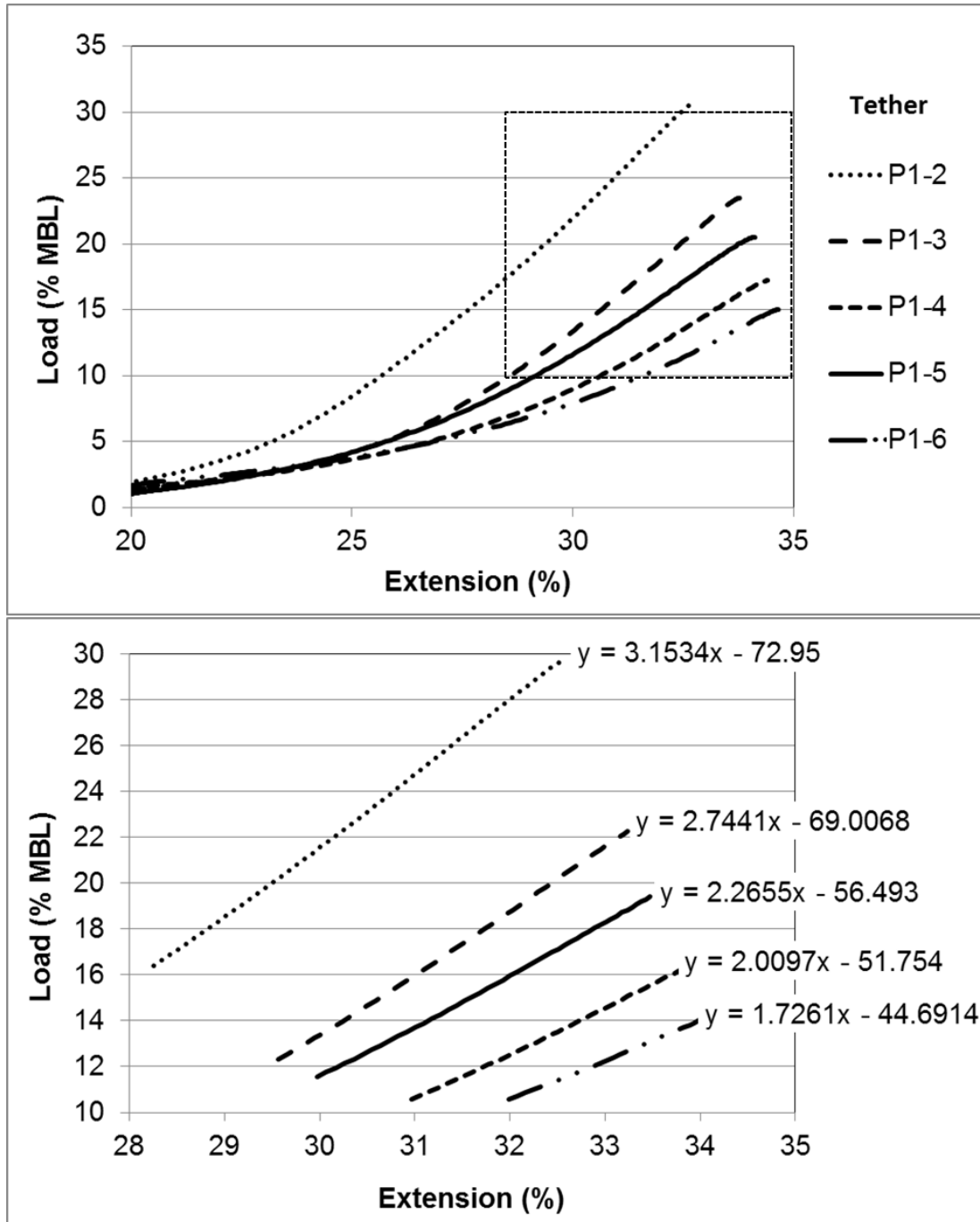
Figure 2.35: P-1 Series Tether extension properties. Overview (top), focus on area of interest (bottom). Replicated from Gordelier *et al.* (2015).
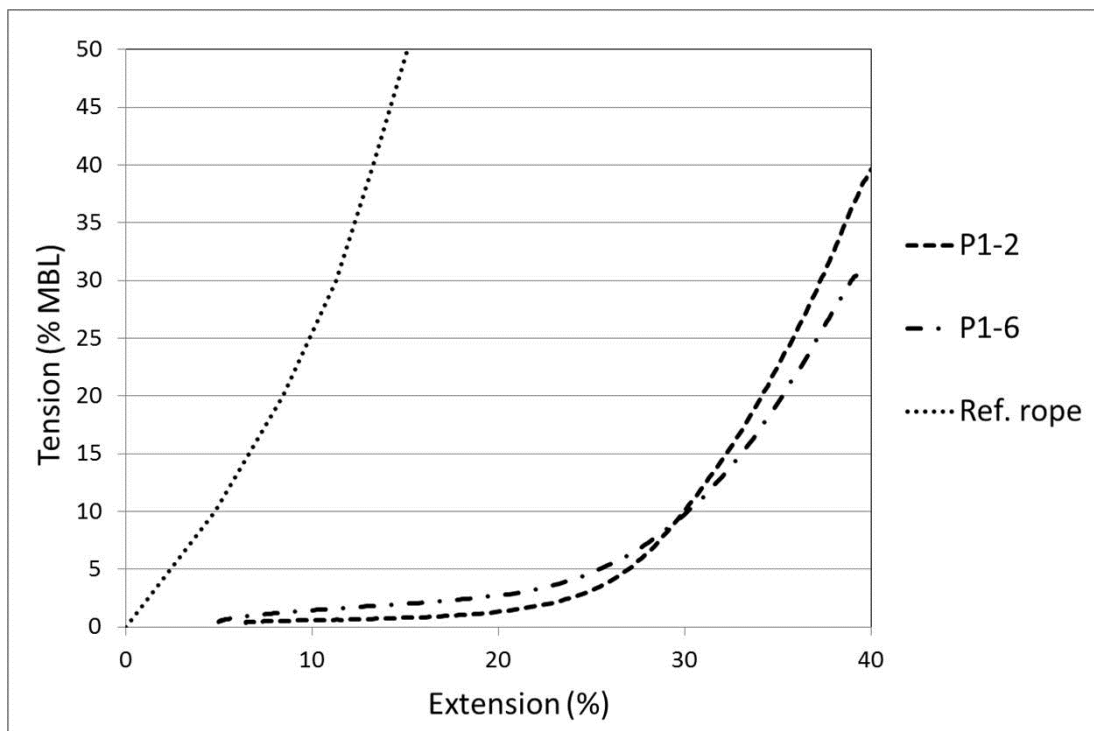
Figure 2.36: Demonstrating the compliance of the Exeter Tether in relation to a double braid polyester reference rope, in addition two phases of operation are clearly visible. Replicated from Gordelier *et al.* (2015).

Chapter 3

Research approach

Contents

Before presenting the individual reliability case studies in Chapters 4 and 5, this Chapter outlines the general approach taken with each case study, and details the test facilities utilised for both assessments. Firstly, Section 3.1 details the overarching reliability approach with reference to guidance documents. This section goes on to identify the key test approaches employed for each component reliability assessment. Section 3.2 details the test facilities utilised for the practical aspects of the reliability assessments, commenting on their suitability for the research objectives. In addition to outlining the key features of these test facilities, calibration and data accuracy is also presented. Finally, Section 3.2.4 details the inspection techniques used to identify damage within the shackles presented in the first reliability case study, Chapter 4.

3.1 Reliability methods

As outlined in the Introduction (Chapter 1) this Thesis aims to assess the reliability of mooring systems for WEC devices at a component level, implementing a detailed reliability study for:

1. A standard component

2. A novel component

DNV guidance outlining the requirements for the certification of components detail the different requirements for standard and novel technologies. This guidance is outlined in Chapter 2, Section 2.5.4 which focuses on DNV document DNV-OSS-312 *Certification of tidal and wave energy converters* (Det Norske Veritas, 2008).

Using the matrix from Det Norske Veritas (2008), detailed in Figure 2.24, Page 101, the two case studies can be classified:

1. **Standard component: Shackle.** Technology status: Proven. Application area: New. The shackle is therefore classed as (2) New technology: New technical uncertainties. (Although shackles have been used for many years in mooring systems within the oil and gas industry as discussed in Chapter 2, the use of shackles in mooring systems for highly dynamic wave energy converters is relatively novel with new design challenges.)

2. **Novel component: Exeter tether.** Technology status: New or unproven. Application area: New. Therefore the tether is classed as (4) New technology: Demanding new technical challenges.

Interestingly, using the approach outlined by DNV, despite being a well known technology the fact that the shackle is being assessed for a relativity unknown application area means it is defined as a 'new technology'. It is however only specified as having 'new technical uncertainties' compared to the 'demanding' challenges of the novel mooring tether. The requirements of the certification process are then detailed with reference to these definitions, as described in the Literature Review by Figure 2.25, Page 102. This process sets out the additional demands on the certification of any technology classified as new. Although the components investigated through these case

Nylon rope
20m

10t
swivel

Studless chain
36m

Stud link chain
5m

Figure 3.1: Graphical representation of a typical mooring limb design from SWMTF. A combination of 9.5t and 25t D shackles are used to link different components of the mooring system. From left to right the mooring is aligned from top to sea bed.

studies are not going through the full certification process, referring to the requirements set out by DNV provides a useful framework to inform the approach applied to the specific case studies. The approach for each case study is outlined in the next two sections.

3.1.1 Reliability assessment of a standard component

A conventional D shackle was selected as the standard mooring component for an investigation into reliability methods and a review of safety factors applied in mooring design. This component was selected as shackles are used extensively throughout a typical mooring limb to connect different sections of rope and chain together. As an example of the frequent use of shackles throughout a mooring limb Figure 3.1 is a representation of the mooring limb design for SWMTF[1]. For simplicity, this figure just shows the central part of the mooring and does not include the load cells and connecting shackles at the buoy end of the mooring, nor the connection arrangement at the anchor end (these add an additional 3 shackles to the whole mooring limb). In the section of the mooring limb detailed there are 6 shackles used along the length of the mooring limb, from the thrash zone at the top to the ground chain on the sea bed. This extensive use of connecting shackles makes them an ideal component for this study.

As detailed in Figure 2.24 Page 101 a mooring shackle in this application is considered to have 'new technical uncertainties' and therefore, amongst other things, requires a reliability assessment. In the case study presented in this Thesis, the aim is to investigate the safety margins present for shackle use in this new application area (WEC

---

[1]South West Mooring Test Facility, see Section 3.2.1, page 136

mooring system design) that has new technical uncertainties. Safety factors are applied at different stages throughout the mooring design process:

- During component manufacture safety factors are applied to account for manufacturing and materials variability (intrinsic variability).

- During mooring system design further safety factors are added. In addition to the intrinsic variability discussed above, these safety factors will take into account extrinsic variability in operating conditions such as wave climate.

The reliability assessment involves the approaches outlined in Figure 3.2. The key steps of the assessment are:

1 **Numerical investigation:** A finite element model of the shackle is developed and subjected to a variety of different load cases. This model has three main purposes:

   (a) Identify areas of weakness within the shackle

   (b) Estimate loads at which failure should be anticipated

   (c) Calculate stress concentration factors to apply to analytical estimations

2 **Laboratory investigation:** In a controlled laboratory environment at the DMaC (Section 3.2.2, Page 139) an investigation is conducted into the yield, break and fatigue performance of the specified shackle.

3 **Field investigation:** A set of shackles are deployed on a mooring limb of the SWMTF (Section 3.2.1, Page 136) and exposed to real mooring loads.

These key steps are conducted and throughout the process the results will be compared with reference to the guidance on mooring system design (Det Norske Veritas, 2010a). The process is not a linear process, and following sea deployment further laboratory testing is conducted on the shackles.

3.1.2 Reliability assessment of a novel component

The aim of the Exeter Tether is to improve overall system reliability by reducing peak and fatigue loads as detailed by Parish (2015) and Gordelier *et al.* (2015). However, any novel component introduces a whole range of new reliability considerations into
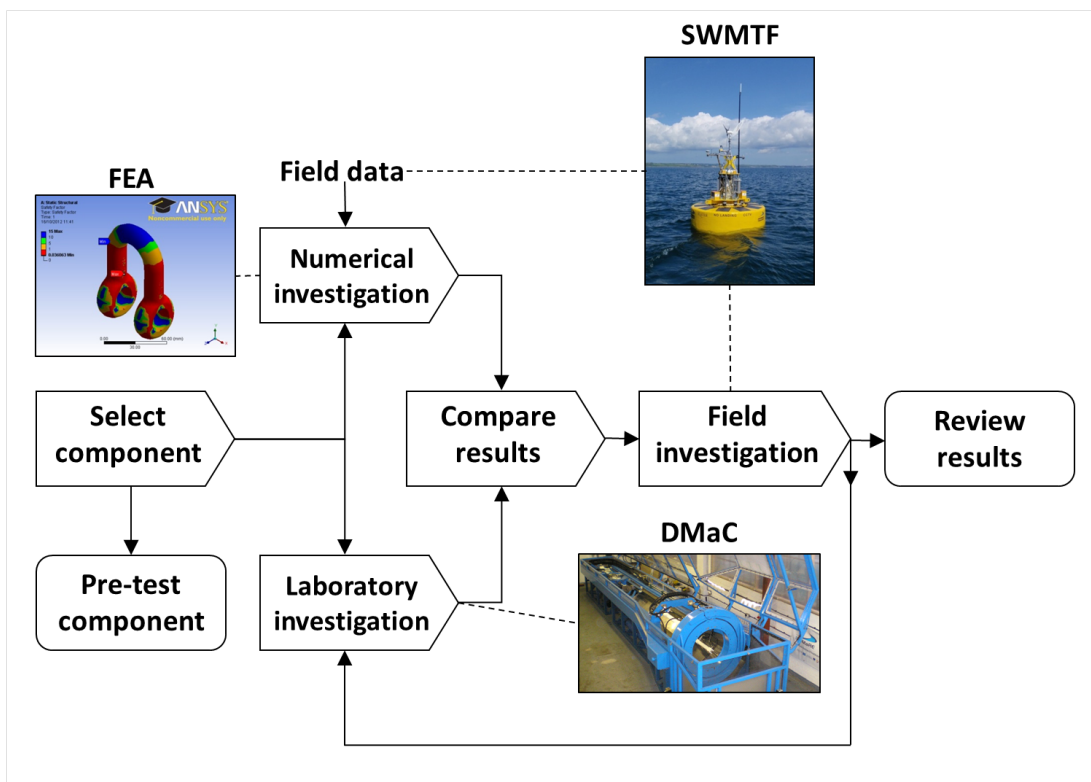
Figure 3.2: Outline method for the reliability assessment of a shackle.

a system, and the key reliability considerations for the Exeter Tether are investigated and presented in Chapter 5 of this Thesis.

As detailed in Det Norske Veritas (2008), the route to certification for a novel component is complex. The aim of the research presented in this Thesis is to conduct a reliability assessment of the tether (the last step in Figure 2.25, Page 102), not to gain full certification. However this guidance does provide a helpful framework for development, and a very good place to start is with *'Failure mode identification and risk ranking'* referred to in this Thesis as 'failure mode and effect analysis' (FMEA). The concept of a FMEA was first introduced in the Literature Review (Section 2.3.2.1, Page 59). A FMEA should not be used as a static tool but should be revisited through the design evolution process. Throughout the early design stages of the tether, FMEA have been used to make design decisions on the optimal development route (Parish, 2015). In the context of this Thesis it will be used to set out the critical areas for reliability assessment of the novel tether.

The FMEA conducted for the tether is detailed in Chapter 4, Table 5.1, Page 239. A diagram summarising the most important reliability considerations for particular tether components derived from this analysis is detailed in Figure 3.3. The purpose of this work is to focus on novel reliability aspects of the tether. The FMEA shows that failure of both the polyester rope and the eye splice have severe consequences, however, these are existing components, widely used in the industry and with standard testing methods. Therefore work presented in this Thesis will not focus on these reliability considerations. Instead, the focus will be on those reliability aspects of the tether that are unique to this design, these include:

- Component interaction within the tether assembly

- Durability of the polymer core

- Durability of the anti friction membrane

Referring back to the Literature Review presented in Chapter 2, durability encompasses reliability and holding capacity and accounts for fatigue damage, wear, corrosion and other changes to material properties (Weller *et al.*, 2014b). In relation to the tether this definition is very important as the changes in material properties of the different
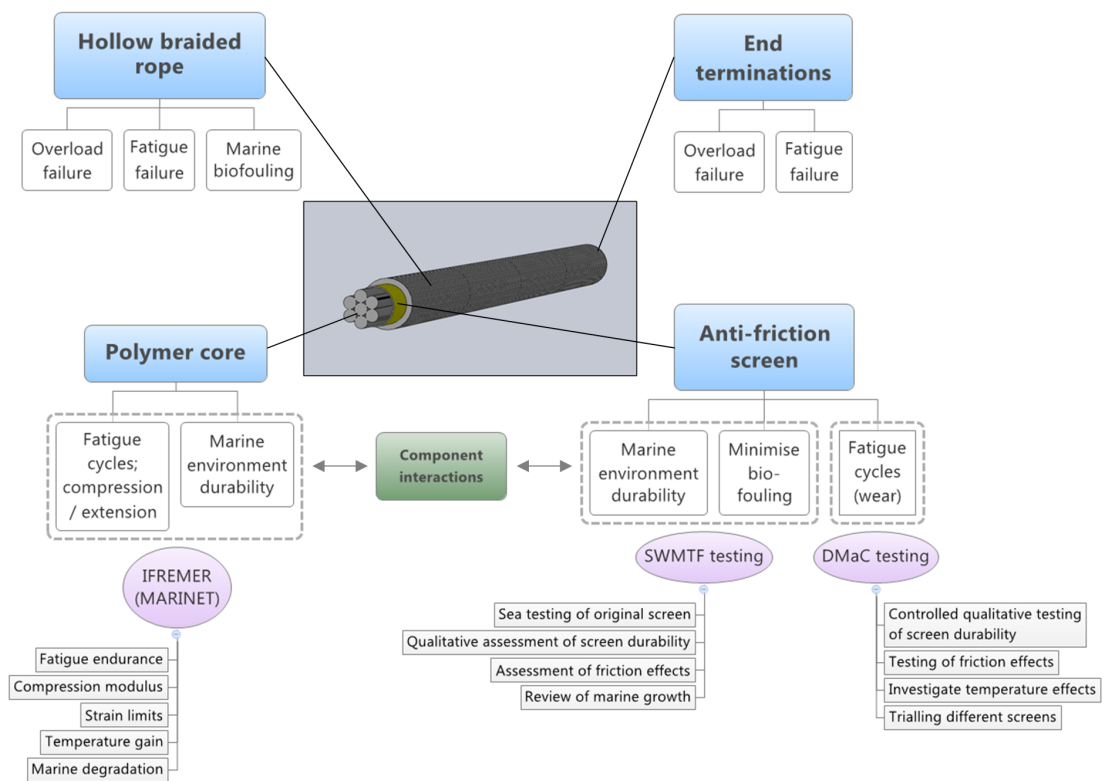
Figure 3.3: Key component reliability considerations for the Exeter Tether with proposed test methods detailed

components of the tether are critical to tether operation.

Global models of the Exeter Tether have been developed to analyse the potential load mitigation offered (Parish, 2015; Thies *et al.*, 2015). These analyses will be referred to during this Thesis however further modelling of the tether is not conducted. The reliability case study of the Exeter Tether focuses on physical testing of different aspects of the tether, identifying priority areas for further development to ensure long term durability. This approach is supported by Det Norske Veritas (2008) which suggests for novel components a qualitative approach may be more practical in the early development phase. To investigate the key reliability considerations identified above, four test methods are identified:

1 **Tether assembly durability trials, laboratory testing.** Conducted at the DMaC test facility, this work includes:

- Long term fatigue testing of tether assembly durability. This enables the quantification of the fatigue performance of the tether and in addition the identification of any durability issues regarding the interaction of the rope, core and screen.

- Benchmarking tether performance both before and after sea trials to quantify marine durability by measuring the affect on tether performance following exposure to a marine environment.

2 **Tether assembly durability trials, field testing.** Conducted at the SWMTF this work includes:

- Exposing the tether to the marine environment and realistic load conditions on the SWMFT to observe any changes to tether operation.

- Quantitative assessment using DMaC to compare tether operation before and after field deployment at SWMTF (linked to item 1).

- Qualitative assessment of tether component durability in the marine environment following a field deployment at SWMTF.

- Qualitative assessment of the impacts of bio-fouling on the tether following a field deployment at SWMTF.

3 **Polymer core durability.** This work was predominantly conducted at the IFREMER [1] Brittany Centre (Section 3.2.3). The following themes are investigated:

- Material degradation due to ageing of polymer. Material properties are compared for the polymer in new and aged condition to observe any degradation caused by ageing in the marine environment. Both tensile and compression tests are conducted.

- Material degradation due to repeated compression fatigue loading. The operation of the tether demands the repeated compression of the core bundle, the long term affects of this on key material properties are investigated.

- To inform the above tests 'core bundle' tests are conducted, observing the deformation of the individual cords when the entire core bundle is subject to radial compression.

- Other material tests including 'Dynamic Mechanical Analysis' to observe the evolution of modulus with respect to temperature.

4 **Anti-friction screen durability trials:** The tether assembly investigations inform this aspect of work which focuses on trialling alternative anti-friction screens for the tether.

---

[1]L'Institut Français de Recherche pour l'Expoloitation de la Mer

3.2 Test facilities

3.2.1 South West Mooring Test Facility (SWMTF)

The SWMTF is an at-sea test facility, located just inside the Harbour Limits of Falmouth Bay, Cornwall (Figure 3.4) and operated by the University of Exeter. The facility is designed to facilitate research in mooring components by providing a platform to expose them to realistic sea conditions. The facility can comprehensively monitor sea states and the imposed loads on mooring arrangements. The two main features of the test facility are the fully autonomous instrumented buoy and the sea-bed mounted Acoustic Doppler Current Profiler (ADCP) unit. The instrumented buoy is installed with a three catenary limb mooring system, each mooring limb has full monitoring of load conditions through both an in-line and a tri-axial load cell. Mooring components under investigation can be installed onto the buoy mooring limbs to provide a review of component response to the fully documented operating environment. Dynamic data and load data monitored by the buoy is managed by an on-board SCADA system, which transmits to a local shore station via a dedicated Wi-Fi bridge (Parish, 2015). In addition to the instrumented buoy, an Acoustic Doppler Current Profiler (ADCP) is installed on the seabed adjacent to the buoy. This continuously records wave and current data in the vicinity of the test buoy, with the raw data being manually recovered from the ADCP following retrieval. To compliment the ability to test mooring components at sea on the SWMTF, data collected from the SWMTF can also inform testing regimes at DMaC for accelerated service simulation testing purposes in more controlled conditions. Full specification of the test facility can be accessed on-line. (Renewable Energy Research Group - University of Exeter, 2013c).

As the test facility is located on the south coast of Cornwall the wave climate is relatively sheltered, making the SWMFT a good location for testing prototype mooring components that have not been exposed to real sea conditions before. Figure 3.6 details typical annual wave statistics for the SWMFT location based on a SWAN model utilising boundary conditions from the UK Met Office's UK waters wave model (Johanning *et al.*, 2011). In addition to the relatively sheltered conditions there is quick and easy access to the well equipped Falmouth docks to facilitate deployment and retrieval.

This test facility is particularly well suited to the work in this Thesis as access to real load data measured at the SWMTF informs numerical modelling in the reliability

Figure 3.4: South West Mooring Test Facility Location, Falmouth, UK. Reproduced from Parish (2015). ©Crown Copyright and/or database rights. Reproduced by permission of the Controller of Her Majestys Stationery Office and the UK Hydrographic Office (www.ukho.gov.uk).

Figure 3.5: South West Mooring Test Facility, Falmouth, UK.
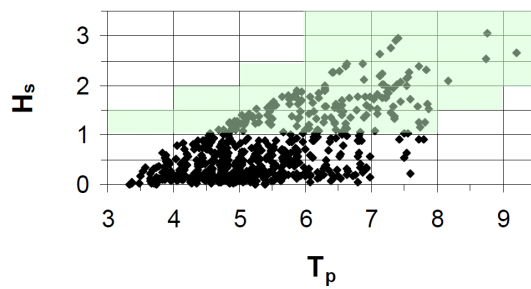
Figure 3.6: Annual wave statistics for SWMTF location, replicated from (Johanning *et al.*, 2011)

study presented in Chapter 4, strengthening the validity of the models. In addition, the ability to expose components to realistic operating conditions significantly strengthens the case studies presented in both Chapter 4 and 5, by allowing a meaningful assessment of operational durability.

The data used to inform the numerical modelling that will be presented in Chapter 4 was collected during a SWMTF deployment period from 16th September 2010 - 7th June 2011. Full data analysis of mooring load measurements from the in-line load cells collected during this deployment was conducted by Harnois (2014). During the deployment load data was collected at a frequency of 20Hz and saved into separate files every 10 minutes. Following the deployment Harnois processed and corrected the data (for example to account for a drift occurring on one of the load cells) to establish maximum and mean load measurements. A maximum load of 52kN was recorded on mooring limb 1 on 17th November 2010 (Harnois, 2014).

The components presented in Chapters 4 and 5 were deployed on the SWMTF data buoy during a subsequent deployment from 4th June 2013 - 26th November 2013: The mooring shackles (Chapter 4) were deployed on mooring limb 3; the P1 Exeter Tether Prototypes (Chapter 5) were deployed on mooring limb 1. Of the three mooring limbs on the data buoy, these two mooring limbs at 185°(limb 1) and 65°(limb 3) from North were likely to experience the highest mooring loads due to the dominant wave conditions at the site as observed during previous deployments (Harnois, 2014; Parish, 2015). Figure 3.7 outlines the mooring configurations during the deployment of the components under investigation in this Thesis.

3.2.2 Dynamic Marine Component Test Facility (DMaC)

The DMaC is a test facility operated by the University of Exeter and based in Falmouth, UK. It has been specifically designed to subject components to the loads and motions experienced by mooring systems in the marine operational environment.

The development of the test facility is detailed in Johanning *et al.* (2010) and Thies & Johanning (2010) and a full specification is provided on-line (Renewable Energy Research Group - University of Exeter, 2013a). Principal features of the system relevant to this work are outlined below, and an image of the facility is provided in Figure 3.8:
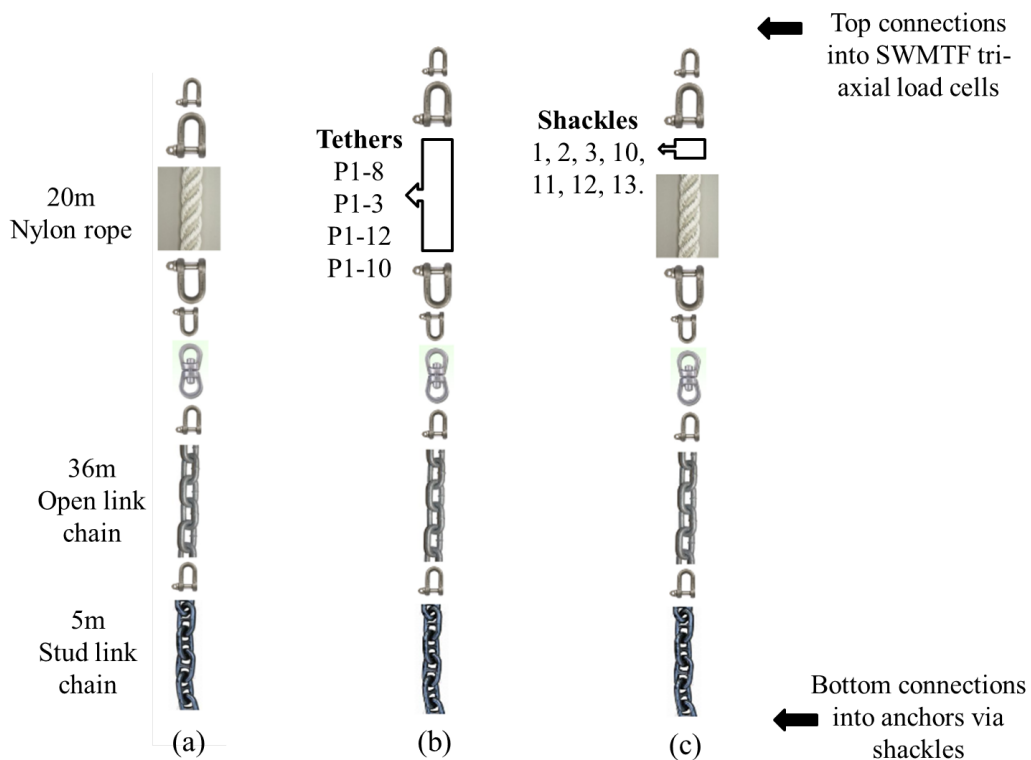
Figure 3.7: SWMTF mooring configuration for component testing: (a) Represents a typical SWMTF mooring limb; (b) Represents Mooring Limb 3 with the deployment of four Exeter Tether prototypes replacing 20m of nylon rope during SWMTF deployment 04/06/2013 - 26/11/2013; (c) Represents Mooring Limb 1 with the deployment of 7 test shackles, these were installed using 2m of back up chain for protection in the event of a shackle failure during SWMTF deployment 04/06/2013 - 26/11/2013.

Figure 3.8: Dynamic Marine Component Test Facility, Falmouth, UK.

- Fully submersible test area for wet testing. Maximum dimensions 6m length, 0.8m diameter.

- Linear hydraulic actuator with 1m stroke to deliver tension or compression forces; 30t dynamically, 45t statically.

- Moving headstock with two degrees of freedom (to replicate pitch and roll). Displacement in X and Y direction: $+/-30°$.

- Fully autonomous control centre with programmable force or displacement driven test regimes.

- Combined sampling frequency of 250kHz for accurate data logging.

The fully programmable control enables force driven or displacement driven tests to simulate real sea state conditions in a controlled (and repeatable) laboratory environment. The test facility has been used to investigate varied components including umbilical cables, bend restrictors (Thies *et al.*, 2014a), mooring systems (Thies *et al.*, 2014b) and synthetic ropes (Weller *et al.*, 2015b).

There are some key features that make this test facility particularly well suited to the test work conducted in this Thesis. Firstly, the reliability assessment of the mooring shackle (Chapter 4) requires exposure to thousands of cycles in order to assess fatigue response. The DMaC test facility Z ram actuator is capable of very high frequency motion (up to 10Hz at 0.01m stroke). This high frequency motion facilitates fatigue testing by considerably speeding up the whole process. Secondly, the unique ability to fully flood the test areas makes the DMaC particularly well suited to testing of the Exeter Tether which is detailed in Chapter 5. For this component the water will provide a level of lubrication to the operating tether. Submerged testing is crucial to develop a realistic understanding of the operation of the tether and any reliability issues. Dry testing or even wet testing using a drip feeder (as used in similar test facilities) would provide an unrealistic representation of the true operational characteristics of the tether as evidenced by Parish (2015).

An additional feature of the DMaC test facility, developed specifically for the P1-Series tether testing, is a pre-tension adjuster. This was fitted onto the back plate of the headstock (Figure 3.9). This platen increases the test bed length of DMaC by 300mm and additionally incorporates an M64 thread which provides further adjustable travel up to 800mm. This feature was installed to facilitate the installation and testing of the tethers by enabling slack to be removed from the tether and a pre-tension to be set without using any of the 1000mm travel provided by DMaC's linear actuator.

3.2.2.1 Calibration of DMaC

During all work conducted on DMaC test facility for this Thesis, it is operated purely as a tensile test machine; there are no requirements for bending of the specimens using the headstock rotation. Therefore the calibration of the pancake load cell controlling the linear actuator (or Z ram) is critical for this work. This is a 444kN load cell, Model 3232, Interface Force Measurements Ltd. Depending on the test arrangement, there are two possible locations for the load cell and, in addition to an annual calibration, whenever the load cell is re-positioned it must be re-calibrated. This work was done in conjunction with Parish, and the calibration procedure is also documented by Parish (2015).

During the test work reported in this Thesis, a full calibration of the DMaC tailstock load cell was conducted four times on 10/01/2013, 09/04/2014, 28/11/2014,

Figure 3.9: DMaC pre-tension adjuster which enables slack to be removed from the system and a pre-tension to be set prior to dynamic testing.

02/12/2015. The calibration process will be outlined here, and data from the last calibration, conducted on 02/12/2015 will be presented to detail the calibration process.

All of the reference load cells used for calibration purposes at the DMaC test facility are annually calibrated by an accredited test house. The calibration conducted on 02/12/2015 utilised a 10,000kg S-beam load cell as a reference cell. The calibration certificate for this load cell is included in Appendix A. The calibration load cell was installed in DMaC using webbing slings and shackles to connect into the headstock and Z ram as detailed in Figure 3.10. The load cell was then energised to 10VDC using a separate power supply and the signal leads from the load cell were connected into a voltmeter with a sensitivity of 10 microvolts. The calibration set-up is therefore completely independent to the DMaC control and data acquisition system.

A specific force driven test script for calibration purposes was developed for DMaC that increases the load in specified steps from 2kN to 50kN. At each step the load is held for 5 seconds in order that a reading from the voltmeter connected to the calibration load cell can be recorded. Simultaneously, the DMaC data acquisition system automatically records the load measured by the DMaC Z ram load cell.

To compare results from each load cell the voltage reading from the calibration load cell was converted to load in N using the offset and gain values as specified in the
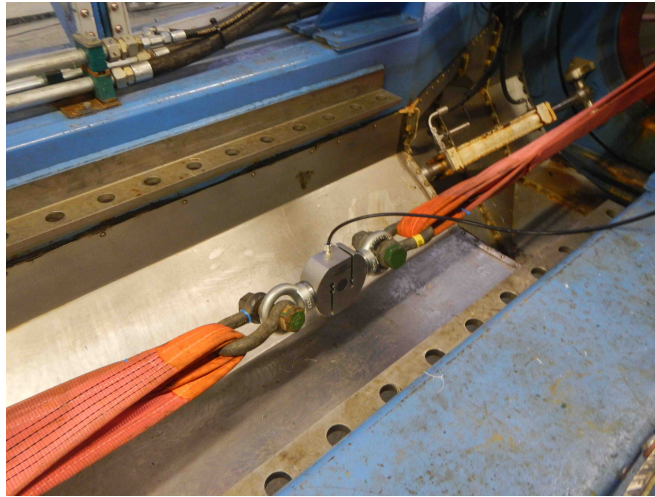
Figure 3.10: Reference load cell installation within DMaC for calibration of DMaC linear transducer load cell.

calibration certificate. This was then plotted against itself to provide a load reference line for comparison to DMaC's load cell reading. The DMaC load cell data is then plotted against the calibration load cell data on the same graph, and a line of best fit established, allowing direct comparison to the load reference line (Figure 3.11).

Any error identified between the two data lines was corrected via an adjustment to the parameters applied to the DMaC load cell; the gain value was altered to adjust the gradient of the line, and the offset value was altered to adjust the difference between the two lines. Following these adjustments the calibration process was repeated to check the alignment of the load cell readings. Further alterations to the gain and offset values were implemented if necessary, until an acceptable alignment was achieved. The acceptance criteria for each calibration was specified as a maximum error of 250N and a mean error below 100N. This particular calibration required three iterations of gain and offset values to achieve an acceptable correlation, however each calibration procedure was slightly different. Data from each iteration is detailed in Figure 3.11, which highlights the equation for each line of best fit and the R^2 value (i.e. the square of the Pearson product moment correlation coefficient which quantifies how well the data correlates to the line of best fit).

The final gain and offset values in the last image of Figure 3.11 were used as the new calibrated DMaC parameters. In the load range of the calibration (0 - 120kN)
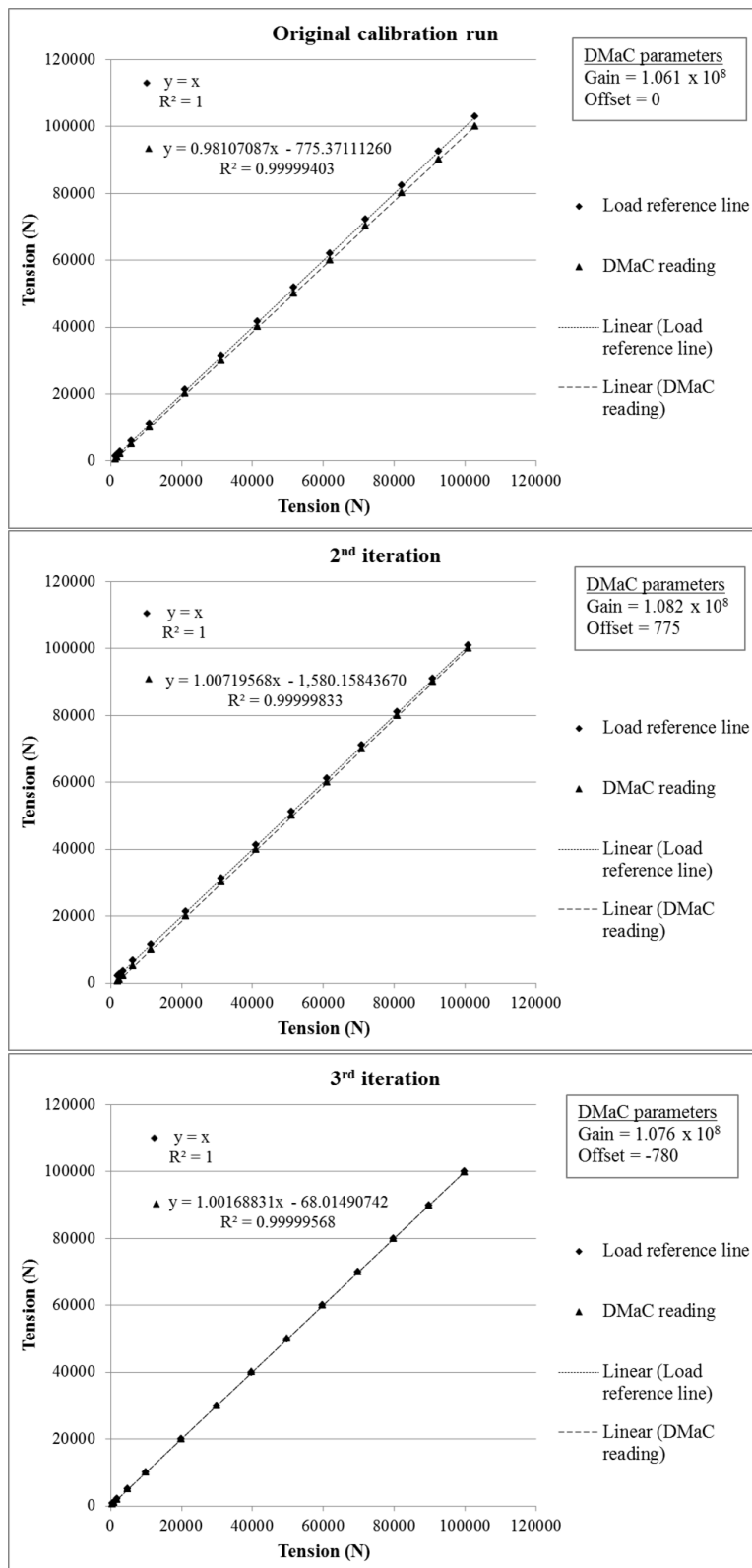
Figure 3.11: Outlining the method of calibration for the DMaC Z ram load cell using data from calibration conducted on 02/12/2015.

Table 3.1: DMaC Z ram load cell parameters following calibration.

Date of calibration	DMaC parameters	
	Gain (N per V/V)	Offset (N)
10/01/2013	1.060E-08	1330
09/04/2014	1.089E-08	2000
28/11/2014	1.064E-08	1700
02/12/2015	1.076E-08	780

these values resulted in a maximum error of 205N and an average error of 14N.

The calibration method detailed here was repeated during each DMaC calibration conducted, and the final DMaC Z ram load cell parameters utilised following each calibration are detailed in Table 3.1.

3.2.2.2 DMaC measurement accuracy and data acquisition

As detailed by (Parish, 2015) the DMaC Z ram load cell is rated to 444kN with the manufacturer specifying a maximum error band of $\pm 0.06\%$ of full scale, which represents a maximum potential error band of ± 266N.

The extension of the Z ram linear actuator is measured by a linear encoder for which the manufacturer specified accuracy is $\pm 20\mu$m per m. With a maximum working stroke of 1m the maximum potential error is therefore $\pm 20\mu$m.

The data acquisition frequency can be specified individually for each DMaC test conducted, for the test work presented here a default data acquisition frequency of 50Hz was used.

3.2.3 IFREMER Materials in a Marine Environment Laboratory

One of the key aspects of investigating the durability of the Exeter Tether (Chapter 4) was to assess the affect of the marine environment on key material properties. To facilitate this aspect of the work an application was made to the MARINET FP7 programme (funded by the European Commission) to access the IFREMER Materials in a Marine Environment Laboratory, based in the IFREMER Brittany Centre, France.

Two weeks test time was awarded through this programme to focus on material testing for the Exeter Tether.

Facilities unique to this test laboratory that made it particularly suitable for this test work include the ability to age materials in natural seawater (pumped from the Brest Estuary around the laboratory) and accelerated ageing where the seawater temperature is heated to controlled temperatures to speed up the ageing process. In addition, facilities to fatigue multiple samples of material in sea water and to conduct ISO standard polymer tests on multiple samples as well as bespoke tests specific to the tether operation were all available.

The breadth of tests conducted over the time allocated in this facility is demonstrated by the schematic detailed in Figure 3.12.

Test equipment utilised at the IFREMER laboratory included:

- Instron 5566 load frame with 500N load cell (transverse displacement with no external extensometer). This was used for all tensile tests, including ISO37:2005.

- Instron 5566 load frame with 1,000N load cell. This was used for compression test measurements, including ISO 7743:2011.

- A bespoke fatigue test machine developed by IFREMER composed of a Parker electrical displacement piston PRA3810DS, with maximum force 1860N and maximum frequency 7Hz. This was used for tension fatigue testing of the samples and enabled 7 specimens to be simultaneously tested.

- MTS Systems Corporation, compression and tensile test machine, 100kN load cell. This was used for the compression fatigue cycling of samples.

- MTS Systems Corporation, compression and tensile test machine, 25kN load cell. This was used for further compression fatigue cycling.

- A Flir Thermovision A20 thermal imaging camera. This was used for temperature investigations into the self heating of the polymer material.

- Metravib DMA+150. This was used for Dynamic Mechanical Analysis of polymer samples.
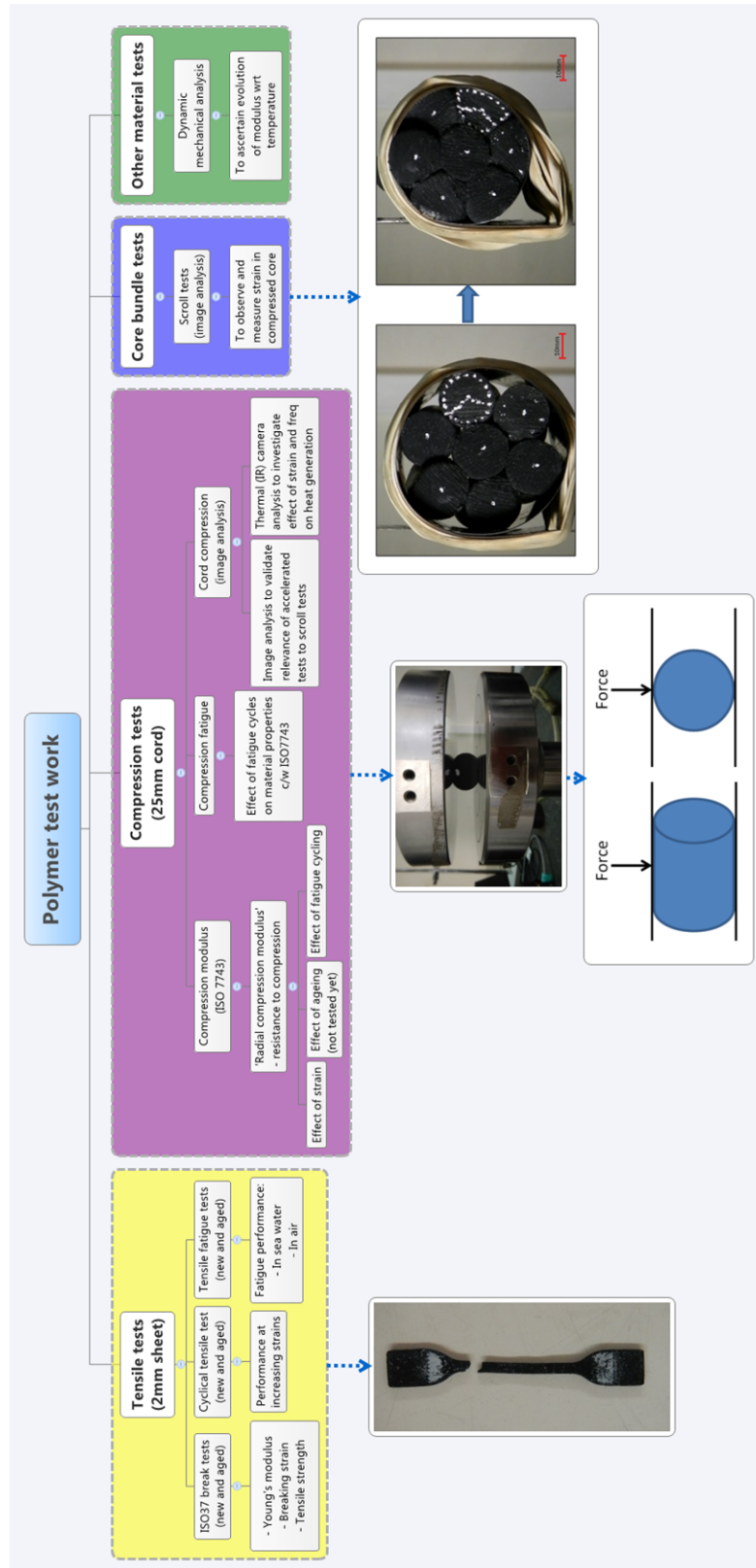
Figure 3.12: IFREMER test scope.

3.2.3.1 Calibration of test equipment at IFREMER

The IFREMER test laboratories are accredited to ISO 9001 Quality Management Systems. As part of this certification included in their Quality Management System an annual calibration of all test equipment is conducted.

3.2.4 Inspection and measurement techniques

The reliability assessment presented in Chapter 4 investigated the use of two key approaches for the physical identification of damage in the shackles. Firstly the use of X-Ray imaging to identify internal damage of the shackles was investigated, however it was found that the strength of the X-ray facilities available was not sufficient to penetrate the steel shackles and hence the resulting images could not be used to identify internal damage. The second approach utilised was 'dye penetrant inspection' which is a non destructive testing method for identifying fatigue cracks in components. This approach was found to successfully identify cracks in the shackles and was therefore the approach adopted to qualitatively assess the shackles for damage at the different stages of testing. The dye penetrant approach requires the generous application of dye penetrant over the cleaned surface of a component. The excess dye is then removed and a thin coating of developer is applied to the component. The developer is a dry, powder like substance that draws out the dye from any cracks that may be present in the component, making them clearly identifiable with the naked eye. The method is relatively quick to apply and non-destructive, so was the ideal technique for investigating any damage within the shackles during testing for the reliability assessment conducted in Chapter 4.

With the key methods and facilities outlined the next two chapters will present the reliability assessments. Chapter 4 will present the reliability assessment of a standard mooring component, a shackle. Chapter 5 will present the reliability assessment of a novel mooring component, the Exeter Tether. Each of these chapters will present an overview of the components, the specific methods applied, the results and a discussion section.

Chapter 4

Assessing safety margins for mooring system components: Reliability assessment of a standard mooring component

Contents

4.1   Introduction

As outlined in Chapter 3 the component selected for this investigation is a standard shackle. After outlining the specific shackle under investigation (Section 4.2), the following chapter will detail the methods applied (Section 4.3) and the results obtained (Section 4.4) for this reliability assessment. A detailed discussion of the results with reference to the wider literature is conducted in Section 4.5. A broader Discussion from this work, with reference to the research questions set out in Chapter 1, is detailed in the Thesis Discussion, Chapter 6. Final conclusions and next steps for this work are detailed in the Conclusions section, Chapter 7.

4.2   Shackle Selection

The shackle specification selected for this research should be appropriate for all steps of the investigation so that a set of identical shackles could be used throughout this study. Within reason there are no scale limitations for numerical modelling; DMaC testing can operate up to 30t dynamically; this leaves the load range of SWMTF as the deciding envelope to select the shackle specification for this work:

4.2.1   SWMTF working loads

The selected shackle must be appropriately rated to withstand the extreme loads imposed on the mooring system at SWMTF. In addition to this, as the effects of fatigue are of interest, it is important not to oversize the shackle and to ensure it remains susceptible to fatigue damage. As detailed in Section 3.2.1 data from the deployment over the period 16th September 2010 - 7th June 2011 is used as a reference for the load case. During this time a peak load of 52.5kN was measured but the majority of measured loads were below 20kN. (Harnois, 2014).

4.2.2 Fatigue considerations

To ensure the specified shackle is susceptible to fatigue loads it would be advantageous to have an understanding of the fatigue life and fatigue limit of potential options. A general definition of the fatigue limit is provided by Schijve (2003) *'the stress amplitude for which the fatigue life becomes infinite in view of the asymptotic character of the S-N curve'*. However, there is very limited material data available from shackle suppliers. Although the yield strength and the tensile strength is often provided, specific S-N curves detailing fatigue response are scarce. Defining the S-N response and fatigue limit of the different shackle options through experimentation would be a large undertaking, and is beyond the scope of this work, so estimation techniques were investigated. Various methods have been suggested to estimate fatigue limits for different materials (Bellows *et al.*, 1999; Dengel & Harig, 1980; Pascual & Meeker, 1999). However, a review paper conducted by Schijve (2003) concludes that fatigue limit approximations are limited and experimental techniques remain the most accurate approach to ascertain the fatigue limit. The contribution of computer modelling to the understanding of fatigue prediction is not addressed in Schijve's paper, and would prove an interesting area to further explore. Given there is no quick estimation of fatigue response, a further source of information to refer to for assistance with shackle specification is the DNV guidance previously discussed.

4.2.2.1 Shackle guidance

In the DNV guidance for position mooring (Det Norske Veritas, 2010a) reference is made to the S-N curves detailed in their *Recommended practice for fatigue design of offshore steel structures* (Det Norske Veritas, 2011). This second document provides the parameters for numerous S-N curves, including details for category B1 which Det Norske Veritas (2010a) refers to as appropriate for calculating the fatigue life of a long term mooring shackle. S-N curves are experimentally derived and provide information relating stress range to cycles to failure for a given material or component. The S-N curves provided in Det Norske Veritas (2011) are based on the *'mean minus two standard deviation curves for relevant experimental data'* and are thus associated with 97.7% probability of survival. The curves are based on tension-tension fatigue testing.

S-N Curve (B1)	Cycle number	Curve parameters	
		m_1	$log\bar{a}$
Air	$N \leq 10^7$ cycles	4	15.117
	$N > 10^7$ cycles	5	17.146
Sea water: Free corrosion	All cycles	3	12.436
Sea water: Cathodic protection	$N \leq 10^6$ cycles	4	14.917
	$N > 10^6$ cycles	5	17.146

Table 4.1: S-N parameters for B1 category, summarised from Det Norske Veritas (2011)

For clarity, the S-N curves detailed in relation to long term mooring shackles will be explained here. The concept of the S-N curve is first introduced in Chapter 2, Section 2.3.2.6, Page 65. The general equation for an S-N curve is:

$$logN = log\bar{a} - mlog\Delta\sigma \qquad (4.1)$$

Where:

$N =$ Number of cycles to failure

$\bar{a} =$ Intercept of the x-axis

$m =$ Slope of the S-N curve

$\Delta\sigma =$ Stress range

Within the guidance values are provided for different S-N curves within the B1 construction category. The curves detailed include fatigue life in air, in seawater with cathodic protection and in seawater with free corrosion. The parameters for these curves are provided in Table 4.1. The curves themselves are plotted in Figure 4.1. These curves provide estimations for the fatigue life, in terms of number of cycles at a defined stress range, but do not identify a fatigue limit. The curves were therefore used to specify a shackle ensuring that the fatigue life of the shackle exceeded the worst case load profile for the proposed deployment time.
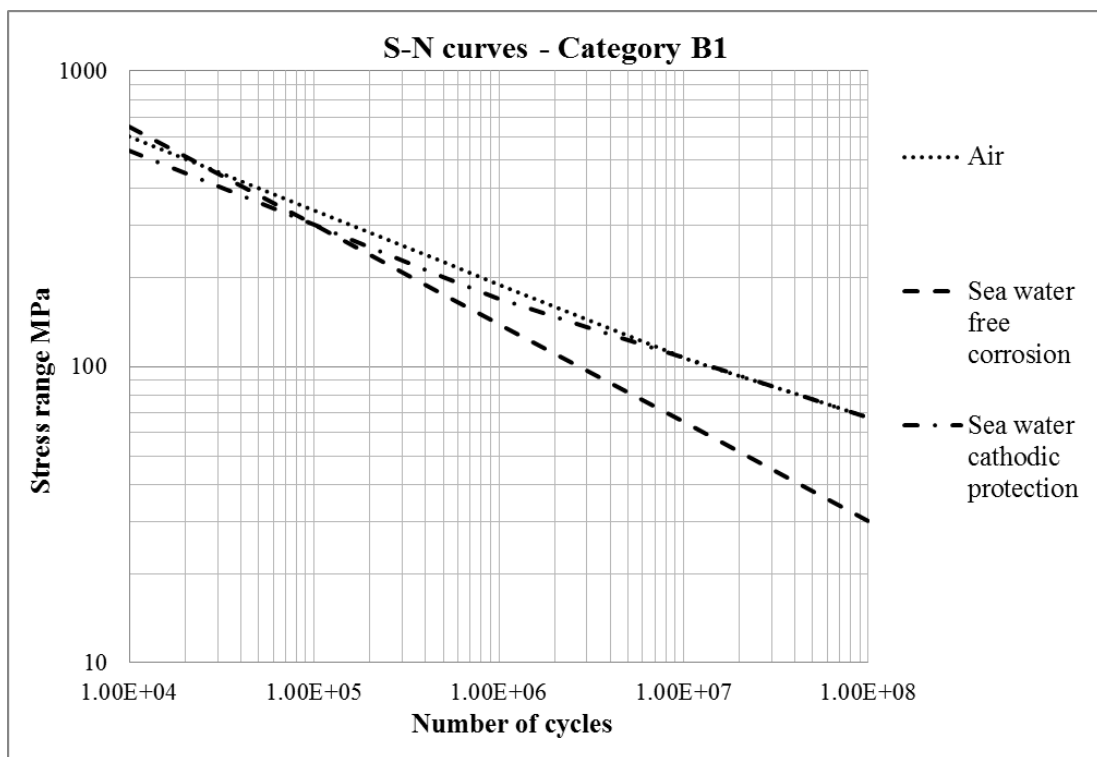
Figure 4.1: S-N curves for B1 category, summarised from Det Norske Veritas (2011)

4.2.3   Selected shackle specification

Shackles are specified by a Safe Working Load (SWL) or Working Load Limit (WLL). This is the maximum load the shackle should be exposed to in use. A Minimum Breaking Load (MBL) is also specified, which is the minimum load required to cause failure of the shackle. The MBL is related to the WLL by a safety factor (SF) as detailed in equation 4.2:

$$MBL = WLL \times SF \tag{4.2}$$

The safety factor applied ranges depending on the specification but is often 4 - 6. Shackles are generally specified in tonnes.

Given the considerations discussed above, a shackle with an MBL from 10 - 14 tonnes was sought for the case study; this should avoid complete failure at SWMTF but allow some fatigue damage in the region of mooring forces anticipated at the SWMTF. A further limiting factor for the specification of the shackle was also dimensions; as shackle design has developed, shackle dimensions have reduced resulting in very strong shackles at a minimal size. This was a consideration in specifying the shackle as the dimensions must enable the shackle to be installed into the existing mooring line system of the SWMTF without significant alteration.

Given the above requirements the following shackle was specified:

- British standard 3032

- Galvanized steel shackle

- Working load limit: 2.5t (24.5kN)

- FoS: 5

- Minimum breaking load: 12.5t (122.6kN)

- Material yield point: 890MPa

- Material ultimate strength: 1010MPa

- Dimensions detailed in Figure 4.2
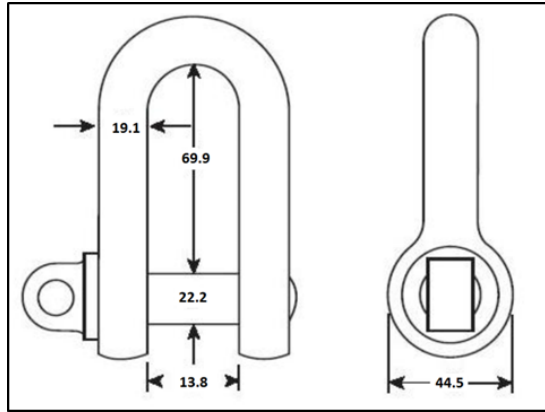
Figure 4.2: Specified shackle dimensions

The maximum load of 52.5kN measured at SWMTF is higher than the WLL of 24.5kN but well within the minimum breaking load of the shackle (122.6kN). In terms of fatigue life, at the peak measured load of 52.5kN, the nominal tensile stress in the selected shackle bow is 91.6MPa (the equation for this is fully detailed in Equation 4.3, Section 4.3.3, 175). Referring to the applicable S-N curve detailed in Figure 4.1 this relates to 1.86E+7 cycles to failure. At a typical wave period of 8 seconds this equates to a fatigue failure at 4.7 years. As this is based on the peak load measurement the actual load profile that the shackle will be exposed to will be considerably less so this can be regarded as a very conservative estimate. It was therefore assumed that the specified shackle would comfortably survive a 6 month field deployment, whilst being exposed to a certain level of fatigue damage.

A total of 15 shackles were ordered, with the intention of using 2 shackles to define shackle breaking load and yield load, the the remainder to investigate the fatigue performance of the shackles in controlled laboratory testing and during field trials.

4.3   Method

4.3.1   Shackle numerical investigation

Following a review of commercial FEA packages, ANSYS Mechanical was selected to conduct the numerical modelling. The main reason this software was selected was due to the Fatigue Tool available in mechanical analysis which was required for a full analysis of the shackle.

Before introducing the numerical model set up, it should be highlighted that there are several challenges regarding the numerical modelling of the stresses within a component such as a shackle. The load contact areas and resulting Hertzian contact stress is complex to model as highlighted by (Oysu, 2007) and requires particular attention. Capturing this accurately in a 3D finite element numerical model is challenging. Optimisation of the contact areas will be further discussed in Section 4.3.1.1, Page 159. In addition, the complex stress distribution within the shackle assembly, which includes direct, bending and shear stresses is challenging to model and extracting the relevant results is also a complex task. These shortcomings when using FEA to model a complex system such as the shackle assembly should be highlighted at this stage. The numerical model will provide some indication of the stress distribution within the shackle and potential weak points susceptible to failure; however absolute values should be used with caution. Given the numerical model developed for this work is linear elastic, it should also be noted that absolute stress values beyond the yield strength of the material will be inaccurate. It is important to consider these shortcomings when drawing any conclusions from such a model.

4.3.1.1   Model set up and boundary conditions

CAD[1] models of the shackle and the pin provided by the shackle supplier were imported into ANSYS. The models were meshed using tetrahedron elements; these are the default element type and are suitable for adaptive refinement of the mesh, a process whereby the mesh is optimised at particular locations of the model that require a more accurate solution. A material designated 'Certex Steel' was created and assigned the material properties specified by the shackle supplier as detailed in Section 4.2 and applied to the parts within the shackle models.

The first FEA models developed were separate models for the pin and the bow of the shackle with loads and boundary conditions applied to each part individually. However, significant stress concentrations developed where the boundary conditions were applied to each of models, so an assembly model was developed incorporating both the pin and the bow. Although this reduced some of the unrealistic stress concentrations, the boundary condition applied to the top of the bow where the displacement was fixed (essentially to anchor the model in space), still showed significant stress concentrations

---

[1]Computer Aided Design.
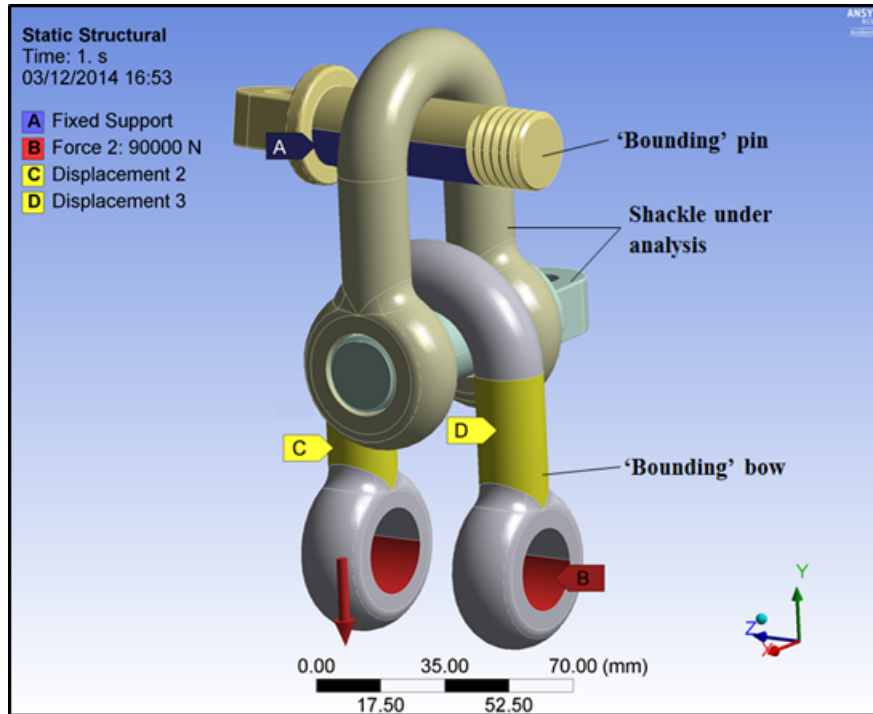
Figure 4.3: FEA model set up, including the use of a 'bounding' pin and bow to apply the boundary conditions. In this figure a load of 90,000N is applied as Force B, however this was altered for different investigations. The fixed supports and displacements labelled A, C and D were consistent for all of the models reported. Support A was fixed in all directions, whilst C and D were restricted from movement in X and Z directions but free to move in the Y direction.

around the edges of the boundary condition. To overcome the issue of the applied boundary conditions directly affecting the parts of interest, two additional parts were added into the model. Referred to as 'bounding' parts in this work, the boundary conditions were then applied to the 'bounding' parts, leaving the shackle under analysis free of any boundary conditions and hence free of unrealistic stress concentrations. Figure 4.3 details the model set up including the bounding pin and bounding bow with the applied boundary conditions.

The boundary conditions detailed in Figure 4.3 include (A) which is a fixed support on the bounding pin; fixed in all directions this condition essentially anchors the model in space. Fixed displacements (C) and (D) were included to prevent the arms of the bounding bow from pulling together when a load was applied; these surfaces were fixed

from movement in the X and Z directions but free to move in the Y direction. Finally, a force was applied, labelled (B), this force was evenly distributed across the two eyes of the bounding bow as detailed in the figure.

4.3.1.2   Contact regions and element types

Creating the model described above by incorporating the bounding pin and bow eliminated unrealistic stresses occurring on the shackle under investigation, however it significantly increased the complexity of the model by introducing multiple 'contact regions'. Contact regions are created when two separate components meet, and for an FEA model processing multiple contact regions can be computationally expensive. As detailed in ANSYS (2013), contact regions have particular properties, namely they:

- *"Do not 'inter-penetrate'*

- *Can transmit compressive normal forces and tangential friction forces*

- *Can be bonded together (linear)*

- *Can separate and collide (non-linear)"*

Each contact region can be defined individually depending on the requirements of the model. The relevant contact types for 3D models are detailed in ANSYS (2013) and are summarised below:

- **Bonded:** No sliding or separation can occur between faces which are essentially glued together. This allows for a linear solution as the contact area remains constant during load application.

- **Frictionless:** Zero coefficient of friction allowing free sliding of surfaces. Standard unilateral contact so gaps can occur resulting in a normal pressure of zero. This is a non-linear contact.

- **Rough:** This contact assumes perfectly rough frictional contact with no sliding. As above, gaps can occur resulting in a normal pressure of zero. This is also a non-linear contact.

Table 4.2: FEA model contact type for each specified contact region as detailed in
Figure 4.4. Bow model has contact types specified for an optimum solution for the
main bow; pin model has contact types specified for an optimum solution for the main
pin.

Label	Components		Contact type (Bow model)	Contact type (Pin model)
A	Bounding pin	Main bow	Frictional	Bonded
B	Main pin	Bounding bow	Bonded	Frictional
C	Main bow	Main pin thread	Bonded	Bonded
D	Main bow	Main pin face	Bonded	Bonded
E	Main bow	Main pin barrel	Bonded	Bonded

- **Frictional:** This contact allows the specification of a coefficient of friction, and
  hence contact surfaces can carry shear stresses up to a certain limit before sliding
  occurs. Again, gaps can occur resulting in a normal pressure of zero. This is also
  a non-linear contact.

When creating a model the choice of contact type will affect the solution time of
the model, with non-linear contacts increasing the solution time and sometimes leading
to convergence issues. Despite being computationally demanding, if calculating the
stresses around a contact area is important then the non-linear contacts are preferential
as they provide a more accurate representation of the contact area.

When developing the shackle model, due to the large number of contacts present,
the choice of contact type had a large effect on the stability of the models, with the
more accurate 'frictional' contact causing convergence issues. To resolve this problem
two separate models were developed; one with contact types specified to optimise the
solution for the shackle pin, and the other with contact types specified to optimise the
solution for the shackle bow.

Figure 4.4 details all the contact areas present in all the shackle models, and Table
4.2 details the specified contact types assigned to each specific model developed. An
ideal model would have a frictional contact type specified for region A and region B
but this led to an unstable model so two separate models were developed.

The frictional contact regions were assigned a coefficient of friction of 0.5 based on
a typical static coefficient of friction for steel (Oberg *et al.*, 1984).
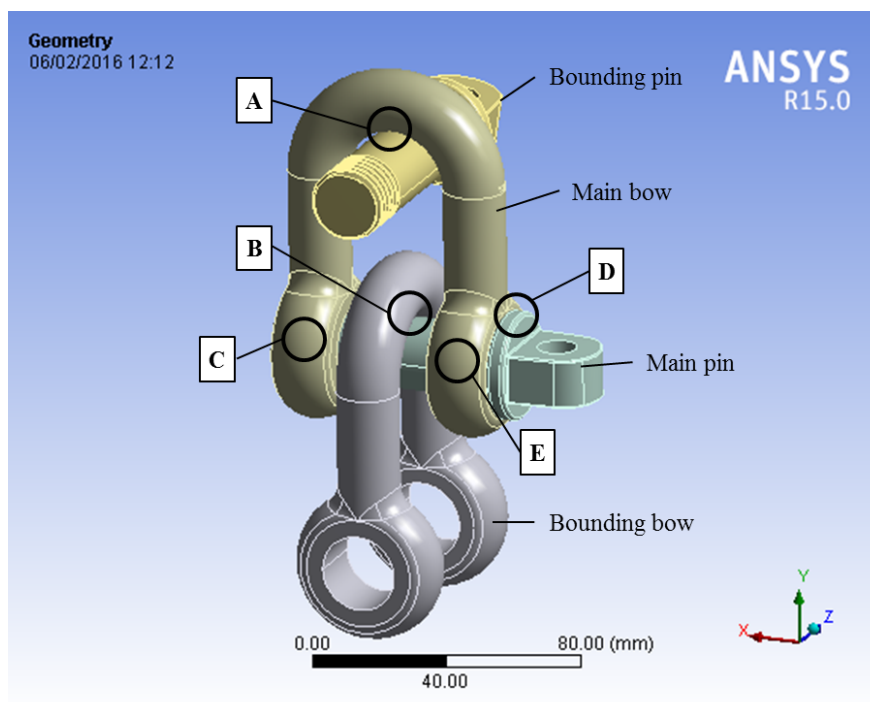
Figure 4.4: FEA model contact region specification to read in conjunction with Table 4.2.

The majority of the elements within the FEA model are SOLID187 elements. These
are 3-D, quadratic, 10-node tetrahedral elements as detailed in ANSYS (2013). Where
contact regions are defined in the model, CONTA174 and TARGE170 elements are
used to define the contact and target surfaces respectively. These 3-D elements are
assigned to the defined contact areas and allow contact to be broken and re-established
and sliding to occur with Coulomb friction.

4.3.1.3 Mesh optimisation

ANSYS default tetrahedron elements were used to mesh the parts within the assembly.
A 'relevance centre' of fine was specified (relevance centre dictates the 'fineness' of the
mesh (ANSYS, 2013)) with 'smoothing' set to medium (smoothing iterations are used
to improve element quality). The non-linear interactions between the components at
the contact regions specified frictional above (either A or B depending on the model)
are critical regions in terms of the load path through the assembly and the stress
developing within the components. To further improve the solutions obtained at these
points, mesh optimisation was undertaken to improve the mesh around the contact
area and hence resolve to a more accurate solution. A 4mm 'sphere of influence' was
created at the contact point with 1mm specified element size.

4.3.1.4 Model evaluation

Due to the use of non-linear contacts in the model development, multiple refinement
iterations were conducted by ANSYS to converge on an accurate solution. In a sta-
ble model the solution at each iteration is closer than the last and a final solution is
achieved when the change between iterations is less than a pre-defined value (ANSYS
default is 20%).

In addition to the ANSYS default convergence, specific convergence criteria can be
user defined for a particular result of interest. Adaptive convergence can be selected so
that at each iteration the mesh is optimised in order to achieve an improved solution.
Again, due to the criticality of the contact regions in the models discussed, convergence
criteria were specified for these models. Convergence criteria were set for the equiva-
lent stress on the contact surface of the bow (in the bow optimised model) or the pin
(in the pin optimised model). A 10% allowable change convergence criterion between

iterations of was set.

Analytical estimations should be used to evaluate the FEA models to ensure the results obtained are within the expected range. Nominal stress within the bow arms was evaluated using Equation 4.3:

$$\sigma_{nom} = \frac{F}{A} \tag{4.3}$$

Where:

σ_{nom} = nominal stress

F = applied load

A = area (in this case 2 x the cross sectional area of the bow arm)

The calculated nominal stress was compared to the principal stress calculated by the FEA model for the centre of the bow arms to ensure it is in the correct region.

In addition to the nominal stress, the contact stress can be calculated by assuming the contact of the pin and the bow can be represented by the contact between two cylinders. This method is detailed by Pilkey (2005) and shown in Equation 4.4:

$$\sigma_c = 0.579 n_c [\frac{F}{K^2 \gamma^2}]^{\frac{1}{3}} \tag{4.4}$$

Where:

σ_c = contact stress

n_c = the ratio between cylinder diameters, D_1 (19mm) and D_2 (22mm). The ratio of $\frac{D_1}{D_2}$ = 0.8636 and using the look up table published by Pilkey (2005) this equates to $n_c = 0.998565$.

F = applied load

$K = \frac{D_1 D_2}{D_1 + D_2} = 10.2$

$\gamma = \frac{1-v_1^2}{E_1} + \frac{1-v_2^2}{E_2}$

v = Poisson's ratio

E = Young's Modulus

When both cylinders are made from the same material, as is the case with the shackle model, γ simplifies to $\gamma = \frac{2-2v^2}{E}$. Assuming typical values for high tensile steel of $E = 2000GPa$ and $v = 0.3$ (Young & Budynas, 2002), $\gamma = 0.0000091(\frac{1}{MPa})$
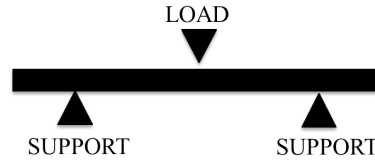
Figure 4.5: A schematic of the approach used to evaluate the stress within the shackle pin model by assuming beam bending using the three point bend model.

A contact tool was inserted into the FEA model and used to calculate the pressure between two contact areas within the model. This was directly compared to the contact stress calculated analytically to evaluate the model.

To evaluate the pin optimised model bending equations were utilised, modelling the pin as a beam. A 'three point bend' test condition was assumed as detailed in Figure 4.5. Although this does not directly replicate the physical bounding of the pin within the bow eyes it should provide some assurance that the values calculated by the FEA model are in the correct region. The maximum bending stress can be calculated by modelling the pin as a 'slender circular beam' with support at either end (provided by the eyes of the bow) and the load applied centrally. The maximum bending stress is calculated by Equation 4.5 (Young & Budynas, 2002):

$$\sigma_b = \frac{FL}{\pi R^3} \tag{4.5}$$

Where:
σ_b = maximum bending stress
F = applied load
L = support span (in this case, distance between shackle eyes)
R = radius of pin.
This model assumes that the pin is free to pivot at either end with no restriction; this is a simplification of the physical situation but should enable some assessment of the FEA model.

Equation 4.5 was used to calculate an estimate for the maximum bending stress in the pin and this value was compared to the maximum principal stress extracted from the FEA model of the pin at the furthest distance from the neutral axis (where the peak bending stress occurred).

4.3.1.5   Load specification

As detailed in Figure 4.3, a load was applied in the negative Y direction, distributed over the eyes of the bounding bow. In the numerical model the load was parametrised and a 'parameter set' developed to calculate key model results at a range of load levels.

Particular load cases of interest for this work include:

1. Maximum mooring load measured at SWMTF: 52.5kN (Harnois, 2014).

2. Specified working load limit of shackle: 24.5kN

3. Maximum load specified for fatigue testing load range: 90kN (as detailed in Section 4.3.2.2, Page 172)

4. Specified minimum breaking load of shackle: 122.6kN

5. Mean measured breaking load of shackle: 201.5kN (as detailed in Section 4.4.2.1, Page 195).

4.3.1.6   Result selection

Numerous results are obtainable from the FEA models. In this Chapter a selection of the most appropriate results from the models are presented.

To understand the potential failure modes in the context of fracture mechanics, a brief overview of the potential modes of crack failure (Anderson & Anderson, 2005) is included here. These are detailed in Figure 4.6 and include:

- Mode I: Opening mode, where the principal stress is applied normal to the crack plane.

- Mode II: In plane shear, where a shear stress acts parallel to the plane of the crack and slides one crack face over another (also known as sliding mode).

- Mode III: Out of plane shear, where a shear stress acts parallel to the plane of the crack but out of plane (also known as tearing mode).

In terms of results selection for the numerical model, it is important to highlight that a crack can be loaded in any of these three modes or a combination of these modes. The results output from the numerical model will therefore be a simplification
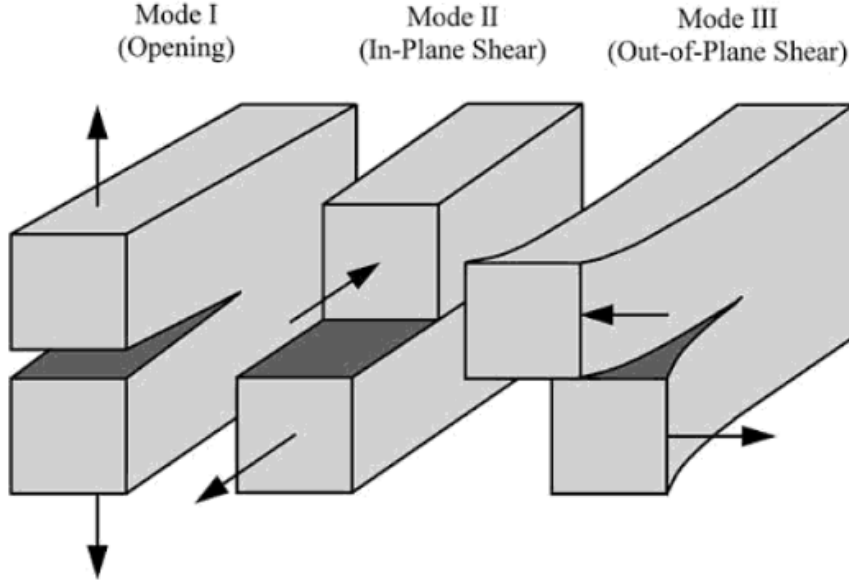
Figure 4.6: Three fracture modes, replicated from (Anderson & Anderson, 2005)

of the real stress state within the shackle. Results from physical testing of the shackles will be informative for the numerical modelling as it will highlight the failure modes of the shackles and hence the corresponding stress state can be investigated from the numerical models.

Equivalent stress, σ_v, (also known as von Mises stress) is a useful value as it describes a complex three-dimensional stress state with one value. This value can then be compared against the yield or ultimate strength of the material. The full calculation for equivalent stress accounts for the principal stresses and the shear stresses as shown in Equation 4.6, however ANSYS utilises a common simplification, just accounting for the principal stresses as detailed in Equation 4.7 (ANSYS, 2013):

$$\sigma_v = \sqrt{\frac{(\sigma_{11} - \sigma_{22})^2 + (\sigma_{22} - \sigma_{33})^2 + (\sigma_{11} - \sigma_{33})^2 + 6(\sigma_{12}^2 + \sigma_{23}^2 + \sigma_{31}^2)}{2}} \qquad (4.6)$$

$$\sigma_v = \sqrt{\frac{(\sigma_{11} - \sigma_{22})^2 + (\sigma_{22} - \sigma_{33})^2 + (\sigma_{11} - \sigma_{33})^2}{2}} \qquad (4.7)$$

Where:

σ_{11}, σ_{22} and σ_{33} = principal stresses

σ_{12}, σ_{23} and σ_{31} = shear stresses

Equivalent stress is a quick approach for reviewing the overall stress state of a component, however, all results are absolute due to the squaring of the terms (as detailed in Equations 4.6 and 4.7). Tensile stresses are of more concern in the shackle assembly, as compressive stresses are not likely to lead to fatigue failure, so knowledge of whether the stress is compressive or tensile is important. Due to this shortcoming with equivalent stress, maximum principal stress results were also assessed which allowed the results to be reviewed in relation to the tensile or compressive nature of the stress. The principal stresses occur normal to the principal planes, which are identified as a set of mutually perpendicular planes where the shear stress is zero. The maximum principal stress is therefore the largest normal stress occurring on all conceivable planes through a point, which makes it a useful failure criterion (Nash, 1992).

In addition to detailing specific stresses, ANSYS can also be used to review safety factors present in a component in relation to either the material ultimate tensile strength or the material yield strength. Plotting these results in contours is a useful way to visualise results as anything with a factor of safety (FOS) of 1 or less suggests the calculated maximum principal stress has exceeded the ultimate tensile strength or yield strength (whichever is specified) of the material. In the results presented for the shackle model, the safety factors presented are based on maximum tensile stress theory and in relation to ultimate tensile strength. This theory is based on failure occurring when the maximum principal stress exceeds a tensile stress limit (ultimate tensile strength in this case). The theory is expressed as a design goal by ANSYS (2013) and detailed in Equation 4.8.

$$\frac{\sigma_1}{\sigma_u} < 1 \tag{4.8}$$

Where:

σ_1 = Maximum principal stress

σ_u = Ultimate tensile strength

4.3.1.7 Numerical modelling of fatigue performance

Although the static models of the shackle are very informative for identifying areas of weakness within the shackle and predicting the potential failure load of the shackle, they

do not fully reflect the loading profile the shackle will be subjected to during operation. Any component installed on a WEC mooring line will be exposed to cyclical, fatigue loads. In the work presented in this Chapter, the experimental methods will expose a series of test shackles to a fatigue testing regime. The full details of the test regime are provided in Section 4.3.2.2, but for the purposes of defining the numerical modelling parameters in this section, the experimental testing fatigue load regime is 10 - 90kN.

A 'Fatigue Tool' was created within the numerical model to estimate the fatigue life of the shackle when subject to a cyclical applied load of 90kN. A loading ratio of 0.1111 was specified to account for the ratio between minimum and maximum applied loads (10kN and 90kN respectively) based on Equation 4.9 (Boyce & Ritchie, 2001).

$$R = \frac{L_{min}}{L_{max}} \quad (4.9)$$

Where:

R = Loading Ratio

L_{min} = Minimum applied load

L_{max} = Maximum applied load

A stress-life approach was specified (based on the use of the DNV S-N curve for air as detailed in Figure 4.1, Page 156) and the tool was set to calculate fatigue life based on maximum principal stress.

4.3.2 Shackle experimental methods

Prior to starting any experimental testing using the DMaC test facility, 'Dye penetrant inspection' (DPI) as described in Chapter 3, Page 149 was used to assess the shackles as received from the suppliers and ensure that no fatigue cracks were present.

4.3.2.1 Experimental Ultimate Limit State

The purpose of these tests was to evaluate shackle ultimate tensile strength for comparison to supplier specification. This enabled the 'embedded safety factor' present within the shackle to be established, this embedded safety factor is additional to the safety factor specified by the shackle supplier. Further to this, the yield point of the shackle
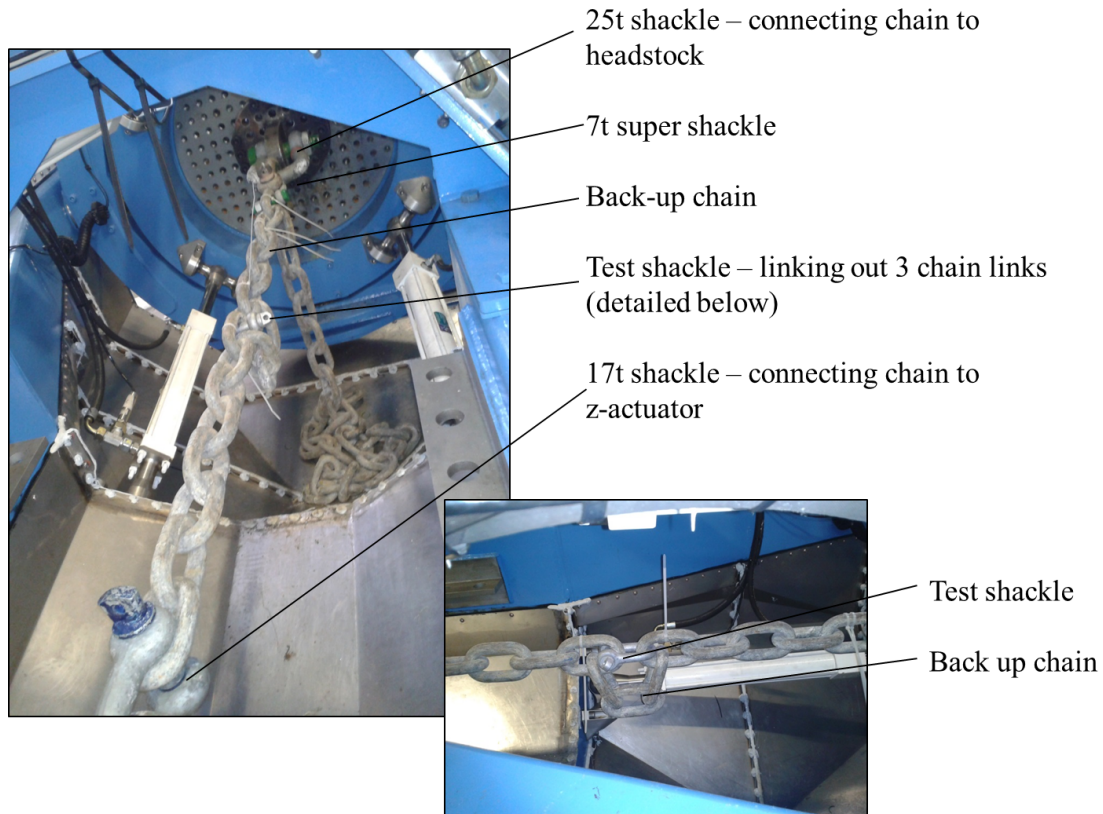
Figure 4.7: Ultimate strength test shackle arrangement in DMaC

was to be established to inform the accelerated testing regime (fatigue tests).

Experimental set up

Each test shackle was installed in DMaC utilising a chain which was attached to the headstock and Z-ram with a series of larger shackles. The shackle under test was installed by linking out three links of the chain, insuring that if the shackle should break unexpectedly, the chain would act as a back-up line and no damage would be caused. Figure 4.7 details the set up within DMaC.

Experimental procedure

171

4. ASSESSING SAFETY MARGINS FOR MOORING SYSTEM COMPONENTS: RELIABILITY ASSESSMENT OF A STANDARD MOORING COMPONENT

Before conducting the final break test, some low level force driven tests were conducted to ascertain the response of the chain arrangement. Although minimal extension was expected from the chain, some force driven characterisation tests were conducted both with and without the shackle in the set up, to ensure extension could be attributed to the shackle rather than the chain. These preliminary tests were always conducted in force mode to ensure no excessive loads were applied to the shackle prior to the break test. The maximum load applied during these tests was 100,000N, below the MBL of the shackle.

The final break tests were conducted with DMaC in displacement mode as this provides more control at the point of break. A displacement of 0.1m was specified to ensure complete failure of the shackle in one cycle. Two separate ultimate strength tests were conducted on Shackle A and Shackle B.

4.3.2.2 Experimental Fatigue Limit State

Any mooring system for a floating body will be subjected to repeated cyclical loading based on the rise and fall of waves. This series of fatigue tests were intended to provide 'accelerated testing' of a set of shackles to establish a longer term response to fatigue loading. This series of testing had two main intentions:

1. Observe the fatigue performance of a set of shackles

2. Pre-age a set of shackles for further field testing at the SWMTF.

To investigate the different stages of fatigue failure, from the development of the initial fatigue crack to the final failure, different shackles were exposed to a range of fatigue regimes. The range of fatigue exposure could be achieved by either altering the amplitude of the load applied, or by altering the number of loading cycles. To keep the complexity of the testing to a minimum, constant amplitude loading was conducted and different fatigue exposure levels were defined by altering the number of cycles. This allowed multiple shackles to be tested in series, exposed to an identical load range with select shackles being removed from the testing after a certain number of fatigue cycles had been conducted.

To ensure the fatigue tests were conducted below the yield point of the shackles, results from the ultimate strength tests were used to define the loading regime for the

fatigue tests. In addition, to avoid the load dropping off entirely at the lower end of the load range (and to more realistically represent the pre-load of a mooring system) a minimum load of 10kN was specified. The final specified load range for the fatigue testing was therefore 10kN - 90kN.

A final variable for this experimental set up was the frequency of the loading regime. A typical wave period observed at the SWMTF will range between 2s - 10s (Harnois *et al.*, 2013) relating to frequencies of 0.5Hz - 0.1Hz respectively. The intention of accelerated testing is to speed up the testing process by subjecting a sample to loads at an increased rate to establish a better understanding of longer term fatigue performance. The ultimate aim is to optimise the frequency of the fatigue cycles to minimise test time, whilst ensuring the required loads can still be achieved. To this end, a range of frequencies were tested at the specified load range (10kN - 90kN). 2Hz was concluded to be the highest frequency possible whilst still achieving good accuracy in meeting the peak loads.

The final fatigue testing regime was therefore a load range of 10kN - 90kN at a cycle frequency of 2Hz.

Observing DMaC operation during the ultimate strength test it was felt the back-up chain was not necessary for these tests; the DMaC control system coped well responding to the sudden 'no-load' immediately after a failure. The shackles for these tests were therefore installed in DMaC using the chain and some additional shackles as detailed in Figure 4.8, without the back-up system. Initially six shackles were installed in series (Figure 4.8), with some shackles removed and others added throughout the testing regime to provide a set of aged shackles with varying fatigue exposure.

The first series of fatigue tests were conducted on 8 shackles, numbered 4 to 11. Following this first series of tests, DPI testing was used to observe the formation of any fatigue cracks in the shackles. Different shackles were exposed to a different number of fatigue cycles; some were cycled to failure, others were cycled to induce fatigue cracks, whilst others were exposed to even less cycles to pre-age them for the SWMTF deployment. Following inspection with DPI, those shackles that had been exposed to the lowest fatigue cycling regime were then deployed on the SWMTF as detailed below in Section 4.3.2.3.

On retrieval from the SWMTF the remaining shackles were exposed to a second series of fatigue cycles, at the same specified parameters as the first (2Hz, 10 - 90kN).
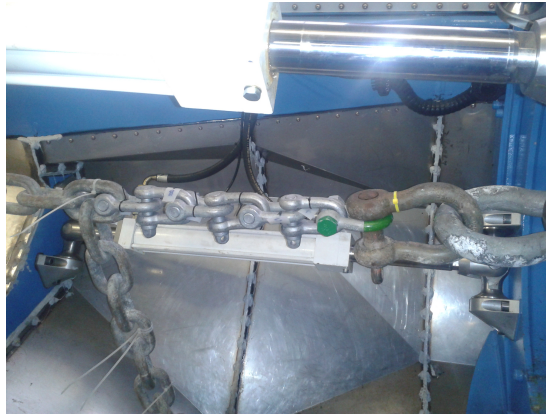
Figure 4.8: Fatigue test shackle arrangement in DMaC

The shackles in this series of tests were all cycled to failure and the failure mechanism for each shackle was noted. The range of cycles to failure and failure mechanism is detailed in Results Section 4.4.3. Table 4.3 outlines the shackle numbers and whether they were exposed to the first series of fatigue tests, the SWTMFT deployment and / or the second series of fatigue tests.

4.3.2.3 Experimental field testing

Following the experimental fatigue tests, to enable exposure to real sea conditions, a set of shackles were deployed on a mooring limb of the SWMTF data buoy. These shackles included 5 new, un-fatigued shackles (Shackles 1, 2, 3, 12 and 13), and 2 shackles that had undergone 5,034 cycles of fatigue testing (Shackles 10 and 11) as specified in the previous section. DPI was used to visually check the shackles for fatigue cracks following the accelerated fatigue testing and no cracks were observed prior to deployment.

As discussed in Chapter 3 these seven shackles were deployed on mooring limb 3 during the period 4$^{\text{th}}$ June 2013 - 26$^{\text{th}}$ November 2013. To protect the SWMTF in the event of a shackle failure, the shackles were inserted onto the mooring limb linking out a portion of 2m DN24 open link galvanised chain. Should a shackle fail, the chain would then act as a back up for the mooring system. Two 9.5 tonne super shackles were used to link the test shackles into the chain, and sacrificial anodes were installed on each of these super shackles to minimise corrosion of the test shackles. The mooring limb set up can be seen in Figure 4.9, taken during the deployment.

Table 4.3: Shackle test exposure summary. Shackles 6 and 9 failed during Fatigue 1st series so no option of SWMFT deployment or 2nd series fatigue testing.

Shackle Number	Fatigue 1st series	SWMTF deployment	Fatigue 2nd series
1	✗	✓	✓
2	✗	✓	✓
3	✗	✓	✓
4	✓	✗	✓
5	✓	✗	✓
6	✓		
7	✓	✗	✗
8	✓	✗	✗
9	✓		
10	✓	✓	✓
11	✓	✓	✓
12	✗	✓	✓
13	✗	✓	✓

Following the SWMFT deployment, the shackles were retrieved and again subjected to DPI to investigate the development of any cracks. The shackles were then re-installed into DMaC and exposed to further fatigue cycling to failure, under the same test parameters as detailed for the original fatigue testing; namely 2Hz cycle frequency and a cyclical load of 10 - 90kN.

4.3.3 Shackle analytical fatigue estimations

As detailed in Section 4.2.2.1, Det Norske Veritas (2011) provide S-N parameters that can be utilised for the fatigue life estimation of shackles in mooring systems. Det Norske Veritas (2010a) states the S-N curves should be used with *"appropriate stress concentration factors (SCF) obtained by a finite element method"*. Figure 4.1, Page 156 detailed the range of S-N curves specified in this standard; the laboratory fatigue testing presented within this Thesis was conducted in air, so the relevant S-N curve for fatigue in air was utilised. The S-N curve relates the applied stress range of the cyclical loading to the number of cycles to failure. To compare this in practice to the WLL of the shackle or to relate this to the load applied during physical tests, the stress generated from a given applied load must be calculated. The nominal tensile stress is
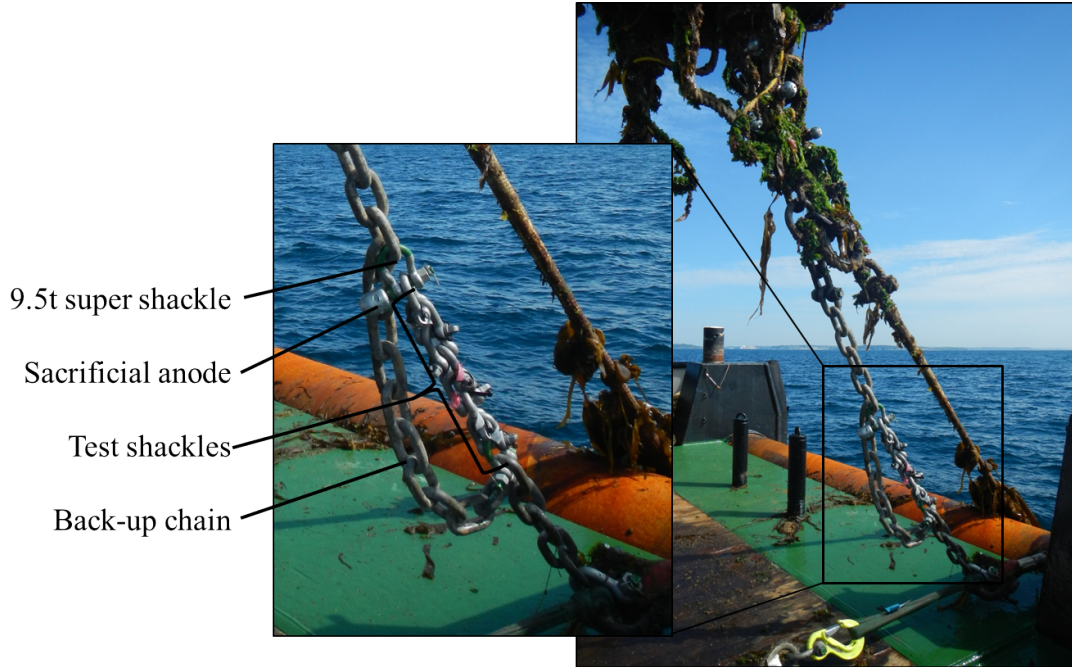
Figure 4.9: Field test shackle arrangement for SWMTF deployment

calculated using Equation 4.3 detailed on Page 165.

The nominal tensile stress is calculated at the maximum load of the fatigue cycles, σ_{max}, and at the minimum load of the fatigue cycles, σ_{min}. The nominal stress amplitude, σ_a, is simply calculated by:

$$\sigma_a = \frac{\sigma_{max} - \sigma_{min}}{2} \tag{4.10}$$

The nominal stress range, $\Delta\sigma_{nom}$, can then be calculated by:

$$\Delta\sigma_{nom} = 2\sigma_a \tag{4.11}$$

Once the nominal stress range is established, this must be multiplied by an appropriate stress concentration factor to calculate a stress range for use with the S-N curve.

4.3.3.1 Stress concentration factor

A stress concentration factor (K_t) defines the maximum stress in a component in relation to the nominal stress. Numerical models of components can be interrogated to display the maximum principal stress (σ_{Pmax}) at particular points of interest within

the component. The stress at a particular point is divided by the nominal stress to provide a value for the stress concentration factor, K_t at that point, as detailed in Equation 4.12.

$$K_t = \frac{\sigma_{max}}{\sigma_{nom}} \tag{4.12}$$

For this work, the numerical model introduced in Section 4.3.1 was used to quantify the stress concentration factors within the shackle assembly. Results from the numerical model presented in the Results Section 4.4.1.4, Page 185, were used to identify the paths anticipated to capture the peak stress concentrations in the model, in addition to providing an overview of the stress distribution within the assembly. The paths run through the centre of the cross section of the model and 12 equidistant points were set up along each path to extract the maximum principal stress. As previously discussed in Section 4.3.1 two separate FEA models were developed; one optimised for the bow results and one optimised for the pin results. These separate models were used to define the paths detailed in Figure 4.10, with paths 1, 2, 3 and 7 set up in the bow optimised model and paths 4, 5 and 6 set up in the pin optimised model. As the calculation of K_t was ultimately for use with the fatigue results, the load in the FEA model was set at 90kN, representing the peak load used for the fatigue testing regime.

It should be noted that this approach, utilising maximum principal stress, is only strictly applicable for load paths 3 and 7 where the loading will be predominantly tensile (leading to failure Mode I as discussed in Section 4.3.1.6, Page 167). Failures occurring on load paths 1, 4, 5 and 6 are likely to be shear stress dominated (Mode II) whilst failures on load path 2 will be subject to a combination of tensile and shear loading. However, given the calculated value for K_t is for use with the DNV S-N curve (presented in Section 4.2.2.1, Page 156) which represents tension-tension fatigue life, the above approach utilising principal stress will be utilised across all the identified paths for illustrative purposes. This simplification highlights the complexity of the analysis and the limitations in the analytical assessment which overlooks some of the complexities of the stress distribution within the shackle components.

The maximum principal stress was extracted along each path and divided by the calculated nominal stress to produce a stress concentration factor. The maximum stress concentration factor was then applied to the calculated nominal tensile stress range to
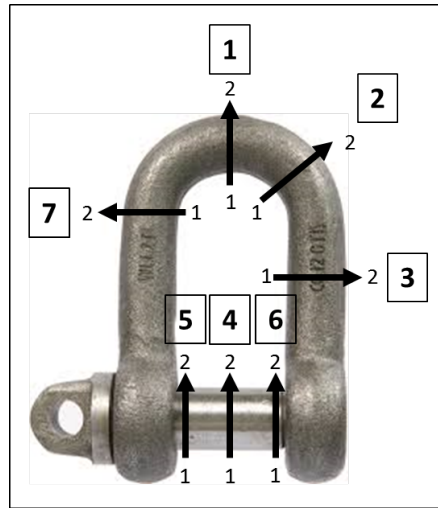
Figure 4.10: Path set up within shackle FEA models to extract maximum principal stress along each path. Boxed number indicates number of path, smaller 1 - 2 on arrow indicates the direction from start to end of path. Paths 1, 2, 3 and 7 were set up in the bow optimised model, whilst paths 4-6 were set up in the pin optimised model.

provide a final stress range for use with the S-N curve in order to estimate cycles to failure analytically.
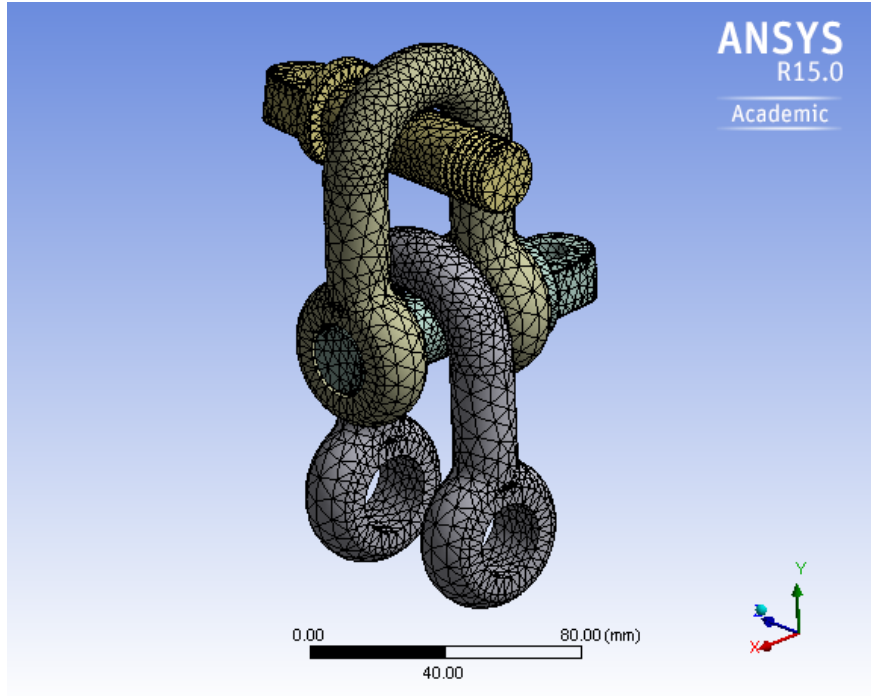
Figure 4.11: Generated shackle assembly mesh.

4.4 Results

The results section is presented to reflect the order in which the methods section was described, beginning with the numerical investigation.

4.4.1 Shackle numerical investigation

4.4.1.1 Mesh optimisation

The generated mesh for the model assembly can be seen in Figure 4.11. In this Figure, different parts are highlighted with different colours to identify them as separate parts, however all parts were assigned 'Certex steel' material properties.

The mesh optimisation conducted using a 'sphere of influence' with a reduced element size of 1mm can be seen in Figure 4.12. This mesh optimisation was conducted at the interaction between the main shackle bow and bounding pin to improve the quality of the results in these critical areas.

179
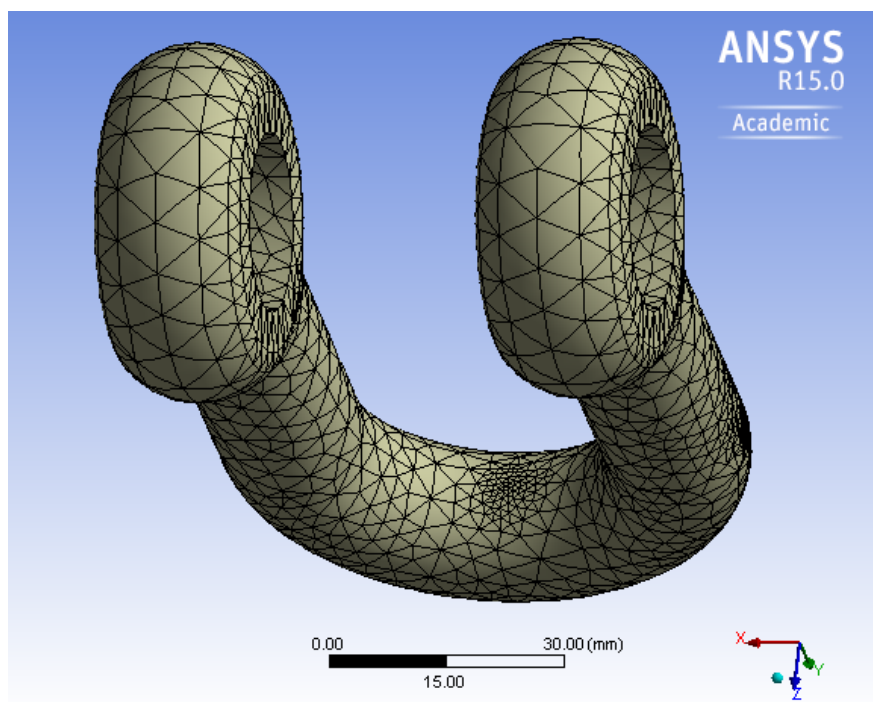
Figure 4.12: Resultant mesh following mesh optimisation for contact region on main shackle bow.
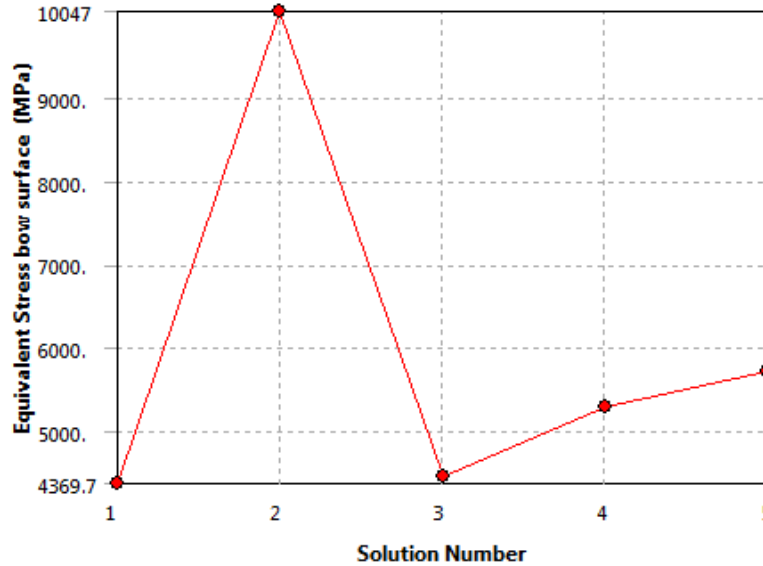
Figure 4.13: Convergence results for bow optimised model subject to a load of 201.5kN. Convergence criteria specified for equivalent stress on the bow surface. Convergence criteria was specified as a maximum change of 10% and was achieved after 5 iterations.

4.4.1.2   Model convergence

Following the development process outlined in Section 4.3.1 two final models were developed, one optimised for the shackle bow and one optimised for the shackle pin. Numerous models for each optimised model configuration were processed, changing only the applied load to represent different scenarios as listed in Section 4.3.1.5, Page 167.

In addition to the default convergence criteria in ANSYS, specific convergence criteria were specified to ensure the model was converging to a stable result. The convergence criteria specified was based on equivalent stress on the surface between the bow and pin interaction. Referring to Figure 4.4, Page 163 for the bow optimised model this was
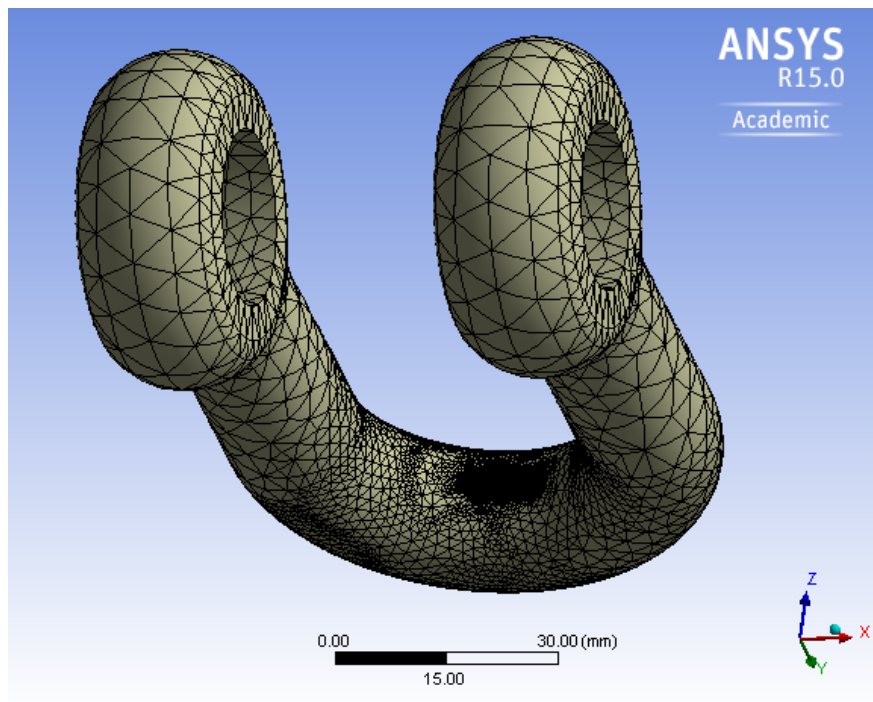
Figure 4.14: Shackle bow mesh following convergence detailed in Figure 4.13. Model is bow optimised model subject to a load of 201.5kN.

contact region A, for the pin optimised model this was contact region B. A maximum allowable change of 10% between iterations was specified. Figure 4.13 demonstrates an example of the converged results achieved; this specific convergence result is for the bow optimised model subject to a load of 201.5kN (mean measured breaking load of the shackles). This model took 5 iterations to converge on a final solution that met the requirement of less than 10% change, in this example the final change was 7.9%. This example does not highlight an optimal convergence route, which would see the value for equivalent stress gradually converging to a steady value; the large increase in Step 2 clearly interrupts this. However, the specified convergence criteria have been satisfied between Steps 4 and 5 and hence the model is considered to have converged. Figure 4.13 also details the increased FEA model size required to converge on a solution, with the final converged model using 216,045 elements in comparison to the initial model using 58,642 elements. Figure 4.14 details the converged mesh generated following the 5 iterations listed in Figure 4.13.

Following model convergence it was necessary to evaluate the models against analyt-

Figure 4.15: Path location specified in FEA model for the extraction of the maximum principal stress value for analytical evaluation.

ical estimations to ensure calculated values were in the correct region. This is detailed in the next section.

4.4.1.3 Model evaluation

As detailed for Model Convergence, it is not necessary to report model evaluation for every load case. To demonstrate the analytical evaluation of the FEA models, the process will be reported for the load case of 122.6kN (representing the shackle supplied MBL).

At a load of 122.6kN, the nominal tensile stress calculated using Equation 4.3, Page 165 is 213.9MPa. To compare this figure to the results from the FEA model the relevant results for the principal stress can be extracted along a path. Figure 4.15 details the location of a path created through the cross section of the FEA model to enable extraction of results. Figure 4.16 details the results for MP stress extracted along this path. The results at the centre of the bow arm should be equivalent to the calculated value for nominal tensile stress. By interpolating the results at the centre of the bow, the FEA model calculated value for maximum principal stress equals 188.6MPa. This result agrees with the analytically calculated value to within 12% and confirms the FEA model is generating results of an appropriate order.

The contact stress between the main pin and main bow was calculated using Equation 4.4, Page 165. At an applied load of 122.6kN the calculated contact stress is
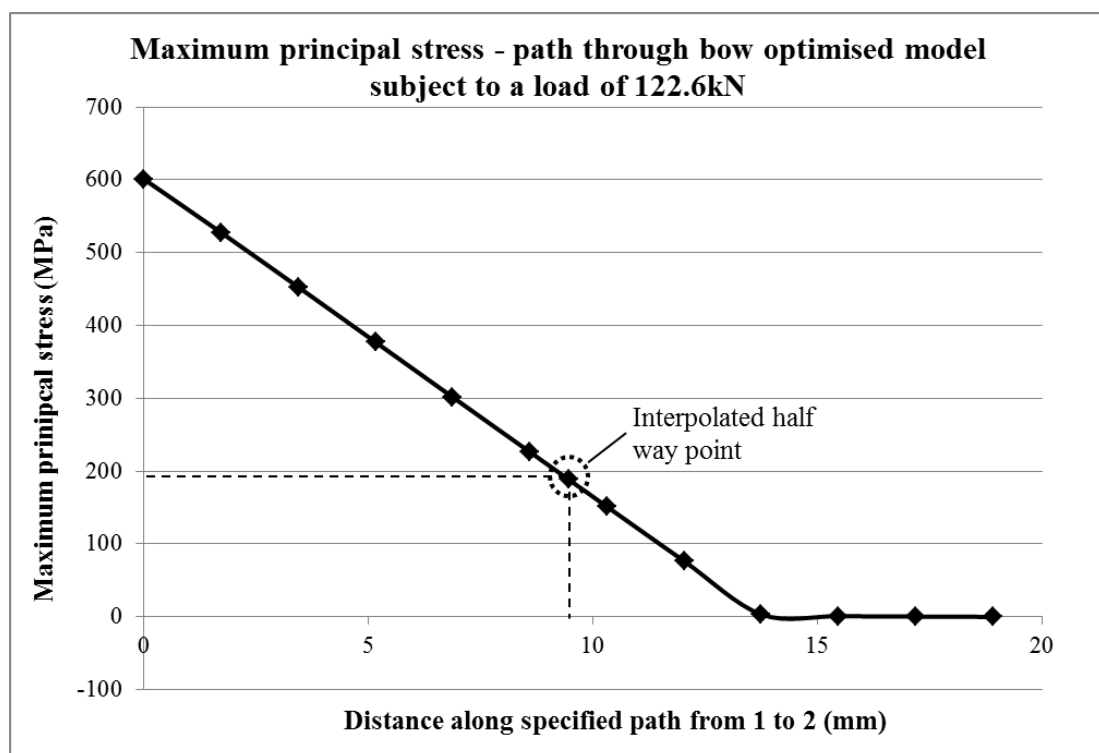
Figure 4.16: FEA results for maximum principal stress plotted along a path through the central cross section of the bow arm (as detailed in Figure 4.15) in the bow optimised model when subject to a load of 122.6kN. Interpolation at half way point highlighted.

14,015.1MPa. To compare this directly to the FEA model, a 'Contact tool' is created and the pressure at the contact region was selected as an output from this tool. The maximum value for pressure calculated by the FEA model at this contact area was 13,066MPa. This result is 7% less than the numerical calculation again confirming the FEA model is generating results of the correct order.

To evaluate the pin model at an applied load of 122.6kN, Equation 4.5, Page 166 for beam bending as detailed in Section 4.3.1.4 was utilised. A maximum bending stress of 908.9MPa was calculated. To compare this to the FEA model the maximum principal stress was extracted at the outer edge of the shackle pin (where the maximum bending stress occurred). The stress calculated by the FEA model at this point was 1055.7MPa. This value is 16% higher than the calculation assuming a 3 point bend test. However, given the analytical calculation is only an approximation of the physical arrangement, this result was accepted as confirming the FEA model was calculating values to the correct order of magnitude.

4.4.1.4 Model results

To assess the model results a straightforward option would be to use the maximum or minimum value for a selected result (e.g. stress or safety factor) as these values are specifically identified by the plot legend. However in the bow model, despite being evaluated using the analytical calculations detailed in Section 4.4.1.3, a minute area of extremely high tensile stress was observed, adjacent to the contact area of high compression. An example of this is detailed in Figure 4.17 for the bow model subjected to 122.6kN. In this figure, the principal stress in this area peaks at 38,615MPa, however the maximum principal stress observed in the remainder of the model peaks at 2,519MPa. It should be noted the very large stress of 38,615MPa is a result of the FEA model being linear elastic i.e. there was no plastic behaviour defined for the material. The value of calculated stress far exceeds the real yield and ultimate strength of the material i.e. 890MPa and 1010MPa respectively. Because of the linear elastic nature of the model, the calculated stresses in the shackle beyond the point at which parts of it would have reached and exceeded yield stresses are increasingly inaccurate. This is because no account is made in the model for the plastic flow of material at stress concentrations or at areas of geometric non-linearity in the real shackle. The model will therefore be useful in determining absolute stresses and stress concentrations before
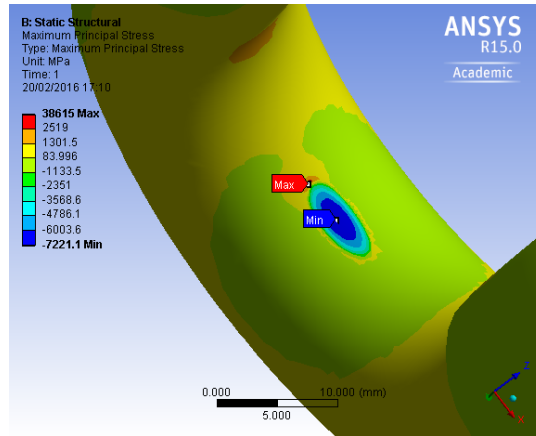
Figure 4.17: Contour plot of maximum principal stress for the bow optimised model subjected to a load of 122.6kN. Localised area of high stress identified by 'Max' label.

yield onset, but should not be relied upon beyond the onset of yield. This particular area of high stress is likely to have been caused by the frictional contact between the bow and the bounding pin. The mesh optimisation applied to this area may have further exaggerated this stress, which is extremely localised and focused on the surface of the bow. Physically, such a localised surface stress would lead to some local material yielding but not a complete failure, and it was therefore decided that this localised area of results should not be included in the presented results. Due to this feature (which occurred in the bow models at all loads), the maximum and minimum values could not be simply extracted from the models and therefore model parametrisation (where specific results are automatically extracted under a range of conditions such as increasing load) could not be used.

As an alternative to using the maximum and minimum values, the equivalent stress plots were used to identify areas of peak stress. Further paths were then established in the models capturing these areas of peak stress to facilitate the extraction of results along these critical paths. These paths were also used to extract data to establish the stress concentration factor, K_t, as described in Section 4.3.3.1, Page 176. Figure 4.10, Page 178 details the locations of these paths. Paths 1, 2, and 7 were anticipated to capture the peak tensile and compressive stresses in the bow, whilst path 3 was established for model analytical evaluation (as discussed in Section 4.4.1.3). These four paths were established in the models optimised for the bow, whilst paths 4, 5 and 6

were established to investigate the stress distributions in the model optimised for the pin.

As discussed in Section 4.3.1, although the equivalent stress plot is useful for a brief overview of the stress distribution within a component, due to the squaring of the terms in Equation 4.7 Page 168, it does not allow for an understanding of the tensile or compressive nature of the stress. As fatigue failures originate in areas of tensile stress (Koh, 1991), it is critical in this analysis to establish whether stresses are tensile or compressive. Therefore further results presented will be based on maximum principal stress (which accounts for the compressive or tensile nature of a stress).

As discussed in Section 4.3.3.1 Page 176, these results are only strictly valid for Paths 3 and 7 where the failure mode is tensile dominated. Failures along the other paths will be dominated by shear loading or a combination of shear and tensile loading and therefore this approach using the maximum principal stress is less applicable. However, given the B1 S-N curve (Det Norske Veritas, 2011) is based on tensile-tensile loading, and there is not an equivalent S-N cure for shear loading, this assessment using maximum principal stress was conducted along all paths for illustrative purposes. Given the peak value for K_t occurs on Path 7, which is subject to predominantly tensile loading, this is a valid result to take forward for use with the S-N curve.

The maximum principal stress values were extracted along each of the described paths and for each load case. Examples of the data extracted can be seen in Figure 4.18 and Figure 4.19 for an applied load case of 122.6kN for the bow and pin optimised models respectively.

The peak maximum principal stress value was then identified for each load case model. At all load iterations of the bow optimised model the peak value occurred at the commencement of the bend in the bow (the beginning of Path 7). At all load iterations of the pin optimised model the peak value occurred on the underside of the pin (at the beginning of path 4). The peak maximum principal stress results for both the bow and pin model across a range of load cases are detailed in Figure 4.20.

In addition to the peak maximum principal stress values, Figure 4.20 also details the minimum safety factor at each load case. The safety factor plotted here is based on the calculated maximum principal stress in relation to the ultimate tensile strength of the material. The safety factor is based on the design Equation 4.8 detailed on Page 169 and highlights any areas where the generated stress exceeds the strength of the
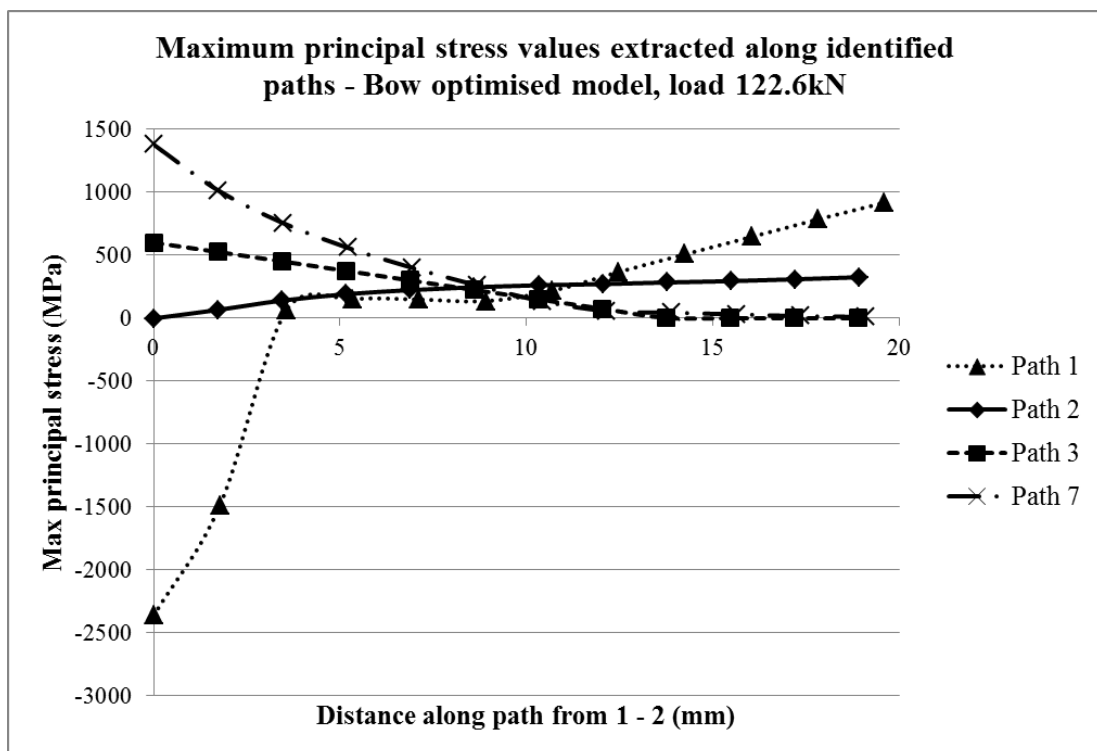
Figure 4.18: Maximum principal stress values calculated for the bow optimised model at an applied load of 122.6kN and extracted along paths as detailed in Figure 4.10, Page 178.
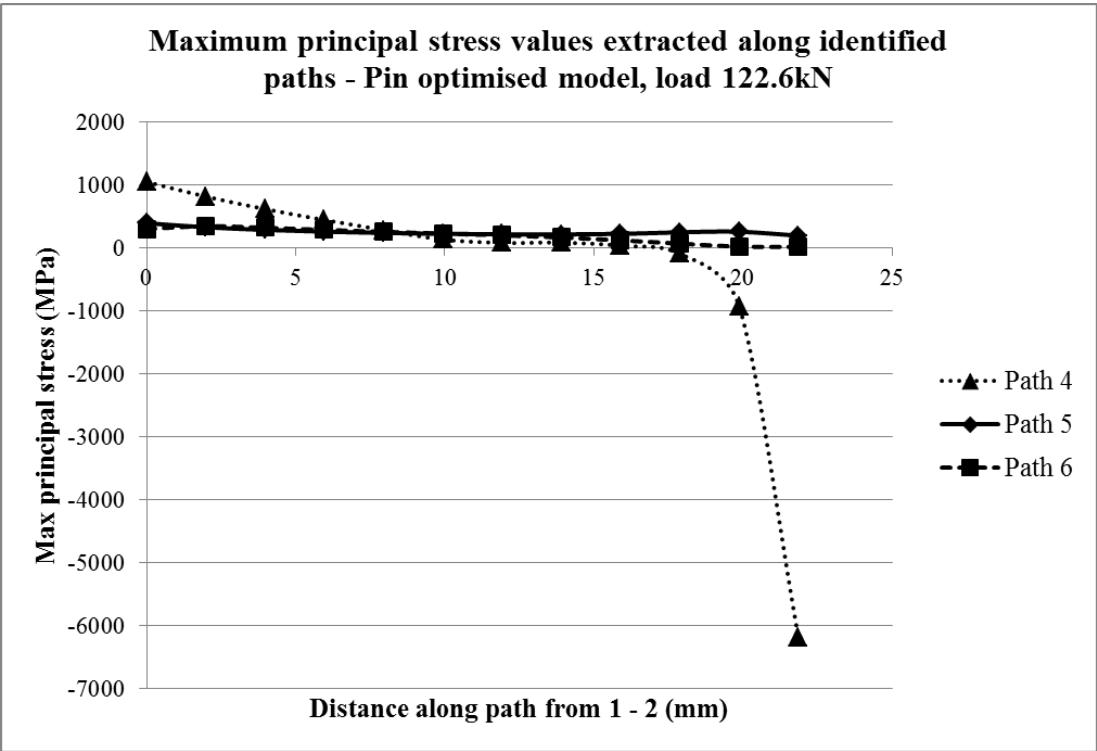
Figure 4.19: Maximum principal stress values calculated for the pin optimised model at an applied load of 122.6kN and extracted along paths as detailed in Figure 4.10, Page 178.
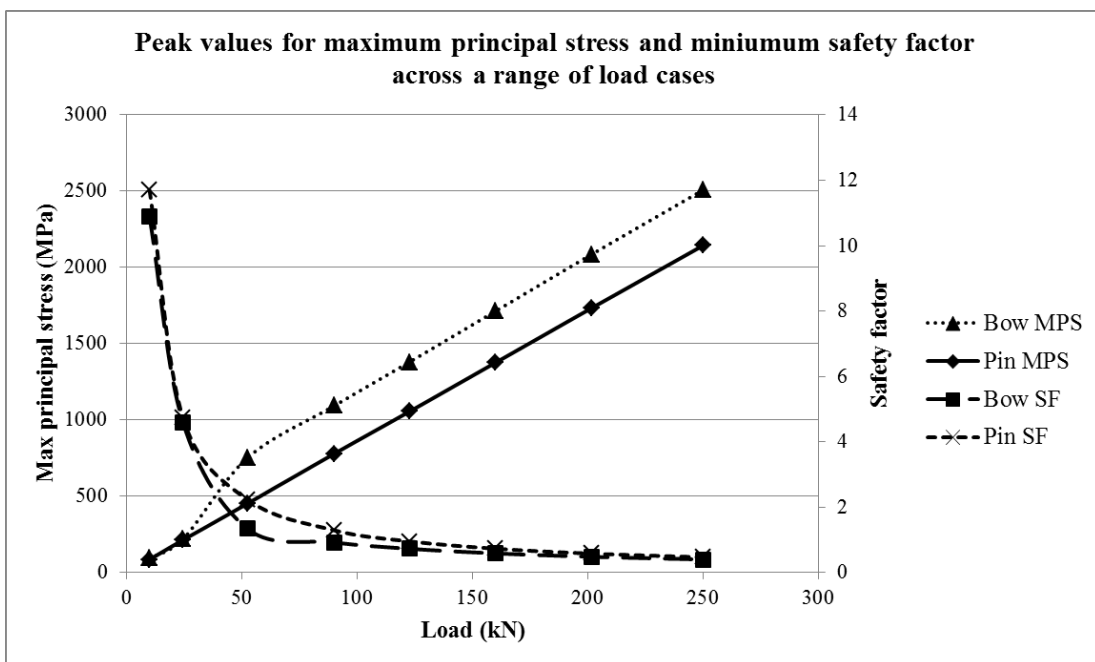
Figure 4.20: Peak values of maximum principal stress (MPS) and minimum safety factor (SF) calculated for FEA models subjected to a range of load conditions. Peak values identified from data extracted along paths set up as detailed in Figure 4.10, Page 178. Safety factors are based on maximum principal stress in relation to the ultimate strength of the material.

material as these have a value of less than 1. The onset of failure can be assumed to commence at this condition. Any values over 1 imply a factor of safety (FOS) on the design, e.g. a value of 2 equates to the material having twice the strength necessary to withstand the stress.

In addition to plotting peak values extracted from the FEA models, the safety factor results also provided a very informative contour plot. Such a plot quickly allowed a review of weak areas within the shackle and an identification of where failures are likely to originate and at what loads. Figure 4.20 details the safety factor plots for the loads of interest identified in Section 4.3.1, Page 158.

Key areas of weakness in the shackle were identified from these plots with areas of concern at each load case identified in red highlighting an ultimate tensile strength safety factor of less than 1. The bow model suggested failures are likely to initiate on the inside surface of the commencement of the bend in the bow, with material in this region displaying a FOS < 1 from a load of 90kN (the fatigue test range). Another weak area of the bow was shown to be the top of the bow curvature, although areas displaying a FOS < 1 were not observed in this region until a load of 201.5kN (the mean measured breaking load of the shackles). In the pin model, the weakest part of the component was identified as the centre on the bottom surface of the pin, opposite the applied load from the bounding bow. A small amount of material in this area began to show a FOS < 1 from a load of 122.6kN (the specified MBL of the shackle).

4.4.1.5 Numerical modelling of fatigue performance

As with the previous results discussed, the areas of highly compressive stresses at the contact regions dominated the fatigue modelling results. Figure 4.21 details the predicted life for the bow and the pin models and shows the effect of the highly compressive stresses at the contact regions.

It was anticipated that the numerical modelling tool would be more sophisticated, however as these compressive results were still being considered in the fatigue life calculation the same paths as detailed in Figure 4.10 were used to interrogate the model and extract data at the regions of peak tensile load. From the work presented in the previous section the peak tensile stress for the bow optimised model occurred on Path 7 and for the pin optimised model it occurred on Path 4. Based on these identified regions of peak maximum principal stress the numerical estimation of cycles to failure
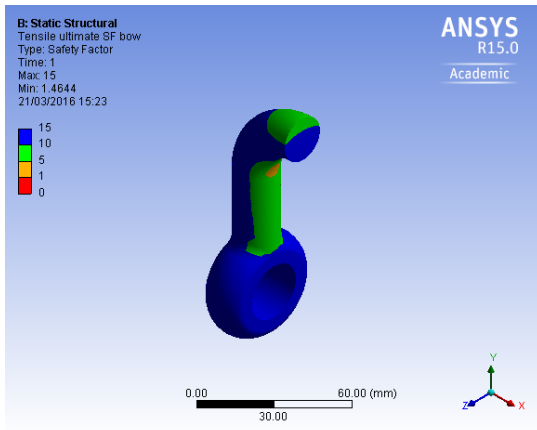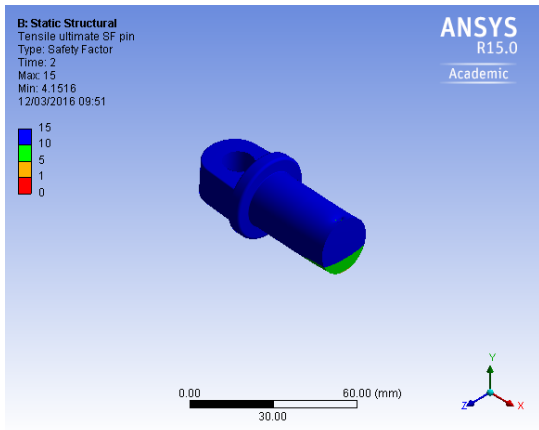
(a) 24.5kN bow model.

(b) 24.5kN pin model.
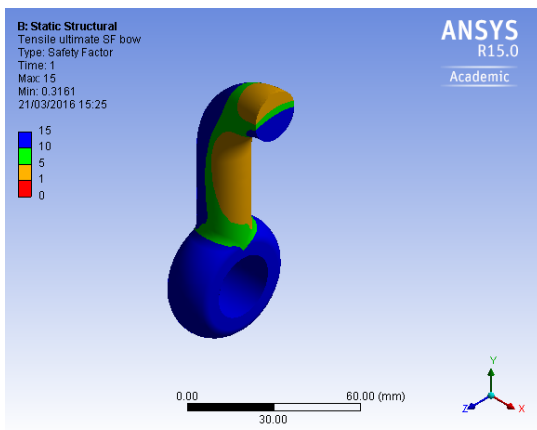
(c) 52.5kN bow model.
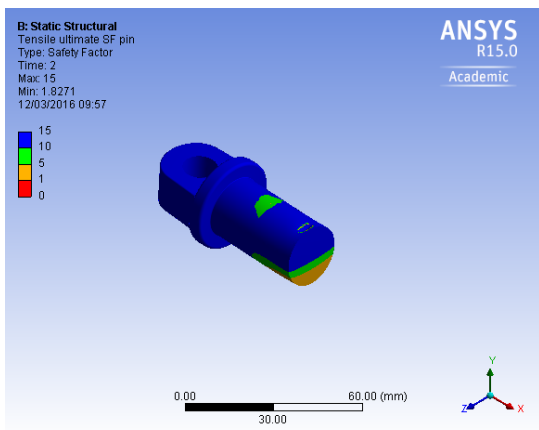
(d) 52.5kN pin model.
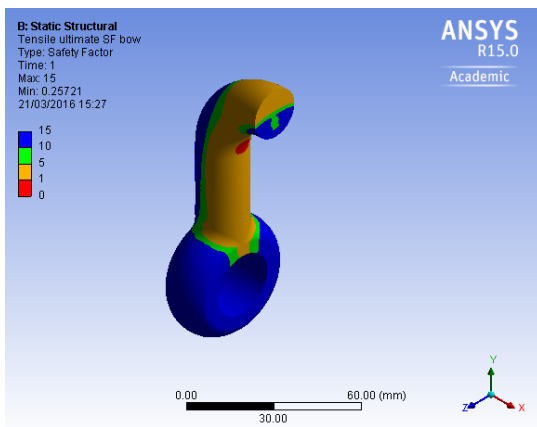
(e) 90kN bow model.
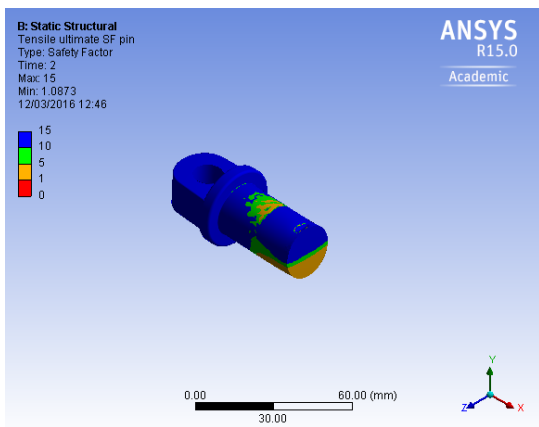
(f) 90kN pin model.
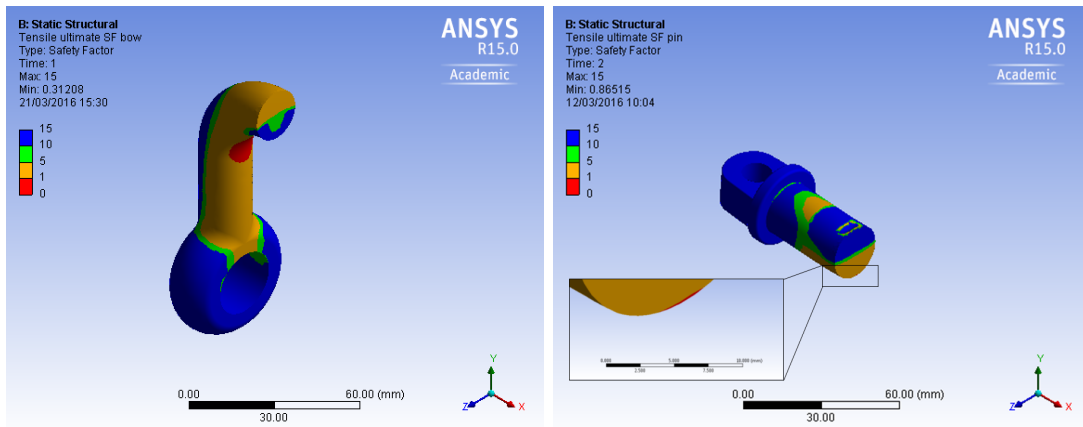
(g) 122.6kN bow model.

(h) 122.6kN pin model.
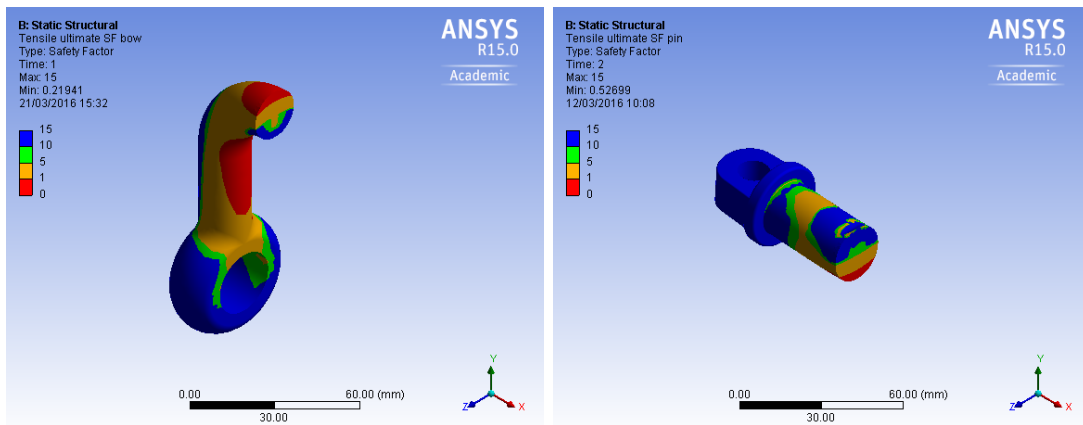
(i) 201.5kN bow model.

(j) 201.5kN pin model.

Figure 4.20: Safety factor contour plots for bow and pin optimised model over a range of applied loads. (a) & (b): 24.5kN, WLL of shackle. (c) & (d): 52.5kN, peak mooring load measured at SWMTF. (e) & (f): 90kN, peak load for fatigue testing. (g) & (h): 122.6kN, MBL of shackle. (i) & (j): 201.5kN, mean measured breaking load of shackle. Other components removed from image and section plane used to enable visualisation of safety factor through cross section. Safety factor plotted is based on maximum principal stress in relation to ultimate tensile strength of the material.
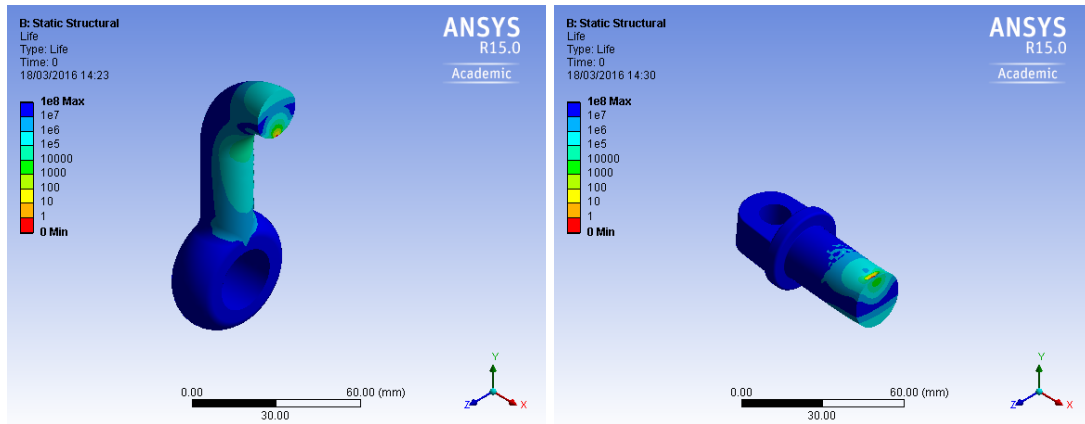
<table>
<tr><td>(a) 90kN bow model.</td><td>(b) 90kN pin model.</td></tr>
</table>

Figure 4.21: Fatigue life for the bow and pin optimised model. Contour plots represent number of cycles to failure based on an applied cyclical load of 90kN with a min/max loading ratio R of 0.1111.

was calculated as 89,856 cycles for the pin optimised model and 23,462 cycles for the bow optimised model. It should be noted here that this assessment did not consider shear stress and focused on maximum principal stress due to the fact the B1 S-N curve (Det Norske Veritas, 2011) is based on tensile-tensile loading.

The results from the numerical fatigue investigation represent the last results to be presented from the numerical modelling; the next section will present the results from the experimental methods.

4.4.2 Shackle experimental methods

This section will present the results from the Ultimate Limit State tests and the Fatigue Limit State tests conducted at DMaC, and the field testing conducted at the SWMTF.

4.4.2.1 Experimental Ultimate Limit State

The linear displacement of 0.1m specified in the DMaC test script successfully broke Shackle A and Shackle B in two separate ultimate strength tests. The tension - extension results for both these tests are detailed in Figure 4.22 and the WLL and MBL specified by the shackle supplier has also been detailed on this figure to put the ultimate strength of the shackles in perspective.
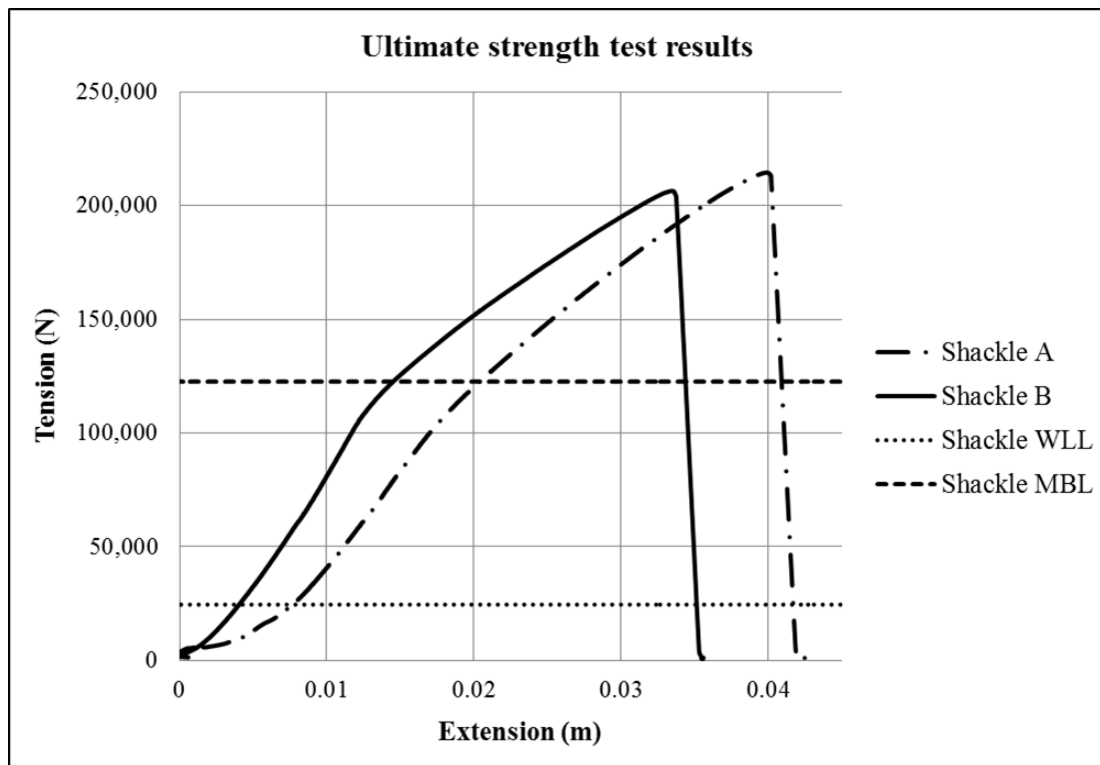
Figure 4.22: Tension - extension results from DMaC for the ultimate strength tests conducted on Shackle A and Shackle B. Specified working load limit (WLL) and minimum breaking load (MBL) have been detailed for comparison.

The average breaking load of the shackles was 210.5kN and the shackles began to yield at approximately 110kN. Both the failures occurred on the thread of the pin and

| (a) | (b) |

Figure 4.23: Ultimate strength failure modes. (a) Shackle A and (b) Shackle B.

are detailed in Figure 4.23.

4.4.2.2 Experimental Fatigue Limit State

The results from the ultimate strength tests were used to specify the accelerated testing regime to ensure the testing remained in the elastic region of the shackle behaviour, below the shackle yield point. Based on the observed yield of the shackles at approximately 110kN, the accelerated testing range was specified as a sinusoidal wave of magnitude 10kN - 90kN and 2Hz frequency (following provisional testing conducted as described in Section 4.3, DMaC could comfortably achieve this regime). A test script was written to this specification which totalled 14,976 cycles in just over 2 hours.

The first series of fatigue testing was conducted, initially with six test shackles installed in DMaC. The above test script was repeated until a failure occurred in Shackle 6 at 19,942 cycles. The failure occurred in the Shackle bow as detailed in Figure 4.24a. At this point DPI was used to inspect all shackles for the development of fatigue cracks; none were observed.

In addition to the broken Shackle 6, Shackles 4 and 5 were also removed from the testing at this point. The remaining three shackles (7, 8 and 9) with an additional two new shackles (4 and 5) were installed in DMaC, and the test script was repeated until a further failure occurred in Shackle 9 at 24,976. This failure occurred in the shackle pin as detailed in Figure 4.24b. All shackles were removed from DMaC at this point and further DPI was conducted. This series of DPI identified the development of hairline

(a)   (b)
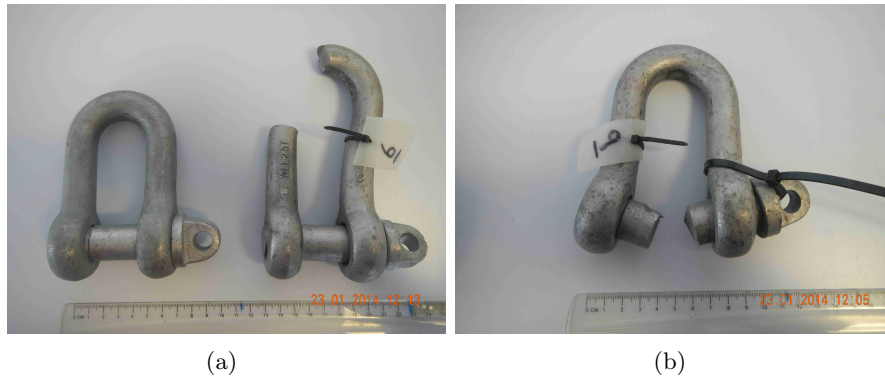
Figure 4.24: Shackle fatigue failures with a new, undamaged shackle for comparison. (a) Shackle 6, failure occurred at 19,942 cycles; (b) Shackle 9, failure occurred at 24,976 cycles.

Figure 4.25: Shackle fatigue crack identification using DPI. Fatigue crack as developed on Shackle 7 at 27,976 cycles.

fatigue cracks on the shackle pin of Shackles 7 and 8, which had also been subjected to 24,976 cycles. Figure 4.25 details an example of fatigue crack identification using DPI. Table 4.4 details the total shackle exposure and results from the first series of fatigue testing.

Following this initial set of fatigue testing, Shackles 10 and 11 together with new Shackles 1, 2, 3, 12 and 13 were deployed at SWMFT for a period approaching 6 months as outlined in Section 4.3.2.3, Page 174.

On recovery from the SWMTF, further DPI was conducted and no fatigue cracks were identified following the sea deployment. A further series of fatigue testing was

4. ASSESSING SAFETY MARGINS FOR MOORING SYSTEM COMPONENTS: RELIABILITY ASSESSMENT OF A STANDARD MOORING COMPONENT

Table 4.4: Summary table outlining the first series of fatigue testing. Fatigue cycle number relates to fatigue cycles of 10-90kN at a frequency of 2Hz.

Shackle No.	Fatigue cycles	Result
4	19952	No damage observed
5	19952	No damage observed
6	19952	Break in bow
7	24976	Fatigue crack pin
8	24976	Fatigue crack pin
9	24976	Break in pin
10	5034	No damage observed
11	5034	No damage observed

then instigated at the DMaC test facility, to the same specified parameters, this will be referred to as the 'second series of fatigue testing'.

During the first 37,200 cycles of this subsequent testing, the DMaC test facility was not reaching the peak load of 90kN and was peaking at a load of 85kN. A correction can be made for this shortfall by assuming the Palmgren-Miner damage model applies and using this along with the S-N curve specified in Figure 4.1, Page 156. The Palmgren-Miner damage model is fully detailed in the Literature Review, Section 2.3.2.6, Page 65.

The nominal tensile stress in the shackle bow arms is calculated at a load of 85kN based on Equation 4.3, Page 165. Utilising the Palmgren-Miner rule with the appropriate S-N curve (Figure 4.1), the damage caused by the 37,000 cycles at a peak load of 85kN can be estimated. The Palmgren-Miner rule is then used to estimate the number of fatigue cycles at the higher load (90kN) that would equate to the equivalent amount of damage. The key values for this are outlined in Table 4.5.

Following the initial 37,200 cycles at a lower load, some adjustments were made to DMaC (an additional hydraulic pump was switched on to provide the capacity for increased hydraulic pressure and the PID controls were adjusted). The subsequent fatigue cycles were able to achieve the specified loads.

The remaining shackles were cycled to failure at the specified load regime. Table 4.6 details the total cycles to failure and failure mode for each shackle included in both

Table 4.5: Key figures for the Palmgren-Miner calculation used to calculate an equivalent cycle number at the higher load of 90kN following 37,000 cycles at a reduced peak load of 85kN.

Parameters for 85kN peak load	No. cycles	37,200	cycles
	Peak load	85	kN
	Nominal tensile stress at 85kN	148.33	MPa
	Cycles to failure at peak load 85kN (from SN curve)	2.70E+06	cycles
	Calculated % damage	1.38%	
Parameters for 90kN peak load	Peak load	90	kN
	Nominal tensile stress at 95kN	157.06	MPa
	Cycles to failure at peak load 95kN (from SN curve)	2.15E+06	cycles
	Equivalent cycle no. at 90kN to achieve calculated % damage	29,622	cycles

the first and second series of DMaC fatigue testing.

As detailed in Table 4.6 a large range of failure modes were observed during the fatigue tests. These can be broadly classified into four different failure modes as detailed in Figure 4.26. The spread of failure modes with respect to cycle number is addressed in the Discussion, Section 4.5.2.2.

4.4.2.3 Experimental field testing

The intention of this section of work was to deploy selected shackles onto a mooring limb of the SWMTF where they would be subjected to real mooring loads with detailed load monitoring for analysis. The shackles were successfully deployed and survived the full duration of the field testing, however, due to load cell failures, load data during the deployment was not available. The load history of each shackle could therefore not be calculated. Despite not having load data available from this deployment, the further testing of the shackles at the DMaC test facility following the sea deployment provided information regarding the effect of the sea deployment on the fatigue life of the shackles, and will be addressed in the Discussion (Section 4.5).

Table 4.6: Summary of first and second series of fatigue testing.

Shackle Number	Fatigue cycles				Total cycles: 1st + 2nd series	SWMTF deployment?	Failure Mode and details
	1st series	2nd series					
	10-90kN cycles	10-85kN cycles	Equivalent 10-90kN cycles	Further 10-90kN cycles			
1	0	37,200	29,622	7,364	36,986	Y	Mode B: Centre of pin, with crack developing on bow
2	0	37,200	29,622	52,258	81,880	Y	Mode D: Bow break across thread
3	0	37,200	29,622	44,574	74,196	Y	Mode A: Centre of bow, with large crack in pin and 'corner' of bow
4	19,952	37,200	29,622	5,880	55,454	N	Mode C: 'Corner' of bow, large deformation
5	19,952	37,200	29,622	35,680	85,254	N	Mode A: Centre of bow
6	19,952				19,952	N	Mode C: 'Corner' of bow, large deformation
7	24,976				24,976	N	**No break** but fatigue crack, centre of pin (Mode B)
8	24,976				24,976	N	**No break** but fatigue crack, centre of pin (Mode B)
9	24,976				24,976	N	Mode B: Centre of pin
10	5,034	37,200	29,622	66,870	101,526	Y	Mode A: Centre of bow
11	5,034	37,200	29,622	20,544	55,200	Y	Mode A: Centre of bow but also large crack on 'corner' of bow
12	0	37,200	29,622	5,996	35,618	Y	Mode B: Centre of pin with crack developing on 'corner' of bow
13	0	37,200	29,622	69,632	99,254	Y	Mode D: Bow eye failure (unthreaded)

Failure Mode A **Failure Mode B** **Failure Mode C** **Failure Mode D**
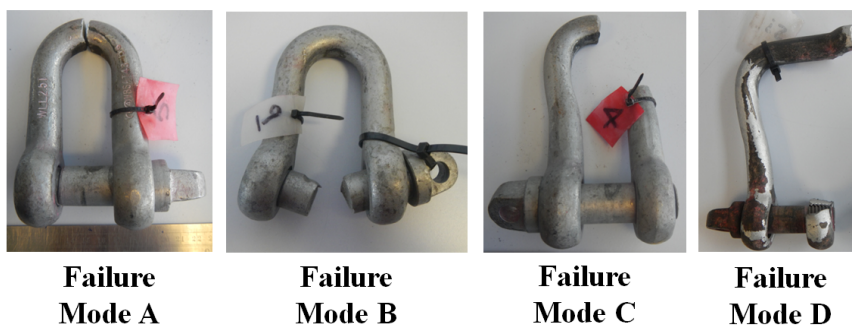
Figure 4.26: Failure mode classification following Series 1 and 2 of fatigue testing. Failure Mode A: Shackles 3, 5, 10 and 11. Failure Mode B: Shackles 1, 9 and 12. Failure Mode C: Shackle 4 and 6. Failure Mode D: Shackles 2 and 13 (although failure occurred on the threaded side of the shackle bow in Shackle 2 and the opposite side for Shackle 13.)

4.4.3 Shackle analytical fatigue estimations

The accelerated fatigue loading regime conducted at the DMaC test facility subjected the test shackles to fatigue cycles at a load range of 10-90kN and frequency of 2Hz. To estimate the anticipated cycles to failure using the air S-N curve detailed in Figure 4.1, Page 156, the stress range of the testing was calculated. The nominal tensile stress range for this testing regime was calculated as 139.6MPa (calculated using Equations 4.3, 4.10, 4.11, Page 176).

To use this with the S-N curve it was necessary to apply an appropriate stress concentration factor.

4.4.3.1 Stress concentration factor

As outlined in Section 4.3.3.1, Page 176, several 'paths' were set up within the shackle models to extract the principal stress at specific locations. In accordance with Equation 4.12 this was divided by the nominal stress to calculate the stress concentration factor at each location. Values of K_t calculated from the principal stress along each path are plotted in Figure 4.27.

Tensile stress is the critical stress in promoting fatigue failures so positive values of K_t (representing a tensile stress) are the most crucial for this assessment. The highest tensile value for K_t was 6.96, located at the start of Path 7 (the inside of the start of the bend in the bow), followed by 4.96 at the start of Path 4 (on the bottom face of the pin) and 4.35 at the end of Path 1 (the top face of the shackle bow). The very negative K_t values observed at the start of Path 1 and the end of Path 4 represent the highly compressive stress generated in the contact area between the test shackle and the bounding pin and bow.

As discussed in Section 4.3.3.1 Page 176, the stress concentration values plotted in Figure 4.27 are only strictly applicable for Paths 3 and 7 where the loading is predominantly tensile (Mode I). Given the peak calculated value of K_t occurs on Path 7 this is therefore a valid figure to take forward for use with the S-N curve to estimate the fatigue life of the shackle.

The nominal stress used in these calculations is based on the tensile stress generated in the bow arms, it is therefore represented by load path 3. At the centre of path 3 the K_t value is approximately 1 which indicates the model is accurate as the stress at
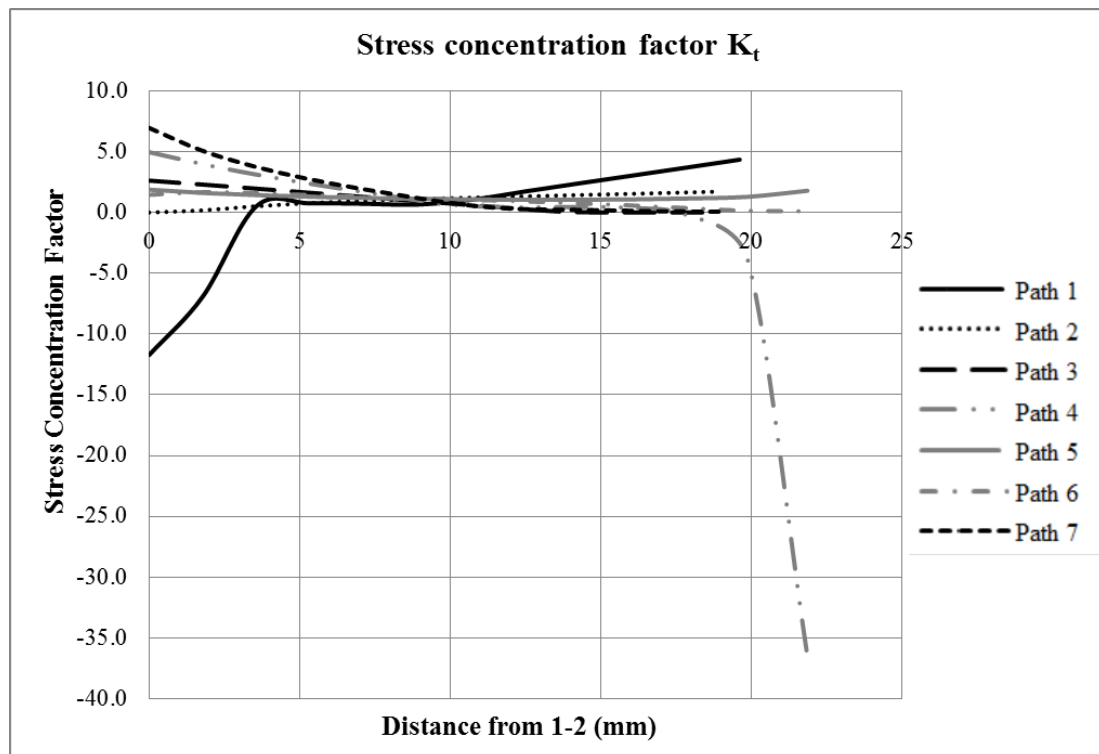
Figure 4.27: Results for stress concentration factor, K_t, along 7 paths specified in FEA
models when subject to a load of 90kN representing the peak load of the shackle fatigue
tests. Figure 4.10, Page 178 details the path configuration. Results calculated using
Equation 4.12, Page 177. Black lines plotted represent bow optimised model; grey lines
represent pin optimised model.

this point should equal the nominal tensile stress (as described in the model evaluation presented in Section 4.4.1.3, Page 183).

It should also be noted here that the values for Kt are an output from the linear elastic FEA model. As discussed in Section 4.4.1 any values of Kt taken from the model when parts of it are beyond the yield strength of the material may be inaccurate as the model is not configured to assess plastic deformation. Given that the yield strength and ultimate strength of the steel are 890MPa and 1010MPa respectively any values of Kt over 6.4 relate to peak results for maximum principal stress greater than the ultimate strength of the shackle. As previously discussed the accuracy of the numerical model is limited beyond the onset of yield. For the purposes of this assessment however, the peak value of 6.96 was used for the fatigue assessment.

The peak stress concentration factor of 6.96 was multiplied by the nominal stress range to calculate the stress range for use with the S-N curve. Figure 4.28 details the S-N design curve highlighting the estimated cycles to failure along with the actual fatigue failures observed from the test shackles. As the S-N design curves published by Det Norske Veritas (2011) are based on mean results minus two standard deviations, vertical lines are added to the figure highlighting mean cycles to failure, and $\pm$ one and two standard deviations for the shackle results.

Based on Figure 4.28, the estimated cycles to failure from the design S-N curve is 1,470. This can be directly compared to the experimental testing results which established a mean minus two standard deviations cycles to failure of 2,380. The analytical result from the S-N curve is therefore shown to be slightly conservative. This result will be further explored in the Discussion, Section 4.5.3, Page 218.

4.5 Discussion

This Discussion section will be structured to reflect the order of the results presented. Starting with the Numerical Investigation (Section 4.5.1), followed by the Experimental Investigation (Section 4.5.2) and the Analytical Estimations (Section 4.5.3). A broader discussion of the work is conducted in the Thesis Discussion, Chapter 7, with reference to the research questions.
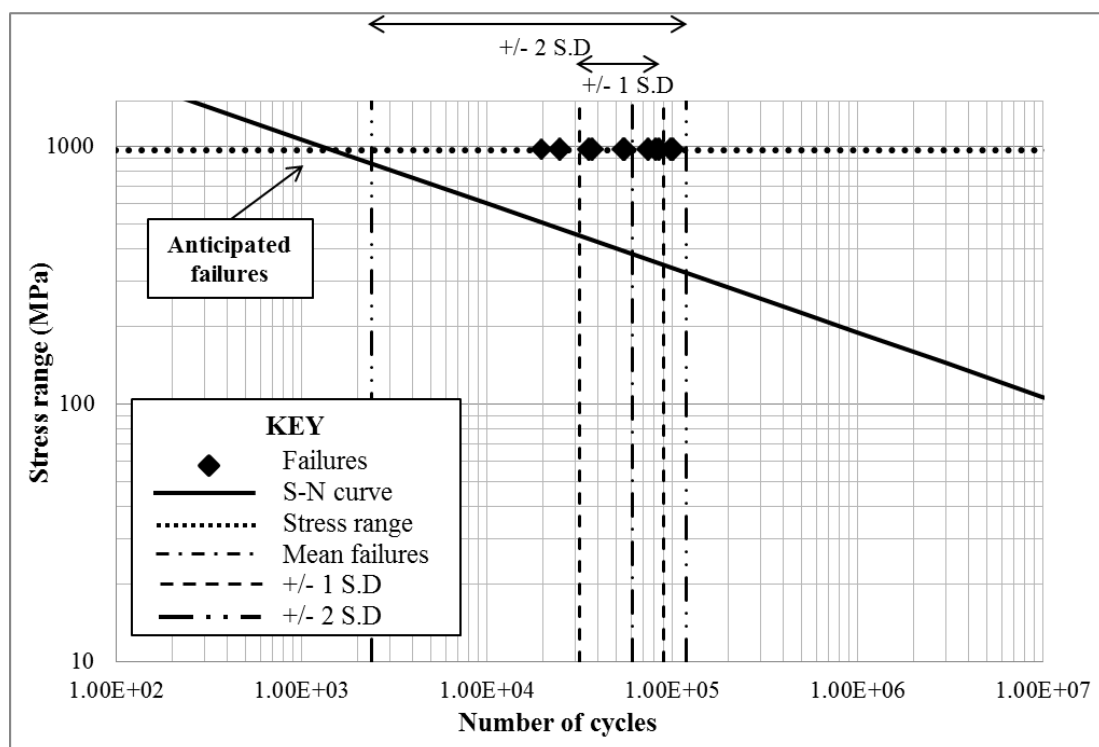
Figure 4.28: S-N design curve for shackles in air (Det Norske Veritas, 2011) with shackle failure results plotted. The mean and $\pm$ one and two standard deviations of the cycles to failure have also been plotted.

	Analytical calculation	FEA model result	Error
Bow nominal tensile stress (MPa)	213.9	188.6	12%
Bow contact stress (MPa)	14015	13066	7%
Pin bending stress (MPa)	908.9	1055.7	-16%

Figure 4.29: Summary results for FEA evaluation based on bow optimised model with an applied load of 122.6kN.

4.5.1 Shackle numerical investigation

Two separate models of the shackle were developed; one optimised to extract solutions for the shackle bow and the other to extract solutions for the shackle pin. Both utilised 'bounding' components to apply the boundary conditions and ensure no unrealistic stress concentrations developed on the component under analysis. Mesh optimisation and convergence criteria were specified to obtain optimum solutions. The FEA models were evaluated using analytical solutions, Table 4.29 summarises the results from the FEA model analytical evaluation.

In terms of bow nominal stress the FEA calculated stress directly at the centre of the bow arm was 12% lower than the analytically calculated value, however just 0.6mm away from this central point the stress is equal; based on this the bow model was assumed to be acceptable. For the contact stress results the analytical calculation assumes two contacting cylinders and a point contact. In the FEA model the stress was distributed over a larger area so it was anticipated the FEA model would have a lower contact stress than the analytical solution. This was observed in the results and again the model was deemed acceptable. Finally the FEA model result for the pin bending stress was 16% higher than the analytical solution. As detailed in Section 4.3.1.4, the 3 point bending assumption used for the analytical calculation is a large simplification of the pin set-up within the bow eyes, and a significant difference was expected between these results. 16% is still a relatively good agreement and is an acceptable result to accept the FEA model. Having evaluated the FEA models analytically it was possible to extract results at a range of load values.

4.5.1.1 Discussion of numerical model results

The FEA models facilitated the identification of the weakest parts of the shackle assembly, where failures are most likely to initiate. As tensile loads are most likely to lead to a fatigue failure these were the focus for the investigation, with the safety factor set to assess maximum tensile stress. The highly compressive stresses generated at the contact areas between the bounding components were therefore not considered in the assessment. The weakest part of the assembly was identified as the inside surface of the commencement of the bend in the bow. Other areas identified as weak within the shackle were the top of the bow and the underside of the pin.

To estimate the load at which failure might commence for each of the models, Figure 4.30 is included. It is a detailed section of the original Figure 4.20 presented in the results section Page 190, with a focus on the minimum safety factors for the bow and pin optimised model to allow an estimate of the load at which the minimum FOS = 1 should be expected for each model. This diagram estimates loads of approximately 63kN and 117kN to result in a FOS = 1 for the bow and pin models respectively. At these loads as the generated stress in the model is equal to the ultimate tensile strength of the material, the onset of failure would be anticipated. In a real situation both the pin and the bow would be subject to the same load; failure of the bow is therefore the predominant failure mode anticipated from the FEA models.

Relating these loads to the shackle specification, the shackle WLL was specified as 24.5kN with a specified design factor of safety of 5, giving a MBL of 122.6kN. The numerical model suggested the WLL was adequate, with over double the load required to initiate a failure (FOS >> 2). However, the 63kN load for the onset of failure approximated from the numerical model is just 51% of the specified MBL, suggesting the shackle is weaker than the specification. It should be noted however, that the numerical models are identifying an area within the shackle where the applied loads are exceeding the material strength. This particular area of the component will fail, however the entire component will not fail at this point so the numerical model can be considered conservative.
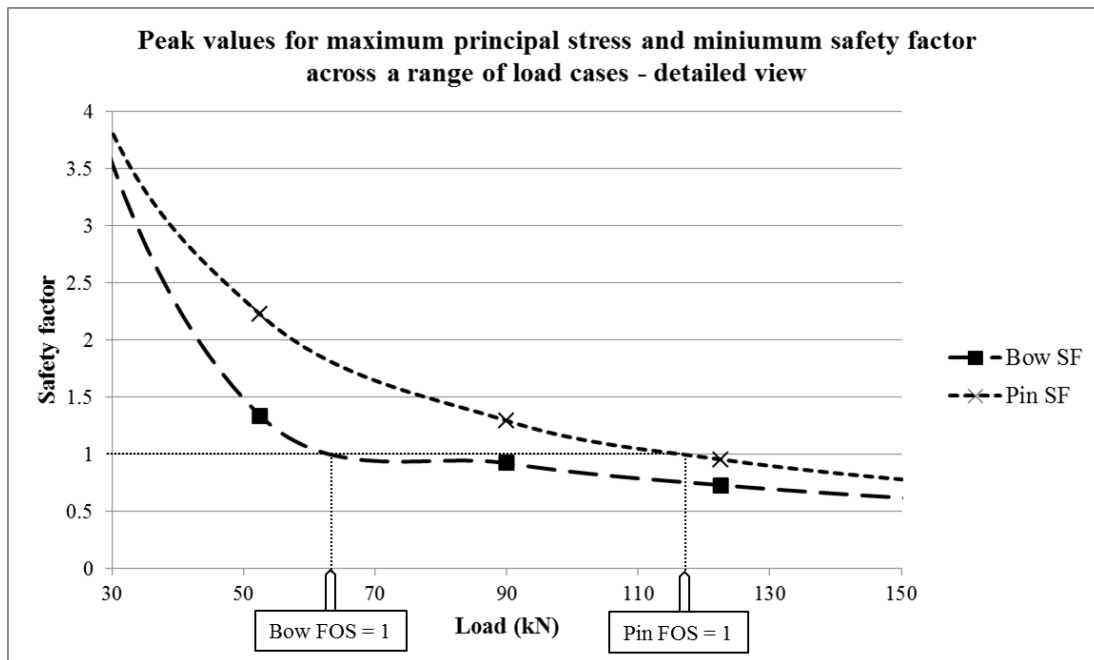
Figure 4.30: Detailed view of minimum safety factor calculated for FEA models subjected to a range of load conditions (original figure presented on page 190). Peak values identified from data extracted along paths set up as detailed in Figure 4.10, Page 178. Safety factors are based on maximum principal stress in relation to the ultimate strength of the material. Detailed view to allow an estimation of the load at which FOS = 1 should be anticipated.

4. ASSESSING SAFETY MARGINS FOR MOORING SYSTEM COMPONENTS: RELIABILITY ASSESSMENT OF A STANDARD MOORING COMPONENT

In addition to comparing the results from the numerical modelling to the shackle specification, they can be compared directly to the results from the experimental methods and to the estimates from the analytical assessment.

4.5.1.2 Comparing numerical model results to experimental results

Ultimate limit state

Relating the failure load predicted by the numerical models to the results of the ultimate strength tests, the failure mode observed in the break tests (both failed via a fracture across the pin at the beginning of the pin thread) was not predicted by the numerical models. This can be illustrated with reference to Figure 4.19, Page 189 which provided detailed maximum principal stress plots at paths identified within the pin when subject to a load of 122.6kN. Path 6, set up to extract results across the pin diameter adjacent to the thread, showed tensile stresses peaking at 353MPa; this was just 33% of the maximum principal stress occurring on the outer edge of the underside of the pin (1056MPa). The thread cut into the pin will clearly act as a stress raiser and it is likely the extent of this effect was not identified in the numerical modelling due to limitations in the modelling of the shackle threaded areas. With regard to the load at which the failures occurred, the shackles tested during the ultimate tensile strength tests survived to an average load of 110kN before failure, 1.75 times the 63kN predicted by the numerical models as the onset of failure.

Fatigue limit state

In addition to reviewing the static loads, a fatigue analysis was conducted using the numerical models. This estimated the cycles to failure of the bow optimised model to be 23,462 in comparison to the pin optimised model cycles to failure of 89,856. In reality the two components would be part of one assembly so the anticipated failure rate would be dominated by the lower cycles to failure calculated for the bow optimised model (24,432 cycles).

Comparing the fatigue calculations from the numerical models to the fatigue failures observed during the shackle experimental testing, some correlation is observed. The earliest failure occurred at 19,952 cycles in the 'corner' of the bow (identified as Failure

Mode C in Figure 4.26, Page 200). This was predicted as the weakest area of the shackle by the numerical models with an anticipated cycles to failure of 24,432. Of the eleven fatigue failures, two failures occurred at this location with an additional four failures displaying significant cracks at this location.

The most common failure observed during the fatigue testing was the top centre of the bow (Failure Mode A); four shackles failed through this mode. This area was identified as one of the weaker areas of the shackle assembly by the numerical models, although it was not anticipated to be the predominant failure mode. The next most common failure mode was at the centre of the pin (Failure Mode B) with three failures in this location; this was predicted by numerical modelling as the weakest part of the pin. The least common failure mode observed during the physical fatigue tests was across the bow eye; one failure occurred across the threaded bow eye and a second occurred across the un-threaded bow eye. These were not predicted as weak areas of the bow by the numerical models and it should be noted that Failure Modes A and B will be dominated by shear loading which was not assessed in the numerical models.

As anticipated, there was significant scatter in the results from the fatigue testing regime, and this will be further discussed in Section 4.5.2.2. The average cycles to failure failure was 60,936 showing that, on average, the shackles performed significantly better than predicted by the numerical modelling, which estimated 24,432 cycles to failure. It should be highlighted again that the numerical model predictions are based on local failure occurring at the weakest part of the shackle and whole component failure should not be assumed to occur at that point. The numerical models should therefore be conservative, and one would expect the observed physical cycles to failure to exceed those predicted by the numerical models. It is therefore surprising that the earliest shackle failure, occurred at 19,952 cycles, a lower cycle number than the 24,432 predicted by the numerical model.

4.5.1.3 Numerical modelling limitations

The main limitation of this work was the required simplification of the numerical models to obtain a solution. As discussed in the Method Section 4.3.1 the most accurate numerical model would have modelled the interactions between the bounding pin/bow with the shackle under investigation as frictional. However, this non-linear contact

type proved too numerically demanding for the software and was unable to resolve. Both Pacheco *et al.* (2003) and Danko (2014) demonstrate the difficulty of accurately modelling these contact areas in their independent work which required the numerical modelling of contacting chain links. In both these studies the contact area was of primary importance so a $\frac{1}{8}$ model of a chain link was created incorporating 3 planes of symmetry to reduce computational demand. For the work presented in this Chapter, the compressive contact stress was not critical and of greater importance was the tensile stress distribution throughout the shackle assembly. A compromise was found by developing two consecutive models, one optimised for the bow and the other optimised for the pin. This allowed valid results to be obtained for each component for the purposes of this investigation.

The predominant focus for the numerical modelling approach was to extract results for maximum principal stress. Due to the linear elastic configuration of the model these results were only valid up to the point of yield. Maximum principal stress was assessed along various paths set up in the shackle model to develop stress concentration factors for use with the B1 tension-tension S-N curve (Det Norske Veritas, 2011) to estimate fatigue life. The results from the physical fatigue testing however have shown many of the fatigue failures occur under shear dominated loading. A further extension to this work would therefore be an assessment of the shear stresses within the numerical model. Given there is currently not a shear S-N curve to use with these results, the focus for the work presented here has been to use principal stress for the assessment. This clearly has limitations and is appropriate for the stresses developed on Paths 3 and 7 (Figure 4.10, Page 178), but less appropriate for the other paths identified. Given the peak K_t value was found on Path 7 this has been deemed valid for the fatigue assessment presented here.

The literature review presented in Chapter 2, Section 2.3.4 compares the positives and negatives of reliability assessment approaches. This section suggests that numerical modelling is cheap and quick to apply. Although numerical modelling certainly avoids the capital costs involved with physical testing, extracting accurate results from the numerical models can be a time consuming process. This piece of work has demonstrated that although results can quickly be established for a model, without fully investigating each model, inaccurate results could easily be presented. Advances in numerical

modelling have allowed for 'parametrisation' of key outputs but this can not always speed up the modelling process and manually extracting data from specific models may be necessary, as shown in the work presented here. It is even suggested by some that in particular cases a simple break test of a sample may be quicker and more accurate than detailed numerical modelling (Noble Denton Euorpe Limited, 2006).

4.5.1.4 Numerical modelling summary

In summary, the numerical models allowed for the identification of weak areas within the shackle assembly where failures were likely to initiate. The models also provided a prediction of the anticipated loading that was likely to initiate failure. Physical testing of a set of shackles allowed for direct comparison to the numerical modelling. This found that during ultimate strength tests the numerical models did not predict the correct area of failure and the average failure load of the shackles (110kN) was significantly higher than the load to initiate failure predicted by the numerical model (63kN). A more realistic loading regime for the shackles deployed in a WEC mooring system was represented by a fatigue testing regime. A range of fatigue failures was observed in the physical testing and three of the four failure modes were well predicted by the numerical models. In addition, the numerical modelling estimated the fatigue life of the shackle to be 24,432 cycles and during physical testing the first failure occurred just below this at 19,952 cycles. The remaining ten failures were at higher cycle numbers than predicted by the numerical modelling, with an average cycles to failure of 60,936. Overall, the numerical models proved conservative across both static and fatigue loading. This was anticipated as the numerical models were used to identify loads exceeding the strength of the weakest part of the shackle i.e. this point is not concurrent with complete shackle failure, only the onset of failure in one area of the shackle. The conservative nature of the numerical modelling predictions is clearly preferred to the models over predicting the strength of the shackle components. The identification of weak areas within the shackle from the numerical models has the additional benefit of informing the inspection techniques used to identify fatigue cracks within components. As detailed in Chapter 3, Page 149 dye penetrant inspection was used in the experimental aspects of this work to identify fatigue cracks. Although this approach identified cracks over the entire component, being able to pay particular attention to certain areas where cracks are

likely to initiate has the potential to speed up this process when assessing multiple components.

4.5.2 Shackle experimental methods

4.5.2.1 Experimental ultimate limit state

The average failure load during the ultimate strength test was 210.5kN, and the two test results agree within 4%. The difference observed in the 0-50kN load-displacement plot (Figure 4.22, Page 195) is due to the different 'bedding in' regimes, where Shackle B was subjected to pre-tests to observe the low load behaviour Shackle A was not subjected to such tests. The initial load up for Shackle A therefore shows greater extension whilst the chain links in the set up are adjusting to their optimum position.

Comparing these results to the shackle supplier specification, the shackles exceeded the specified loads surviving beyond 200kN despite having a WLL of 24.5kN and an MBL of 122.6kN. The average embedded component safety factors are therefore 8.6 on the specified WLL and 1.7 on the specified MBL. The results show that both shackles appear to yield at approximately 110kN, which is a safety factor of 4.5 on the specified WLL but, as expected, is below the specified MBL of the shackle.

In terms of the material properties of the supplied shackle, the specified material ultimate strength is 1010MPa and the specified yield point is 890MPa. To compare this to the results from the shackle ultimate strength tests the nominal stress was calculated using Equation 4.3, Page 165. The average failure load of 210.5kN equates to a nominal tensile stress of 367.3MPa, and the approximate yield load of 110kN equates to a nominal tensile stress of 192MPa. These are considerably less than the specified material properties with the ultimate strength 64% below and the yield strength 78% below the specified material properties.

This difference is due to the calculation used for the nominal tensile stress which does not take into consideration the complex distribution of stresses within the shackle. Although the nominal stress calculation is a good approximation of the stress developed in the parallel parts of the shackle bow arms, considerable stress concentrations will develop in other parts of the shackle geometry that will be higher than the calculated nominal stress. It is in these regions that failures will initiate. Further discussion of

the stress distribution within the shackle and the calculation of stress concentration factors is detailed in Section 4.5.3.1, Page 219.

Putting these results in wider context the DNV guidance for mooring design (Det Norske Veritas, 2010a) as detailed in Chapter 2, Section 2.5.5, should be referred to. Assuming design for ultimate limit state, with the lower consequence class 1 and a quasi-static analysis type, the specified safety factor is 1.70. If this mooring design safety factor is applied to the specified shackle WLL a total safety factor of 14.6 would be present in the mooring design.

The main limitation for this section of work is the limited sample numbers used to calculate the average shackle strength. Two samples were used and testing additional shackles would have further verified the figure of 210.5kN obtained. However, with limited resources available, given the two failure loads agreed within 4%, it was decided that the remaining shackles should be utilised for fatigue testing, where it is generally accepted a large number of samples are required to obtain representative data (Det Norske Veritas (2011) suggests a minimum of 15 specimens).

In summary, the aim of this work was to establish the breaking and yield load of the shackles to both inform the fatigue testing regime and to allow a comparison to the shackle supplier specification to establish the embedded component safety factor. In this static loading situation, large safety factors were present with an average safety factor of 8.6 on the specified WLL. Given a typical recommended mooring design safety factor of 1.7 the total resulting system safety factor would be 14.6, the cost implications of this will be further discussed in Chapter 6.

4.5.2.2 Experimental fatigue limit state

Reviewing the results from the first and second series of fatigue testing (presented in Table 4.6, Page 200) the large range of cycles to failure observed is immediately obvious. The mean number of cycles to failure was 60,936 with a standard deviation of 29,278. Scatter is inherent in fatigue failures and is the reason that once a mean S-N curve is established through testing, the design S-N curve is determined as mean minus 2 standard deviations (Det Norske Veritas, 2011). Figure 4.31 illustrates the
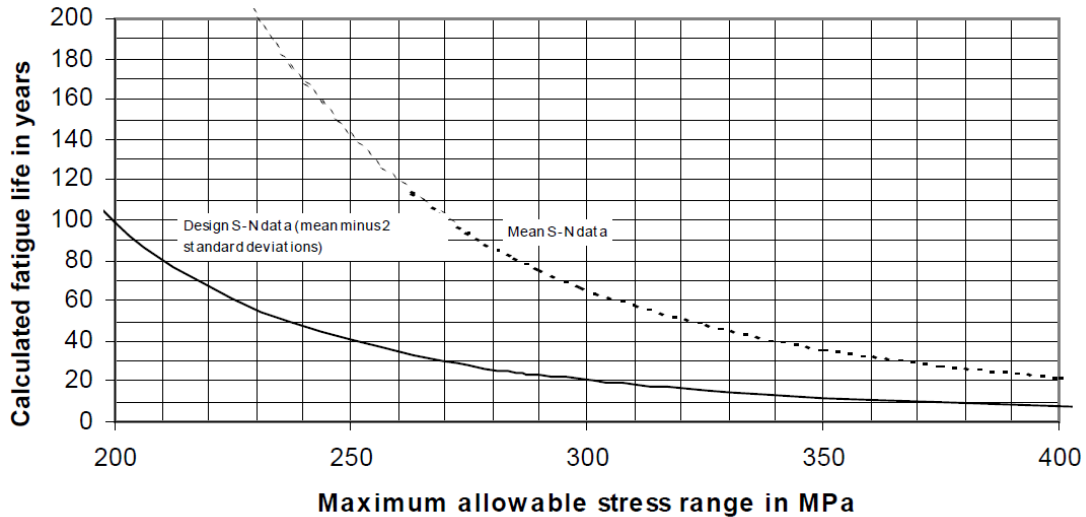
Figure 4.31: Figure replicated from (Det Norske Veritas, 2011) to illustrate the effect of scatter in S-N data on design S-N data which is calculated from mean S-N data minus 2 standard deviations.

large effect this inherent scatter can have on typical design S-N data in comparison to the calculated S-N data.

The failure modes were classified from A - D in Figure 4.26, Page 200 and the type of failure observed appears to be linked to the cycles to failure. The failures occurring at lower cycle numbers are dominated by failure type B (pin failure) and C (bow failure on 'corner') whilst shackles surviving to higher cycle numbers eventually failed via modes A or D (bow failure either A - in centre, or D - across the eye). Figure 4.32 details the spread of results observed with reference to failure mode.

The mean cycles to failure by failure mode type is detailed in Table 4.7 and demonstrates the link described above. Standard deviation is also included in this table to quantify the spread of results for each failure mode.

The range of failure modes observed indicate that the shackle is well designed and does not have one particular weak point where failures repeatedly occur. However, the large spread of cycles to failure demonstrates the scatter that is inherent with fatigue failures and which, in part, contributes to the requirement of safety factors for fatigue limit state of 5 or higher (Det Norske Veritas, 2010a). There is limited literature to compare this work to, however a technical report investigating the fatigue
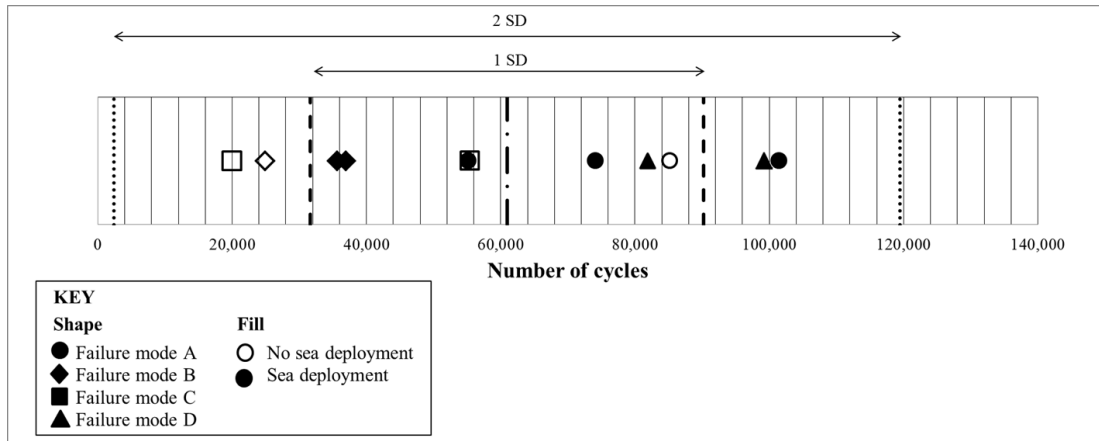
Figure 4.32: Shackle fatigue cycles to failures identified by failure mode and with reference to sea deployment. Based on equivalent 10-90kN cycles at 2Hz. Failure modes identified in Figure 4.26, Page 200.

Table 4.7: Shackle fatigue failure modes with mean cycles to failure and standard deviation identified for each failure mode. Fatigue cycles based on equivalent 10-90kN load cycles at 2Hz. Failure modes identified in Figure 4.26, Page 200

Failure mode	No. failures	Mean cycles to failure	Sample S.D.
All failure modes	11	60,936	29,278
A	4	79,044	19,460
B	3	32,527	6,575
C	2	37,703	25,104
D	2	90,567	12,285

of surface mooring hardware also observed significant scatter in the fatigue performance of shackles (Trask & Weller, 1995), unfortunately the WLL of these shackles is not provided so a detailed comparison cannot be made.

It should be noted, that the shackles used for the work presented in this Thesis were basic galvanized steel shackles, as detailed in Section 4.2. These shackles have not undergone any specialist treatment in order to improve fatigue performance. Alternative shackles are available, such as Van Beest's Green Pin® Super Shackle (Van Beest, 2006) that are manufactured from higher grade steel and to closer tolerances. Shackles such as this would be expected to demonstrate a much smaller range of fatigue results if tested using the same approach. A discussion by Schijve (2009) details the effect of surface finish and surface treatments on the fatigue performance of metals and the complex nature of this topic. Surface treatments such as shot peening increase the surface roughness but improve fatigue performance due to the residual stresses introduced into the surface layer. A study presented by Trask & Weller (1995) demonstrates the improvement in fatigue performance of shot peened shackles, however comments that galvanizing cannot be used following shot peening so alternative corrosion protection is required. The shackles used in the investigation presented in this Thesis were galvanized (to improve corrosion resistance) however it has been suggested that the process of galvanising may actually reduce fatigue performance of steels (Dimatteo *et al.*, 2011).

With reference to the shackle specification, as previously discussed, no specific fatigue performance information was supplied with the shackle. This is standard within industry where basic material properties, MBL and WLL are the extent of the specification (and as detailed for this particular shackle in Section 4.2.3, Page 157). Given the results for the ultimate strength tests, with an average failure load of 210.5kN, and an embedded component safety factor of 8.6 on the WLL, the safety factors under fatigue loading are shown to be more critical. The peak cyclical load for the fatigue testing was 90kN, which is below the specified shackle MBL (122.6kN) and has an associated embedded component safety factor of 3.7 on the specified WLL (24.5kN).

Relating this to the DNV guidance for mooring system design (Det Norske Veritas, 2010a), the safety factor for the fatigue limit state can range from 5 - 8 (as detailed in Chapter 2, Section 2.5.5). Assuming the lower value of 5, the total fatigue safety factor designed into a system based on the WLL of this shackle would therefore be 18.5 (at the load range tested). This result however, is not that informative as the fatigue load

range tested was specified to ensure the testing remained within the elastic region of the shackle behaviour and does not relate to an operational value. Broader and more informative conclusions can be drawn from this work by further analysis of the S-N curve to estimate load to failure at a realistic operational cycle number. This analysis is presented when discussing the analytical fatigue estimations in Section 4.5.3.3.

The main limitation of this work stems from the fact that, due to the requirements of the accelerated testing regime, the constant load range specified for the fatigue testing is not representative of a real mooring load spectrum, such as those presented by Harnois (2014). The accelerated testing regime was set up to investigate the fatigue performance of the shackle in relation to the shackle specified MBL and WLL, and in relation to the general S-N curve provided by DNV (Det Norske Veritas, 2011). To achieve the maximum number of test repeats an identical load range was specified for all shackles. Although this is a simplification of the real loading situation, it allowed for a full appreciation of the inherent scatter present in the fatigue results.

The test facility issues that arose during the second series of fatigue testing and led to six shackles being exposed to 37,200 cycles at a reduced peak load (85kN instead of 90kN) led to a further limitation of this work. To account for the shortfall in load, the Palmgren-Miner damage hypothesis was utilised along with the DNV S-N curve (Det Norske Veritas, 2011) detailed in Figure 4.1. The use of the Palmgren-Miner damage hypothesis is recommended by Det Norske Veritas (2011) and has been extensively applied by others (Christiansen *et al.*, 2013; Jing *et al.*, 2012; Thies *et al.*, 2013a; Xu *et al.*, 2013). However, it does have some limitations as discussed by Cui (2002), with the main limitation being that it does not account for the effect of the load sequence on crack propagation. The crack growth approach is cited as a more accurate fatigue life prediction approach, however it requires knowledge of both the initial crack size (a_0) and the the relationship between crack propagation ($\frac{dA}{dN}$) and stress intensity factor range (δK). Obtaining this information is both timely and expensive so this approach has not been widely adopted by industry (Cui, 2002).

In many of the examples listed above the Palmgren-Miner hypothesis is used to calculate the total damage from a complex series of variable amplitude loading. In contrast, the situation presented in this Thesis has only two simple loading sequences: loading cycles of 10-85kN followed by loading cycles of 10-90kN. Given the main limitation of the Palmgren-Miner approach is that it does not account for the load sequence,

in the situation presented here, the load has increased from one step to the next and is not reduced for subsequent cycles. The main limitation is therefore not a concern and as such the use of this hypothesis is valid for the correction applied to this data set.

In summary, this section of work successfully established the fatigue response of 13 shackles to a fixed loading regime. This allowed a review of the embedded component safety factor at the specified loading regime, and a comparison to the DNV S-N design curve (Det Norske Veritas, 2011) in Section 4.5.3.

4.5.2.3 Experimental field testing

Due to the load cell failure during the SWMTF deployment, it was not possible to calculate the total load exposure of the shackles that were deployed on mooring limb 3 of the SWMTF for a period approaching 6 months. This lack of data proved a major limitation for this section of work.

Following the SWMFT deployment, the shackles were exposed to further fatigue testing at the DMaC test facility and Figure 4.32, Page 215 details the spread of results observed highlighting whether the shackles had been deployed at the SWMTF or not. There appears to be no reduction in cycles to failure for those shackles deployed at the SWMTF.

Although the SWMTF deployment will have caused some fatigue damage, it is likely that the level of loading the shackles were exposed to during the deployment proved insignificant in comparison to the high loading of the DMaC test facility accelerated testing regime (10-90kN). Due to this, no reduction in fatigue performance of these shackles was observed following SWMTF deployment.

4.5.3 Shackle analytical fatigue estimations

The results presented in Section 4.4.3 showed broad agreement between the S-N design curve plotted using the specified parameters from Det Norske Veritas (2011) and the results obtained during the fatigue testing of the shackles, with the S-N curves proving slightly conservative. The anticipated cycles to failure from the S-N curve was estimated as 1,470 and this compared to a measured mean minus two standard deviations cycles to failure of 2,380.

This section will discuss the influence of stress concentration factor, K_t, on the results, as well as the impact of mean stress effects on fatigue results, before using the analytical estimations to consider the results in the context of a realistic operational life.

4.5.3.1 Stress concentration factors

A stress concentration factor, K_t, of 6.96 was established using the numerical models presented in Section 4.4.1.4. As highlighted previously, the method utilised for establishing K_t is only strictly applicable to Paths 3 and 7 (detailed in Figure 4.10, Page 178), where loading will be predominantly tensile (Mode I). Given the peak value for K_t occurs on Path 7 this figure is assumed valid to use with the S-N fatigue life assessment.

This fatigue assessment was conducted at a relatively low load of 90kN to represent the peak loading level used with the physical fatigue testing. It is anticipated that the majority of the shackle will be deforming elastically at this level of loading, and it should be noted that this approach is only valid under the elastic regime. As previously discussed, the linear elastic FEA model will not produce accurate results once plastic deformation occurs beyond the yield point of the material.

The stress concentration factor has a large influence on the results, and Figure 4.33 is included to demonstrate the impact of K_t. This figure compares the calculated cycles to failure using a K_t of 6.96 (1,469 cycles) with the cycles to failure estimated if the nominal stress were used with no K_t applied (3,446,139 cycles). It also assesses the variation of cycles to failure in relation to the sensitivity of K_t, assessing cycles to failure with a K_t of 6.96 $\pm$ 20% (resulting in a range of 708 - 3,585 cycles to failure). This figure demonstrates the significant influence the specified value of K_t has on these results.

Due to the strong effect of the stress concentration factor on the calculated cycles to failure, other literature was sought to provide assurance that the applied value for K_t of 6.96 was not excessive. Although no studies on shackles could be identified, a study by Adziev *et al.* (2004) reviewed the structural integrity of mooring components and calculated stress concentration factors (K_t) for stud-less and stud chain links. These values are detailed in Figure 4.34, and show a peak K_t of 4.5 occurring on the stud-link chain at location B1. This location reflects the identified peak K_t in the equivalent shackle model, providing some support for K_t used for the shackle assessment.
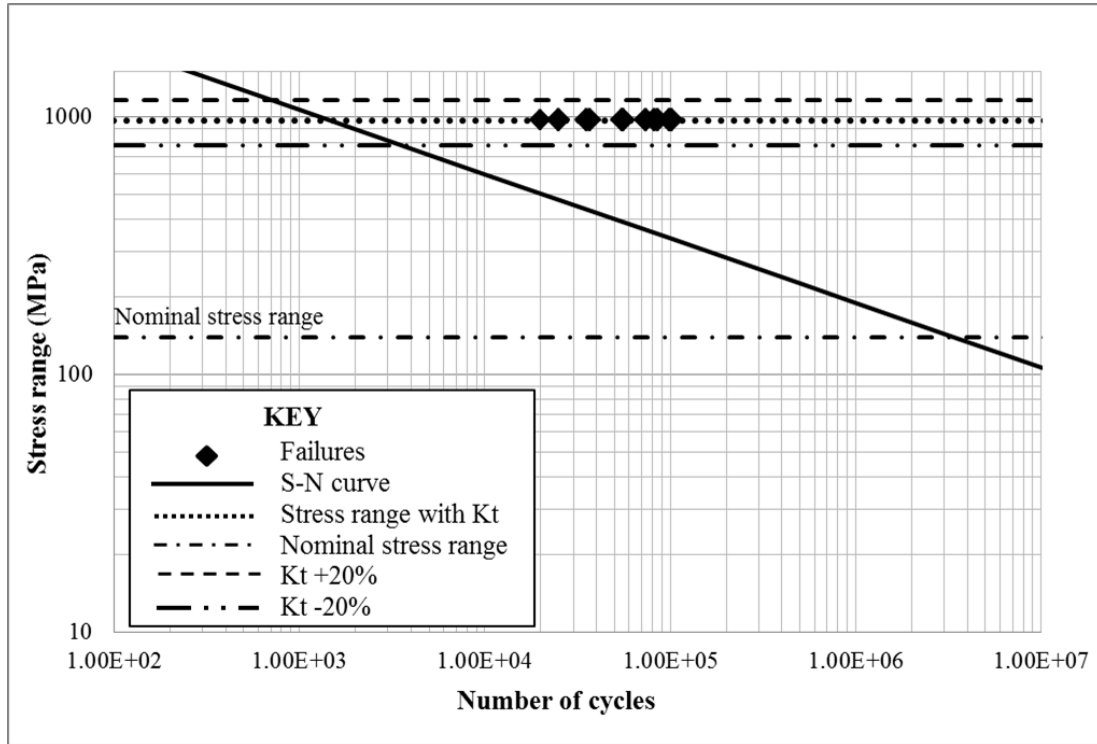
Figure 4.33: A demonstration of the sensitivity of the cycles to failure estimated from the S-N curve to variations in the stress concentration value applied.

Position of analysis	SCF	
	Studless Chain Link	Stud Chain Link
A1	3.9	2.5
A2	3.4	2.3
A3	1.3	1.2
B1	4.0	4.5
B2	2.7	2.9
B3	0.8	0.7
WL1	3.0	1.2
WL2	2.4	1.6
WL3	1.0	1.8
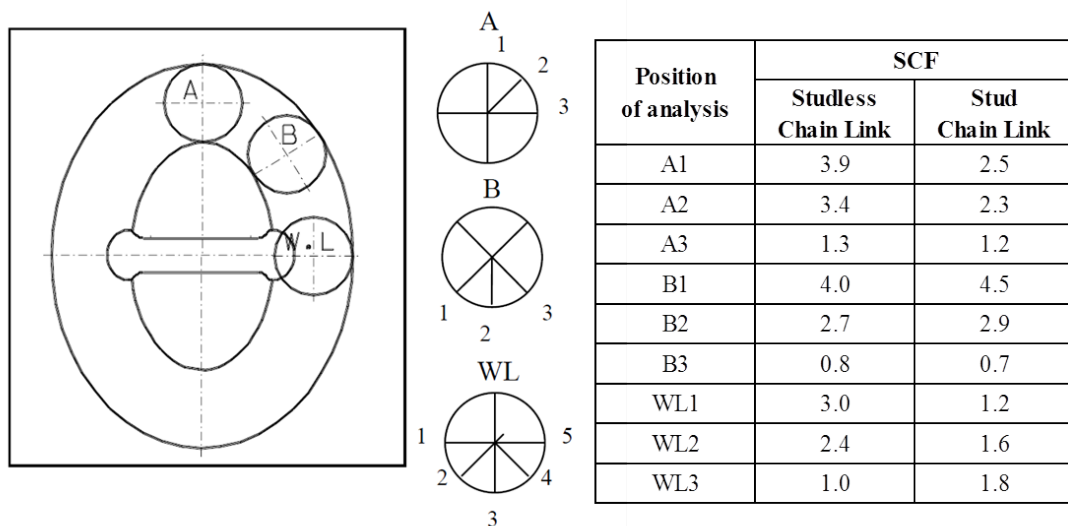
Figure 4.34: Reference stress concentration factors replicated from a study by Bastid & Smith (2013) investigating the structural integrity of mooring components.

Although limited details on stress concentration factors are provided, a further paper by Bastid & Smith (2013) reviews the contact stresses in mooring chain links. This paper also cites the internal face of the commencement of the curved end of the link as the location for the peak K_t, and suggests a K_t of approximately 4 for a standard chain link. Relating these studies back to the shackle model, the load path through a chain link will have a smoother distribution than through a shackle, so the shackle model would be expected to have a higher peak K_t. Given this, the use of a K_t of 6.96 in the shackle model seems broadly appropriate.

Given the limited fatigue data supplied with conventional mooring components, mooring designers must rely on the use of generic S-N curves if they are designing a system with reference to fatigue. This work has shown the large impact of the selected K_t on the estimated cycles to failure using a generic S-N curve. To improve the accuracy of mooring design regarding fatigue, and to provide a consistent approach across the sector, the publication of suitable stress concentration factors for commonly used components would be a great benefit. Given that DNV guidance document *DNV-OS-E301: Position Mooring* (Det Norske Veritas, 2010a) suggests the use of S-N curves published in DNV document *DNV-RP-C203: Fatigue design of offshore steel structures* (Det Norske Veritas, 2011), presenting appropriate values for K_t in these documents would be a useful addition to this guidance.

When reviewing the analytical results in the context of those results obtained through the experimental work, it is clear that failures occurring due to shear stress have not been captured through the analytical assessment. With reference to the locations of the failures in relation to Figure 4.10, Page 178, of 11 fatigue failures observed during experimental testing only two occurred on Path 7. The remaining failures occurred along Paths 1 and 4 and along the shackle eye (which was not captured by the 'paths' set up within the FEA model). The seven failures occurring on Paths 1 and 4 will have been dominated by shear loading (Mode II presented in Section 4.3.1.6, Page 167), and therefore not captured in this analytical assessment. To assess the shear dominated failures using the FEA model, the peak shear stress could be extracted from the FEA model along the identified paths. This could be compared to the nominal shear stress to calculate a shear stress concentration factor $K_{t-shear}$. However, the value of K_t generated here is for use with the B1 S-N Curve (Det Norske Veritas, 2011). This

221

curve is based on tensile-tensile loading and without a specific shear S-N curve, the calculation of $K_{t-shear}$ alone would not resolve this limitation. A further addition to the guidance could therefore be a more detailed consideration of shear failure and the publication of appropriate shear S-N curves for assessment of fatigue life with reference to shear loading.

A further consideration for the analytical assessment is the presence of a mean stress, which also has an effect on fatigue response. This will be explored in the next section.

4.5.3.2 Mean stress effects

During the fatigue testing presented in this chapter, to ensure the alignment of the shackles was maintained throughout the testing, a minimum load of 10kN was specified. The fatigue cycling regime then cycled from 10kN - 90kN with a mean load of 50kN. The standard S-N curve does not account for the presence of a mean stress and assumes fully reversed loading with a mean stress of 0. However, it is widely accepted that mean stress can have an effect on fatigue life of components (Dowling, 2004; Dowling *et al.*, 2009; Koh, 1991; Wehner & Fatemi, 1991; Xia *et al.*, 1996).

The presence of a mean stress is not unique to this testing regime and mooring systems installed for wave energy generators will also have a mean stress (Thies *et al.*, 2013a). The self weight of each mooring limb will create a certain level of pre-tension and some mooring designs will be designed specifying a pre-tension in the system. Ferrario *et al.* (2004) present the design for an oscillating water column wave energy device that has a taut mooring with a pre-tension requirement of 90 tons (882.6kN).

As the presence of a mean stress in the fatigue cycling of a mooring system is a genuine consideration for the design of wave energy converter mooring systems, it is worth spending some time looking into proposed approaches to address the presence of a mean stress. Several different approaches have been developed and a short review of the literature will discuss the most suitable approach for use with the steel shackles specified in this Thesis.

Before outlining the different calculations, some variables that are common across the different techniques will be outlined below:

σ_{min} = minimum stress

σ_{max} = maximum stress

σ_a = stress amplitude = $\frac{\sigma_{max} - \sigma_{min}}{2}$

σ_m = mean stress = $\frac{\sigma_{max} + \sigma_{min}}{2}$

σ_{ar} = stress amplitude for equivalent completely reversed loading

$\Delta\sigma$ = stress range = $2\sigma_a$

σ_u = ultimate tensile strength

σ_y = yield strength

$\widetilde{\sigma_{fB}}$ = true fracture strength

σ_f' = fatigue strength coefficient

Dowling *et al.* (2009) provide a good summary of the different approaches and these will be summarised using the nomenclature described:

- **Gerber relation:** This was the earliest approach developed by Gerber in the 1800s, and has been subtly developed by others over the years. The original Gerber relation is detailed in Equation 4.13.

$$\sigma_{ar} = \frac{\sigma_a}{1 - (\frac{\sigma_m}{\sigma_u})^2} \qquad (4.13)$$

- **Goodman relation:** Detailed in Equation 4.14

$$\sigma_{ar} = \frac{\sigma_a}{1 - (\frac{\sigma_m}{\sigma_u})} \qquad (4.14)$$

- **Soderberg relation:** Detailed in Equation 4.15

$$\sigma_{ar} = \frac{\sigma_a}{1 - (\frac{\sigma_m}{\sigma_y})} \qquad (4.15)$$

- **Morrow relation:** Morrow further developed the basic forms detailed above by introducing a corrected true fracture strength ($\widetilde{\sigma_{fB}}$) in 1968 (Dowling *et al.*, 2009). This is detailed in Equation 4.16.

$$\sigma_{ar} = \frac{\sigma_a}{1 - (\frac{\sigma_m}{\sigma_{fB}})} \qquad (4.16)$$

- **Alternative Morrow:** An alternative form of this replaced the true fracture strength with a fatigue strength coefficient (σ_f') as detailed in Equation 4.17.

$$\sigma_{ar} = \frac{\sigma_a}{1 - (\frac{\sigma_m}{\sigma_f'})} \tag{4.17}$$

For some materials, such as steel, the Morrow and Alternative Morrow relations give similar results as $\sigma_f' \approx \sigma_{fB}$ (Dowling, 2004).

- **SWT relation:** In 1970 Smith, Watson and Topper introduced a new approach often referred to as SWT, and detailed in Equation 4.18 (Smith *et al.*, 1970). Unlike all the other approaches, this approach does not require the use of any material properties.

$$\sigma_{ar} = \sqrt{\sigma_{max}\sigma_a} \tag{4.18}$$

- **Walker relation:** The SWT relation was further developed by Walker, who introduced a material constant, γ. Taking a value between 0 - 1, γ is essentially a measure of the material sensitivity to the effect of mean stress (Dowling *et al.*, 2009; Walker, 1970). Equation 4.19 details the Walker relation.

$$\sigma_{ar} = \sigma_{max}^{1-\gamma}\sigma_a^{\gamma} \tag{4.19}$$

Dowling *et al.* (2009) conducted extensive testing and derived some values for γ. A liner relationship to estimate γ for steels was also derived and detailed in Equation 4.20

$$\gamma = -0.0002\sigma_u + 0.8818 \tag{4.20}$$

Of all the introduced approaches, Equations 4.13, 4.14, 4.15 and 4.18 are the quickest to apply, utilising widely available material properties to estimate the effect of mean stress. Equations 4.16, 4.17 and 4.19 on the other hand, utilise material properties that are less readily available and may need to be empirically obtained.

In the shackle case study presented here, the true fracture area is not available to calculate the true fracture strength, $\widetilde{\sigma_{fB}}$ that is required for Equation 4.16 and to estimate Equation 4.17. However, γ required for Equation 4.19 can be estimated using the empirical linear relationship derived for steels by Dowling *et al.* (2009). For this case study, two possible values of σ_u could be used. Either the value specified in the

material specification from the shackle manufacturers, σ_u of 1010MPa, which gives an estimated γ of 0.6798. Alternatively, the value for σ_u derived from the ultimate limit state tests could be used, σ_u of 366MPa, which gives a γ estimated as 0.8085.

The variety of approaches suggested above produce a large range of estimated values for σ_{ar}. Figure 4.35 details the range of adjusted stress amplitude results. As there was a significant difference between the shackle specified material properties (890MPa and 1010MPa for yield and ultimate strength respectively) and those values obtained through the ultimate limit state tests in Section 4.4.2.1 (192MPa and 366MPa respectively), the adjusted stress amplitude calculations have been conducted separately for each.

Much of the literature compares the accuracy of the mean stress relations discussed to empirical data, often for specific materials. Koh (1991) looked specifically at high strength steel and concluded the SWT (Equation 4.18) provided the most accurate estimate of mean stress effects. The paper also observed the detrimental effect of tensile mean stress on the fatigue life in contrast to the positive effect of compressive mean stress. During the same year Wehner & Fatemi (1991) reviewed mean stress effects on hardened carbon steel. As well as confirming the significant effect tensile mean stress has on the fatigue life of this material, the paper concurs with Koh (1991) that the best correlation to the experimental data is achieved using the SWT approach, with Goodman (Equation 4.14) and Morrow (Equation 4.16) providing some correlation, but Soderberg (Equation 4.15) and Gerber (Equation 4.13) proving unsatisfactory.

Research by Xia *et al.* (1996) looked at the effect of both mean stress and ratcheting strain on the fatigue life of steel. This work also concluded SWT provided the best fit to experimental data when reviewing mean stress effects.

More recently, a thorough review of the accuracy of the different mean stress effects was conducted by Dowling and published in Dowling (2004) and Dowling *et al.* (2009). This research reviews the accuracy of many of the different mean stress relations in comparison to experimental data for a variety of metals including steels, aluminium alloys and a titanium alloy. The conclusions detail the suitability of the different mean stress relations for different metals. For steels, it is concluded that the alternative Morrow equation (Equation 4.17) using the fatigue strength coefficient σ_f' provides accurate use, with SWT (Equation 4.18) providing a good choice for general use (although less
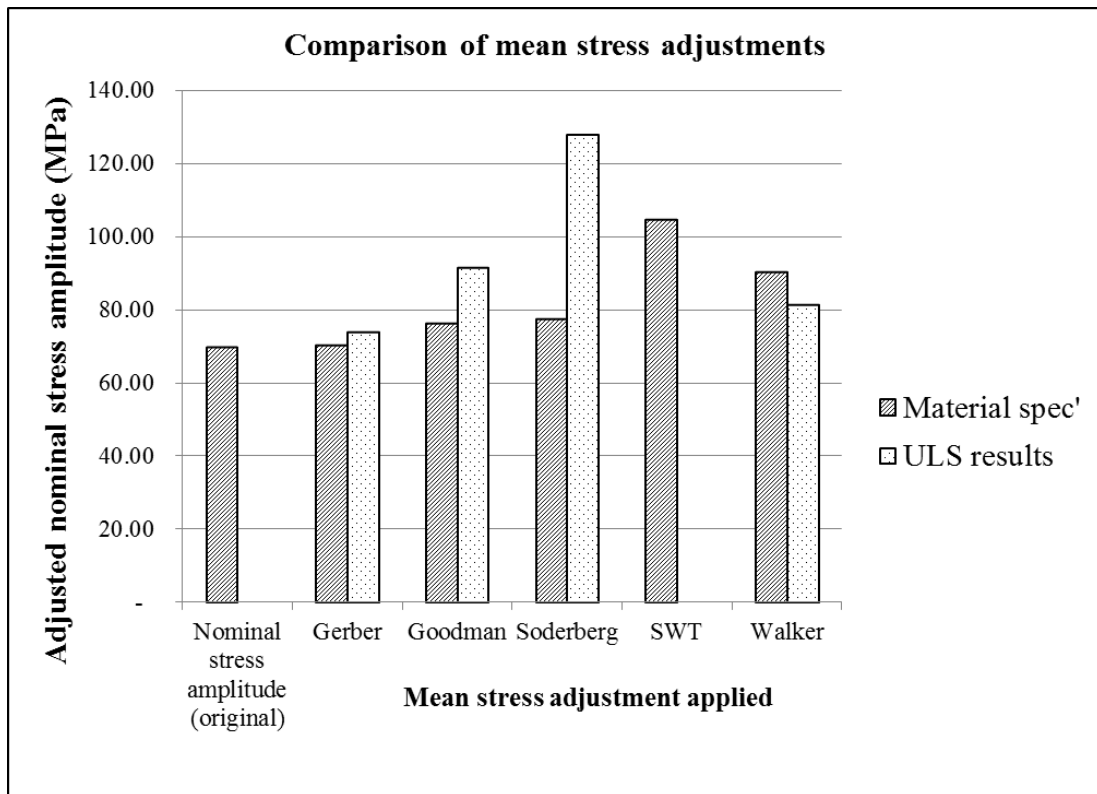
Figure 4.35: Comparison of mean stress adjustment factors applied to the fatigue cycling regime of 10 - 90kN. 'Material spec' results account for values calculated using material properties as specified; 'ULS results' account for values calculated with results from ultimate limit state testing of shackles. Note the original, uncorrected stress amplitude has been included for comparison, and the SWT approach does not require material properties for calculation.

accurate than the Moorow relation for steels). Dowling (2004) concludes that if γ is known or can be accurately estimated then the Walker relation (Equation 4.19) provides the best results for steel. This work is further developed and Dowling *et al.* (2009) present an empirically derived relationship to estimate *gamma* (Equation 4.20). This relationship has been used to calculate the results for the Walker adjustment detailed in Figure 4.35.

Having reviewed the literature, the consensus is that the SWT relation will provide an accurate estimate for the effect of mean stress on fatigue life. Although Dowling *et al.* (2009) have a preference for the Walker equation utilising an estimate for γ, SWT is still accepted as a good choice. Given the consensus from the other papers reviewed, the SWT approach will be used as the mean stress relation when reviewing the results from the shackle fatigue tests presented in this Thesis. Reflecting the previous comment regarding the publication of stress concentration factors in mooring guidance documents (Section 4.5.3.1), given that many mooring system designs for WECs will require a pretension, the publication in guidance documents of a suitable mean stress adjustment factor for use with generic S-N curves would again ensure an accurate and consistent approach was adopted across the sector.

Using the SWT approach the adjusted stress amplitude was calculated and used to define the adjusted stress range for the fatigue testing (twice the stress amplitude). The adjusted stress range was then plotted on the relevant S-N curve to allow an estimation of the cycles to failure and plot the shackle failures observed at the adjusted stress range. Figure 4.36 details the revised plot and includes both (i) the original stress range calculated from the nominal stress multiplied by K_t and (ii) the SWT adjusted stress range for comparison. The estimated cycles to failure from the S-N graph is reduced from 1,469 to 290 when accounting for the effect of the mean stress. This makes the analytical estimation using the S-N curve even more conservative given the experimental results observed mean cycles to failure of 60,936 and mean cycles to failure minus two standard deviations of 2,380 cycles.

4.5.3.3 Operational life

Given the adjustments made to the S-N curve discussed above, which have utilised an appropriate stress concentration factor, K_t and considered mean stress effects, the S-N
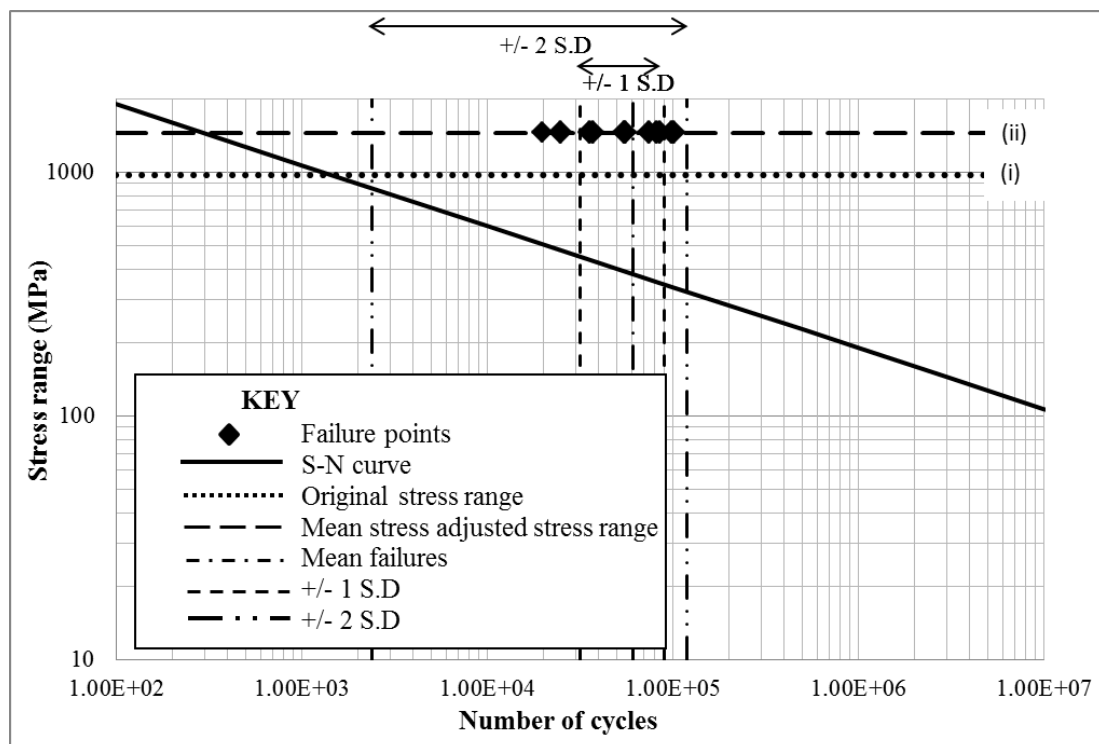
Figure 4.36: S-N curve for shackles in air, with shackle failures plotted at stress range
(ii) adjusted using the SWT approach to account for the mean stress present during the
fatigue testing. The original stress range is also included for comparison and labelled
(i).

curve was established as conservative and could then be used to draw more general conclusions. The experimental fatigue results obtained were conducted at one load range (10-90kN), and the mean cycles to failure at this load range was 60,936 cycles. If a typical wave period, T_p, of 8 seconds is assumed this represents just 5.64 days (or 135.4 hours) of operation. In reality, a conventional mooring system would be expected to be operational for at least 10 years. Using the same typical wave period of 8 seconds this represents 39,420,000 cycles (3.90E+07 cycles).

The S-N curve first presented in Section 4.2.3, Figure 4.1, Page 156, can be used to estimate the maximum stress range that could be applied when assuming 3.90E+07 cycles, representing 10 years of operation. The S-N curve was extended to accommodate this high cycle number and is detailed in Figure 4.37 to show the maximum stress range that could be applied assuming constant amplitude loading for a 10 year deployment with a T_p of 8s (this is a simplified situation for illustrative purposes, a real deployment would have a variable load and wave period).

The maximum stress range identified from Figure 4.37 was 81.29MPa. Taking into account the 6.96 stress concentration factor K_t, and working backwards through the SWT mean stress adjustment applied, this relates to a non-mean stress adjusted nominal stress amplitude, σ_{nom}, of 1.64MPa. Given the same minimum loading (or pre-tension) as applied for the original fatigue testing e.g. 10,000N or a stress of 17.45MPa, this results in a peak stress of 20.74MPa or a peak load of 11,885N.

Summarising this, for a 10 year anticipated deployment, with a pre-tension of 10,000N and a cycle period of 8s, according to the adjusted S-N curve, the maximum load that could be applied whilst avoiding shackle failure is 11,885N. This represents just 49% of the shackle specified WLL (an embedded component safety factor of 0.49) and highlights one of the key concerns surrounding the lack of fatigue data available for mooring components. It should be emphasised that the adjustments made to the S-N curve did result in a conservative fatigue estimate, however, it is still a concern that the anticipated load limit for a 10 year deployment is nearly half of the shackle specified WLL.

To put this into context, if the design safety factors detailed by DNV were applied (with a suggested range of 5 - 8 (Det Norske Veritas, 2010a)) the total system safety factor would range from 2.45 - 3.92, significantly lower than the equivalent resultant safety factor for ultimate limit state of 14.6 (Section 4.5.2.1).
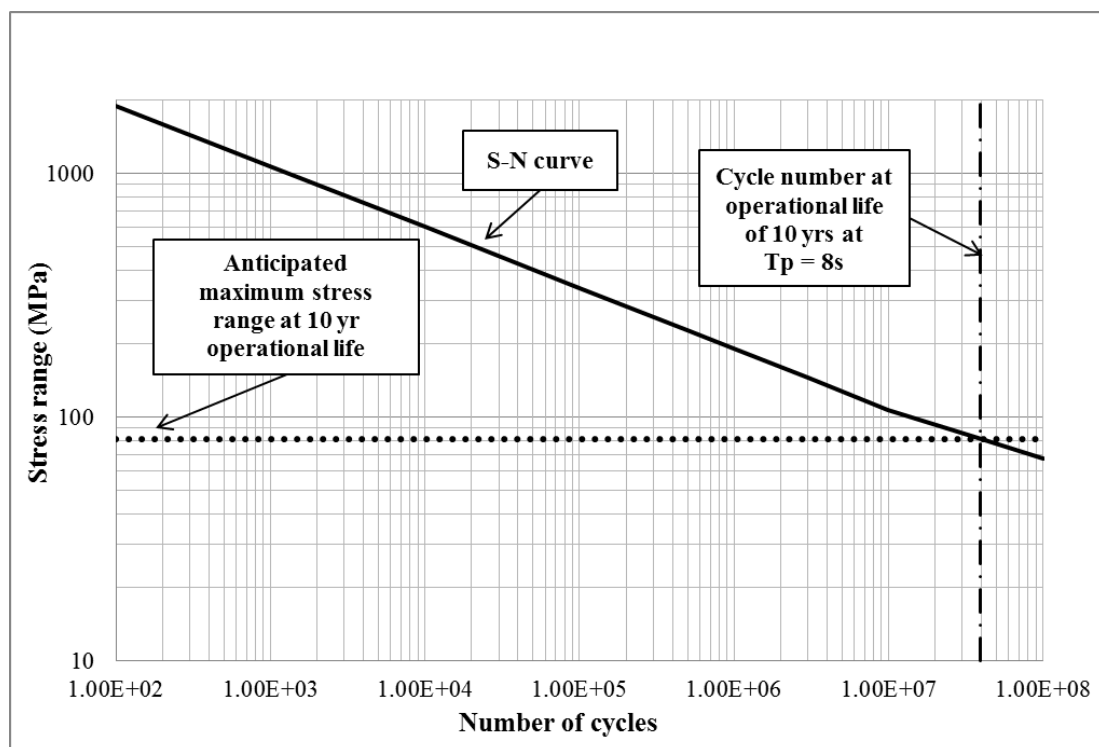
Figure 4.37: S-N design curve for shackles in air (Det Norske Veritas, 2011) with cycle number highlighted for anticipated operational life of 10 years at a cycle period, T_p, of 8s.

4.5.3.4   Analytical fatigue estimations summary

This section has focused on the use of the published S-N curve (Det Norske Veritas, 2011) to assist in the prediction of fatigue failures for the shackles tested as part of this work. The initial results showed that given a K_t of 6.96, the estimated cycles to failure from the S-N curve compared well to those observed in the fatigue limit state testing (S-N estimate of 1,469 cycles compared to fatigue testing of mean minus two standard deviations of 2,379 cycles).

The importance of an accurate stress concentration factor for the given component was discussed. For simple geometries standard formula such as those presented in Young & Budynas (2002) can be used, however for more complex geometries, such as the shackle, FEA models allow a thorough investigation into appropriate stress concentration factors.

The analytical assessment conducted here has used a K_t value based on maximum principal stress for the calculation of fatigue life with the B1 tension-tension S-N curve (Det Norske Veritas, 2011). Given many of the fatigue failures observed through the experimental work occurred in shear it would be appropriate to develop a $K_{t-shear}$. However, given a shear S-N curve is not available for calculation of fatigue life in shear dominated loading, this has not been done. The maximum K_t of 6.96 was observed on a tensile dominated area of the shackle, and therefore this value was considered valid for the fatigue assessment with the tensile-tensile S-N curve.

This discussion has shown that the presence of a mean stress during fatigue cycling requires an adjustment to the calculated stress range used with the S-N curve. Following a short review of the literature the SWT approach was selected as the most appropriate adjustment for the steel shackles and when this was applied to the stress range, a reduced estimated value of 290 CTF was calculated. In wave energy mooring applications a mean stress is likely to be present, so accounting for the mean stress in fatigue life estimations is very important if an accurate prediction of fatigue life is to be made.

Following the adjustments to the S-N curve, the curve was used to estimate the peak loading that could be applied if the shackle were to survive a 10 year deployment with constant loading at a wave period of 8s. A peak applied load of 11,885N was calculated, providing a safety factor of 0.49 on the shackle specified WLL. Applying

the DNV suggested mooring system design safety factors, the total system safety factor
range would be 2.45 - 3.92. This highlights long term fatigue loading as the dominant
concern for system reliability, over ultimate limit state.

Having discussed the results presented in this chapter in detail, a more general
discussion will be provided in the Discussion Chapter 6. Conclusions and next steps
from this work will be detailed in Chapter 7.

Chapter 5

Reliability assessment of a novel mooring component: The Exeter Tether

Contents

5. RELIABILITY ASSESSMENT OF A NOVEL MOORING COMPONENT: THE EXETER TETHER

5.1   Introduction

This chapter details the reliability assessment of a novel mooring component, the Exeter Tether. To put the reliability work conducted into context, Section 2.6 was included in the Literature Review (Chapter 2, Page 112). This outlined the development of the Exeter Tether, which was led by Parish and is fully documented in Parish (2015). With reference to this overview, Section 5.2 details the key reliability considerations for each of the identified components and outlines how they are addressed through the work presented in this Thesis. Following this, Sections 5.3, 5.4 and 5.5 detail the Methods, Results and Discussion of the work undertaken to investigate the reliability of the Exeter Tether. A broader discussion, relating this work to the original research questions is detailed in Chapter 6. Finally, conclusions and further work from this research are detailed in Chapter 7.

5.2   Tether components and reliability considerations

Reliability considerations for each of the Exeter Tether components are discussed in the following sections. They are ordered working from the outside of the tether towards the core: End terminations; hollow braided rope; anti-friction screen; polymer core.

5.2.1   End terminations

The ends of the Tether P1-Series are terminated with a form of Lankhorst Rope's A3 eye splice. The two main reliability considerations for this are:

- Overload failure, caused by peak loads exceeding the breaking load of the eye splice. As detailed in Section 2.6.3.4, if the splice is not accurately manufactured the breaking load of the eye splice is significantly compromised.

- Fatigue failure, from the repeated lower level loads during operation causing friction damage between adjacent yarns of the eye splice, ultimately leading to failure.

These catastrophic failures could potentially lead to the loss of a device. In addition marine growth may also affect the eye splice, with particle ingress creating additional points for friction damage, which could also promote a catastrophic failure.

5.2.2 Hollow braided rope

The key reliability considerations for the rope are similar to those detailed for the eye splice:

- Overload failure, caused by peak loads exceeding the breaking load of the rope.

- Fatigue failure, from the repeated lower level loads during operation causing friction damage between adjacent yarns (Weller *et al.*, 2013).

- Marine growth, this could add significant weight and bulk to the rope and alter the dynamics of the system. In addition, debris from hard shell species could infiltrate the rope yarns and cause increased fibre cutting and abrasion promoting premature failure (Weller *et al.*, 2013).

- Component interactions between the hollow rope and the anti-friction screen. During tether operation these two components continuously rub over one another, potentially leading to wear and premature failure of the rope and/or breakdown of the screen leading to bio-fouling infiltration of the core.

- Finally, any damage caused to the rope during manufacture, shipping or deployment could introduce weaknesses into the load carrying capability of the rope and should also be considered.

These failure mechanisms would also lead to catastrophic failure and potential loss of the device.

5.2.3 Anti-friction screen

The anti-friction screen does not carry any load in the tether, so degradation of the anti-friction screen would not directly lead to catastrophic failure. However, breakdown

of the screen could introduce high friction points that could promote wear of the hollow rope and eventually lead to premature failure. Key reliability considerations are:

- Marine environment durability. Two different screens are under trial in the P1-Series. Dacron is anticipated to have good marine environment durability as it is widely used for boat sail manufacture. The second material under consideration is PVC. Despite being a very durable tape, little is known about the long term effect of the marine environment on PVC.

- Marine bio-fouling. One of the potential functions of the screen is to protect the core from marine bio-fouling ingress. The effects of marine bio-fouling on the screen and whether it can be penetrated are therefore of interest.

- Component interactions. The continuous movement of the rope over the screen during tether operation is likely to cause the most damage to the screen of all the reliability issues discussed. This is a key issue as if the screen begins to break down, it could create high friction areas which would promote wear on the tether rope and ultimately lead to premature failure.

5.2.4 Elastomeric core

Unlike the reliability considerations for the eye splice and the hollow rope, the polymer core carries a minimal load (it is estimated to carry 10% of the total tether load (Parish, 2015)), and therefore any deterioration of the core is unlikely to lead directly to catastrophic failure. However, breakdown of the core materials could change the operating parameters of the tether (as detailed in Section 2.6.4 the material properties of the polymer core directly affect the compliance of the tether). This could in turn lead to higher peak loads which could, in time, lead to a premature failure. The key reliability considerations for the elastomeric core are:

- Fatigue cycling of the core. This includes both radial compression cycling, and axial extension cycling of the core material. The long term affects of these actions on key material properties is unknown.

- Marine environment durability. In contrast to the use of established materials for the rope and eye splice, there is no published data on the affects of the marine

environment on EPDM rubber. EPDM was selected as it has very good water and ozone resistance, as well as good resistance to abrasion and wear (Rinnbauer, 2007), additionally it was widely available off-the-shelf (Parish, 2015). However there is no data on the long term effects of exposure to the marine operating environment, which clearly has the potential to cause material degradation.

- Component interactions between the core, screen and rope. The core and screen are subject to high pressures from the rope during tether operation, the effects of the pressure on the core structure are unknown.

5.2.5   Failure modes and effects analysis

To enable ranking of the reliability considerations of the Exeter Tether, a Failure Modes and Effects Analysis approach has been used, focusing on reliability issues as opposed to complete component failures. The structure and purpose of a FMEA is outlined in the Literature Review, Section 2.3.2.1, Page 59. The FMEA conducted for the Exeter Tether is detailed in Table 5.1. At this stage of component development for such a novel design there are clearly some probabilities and consequences that are hard to quantify and as such it is challenging to use the detailed look up tables presented by DNV (Det Norske Veritas, 2015) and detailed in the Literature Review (Figure 2.16, Page 61). Where knowledge is limited, the most appropriate values have been chosen and the 'remarks' column has been used to detail any uncertainties. Despite the unknowns, this is a very useful exercise for ranking component risks, and the FMEA detailed in Table 5.1 multiplies the probability by the consequence to provide a 'Risk Priority Number' in order to rank the risks.

5.2.6   Summary

Of the reliability issues discussed, Figure 3.3, Page 133 presented in Chapter 3 outlines the most critical reliability considerations identified for each component of the tether and provides a useful summary.

It was not possible to cover all aspects of tether reliability in this Thesis, so it was necessary to select particular components for further investigation. To develop a better understanding of the key reliability threats to the tether, full assembly testing was necessary, both at sea (to observe the effects of the marine environment) and

Table 5.1: Failure modes and effects analysis approach for the Exeter Tether reliability issues. Failure effects marked * may ultimately lead to complete failure due to altered operating parameters, but only the initial effect is listed in this table.

Item	Reliability consideration	Reliability effect	Probability	Consequence	Risk Priority Number	Remarks
Hollow braided rope	Overload	Failure of rope	1	5	5	Informed specification of MBL from **wide** industry knowledge should minimise probability.
	Fatigue failure	Failure of rope	2	5	10	Informed specification of rope with **some** industry knowledge should minimise probability.
	Bio-fouling	Change of device dynamics*	5	2	10	Some information in the literature but more work needed to quantify the effects of bio-fouling. Very likely to occur.
End terminations	Overload	Failure of splice	2	5	10	**Some** industry knowledge regarding eye splice strength should minimise probability.
	Fatigue failure	Failure of splice	3	5	15	**Limited** industry knowledge regarding eye splice fatigue performance.
	Bio-fouling	Bio-fouling infiltration of splice construction*	5	2	10	Some information in the literature but more work needed to quantify the effects of bio-fouling. Very likely to occur.
Polymer core integrity	Fatigue cycles; compression / extension	Altered material properties. Loss of tether performance, altering of loads on device, no reduction of peak loads etc.*	5	3	15	Fatigue cycling of core will definitely occur, with unknown consequences; no existing information on material response.
	Marine environment durability	Altered material properties. Loss of tether performance, altering of loads on device, no reduction of peak loads etc.*	5	3	15	Exposure to marine environment will definitely occur, with unknown consequences; no existing information on material response.
Anti-friction screen	Marine environment durability	Degradation of screen creating rough surface*	3	3	9	Novel application therefore uncertain probability of occurrence and uncertain consequence.
	Bio-fouling	Infiltration of marine debris *	3	2	6	Novel application therefore uncertain probability of occurrence and uncertain consequence.
Component interactions	Rope continuously rubbing over	Degradation of screen creating rough surface*	3	2	6	Likely to be some friction effects from tether operation but novel application so uncertain consequence.
	Rope compression of core / screen	Degradation of screen and/or core: altered material properties. Loss of tether performance, altering of loads on device, no reduction of peak loads etc.*	3	3	9	Likely to be some interaction between components with uncertain consequences.

239

in controlled laboratory conditions. This established the component interactions and highlighted any unforeseen reliability concerns.

In addition, specific component test regimes were conducted to develop understanding of the novel aspects of the tether that had limited relevant literature available. From the FMEA analysis conducted in Table 5.1 the polymer core integrity stands out with a high risk priority number. This high score is due to the high probability (the core will definitely be subjected to numerous fatigue cycles and exposed to the marine environment during operation), and the very limited information currently available about the effects of these two things on the EPDM material. Due to this, polymer core integrity was identified as a key focus for the work presented in this Thesis. Additionally, the novel use of the anti-friction screen had significant uncertainties and was selected as a further focus for this work.

Clearly the consequences of rope or splice failure are severe, and fatigue loading presents a particular concern. However, these are more established fields in the industry and therefore less specific to the development of the tether. Table 5.2 details the test approaches for each of the identified reliability issues.

Table 5.2: Development approaches identified for the Exeter Tether reliability assessment

Item	Reliability consideration	Tether development approach
Tether assembly durability	Overload	Refer to existing work 'Proof of Concept Study'.
	Fatigue	Assembly testing in controlled laboratory conditions: **Section 5.3.1.1. Laboratory assembly assessment - DMaC.**
	Marine environment durability	Assembly sea testing: **Section 5.3.1.2. Field assembly assessment - SWMTF.**
Hollow braided rope	Overload	Not covered in this Thesis: Refer to existing industry practice and literature.
	Fatigue failure	
	Bio-fouling	Sea trials at the SWMTF: **Section 5.3.1.2. Field assembly assessment - SWMTF.**
End terminations	Overload	Not covered in this Thesis: Refer to existing industry practice and literature.
	Fatigue failure	
	Bio-fouling	Sea trials at the SWMTF: **Section 5.3.1.2. Field assembly assessment - SWMTF.**
Polymer core integrity	Fatigue cycles; compression / extension	Material tests in controlled laboratory conditions: **Section 5.3.2. Elastomeric core durability assessment.**
	Marine environment durability	Material tests of aged polymer in controlled laboratory conditions: **Section 5.3.2.1. Elastomeric core durability assessment - Ageing of polymer.** Sea trials at the SWMTF: **Section 5.3.1.2. Field assembly assessment - SWMTF.**
Anti-friction screen	Marine environment durability	Sea trials at the SWMTF: **Section 5.3.1.2 Field assembly assessment - SWMTF.**
	Bio-fouling	
Component interactions	Rope continuously rubbing over screen.	Laboratory testing at DMaC: **Section 5.3.3. Anti-friction membrane investigation.**
	Rope compression of core / screen	Assembly testing: **Section 5.3.1. Tether assembly durability assessment (DMaC & SWMTF)**

5.3 Method

Due to the extensive nature of test work presented in this Chapter, Figure 5.1 has been
included to aid navigation through this section of work.

5.3.1 Tether assembly durability assessment

Tether assembly durability trials focused on the longer term testing of the complete
tether assembly to observe the durability of the system and components when exposed
to extended loading regimes and when deployed in situ in the marine environment. The
next two sections detail each of the methods involved for this test work.

5.3.1.1 Laboratory assembly assessment - DMaC

As discussed in Chapter 2, there is limited guidance regarding standard testing regimes
for mooring systems for wave energy converters, and this is certainly the case for long
term durability testing. However, the oil and gas industry provides a good reference
point for this work. A standard test developed by the Oil Company's International
Marine Forum (OCIMF) to quantify mooring hawser response to tension-tension fatigue
(when the sample remains under tension through the maximum and minimum loads
of the fatigue loading regime), is the 'Thousand Cycle Load Limit' or TCLL (Oil
Companies International Marine Forum, 2000). The TCLL test was conducted on
tether P1-16 and is summarised by Gordelier *et al.* (2015).

Although originally developed for mooring hawsers, the TCLL test has become a
standard industry test to express a rope's performance with regard to tension-tension
fatigue. A good definition of the TCLL test is provided by Lankhorst Ropes: *"TCLL
expresses the maximum percentage of the nominal breaking strength at which a rope can
be cycle loaded 1000 times as tested under strict laboratory conditions."* (Lankhorst
Austraila, 2013).

The principle of the TCLL test is to cycle the specimen for 1,000 cycles at increas-
ing load steps. 1,000 cycles are conducted at 50% NWBS (new wet breaking strength),
then 1,000 cycles at 60% NWBS and so on, each time increasing the load by a further
10%. The key principals of the TCLL test procedure were adhered too with some adap-
tations to make the test more appropriate for the P1-Tether Series and the operating
capabilities of DMaC. The key adaptations were:
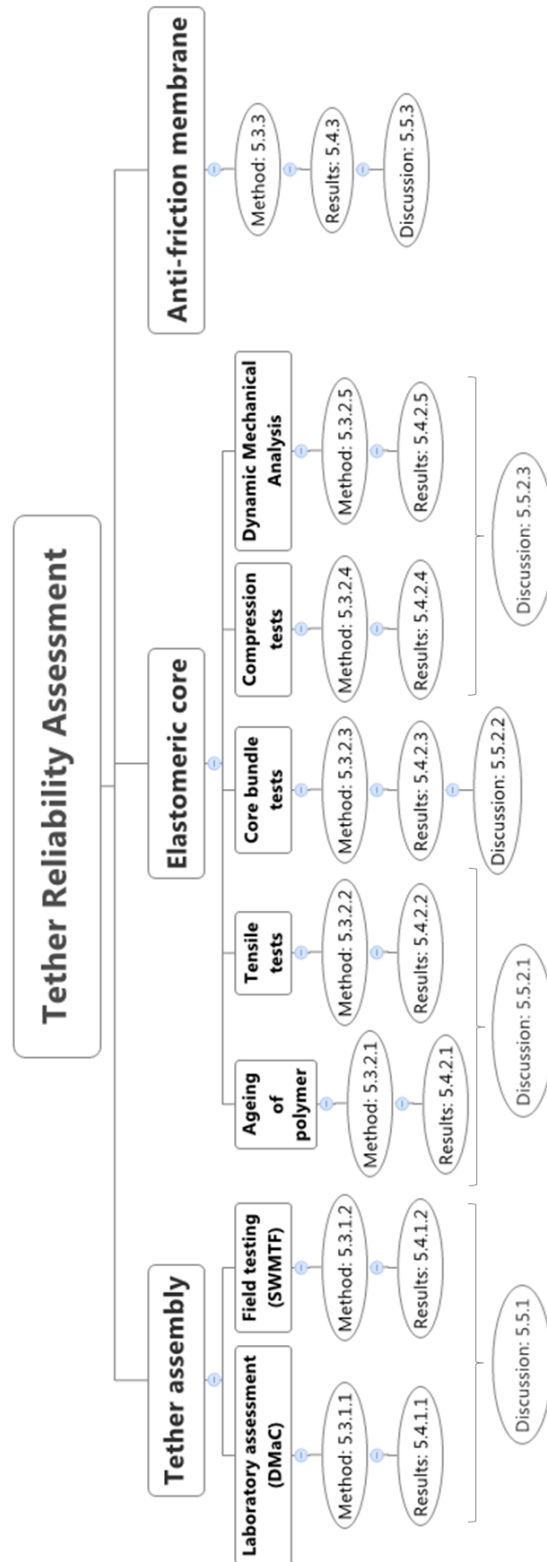
Figure 5.1: Tree diagram to aid navigation through the research presented for the Exeter Tether reliability assessment.

- **Method of soaking during test.** The TCLL test specifies continuous soaking of the test specimen during testing *"including splices but excluding eyes"*. This test specification is likely due to the limitations of most test houses which do not have fully submerged test facilities. A unique feature of DMaC is that the specimen can be fully submerged for the duration of testing. The entire tether was therefore submerged, including eye splices **and** eyes.

- **Frequency of cycling.** The TCLL test specifies a rate of loading for the first test range (50%) to provide a cycle period of between 20-60 seconds. This is a frequency of 0.0167-0.05Hz. However, to better represent the frequency of wave cycling at the SWMTF site, a wave period of 8s was selected, giving a frequency of 0.125Hz. Again, the specified low frequency in the standard may be a result of the limitations of standard test house equipment. Given the capability of DMaC to operate at a higher frequency, better representing operational conditions, this higher frequency was the preferred option for the tether TCLL testing.

- **Rate of loading.** The implications of fixing the cycle frequency as above are that the rate of loading increases with each increase in load step. The TCLL test specifies that the load rate should be adjusted at each increased load step to maintain the same rate of strain. This was adjusted for the tether tests, to maintain a realistic wave period for all the load steps.

- **NWBS.** The TCLL test loads are based on % calculations of average NWBS. For the tether tests the breaking load result is available from the Proof of Concept study. Previously referred to as the MBL, the figure of 222kN was used to represent NWBS in these tests.

- **Test interruptions.** The TCLL Test Procedure permits brief interruptions of up to 1hr between each load step; during the tether tests the load was always maintained above 1% during these interruptions, although this is not stipulated by the guidance.

The potential implications of these alterations to the standard TCLL test procedure is addressed in the Discussion, Section 5.5.

Initially, it was hoped that the TCLL test could be conducted on full scale tethers from the original P1-Prototype series. To this end, tether P1-2 was initially trialled

for the TCLL test, however, when running some conditioning tests with this tether, it became apparent that the loads required to meet the specifications of TCLL were not achievable with a full length tether and the 1m stroke available from DMaC's linear actuator. It was therefore necessary to identify a tether with a reduced working length to conduct the TCLL procedure.

P1-16 was the alternative tether identified. It had a reduced working length of 2m and was manufactured with 70 Shore A EPDM supplied by Polymax with cord diameters of Ø20mm. This tether was modified from P1-14, which was manufactured as part of the original series to investigate the properties of the standard hollow rope with no core. Despite having reduced dimensions, the NWBS of the tether should be representative of the full size tethers as the load carrying rope was manufactured to the same specification. The potential implications of the reduced dimensions of the tether is covered in the Discussion (Section 5.5). As tether P1-16 was a modified tether from the original P1 Series, one eye splice of the tether was constructed by professional rope makers at Lankhorst Ropes, whilst the other eye splice was constructed by the University of Exeter staff to the Lankhorst specification.

Following the original TCLL test conducted with P1-16, design alterations were identified to improve the fatigue performance of the tether. These alterations were made to tether P1-20 and a repeat TCLL test was conducted. P1-20 was developed from the original tether P1-7, with a reduced working length of 2m and was manufactured with full size elastomer cord diameters of Ø25mm. The outer 6 cords were manufactured from Polymax 70 Shore A EPDM, with the inner cord manufactured from Polymax foam 70 Shore A EPDM. P1-20 also had one eye splice manufactured by Lankhorst Ropes and the other manufactured by the University of Exeter.

For each TCLL test conducted, based on the load level and cycle number at failure, it was possible to calculate the TCLL value for each tether using the following calculation as detailed in Oil Companies International Marine Forum (2000):

$$TCLL = 100\% - \frac{6.91(100\% - TLL)}{LnCTF} \tag{5.1}$$

Where:

$TCLL$ = thousand cycle load level

TLL = test load level at which cycles fo failure was determined (maximum load as a %)

CTF = cycles to failure at test load level

6.91 = natural logarithm of 1000

To calculate the CTF at the test load level, the equivalent cycles at higher load levels is required and is also detailed in Oil Companies International Marine Forum (2000):

- 1000 cycles at 50% = 251 cycles at 60%

- 1000 cycles at 50% + 1000 cycles at 60% = 215 cycles at 70%

- 1000 cycles at 50% + 1000 cycles at 60% +1000 cycles at 70% = 113 cycles at 80%

The TCLL value essentially provides a % NWBS value that the sample would fail at when subjected to 1000 cycles (Samson Rope, 2015).

Test schedules

The test schedule followed for the TCLL tests are detailed in Table 5.3. Conditioning tests are required for 'bedding in' of the tether. The purpose of bedding in, detailed by Gordelier *et al.* (2013), is to ensure the individual fibre components of the main body of the rope and the eye splices have found an optimal position and the rope can be considered 'stable'. There is not a standard for bedding-in of conventional fibre ropes but McKenna *et al.* (2000) refers to the Cordage Institute Standard CI-1500A *Test Methods for Fiber Rope* (Cordage Institue, 2015) which recommend 10 cycles to 20% breaking strength followed by ten cycles to 50% breaking strength to stabilise a rope specimen.

Both P1-16 and P1-20 were exposed to the full range of bedding in conditioning tests. These included ETT-03, 04, 05 and 06 as detailed in Table 5.3. In addition to the standard bedding in tests, additional tests were conducted on P1-16 as part of the original primary data collection for the Proof of Concept Study. These tests are also detailed in Table 5.3. During the TCLL test set up for both P1-16 and P1-20 several bedding in tests were repeated to create slack in the tether which could be taken up using DMaC's pre-tension adjuster, to ensure the maximum 1m stroke length of the linear actuator was available for the TCLL tests.

Table 5.3: TCLL test schedule for tethers P1-16 and P1-20.

Tether	Test I.D.	Test script	Test type	Pre-tension (kN)	Peak tension (kN)	Period (s)	Cycles (No.)	Details
P1-16	ETT_03_P1-16	ETT_03	Conditioning	1	10	8	10	Conditioning (prior to primary data collection)
	ETT_04_P1-16	ETT_04	Conditioning	2	20	8	10	Conditioning (prior to primary data collection)
	ETT_05_P1-16	ETT_05	Conditioning	2	40	8	5	Conditioning (prior to primary data collection)
	ETT_06_P1-16	ETT_06	Conditioning	2	60	8	5	Conditioning (prior to primary data collection)
	ETT_09_P1-16	ETT_09	Primary data	1.55	variable	8	5	Displacement driven, 0.25 - 0.5m (peak load 26.9kN).
	ETT_08_P1-16	ETT_08	Primary data	1.55	variable	8	5	Displacement driven, 0.5 - 0.9m (peak load 107.5kN)
	TETT_04_P1-16_01	ETT_04	Conditioning	2	20	8	10	To stretch out tether and take up slack using M64 in preparation for TCLL
	TETT_04_P1-16_02	ETT_04	Conditioning	2	20	8	10	To stretch out tether and take up slack using M64 in preparation for TCLL
	TETT_26_P1-16_01	TETT_26	Durability	2.2	110	8	10	Trial of 10 cycles of TCLL monitoring eye splice
	TETT_26_P1-16_02	TETT_26	Durability	2.2	110	8	10	Trial of 10 cycles of TCLL monitoring eye splice
	TETT_27_P1-16_01	TETT_27	Durability	2.2	110	8	1000	1st TCLL test, 1000 cycles @ 1- 50% NWBL
	TETT_28_P1-16_01	TETT_28	Durability	2.2	132	8	1000	2nd TCLL test, 1000 cycles @ 1- 60% NWBL
	TETT_29_P1-16_01	TETT_29	Durability	2.2	154	8	1000	3rd TCLL test, 1000 cycles @ 1- 70% NWBL
P1-20	ETT-03_P1-20_01	ETT_03	Conditioning	1	10	8	10	Conditioning for TCLL
	ETT-04_P1-20_01	ETT_04	Conditioning	2	20	8	10	Conditioning for TCLL
	ETT-05_P1-20_01	ETT_05	Conditioning	2	40	8	5	Conditioning for TCLL
	ETT-06_P1-20_01	ETT_06	Conditioning	2	60	8	5	Conditioning for TCLL
	ETT-05_P1-20_02	ETT_05	Conditioning	2	40	8	5	To stretch out tether and take up slack using M64 in preparation for TCLL
	ETT-06_P1-20_02	ETT_06	Conditioning	2	60	8	5	To stretch out tether and take up slack using M64 in preparation for TCLL
	TETT-26_P1-20_01	TETT_26	Durability	2.2	110	8	10	Trial of 10 cycles of TCLL
	TETT-27_P1-20_01	TETT_27	Durability	2.2	110	8	1000	1st TCLL test, 1000 cycles @ 1- 50% NWBL
	TETT-28_P1-20_01	TETT_28	Durability	2.2	132	8	1000	2nd TCLL test, 1000 cycles @ 1- 60% NWBL

5. RELIABILITY ASSESSMENT OF A NOVEL MOORING COMPONENT: THE EXETER TETHER

Data processing

During DMaC test work, data for time, displacement and load was saved at a rate of 50Hz. Data processing was conducted using National Instruments DIAdem and Microsoft Excel software.

To attribute the displacement value recorded by the DMaC linear actuator to a strain value for the working portion of the tether it was necessary to account for the extension of the eye splice at either end of the tether. A method for accounting for this extension was developed by Parish (2015) and is reported by Gordelier *et al.* (2015). Following conditioning tests, primary data collection test ETT-08 was conducted on tethers P1-3 and P1-6, using a linear transducer to monitor the eye splice extension. ETT-08 is a displacement driven test, starting from a fixed pre-tension of 1550N, with 5 cycles at an 8 second period and a displacement profile detailed in Figure 5.2. The linear transducer results from the fifth cycle of each test series was used to ascertain the extension of the eye splice, which showed a linear relationship to load. The mean of the extension value for P1-3 and P1-6 was calculated (1.02×10^-3m/kN) and assumed to represent the extension of the eye splices for the P1 test series during loading.

As the TCLL test series utilised eye splices manufactured in house by the UoE and also peaked at higher loads than the functionality tests, there was a concern that the above assumption may not be valid for the TCLL tests. Therefore during the set up of the first TCLL test on tether P1-16, a linear transducer was installed on the eye splice manufactured by UoE located at the headstock end of DMaC. As the TCLL test would run to failure, the linear transducer could not be in situ for the duration of the test as it would be damaged by the final failure of the tether. Therefore a trial test script running for 10 cycles of the 0-50% load range was developed to allow the extension of the eye splice to be monitored at this higher loading level of 110kN. As with the original eye splice extension calculations, the load up data from the fifth cycle of this range was analysed to calculate an extension value in m/kN for the UoE eye splice. The calculated value was then compared to the original eye splice extension value to ensure the original assumption remained valid for the TCLL tests. If the assumption was not valid, then it would be updated to reflect the new extension value calculated. Once a value for eye splice extension was confirmed, this value was doubled (to account for
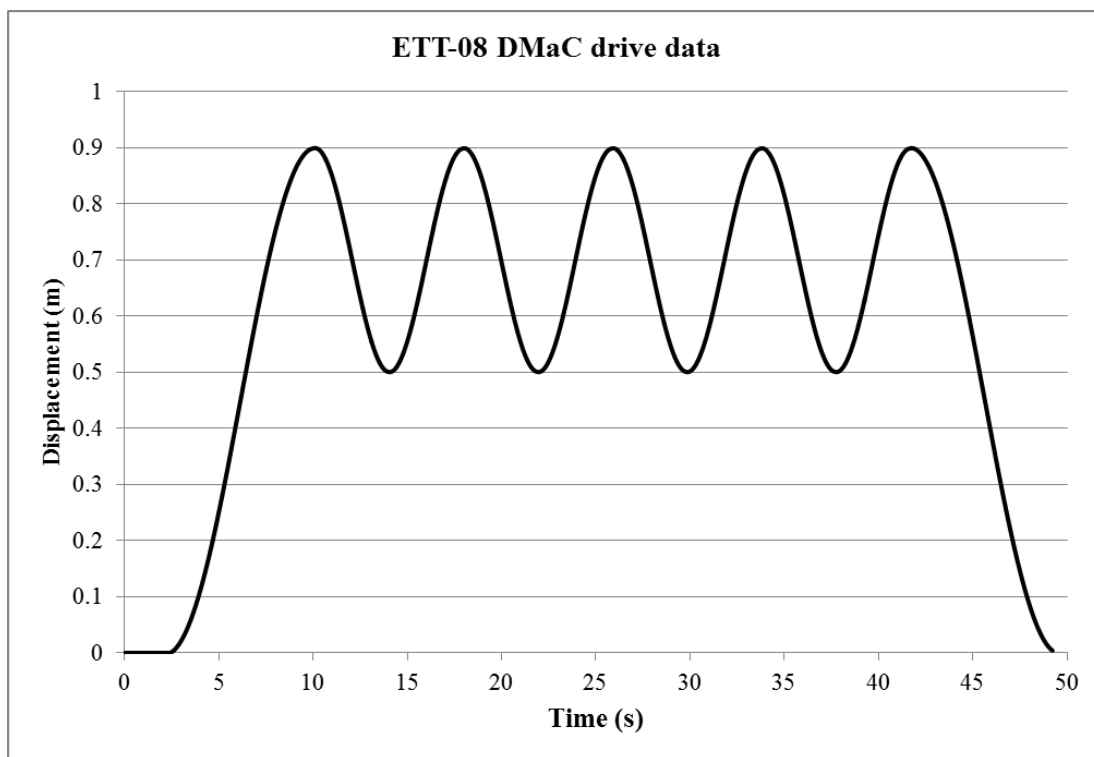
Figure 5.2: Tether test ETT-08 DMaC drive data.

two eye splices), and deducted from the extension results measured by DMaC, with the remaining extension assumed attributable solely to the working portion of the tether.

A key property of interest throughout the TCLL test work was the axial stiffness of the tether, and whether this changed when the tether was exposed to high cycle numbers. From data extracted at particular load cycles of the TCLL test series, the axial stiffness was defined using the 'secant modulus' approach with a load-strain plot. Various approaches can be used to quantifying the axial stiffness of a rope. The secant modulus approach is one of the standard methods suggested by McKenna *et al.* (2000). A secant is drawn between two points on the load up cycle, and the gradient is calculated. This provides an axial stiffness value of kN/strain; as strain is unit-less, the stiffness value unit is kN. This figure essentially provides a value for the load required to achieve a strain of 1 (or an extension of 100%). To compare the stiffness values calculated at each TCLL loading level, for each cycle of interest, the secant was drawn between the loads of 20kN and 90kN. This means that even at the lowest load level of 1 - 50% NWBS (2.2 - 110kN), the specified secant can still be selected within the data. The data at each cycle of interest was linearly interpolated to achieve the exact strain value for the specified load (20 or 90kN). Due to the dynamic nature of these tests (with a cycle period of 8s) this axial stiffness represents the dynamic axial stiffness of the tether.

5.3.1.2   Field assembly assessment - SWMTF

As detailed in the Methodology Chapter (Chapter 3) the South West Mooring Test Facility, was selected as an ideal test bed to expose a selection of tethers from the P1-Prototype series to realistic sea conditions for an extended period of time. Four tethers were connected in series using cow hitches and deployed on mooring limb 1 of the SWMTF buoy. The tethers replaced 20m length of nylon rope used in a standard mooring limb of the SWMTF. The order of deployment of the tethers from buoy to sea-bed was: P1-8, P1-3, P1-12, and P1-10. P1-8 was located in the most exposed position nearest the buoy where both wave action and marine growth is likely to be the most severe.

Two approaches to assessing the tethers following the SWMTF deployment were adopted. Firstly a qualitative durability assessment was conducted, using microscopes to review the tethers and components for signs of damage and bio-fouling ingress. As

a tether with a mid-range polymer hardness (70 Shore A) and exposed to the harshest conditions during the SWMTF deployment, tether P1-8 provided the focus for this post-deployment assessment.

Secondly, DMaC was used to quantitatively assess any alteration in tether performance following sea deployment. Prior to deployment a full range of functionality tests were conducted using DMaC and following deployment these tests were repeated to allow the quantification of the affect of long term exposure to the marine environment on tether functionality. The solid tether constructions P1-3 and P1-8 were used in this quantitative assessment comparing pre and post deployment functionality. Table 5.4 details the DMaC tests conducted both before and after deployment. As with the TCLL tests a series of bedding in conditioning tests were conducted prior to primary data collection for the new tether assemblies. These were repeated following deployment to ensure consistency between pre and post deployment test regimes.

The final comparison between the pre and post SWMTF deployment functionality of the tethers was conducted reviewing data collected from the functionality test ETT-08. This was detailed in Section 5.3.1.1 and the displacement profile for it was detailed in Figure 5.2, Page 249. Data from the fifth cycle was extracted for analysis, and a deduction was made for the eye splice extension in line with the value presented in Section 5.3.1.1 (1.02×10^{-3}m/kN). To account for the eye splice extension following the SWMTF deployment, it was assumed that the stiffness of the eye splice increased in line with the standard increase in stiffness observed between new and worked polyester rope. Published data for the change in stiffness for the 'Viking Braidline' polyester rope was the most appropriate reference rope and detailed an average reduction in extension of 25% (Bridon, 2015a). This reduction in extension was therefore applied to the eye splice extension to calculate a value of (0.76×10^-3m/kN) which was deducted from the measured DMaC extension to provide a final value for the extension of the working portion of the tether. As with the TCLL assessment, the secant modulus approach was again adopted to quantify axial stiffness, this time the modulus was plotted between loads of 10kN to 35kN (as ETT-08 had a reduced load range in comparison to the TCLL tests). Linear interpolation was again used to calculate the exact extension at each specified load and these values were plotted to establish the secant and the gradient of the line providing a value for dynamic axial stiffness. This final calculated

Table 5.4: Full DMaC test schedule for tethers P1-3 and P1-8 prior to and post deployment on SWMTF. Post deployment is labelled 'worked'.

Tether	Test I.D.	Test script	Pre-tension (kN)	Peak tension (kN)	Period (s)	Cycles (No.)	Details
P1-3	ETT_03_P1-3	ETT_03	1	10	8	10	Force driven, conditioning tests
	ETT_04_P1-3	ETT_04	2	20	8	10	Force driven, conditioning tests
	ETT_05_P1-3	ETT_05	2	40	8	5	Force driven, conditioning tests
	ETT_06_P1-3	ETT_06	2	60	8	5	Force driven, conditioning tests
	ETT_07_P1-3	ETT_07	2.5	80	8	5	Force driven, conditioning tests
	ETT_08_P1-3	ETT_08	1.55	variable	8	5	Displacement driven, primary data collection
P1-3 Worked	ETT_03_P1-3W	ETT_03	1	10	8	10	Force driven, conditioning tests
	ETT_04_P1-3W	ETT_04	2	20	8	10	Force driven, conditioning tests
	ETT_05_P1-3W	ETT_05	2	40	8	5	Force driven, conditioning tests
	ETT_06_P1-3W	ETT_06	2	60	8	5	Force driven, conditioning tests
	ETT_08_P1-3W	ETT_08	1.55	variable	8	5	Displacement driven, primary data collection
P1-8	ETT_03_P1-8	ETT_03	1	10	8	10	Force driven, conditioning tests
	ETT_04_P1-8	ETT_04	2	20	8	10	Force driven, conditioning tests
	ETT_05_P1-8	ETT_05	2	40	8	5	Force driven, conditioning tests
	ETT_06_P1-8	ETT_06	2	60	8	5	Force driven, conditioning tests
	ETT_08_P1-8	ETT_08	1.55	variable	8	5	Displacement driven, primary data collection
	ETT_11 to 14	various	1.55	variable	variable	5	Displacement driven, primary data collection (frequency investigation)
P1-8 Worked	ETT_03_P1-8W	ETT_03	1	10	8	10	Force driven, conditioning tests
	ETT_04_P1-8W	ETT_04	2	20	8	10	Force driven, conditioning tests
	ETT_05_P1-8W	ETT_05	2	40	8	5	Force driven, conditioning tests
	ETT_06_P1-8W	ETT_06	2	60	8	5	Force driven, conditioning tests
	ETT_08_P1-8W	ETT_08	1.55	variable	8	5	Displacement driven, primary data collection

value was then compared between the ETT-08 tests conducted pre and post SWMTF deployment.

5.3.2 Elastomeric core durability assessment

As detailed in Chapter 3, the long term durability of the elastomeric core is a key reliability consideration for the operation of the tether. Although a deterioration in material properties would not directly lead to a catastrophic failure, it would alter the operating parameters of the tether, which could lead to increased peak loads and, ultimately, a premature failure.

The elastomeric core durability assessment involved an investigation into the affect of both exposure to the marine environment and the long term mechanical operation of the tether on the elastomeric core material properties. To limit the scope of this study, the majority of the investigation focused on the mid-range polymer EPDM 70.7 Shore A supplied by Ley Rubber Ltd. In addition to the Ø25mm extruded core sections, 2mm thick sheet was also supplied by Ley Rubber Ltd for tensile test work, this had a specified Shore A hardness of 70.

5.3.2.1 Ageing of polymer

A widely used approach for accelerating the effect of polymer ageing in a marine environment is to immerse samples in heated sea water for extended periods of time. There is a significant amount of literature detailing the use of this approach for ageing polymers: Celina *et al.* (2005); Gillen *et al.* (2005); Le Gac *et al.* (2012); Le Saux *et al.* (2014); Scheirs (2000); Wise *et al.* (1995). A linear Arrhenius extrapolation is generally used to relate the accelerated ageing conducted at elevated temperatures and extrapolate this to estimate the affects of longer term ageing at lower temperature. This relationship relates reaction rate to time and temperature through the relationship detailed in Equation 5.3.2.1 (Celina *et al.*, 2005).

$$k = A \times e^{\left(\frac{-E_a}{RT}\right)} \tag{5.2}$$

Where:

k = reaction rate

A = pre-exponential factor

E_a = Arrhenius activation energy

$R =$ the gas constant (8.314J/mol-K)

$T =$ temperature (in K)

Taking the natural logarithms of this equation, reaction rate k can be related to the inverse of temperature $\frac{1}{T}$ via a straight line relationship. As detailed by Celina *et al.* (2005) degradation time t is related to reaction rate by $\frac{1}{k}$.

To date, there is no data available for the specific effect of ageing at an elevated temperature on EPDM and to accurately quantify the Arrhenius relationship specifically for EPDM would require a body of work beyond the scope of this Thesis.

For the research presented here, the EPDM under investigation was immersed in tanks of sea water at a temperature elevated to 60°C. It was assumed that, in accordance with the wealth of literature on polymer ageing, this process acts to speed up the natural ageing process. Based on previous work ageing polymers (Le Gac *et al.*, 2012), 60°C was selected as an appropriate temperature to speed up the ageing process but minimise oxidation of the polymer, which could result in an excessive deterioration of material properties.

Specimens of Ø25mm round and 2mm flat EPDM were taken to the IFREMER test laboratories and immersed in a 60 litre tank filled with natural sea water pumped directly from the Brest Estuary. The water was maintained at a constant temperature of 60°C whilst being continually renewed with fresh water from the estuary at a replacement rate of 60 litres / 24 hour period.

The 2mm sheet samples were immersed in heated sea water for 1 month and then removed for testing. Based on previous work with 2mm sheet natural rubber the samples were assumed to be saturated at this point (Le Gac *et al.*, 2015a). The Ø25mm core samples were not saturated after 1 month immersion so it was necessary to leave these samples for longer to allow further saturation. The weight of the samples was periodically measured and the samples were assumed to be saturated once the weight stabilised. The samples were removed after 13 months of saturation due to time limitations; at this point the weight gain had slowed significantly but not fully stabilised.

Following ageing of the samples, experiments to establish key material properties of both the new and the aged samples were conducted to observe the change in material properties resulting from the ageing process.

Table 5.5: ISO37, 'Sample Size 2' dimensions

Dimension	Description	Length (mm)
A	Overall length	75
B	Width of ends	12.5 ±1
C	Length of narrow portion	25 ±1
D	Width of narrow portion	4±0.1
E	Transition radius outside	8 ±0.5
F	Transition radius inside	12.5 ±1
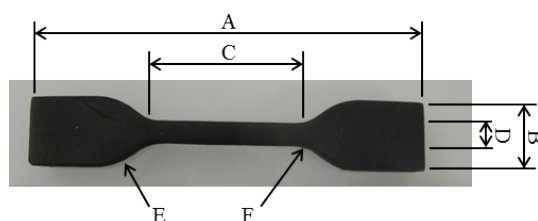
Figure 5.3: ISO37, 'Sample Size 2' dimensions identification

5.3.2.2 Tensile tests

All the tensile tests reported here were conducted on 2mm sheet of 70 Shore A EPDM supplied by Ley Rubber Ltd.

ISO37: Determination of tensile stress-strain properties

A standard test for calculating the tensile stress-strain properties of a polymer is ISO37:2005 (ISO, 2005). 2mm sheet material was used to prepare specimens to 'Sample Size 2' of the standard, with dimensions as detailed in Table 5.5 and Figure 5.3. A die and press were used to cut the samples to identical specification as detailed in Figure 5.4.

An Instron 5566 load frame with a 500N load cell was used to run the tests. Samples were individually clipped into the load frame grips and extended to failure. The standard stipulates a nominal rate of traverse of the moving grip (or extension rate) of 500mm/min. In addition to this, samples were extended to failure at extension rates of 10mm/min and 100mm/min. These alternative rates were used to observe the influ-
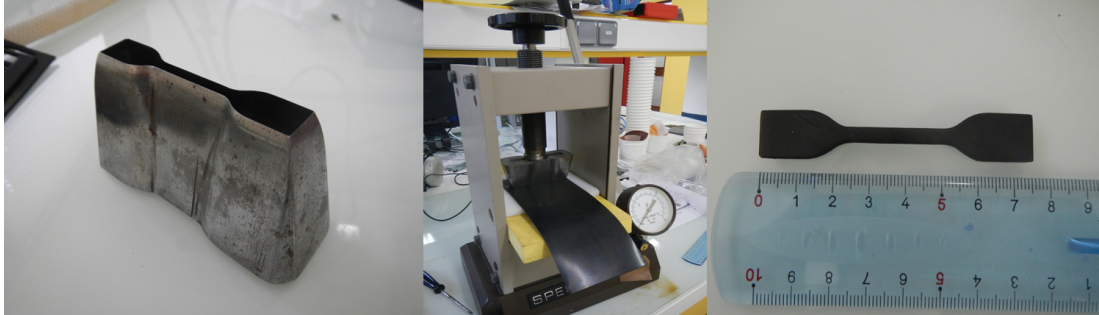
Figure 5.4: Sample preparation for ISO37 standard from left to right: die for cutting samples; press in use with die and 2mm EPDM 70ShA; final specimen example.
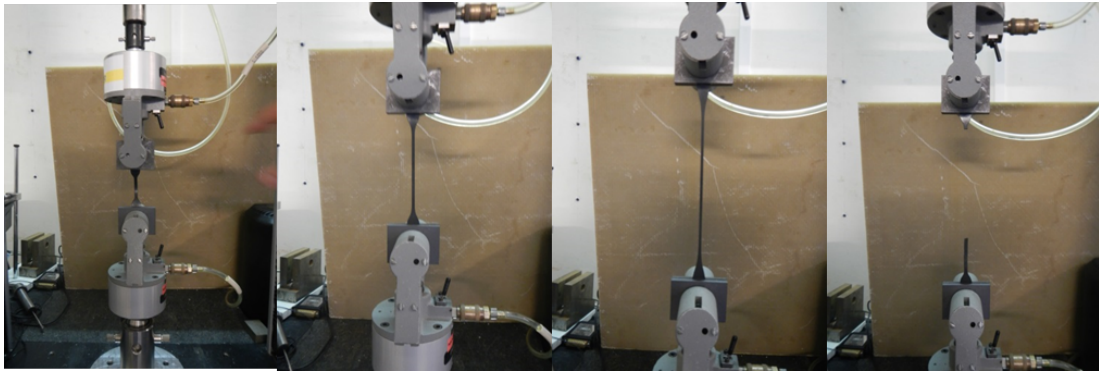
Figure 5.5: Images captured during the ISO37 test procedure

ence of extension rate on the tensile stress-strain properties of the polymer. Figure 5.5 details images captured during a load sequence for the standard ISO37 test.

Before the start of each test, dimensions were taken of each sample using a micrometer to the nearest 10μm. During the test the software monitored the time, displacement and load, and calculated strain and stress at each time step based on the dimensions that were input prior to the start of the test. The automated stress calculations were based on the original cross-sectional area of the sample. Following the test, the data was used to manually calculate various material properties for each sample, including:

- **Tensile strength at break.**

$$TS = \frac{F_m}{Wt} \tag{5.3}$$

  Where:

  $TS =$ tensile strength (MPa)

F_m =maximum load (N)

W =original specimen width (mm)

t =original specimen thickness(mm)

- **Elongation at break (or strain at break).**

$$\varepsilon_b = \frac{(L_b - L_o)}{L_o} \tag{5.4}$$

Where:

ε_b =strain at break

L_b =specimen length at break (mm)

L_o =original specimen length (mm)

- **Young's Modulus.** Unlike many standard engineering materials, polymers display a Young's Modulus that varies with strain. Young's Modulus should therefore be quoted alongside a particular strain. For the purpose of these investigations, values for Young's Modulus are calculated at strains of 1, 2, 3 and 4. Young's Modulus is calculated by the software using:

$$E_x = \frac{\sigma_x}{\varepsilon_x} \tag{5.5}$$

Where:

E_x =Young's Modulus at x (MPa)

σ_x = stress at x (MPa) = $\frac{F_x}{Wt}$

ε_x = strain x = $\frac{(L_x - L_o)}{L_o}$

F_x = load at x (N)

L_x = length at x (mm)

For each strain rate a minimum of 3 samples of both new and aged polymer material were tested in line with the ISO37 requirements.

Tensile fatigue tests

IFREMER have developed a test rig specifically for longer term tension fatigue testing of material samples under exposure to sea water. The test rig is detailed by
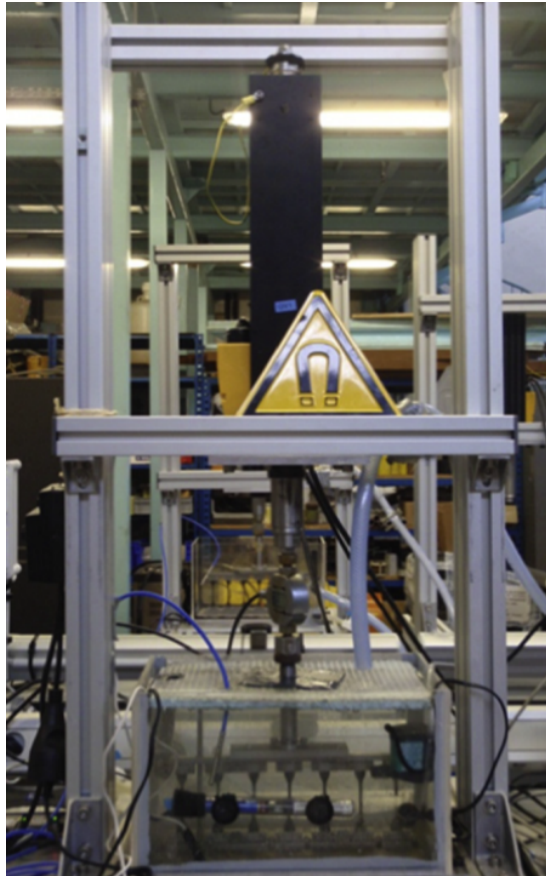
Figure 5.6: IFREMER fatigue testing machine operating with the tank filled with natural sea water. Image replicated from (Le Gac *et al.*, 2015a).

Le Gac *et al.* (2015a) and comprises a Parker electrical displacement controlled piston (PRA3810S) with a maximum force of 1860N and maximum frequency of 7Hz. The piston is controlled via a computer and the test rig allows seven samples of material to be simultaneously exposed to fatigue cycling. The samples can be tested in air, or alternatively, the tank can be filled with natural sea water, pumped from the Brest Estuary, maintained at 25℃ by a submersible heater and renewed at a rate of 4l/h. Figure 5.6 details the test rig operating with samples submerged in sea water. The seawater is heated to 25℃ to minimise any temperature difference between testing in sea water and testing in air. It is therefore assumed that the air temperature is also 25℃.

Specimens of 2mm EPDM rubber were cut to the dimensions for 'Sample Size 2' of
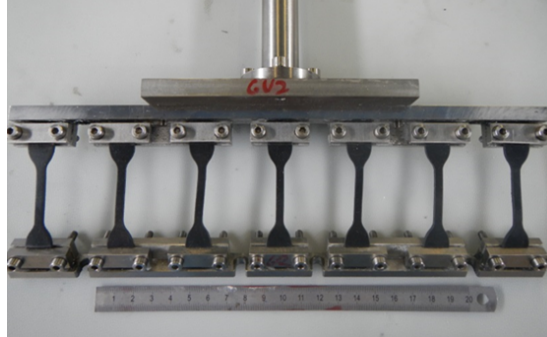
Figure 5.7: Fixture for parallel testing of seven specimen samples.

ISO37 as detailed in Table 5.5 and Figure 5.3, Page 255. The samples were installed in parallel onto a test fixture as detailed in Figure 5.7 and installed into the test machine.

To monitor sample failures, a Logitech[TM] C310 digital camera recorded images at 90s time intervals. Once all of the samples had failed the image recordings were used to determine cycles to failure for each specimen.

The frequency selected to run the testing was specified to optimise the balance between minimising test time and ensuring the samples did not excessively self heat, which can occur if the cycling frequency specified is too high. A separate study into the self-heating effects of natural rubber concluded that a cycle frequency of 2Hz for strains up to 2.5 would maintain a temperature rise below 5°C in air (Le Gac *et al.*, 2015a). As water would speed up the dissipation of heat from the samples, the temperature rise would be less than 5°C in water, so 2Hz was deemed a suitable frequency for the natural rubber tests. For the EPDM polymer tests reported in this Thesis, the sample dimensions are identical to the natural rubber study and the strains do not exceed 2.5. It was anticipated that the self-heating properties of EPDM are similar to natural rubber so 2Hz was also selected as a suitable frequency to run these tests.

Before commencing the tests, the strain required to cause fatigue failure in these test conditions was unknown. For a valid set of results, cycles in the order of 15,000 and over were required, as the image capture has a resolution of 90s, so a low number of cycles would provide a very low test accuracy. Testing started with a strain of 250%, which related to a displacement of 0 - 62.5mm. A suitable number of cycles to failure were not achieved at this strain, so a reduced strain of 200% (displacement of 0 - 50mm) was specified. Again, a suitable number of cycles to failure were not achieved at this

strain so a further strain of 100% was tested (displacement of 0 - 25mm). A sufficient number of cycles to failure were achieved at this strain to provide a meaningful data set, which is presented in the Results Section (5.4.2.2).

5.3.2.3 Core bundle tests

To inform the strain values used for the compression investigations of the Ø25mm cord samples of EPDM, a detailed understanding of the deformation of the core bundle under load was required. Collaborative work was conducted with Parish to measure the overall diameter of the tether assembly under load and ascertain a compressive strain across the diameter of the tether at realistic operating extensions. This test work was conducted at the DMaC test facility using tether P1-2*, which was the original P1-2 tether reduced in length and re-spliced at either end to enable greater extension to be achieved within the stroke length of the DMaC linear actuator. P1-2* was manufactured using the softest polymer with 54 Shore A Hardness which made it the preferred choice for this test as this would obtain the greatest radial compression for a given tensile load. The tether was installed in DMaC and when under zero extension a gauge length of 945mm was marked on the tether as a baseline from which to measure extension. To conduct the test DMaC was operated in manual mode and the Z-ram was retracted in 10mm steps with measurements taken every 100mm. At each measurement interval the gauge length was re-measured, and six diameter readings of the tether were taken (due to the hexagonal core bundle construction there are three high points at the cord corners and three low points across the flat edges, so a measurement was taken across each).

Results from this investigation can simply be used to estimate the compression of individual cords by assuming that the strain is evenly distributed across the diameter of the core bundle. However, the deformation of individual cords is more complex than this, with areas of high compression as well as areas of tension. A further method was required to quantify the deformation within the core bundle in more detail.

To develop an operating model of the tether, Parish developed a bespoke tool to quantify the relationship between circumferential load and radial deformation in order to estimate the pressure within an operating tether. The compression tester, constructed of spring steel, allows an actuator to provide a transverse load which causes the compression of the core bundle diametrically. Figure 5.8 details the test rig under
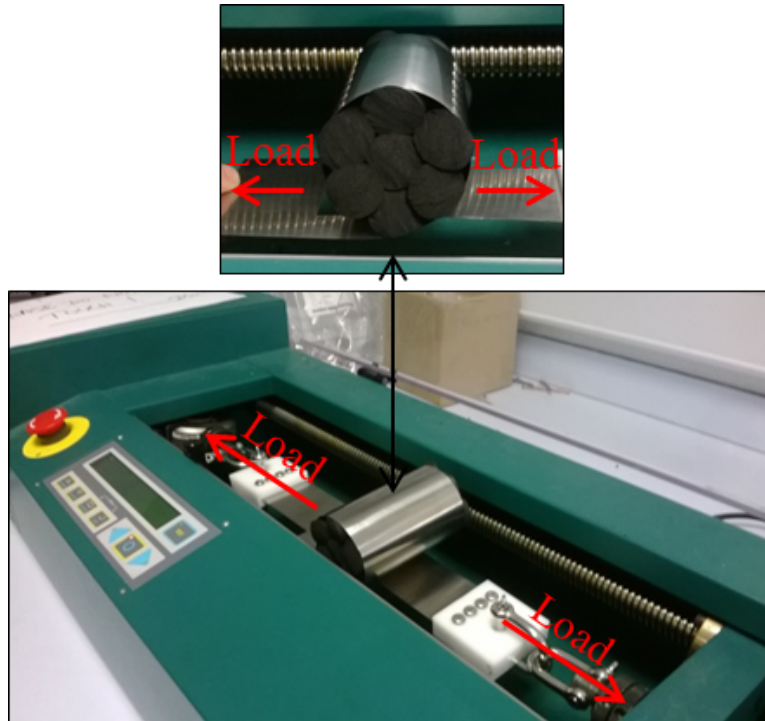
Figure 5.8: 'Scroll test' set up at the University of Exeter. Used to convert transverse load to a diametric compression across the core bundle.

early trials at the University of Exeter. Investigations conducted using this tool are referred to as 'Scroll Tests'.

Although not initially developed for this purpose, the scroll test enabled the observation of the deformation of individual cords within the core bundle which could then be used to inform further compression testing of individual cords. The method used to conduct the scroll test for core bundle deformation measurements is outlined below.

The scroll test was conducted on the full suite of Ley Rubber supplied EPDM polymers (54, 59, 70, 70.7 and 80.7 Shore A). The scroll tests were load limited due to the strength of the spring steel (to allow the flexibility required during the test procedure the spring steel specified was CS95 with a gauge thickness of 0.4mm). Testing was therefore conducted starting at a low load and completing a full set of tests for each polymer specification before increasing the load in steps. This maximised the number of samples taken before the scroll tool failed (although some failures were expected so 3 scroll tools were manufactured to maximise results collected).

5. RELIABILITY ASSESSMENT OF A NOVEL MOORING COMPONENT: THE EXETER TETHER

To allow for a comparison to the 'Compression Modulus' of individual polymer cores some key aspects of the test procedure were developed to align the results with ISO 7743:2011, "Rubber, vulcanized or thermoplastic - determination of compression stress-strain properties" (BSI, 2011). To ensure similarity between the methods the following was specified:

- Cycle number: ISO 7743 specifies 4 compression cycles should be repeated, with data analysed from the 4th cycle. The scroll test was therefore repeated 4 times for each data set, with data analysed from the 4th cycle.

- Compression rate: ISO 7743 compresses the sample at a rate of 10mm/min. Given the scroll test compressed 3 cords diametrically, a diametric speed of 30mm/min was required which converts to a transverse speed for the linear actuator of 70mm/min.

Core bundles were inserted into the scroll tool using a high performance PTFE aerosol to provide lubrication. White correction fluid was used to mark dots on the surface of the polymer cords to facilitate tracking during the test procedure. Shackles were used to connect the scroll tool into the Instron 5566 load frame which was set up with a 10kN load cell. Elastic bands were used to maintain the correct alignment of the spring steel. A video camera was set up on a tripod to record the tests. Figure 5.9 details the test set up.

Given the tests were load limited, the maximum strain was achieved with the softest polymer material, with Shore A hardness of 54. The maximum number of results were therefore taken with this polymer and these results are reviewed in detail and used to calculate the maximum strain of individual cords.

Image analysis software, Image J (University of Wisconsin-Madison, 2015), was used to take measurements from still images taken from the video footage of the scroll tests. At the start of each video, a ruler was held in-line with the test piece to enable Image J to be re-calibrated for each recording, using the correct mm/pixel ratio.

5.3.2.4 Compression tests (25mm cord)

During tether operation, the polymer core bundle is exposed to repeated radial compression cycles. The aim of this section of work is firstly to establish the compression
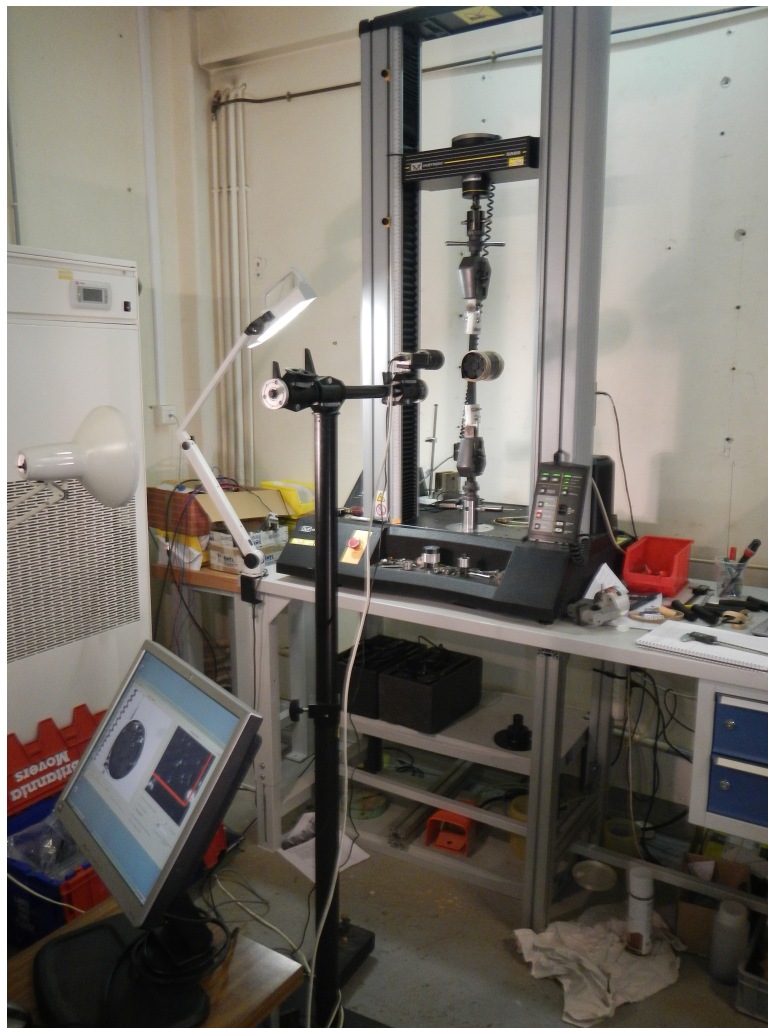
Figure 5.9: 'Scroll test' set up at IFREMER.

Table 5.6: Scroll test schedule

Test name	Polymer specification (Shore A hardness)	Test driving paramater	Maximum Load (N)	Notes
Empty scroll_1	n/a	Displacment	n/a	Empty scroll to test operation
Empty scroll_2	n/a	Displacment	n/a	Empty scroll to test operation
Scroll test_4_50_1	54	Load	1500	
Scroll test_4_50_2	54	Load	3000	
Scroll test_4_90_1	80.7	Load	3000	Scroll broke
Scroll test_5_empty scroll_1	n/a	Displacment	n/a	Empty scroll to test operation
Scroll test 5_70_1	70.7	Load	1500	
Scroll test 5_70_2	70.7	Load	3000	
Scoll test 5_90_1	80.7	Load	3000	
Scoll test 5_60_1	59.0	Load	3000	
Scoll test 5_80_2	70.0	Load	3000	
Scroll test 5_50_1	54.0	Load	4000	
Scroll test 5_50_2	54.0	Load	5000	Scroll broke

.

stress-strain properties of the EPDM cord sections across the range of Shore Hardness values specified using standard test procedure ISO7743; this procedure is specified in the next section. Secondly the aim of this work is to observe how the established stress-strain properties are likely to change when exposed to marine ageing (Page 268) and repeated compression cycles (Page 268). The final section included within the compression testing work uses thermal imaging to assess the heat generation caused by repeated compression cycles of the EPDM polymer (Page 269).

ISO7743: Determination of compression stress-strain properties

A key principal of the Exeter Tether P1 Prototype series is the control of axial stiffness by varying the core material and construction, with each configuration providing a different resistance to compression. The compression stress-strain properties of the core material are therefore critical to the operation of the tether; understanding how these material properties might be affected by ageing of the core material, or exposure to multiple compression fatigue cycles is important for ascertaining long term reliability. ISO7743:2011 'Rubber, vulcanized or thermoplastic - determination of compression stress-strain properties'(BSI, 2011) provides a standard to calculate the compression modulus of a given polymer. This can then be used as a benchmark to compare with further material tests.

The ISO7743 test procedure subjects a cylinder of material to axial compression at a rate of 10mm/min to induce a strain of 0.25. The load is then removed at the same rate, and this is repeated to give four compression cycles in total. Data from the fourth cycle is used to calculate the compression modulus of the material at a strain of 0.1 and a strain of 0.2 (the compression modulus of a polymer varies with strain, so the compression modulus must be specified at a given strain). Compression modulus is calculated in the same way as Young's Modulus detailed in Equation 5.5, Page 257, however unlike the tensile tests conducted before, these tests are conducted in compression. For clarity the equation for compression modulus at a strain of x is:

$$E_{C,x} = \frac{\sigma_x}{\varepsilon_x} \tag{5.6}$$

Where:

$E_{C,x}$ =Compression Modulus at x (MPa)
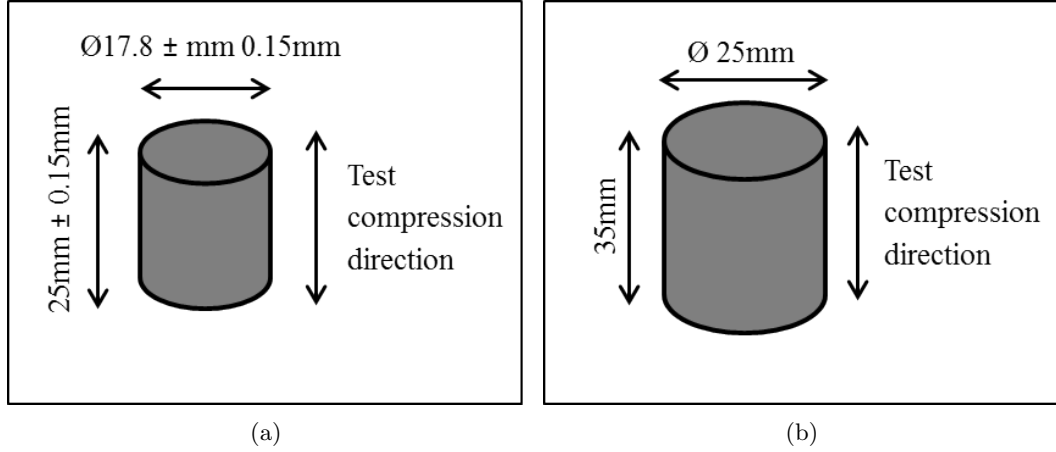
Figure 5.10: ISO 7743 test piece B dimensions (not to scale) (a) dimensions and tolerances as specified in standard; (b) target dimensions scaled to accommodate the 25mm diameter polymer cord.

$\sigma_x = \text{stress at } x \text{ (MPa)} = \frac{F_x}{A}$

$\varepsilon_x = \text{strain at } x = \frac{L_x - L_o}{L_o}$

$F_x = \text{load at } x \text{ (N)}$

$A = \text{area (mm}^2)$

$L_x = \text{length at } x \text{ (mm)}$

$L_o = \text{original length (mm)}$

The ISO standard provides a choice of test pieces and methods. The results presented in this Thesis are based on Test Piece B, Method C. The dimensions for Test Piece B are detailed in Figure 5.10a. However, as the material supplied was in Ø25mm extruded sections, and the compression modulus is affected by both the material properties and the manufacturing process, it was decided to scale Test Piece B so that the test could be conducted on a Ø25mm section. This resulted in the test piece dimensions detailed in Figure 5.10b. This set of tests, compressing the sample axially (along the axis of the extruded polymer) is referred to as the 'Axial Compression Modulus tests'.

In addition to the axial compression modulus tests, of specific interest to the operation of tether is the compressibility of the polymer across the diameter of the polymer cord. This is not a standard ISO test and, unlike the axial compression modulus tests,
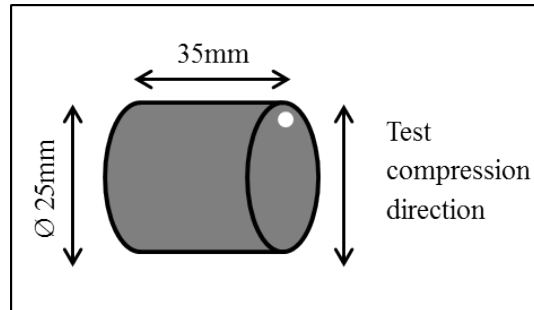
Figure 5.11: Radial compression modulus sample target dimensions and set up. White dot located on sample to ensure consistency between sample measurements and test procedure.

the cross-section of the sample along the axis of this test is not consistent. The compression modulus in this direction is therefore related to both the material properties and the geometry of the sample. Due to this, these results are not comparable to material property specifications from external sources. However, measuring the compression modulus in this direction allows for a direct comparison across the different polymer specifications in the P1 Series, and an understanding of how fatigue loading and ageing of the material affects this crucial behaviour of the polymer cord. The compression modulus in this direction is referred to as the 'Radial Compression Modulus' for ease of reporting, although it should be emphasised that this is not a standard material property.

The dimensions for the radial compression modulus tests are detailed in Figure 5.11. It should be noted that for some of the extruded polymer sections, a 2-3mm flat ridge was evident running along the length of the cord, this was left over from the manufacturing process. To minimise the effect this ridge had on the results, it was ensured that it was at the side of the test piece when conducting the compression testing. A small white dot was painted on the polymer cord to mark the top edge to ensure consistency between measuring the sample dimensions and setting up the test.

Once the samples had been prepared to size, three dimensions were taken of height and width of each sample using a vernier caliper. The minimum height value was used to calculate the distance to achieve 25% strain for the test procedure.

All tests were conducted on the Instron 5566 Load Frame with a 10kN load cell. Three repeat tests were performed for both the axial compression tests and the radial

compression tests.

Although the main material under investigation in the polymer work is EPDM 70.7 Shore A hardness, to inform a comparison across the range of hardness values specified, the test was repeated for the full range of EPDM supplied by Ley Rubber Ltd e.g. 54, 59, 70, 70.7 and 80.7 Shore A.

Once the full range of compression modulus values had been calculated for the polymers, the durability aspect of this work was to understand how this key material property is affected by the operation of the tether. Two aspects of the tether operation that may have an effect on this material property are the long term exposure to the marine environment and the repeated compression cycles that the core is subject to during tether operation. The method for investigating the effect of these two factors on the compression modulus of EPDM is outlined in the following sections.

Aged polymer compression tests

As described in Section 5.3.2.1, the ageing process of polymers in a marine environment can be accelerated by immersion in heated water. Samples of Ø25mm round section of 70.7 Shore A hardness EPDM were immersed in renewed natural sea water, heated to a temperature of 60°C for a period approaching 13 months (15/05/2014 - 10/06/2015).

Following removal from the tanks of water, the ISO 7743 test for compression modulus was conducted on the samples and the results were used to calculate both the Axial Compression Modulus and the Radial Compression Modulus. These results were compared to the original ISO 7743 tests to ascertain the affect of marine ageing on this key material property.

Compression fatigue

During operation the tether extends and contracts to accommodate the wave induced motion of the floating body. This in turn exposes the polymer core to repeated radial compression cycles and axial tension cycles. The radial 'compression fatigue cycling' is a durability concern for the tether as the long term consequences of this action are unknown. To investigate the potential effects of this process, samples of polymer

core were subjected to repeated compression cycles and the ISO 7743 process was used to calculate the Radial Compression Modulus of the sample following the compression cycles. The ISO test was conducted immediately after the compression cycles, and repeated after a delay to observe any time dependency present in the results.

This test work focused on the mid-range polymer, EPDM 70.7 Shore A hardness. The compression fatigue cycling was conducted radially to reflect the compression of the material cord within an operational tether. Material samples were prepared according to the target dimensions in Figure 5.10b, Page Figure 266 and set up in the MTS compression test machine with a 25kN load cell. A small dot of cyanoacrylate was used to locate the underside of the cord to the MTS load platen as during trials the sample had been observed slipping out of the test machine.

As with the tensile fatigue testing, a compromise was required between maximising the number of cycles in a given test window and limiting the self-heating of the sample. Provisional tests indicated that the frequency of compression cycles should be limited to 2Hz as anything beyond this would lead to excessive self-heating of the polymer. The MTS machine was set to operate in displacement mode, with a strain specified based on the average of three measurements of the cord diameter.

A range of compression fatigue tests were conducted with varying cycle numbers and strains. Based on the results from the Scroll Tests, compression values of 20%, 30% and 40% were trialled. The full range of tests conducted is reported in Results (Section 5.4).

Cord compression fatigue with thermal investigation

Provisional tests run in advance of the compression fatigue testing suggested a cycle frequency of 2Hz would limit the self-heating of the samples. When conducting the testing however, during the higher compression tests, a significant increase in temperature was observed. The implications of this are twofold: Firstly, an excessive increase in temperature during the compression fatigue testing could invalidate the results. Secondly, in an operational tether with a bundle of seven cords, the heat dissipation is much more limited than during the laboratory trials on a single cord, so the temperature increase will be more severe. The immersion of an operating tether in sea water may reduce the affects of this to an extent due to increased heat dissipation in water, however, the

temperature increase was an area of concern and required further investigation. Due to these two factors further trials were initiated to investigate the self heating of the EPDM polymer cords under compression.

Again this test work focused on the mid-range EPDM polymer with 70.7 Shore A hardness. The same test set up as utilised for the compression fatigue testing (Section 5.3.2.4) was employed, with the same test machine, the same sample size and the sample being compressed radially. A Flir Thermovision A20 Thermal Camera was set up with an assumed emissivity value of 0.9. Bespoke software developed by IFREMER, CamIR, was used to save thermal images at a frequency of 1Hz. Due to limitations in file size, thermal images from the full test series could not be saved, so image samples were captured periodically throughout the test procedure. To account for temperature changes in the test hall a sample section of EPDM was put in the frame of the camera adjacent to the test piece under compression. This sample was used to define a base temperature so that the temperature difference ($\triangle t$) could be quantified.

Two separate data sets were collected. The first compressed the sample by a peak value of 20%, whilst gradually increasing the cycle frequency from 0.01Hz - 5Hz. The second data set compressed the sample at a constant frequency of 2Hz whilst gradually increasing the peak compression from 20% to 50%. During testing when a test parameter was altered the temperature of the sample was monitored live using the thermal camera. If an increase was detected then further test parameters would not be altered until the temperature increase had stabilised. The temperature was assumed stable if no further temperature increase was detected for a period of 1 minute. At this point the next test parameter was introduced.

Post-processing of the saved images was conducted to identify the maximum change in temperature at each test parameter and to observe the overall effect of frequency and strain on the self heating of the polymer samples. An example of a thermal image is provided in Figure 5.12, which identifies the key components of the image.

5.3.2.5 Dynamic Mechanical Analysis Tests

The final polymer testing to be described in this section is the assessment of the material using Dynamic Mechanical Analysis (DMA). The basic principles of DMA are described by Menard (2008) and PerkinElmer (2008). The process involves measuring the material response to an applied oscillating force. The particular benefit of a
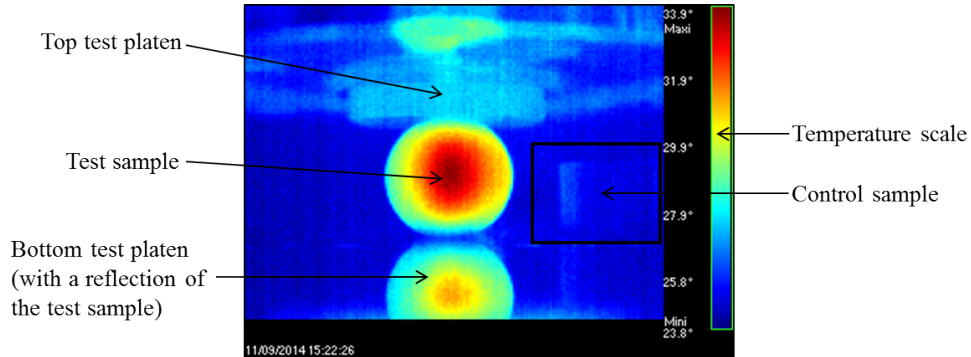
Figure 5.12: Thermal image example recorded during a thermal investigation of 70.7 Shore A hardness EPDM polymer, compressed at 20% strain and at a frequency of 3Hz. Key details are labelled.

DMA test machine is the ability to cyclically apply a constant maximum force whilst sweeping through a range of temperature or frequency values to observe the effect on the material response. The material response is re-measured at each point providing detailed information on the effect of the changing parameter on the evolution of key material properties. Of particular interest for this work was the effect of temperature on the EPDM polymer response. As with previous sections, this work focused on the mid-range polymer with 70.7 Shore A hardness.

The output from a DMA test is the 'Complex Modulus' of the material. The complex modulus is described by:

$$E^* = E' + E''$$ (5.7)

Where:
E^* = Complex Modulus
E' = Storage modulus, also referred to as the real part of the modulus
E'' = Loss modulus, also referred to as the complex part of the modulus

The Storage Modulus E' is the result of interest for this work as it is a measure of the elastic response of a material. Due to the high frequency of this testing and the spot measurement of this value at multiple points, it is not directly comparable to the Young's Modulus described in previous sections, but it is useful in understanding how the material response evolves with temperature.

A DMA $^+$150 Metravib machine was used to conduct the DMA testing. A preliminary test was run to observe the effect of strain rate on E' (the Storage Modulus). This test was used to inform the strain rate specified for the temperature investigation. The strain rate selected was the maximum strain rate possible before permanent damage was induced in the sample.

Once this strain rate was selected, a temperature sweep was conducted ranging from -100°C to +100°C with the temperature changing at a rate of 2°C / minute. A second temperature sweep was conducted ranging from -10°C to +100°C, again with temperature changing at a rate of 2°C / minute.

The DMA testing concludes the methods for the polymer test work. The next section describes the assessment of the anti-friction membrane.

5.3.3 Anti-friction membrane investigation

Following field testing of the tether prototypes, concerns were raised regarding the durability of the Dacron anti-friction membrane. To address these concerns trials of alternative materials were instigated. Research into high strength, low friction materials highlighted UHMWPE (ultra high molecular weight polyethylene) as a material that met many of the requirements for the tether application, including high wear resistance. There are many manufactures of UHMWPE which can be supplied in many different forms from tape to material. The following tapes were procured for these investigations:

- **Endumax® tape TA23.** Manufactured by Teijin, Endumax is a high performance tape manufactured from UHMWPE. Supplied in 133mm wide tape and cut down to 50mm for installation on the tether core bundle. The thickness of the tape was 55 μm.

- **Bell Plastics' Black UHMWPE.** This is Bell Plastics standard high performance UHMWPE tape with added carbon to provide improved UV resistance. This tape was supplied in 100mm width but was cut down to 50mm for installation on the tether core bundle. The thickness of the tape was 200μm.

Reduced diameter Ø20mm cords were used to manufacture the test tethers described below as it was not possible to remove a Ø25mm core bundle from the rope jacket, apply an alternative anti-friction membrane and re-insert the bundle back into the

rope jacket. The diameter of the core bundle was too large to allow for this so a reduced core diameter was necessary, and this in turn altered the braid angle of the rope construction. Due to these altered tether parameters, half of each test tether was manufactured with an alternative anti-friction material and half with the original Dacron material to ensure a like for like comparison of the screens under test. It was anticipated that utilising two layers of material may have some durability advantages by promoting slip between the two layers, so in addition to installing the new materials with 2 layers, this was also trialled with the original Dacron tape during these tests with 2 layers of Dacron applied to tether P1-17* to ensure a fair comparison between all the materials.

Two tethers were assembled, re-cycling existing rope jackets from the P1 Series range. One end of each tether was spliced in accordance with the P1 series, and the other end left open for connection into a collet arrangement. The following details the specification for each tether and Figure 5.13 details the core and anti friction assembly for each tether:

P1-16*

- Rope: The rope was previously P1-16, which was a modified tether made from P1-14 (manufactured as an empty rope in the original P1 range). P1-16 was used for the laboratory tether assembly durability assessment (TCLL tests).

- Anti friction screen (spliced end): Endumax tape TA23 x 2 layers, helically wound around the tether core at a helix angle of approximately 75°.

- Anti friction screen (open end): Dacron x 1 layer, helically wound around the tether core at a helix angle of approximately 80°(as used in the original P1 tethers P1-8 and P1-12).

- Core construction: 7 x Ø20mm 70 Shore A hardness EPDM supplied by Polymax.

P1-17*

- Rope: The rope was previously P1-17 which was a reduced length tether made from the original P1-4 tether and used for the first break test.

273

Figure 5.13: P1-16* and P1-17* anti friction membranes as installed prior to testing. Top image: P1-16* (Left: 1 x layer of Dacron. Right: 2 x layers of Endumax tape TA23). Bottom image: P1-17* (Left: 2 x layers of Dacron. Right: 2 x layers of Bell Plastics Black UHMWPE).

- Anti friction screen (spliced end): Bell Plastics Black UHMWPE x 2 layers, helically wound around the tether core at a helix angle of approximately 80˚.

- Anti friction screen (open end): Dacron x 2 layers, helically wound around the tether core at a helix angle of approximately 75˚.

- Core construction: 7 x Ø20mm 70 Shore A hardness EPDM supplied by Polymax.

To facilitate the testing of the different core constructions, a novel collet arrangement was designed to terminate one end of the tether in a way that enabled the removal of the core for visual assessment at intervals during the testing regime. In practice, the test window did not allow for repeatedly removing and re-installing the test tether in DMaC, which would have been required every time the tether was removed for inspection. The collet arrangement was therefore manufactured and utilised for these tests but visual assessments of the tether at intervals was not possible. Figure 5.14 details the collet design.

To ensure the collet arrangement was strong enough to withstand the forces during the testing it was manufactured from bright mild steel. The use of this material resulted in a heavy component so when installing each test tether in DMaC an overhead crane was used to take the weight of the collet and to avoid any additional catenary being introduced into the test set up due to the weight of the collet pulling the tether down. An additional eye bolt was installed into the top of the collet arrangement to enable the collet to be safely clipped into the overhead crane lifting hook. The overhead crane

Connect into
DMaC with a
shackle around
this shaft

Dowels used for
locating clamp.

Open end of tether is
pulled through this
cavity and mandrel fits
inside open end of
tether. Once the tether
is under tension the
mandrel is pulled into
location.
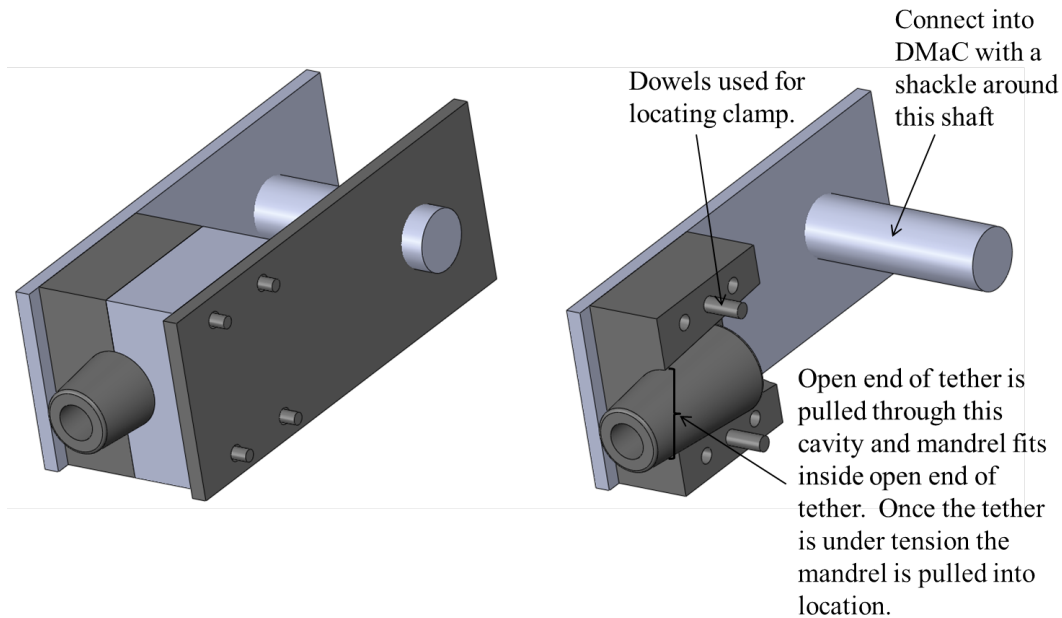
Figure 5.14: Rope collet design. Left image details the complete assembly; right image details cut away view. The deign allowed the empty end of the tether to be pulled through the clamp with the mandrel then fitted into the open end of the tether. Once the tether was put under load the mandrel was then pulled into location within the collet and held the tether firmly in place. Note the entire assembly was manufactured from bright mild steel. Different colours have been used in this assembly visualisation to clearly define different components of the assembly.

was used to support the weight of the collet throughout the test work, and Figure 5.15a details the use of the collet arrangement utilising the eye bolt. In practice, the orientation of the collet during the test set up was introducing twist in the tether. The final set up therefore utilised a strop to support the collet with the crane, rather than clipping the overhead crane directly into the collet eye bolt. Figure 5.15b details the rope clamp supported by the strop during the test set up for the anti-friction membrane durability tests.

The DMaC test regime was specified to subject the anti-friction screens on the tethers to as much movement as possible. It was therefore decided to conduct the testing in displacement mode, with a maximum travel of 0.2m. This value for displacement was selected to expose the tether to a significant amount of strain whilst ensuring

(a)   (b)

Figure 5.15: Rope collet arrangement in situ during anti friction membrane durability testing. (a) details original arrangement using a hook through the eye bolt but this was found to introduce too much twist into the tether set up; (b) details the final arrangement with a strop to support the collet, this arrangement was used for the testing.

it was not likely to break as a failure would nullify all the results. To realistically reflect the operational requirements of the anti-friction screen, DMaC was filled with water throughout these tests (with the exception of the set up tests ETT_03_P1-16 and ETT_03_P1-17 as detailed in Table 5.7).

Bedding in tests as detailed for the previous tether tests were not necessary in this instance as the eye splice end of each tether was the original eye splice used during Proof of Concept test work, so had already been exposed to the full range of bedding in tests. The collet arrangement did not have the bedding in requirements of a fibre rope. Both tethers were exposed to identical test regimes as detailed in Table 5.7. During test TETT_102_P1-17 the collet arrangement slipped out of the strop after 185 cycles so the test was aborted. An additional test script (TETT_104_DM) was therefore written for 815 cycles to ensure the full 1000 cycles were conducted for consistency between the tests on P1-16* and P1-17*.

Table 5.7: Anti friction membrane DMaC test schedule details for tethers P1-16* and P1-17*. Tests were conducted wet unless otherwise stated.

Tether	Test I.D.	Test script	Pre-tension (kN)	Peak tension (kN)	Sinusoidal Cycle Period (s)	Cycles (No)	Details
P1-16*	ETT_03_P1-16	ETT_03	1	10	8	10	Dry cycles to observe test set up before filling DMaC.
	DMaC operated manually		n/a				Manual investigation up to 25kN to observe set up and twist in tether - wet.
	TETT_101_P1-16_01	TETT_101	n/a		8	5	5 cycle test to ensure all operating as expected - wet.
	TETT_102_P1-16_01	TETT_102	n/a		8	1000	Displacement driven with a displacement of 0.2m - wet.
	TETT_103_P1-16_01	TETT_103	n/a		8	500	Displacement driven with a displacement of 0.2m - wet.
	TETT_103_P1-16_02	TETT_103	n/a		8	500	Displacement driven with a displacement of 0.2m - wet.
P1-17*	ETT_03_P1-17	ETT_03	1	10	8	10	Dry cycles to observe test set up before filling DMaC.
	DMaC operated manually		n/a				Manual investigation up to 35kN to observe set up and twist in tether - wet.
	TETT_101_P1-17_01	TETT_101	n/a		8	5	5 cycle test to ensure all operating as expeted - wet.
	TETT_102_P1-17_01	TETT_102	n/a		8	1000	Displacement driven with a displcaement of 0.2m - wet. Aborted at 185 cycles due to collet slip.
	TETT_104_P1-16_01	TETT_104	n/a		8	815	Displacement driven with a displcaement of 0.2m. 815 cycles to reach original 1000 cycle target of TETT_102 - wet.
	TETT_103_P1-16_02	TETT_103	n/a		8	500	Displacement driven with a displcaement of 0.2m - wet.
	TETT_103_P1-16_02	TETT_103	n/a		8	500	Displacement driven with a displcaement of 0.2m - wet.

5.4 Results

This section presents the results for the tether reliability assessment in the same order as the methods outlined in Section 5.3. To aid navigation through the results section, references are provided in each sub-section, linking back to the original method identified.

5.4.1 Tether assembly durability assessment

The tether assembly durability assessment is presented in two sections; 5.4.1.1 presents results from the laboratory testing of the tether at the DMaC test facility and 5.4.1.2 presents results following field testing of the tether at sea on the SWMTF.

5.4.1.1 Laboratory assembly assessment - DMaC

Long term fatigue assessment was conducted on two tether prototypes as outlined in Method Section 5.3.1.1, Page 242. Initially tether P1-16 was tested and results from this are presented below. Design improvements were identified following this testing and further fatigue assessment was conducted on a revised tether, P1-20. Results from this tether are presented following the results for P1-16.

Original fatigue assessment - P1-16

The Thousand Cycle Load Limit (TCLL) test was performed to ascertain the performance of a typical tether when subjected to high level, tension-tension loading over multiple cycles. Initially this test was conducted on P1-16 which survived 1,000 cycles at 1% - 50% NWBS loading and 1,000 cycles at 1% - 60% NWBS loading. The tether failed at a load range of 1% - 70% NWBS loading (2.2 - 153kN) on the 176$^{\text{th}}$ cycle. Based on Equation 5.1, Page 245, the TCLL value for the P1-16 tether was calculated as:

$$TCLL = 100\% - \frac{6.91(100\% - 70\%)}{Ln(215 + 176)} = 65.27\% \tag{5.8}$$

The fatigue failure on P1-16 occurred where the load carrying rope increased in diameter to envelop the core bundle. It is likely that the edge of the core bundle caused wear on the rope, and over the high number of cycles conducted during the TCLL test

Figure 5.16: TCLL failure of tether P1-16. Failure occurred during the 1% - 70% NWBS load range and on the 176th cycle.

the fretting eventually led to complete failure of the rope. Figure 5.16 details tether P1-16 immediately following failure.

In addition to calculating the TCLL value for P1-16, the evolution of axial stiffness of the tether throughout the testing is also of interest to establish any changes to the tether operation caused by this high level of loading. Before quantifying any change to the axial stiffness of the tether it was necessary to check the validity of the assumption for eye splice extension used in the functionality test work (1965.9kN/m). The method for doing this was outlined in Section 5.3.1.1. In order to quantify this, TETT_26 was performed, cycling the tether from 1% - 50% NWBS for 10 cycles whilst monitoring the UoE eye splice. Figure 5.17 details the displacement measured during this test. Load extension data for the first five cycles was extracted and can be seen in Figure 5.18. From this figure it is clear that as the test progressed, the load-extension behaviour of the eye splice began to align to a steady value, indeed it is difficult to distinguish between cycle 4 and cycle 5. Data for the load up of cycle 5 was extracted and plotted in Figure 5.19, along with a line of best fit which is detailed on the graph and shows good correlation to the data with an R^2 value of 0.9981 (the R^2 value is the square of the Pearson product moment correlation coefficient). The gradient of this line relates
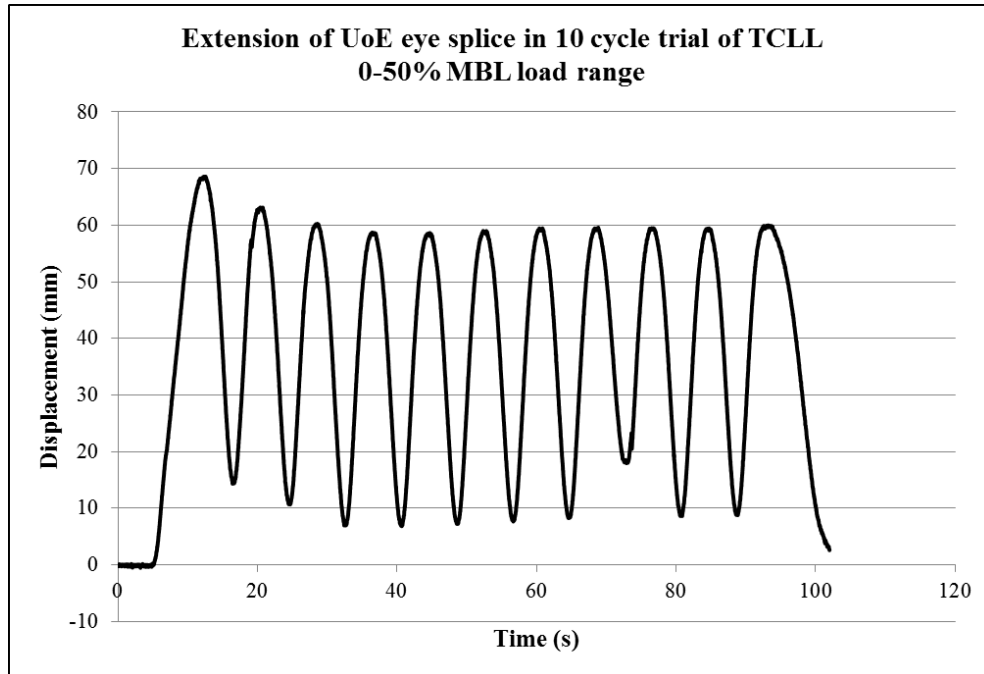
Figure 5.17: Draw wire displacement measurement of UoE eye splice extension during a 10 cycle trial of TCLL in the 1-50% NWBS load range. A glitch occurs in the reading for the 8$^{\text{th}}$ cycle, this is inconsequential as only data from cycle 5 is used for the extension calculation.

to the extension of the eye splice and is 1984.4kN/m. This compares well to the original calculated mean extension of the eye splice, which was 1965.9kN/m. This original value was calculated based on results for two experiments on P1-3 and P1-6, with calculated values of 2065.7kN/m and 1866.2kN/m respectively. The new result is therefore 4% higher than the value for P1-3 and 6% lower than the value for P1-6 which demonstrates the existing assumption for eye splice extension of 1965.9kN/m remains valid for the higher loads used in the TCLL tests and is applied throughout this work.

Once the eye splice extension was calculated, this was deducted from the overall displacement measured by DMaC, to leave the extension of the working portion of the tether. Load and displacement data were then extracted at a selection of cycles for each TCLL loading level. The results from these cycles are detailed in Figure 5.20.

It is clear that as the TCLL tests progress through the cycle numbers, the load-displacement behaviour of the tether cycles begins to align. This is very pronounced
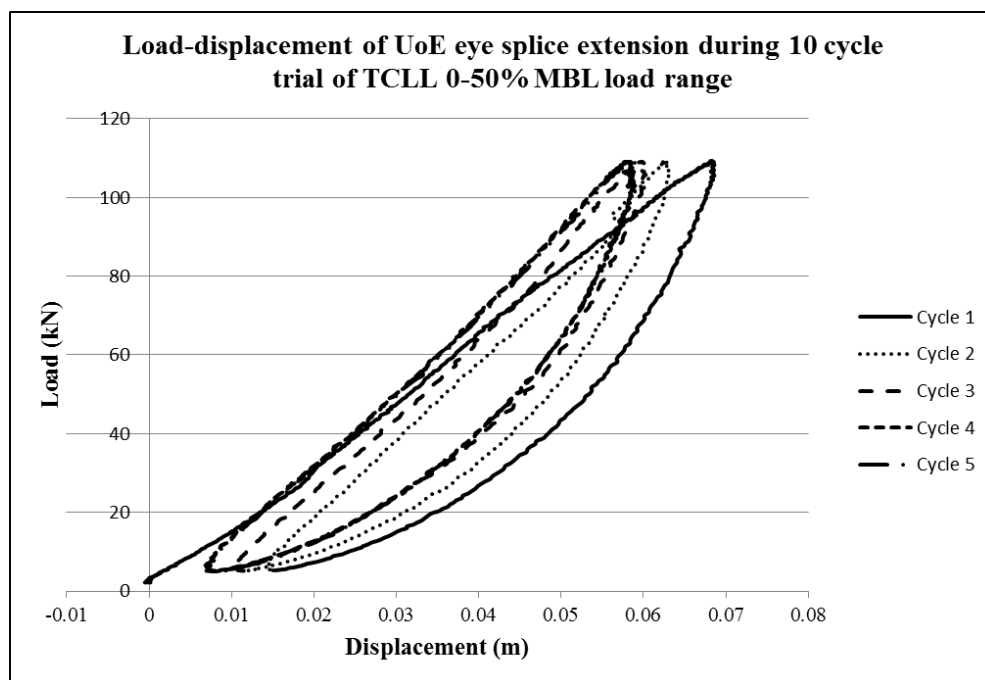
Figure 5.18: Load-displacement performance of UoE eye splice during a 10 cycle trial of TCLL in the 1-50% NWBS load range, first five cycles plotted independently. Cycle 4 and cycle 5 are difficult to distinguish as they are very closely aligned. Cycle 1 is on the far right of the figure with increasing cycle numbers plotted sequentially moving from right to left.
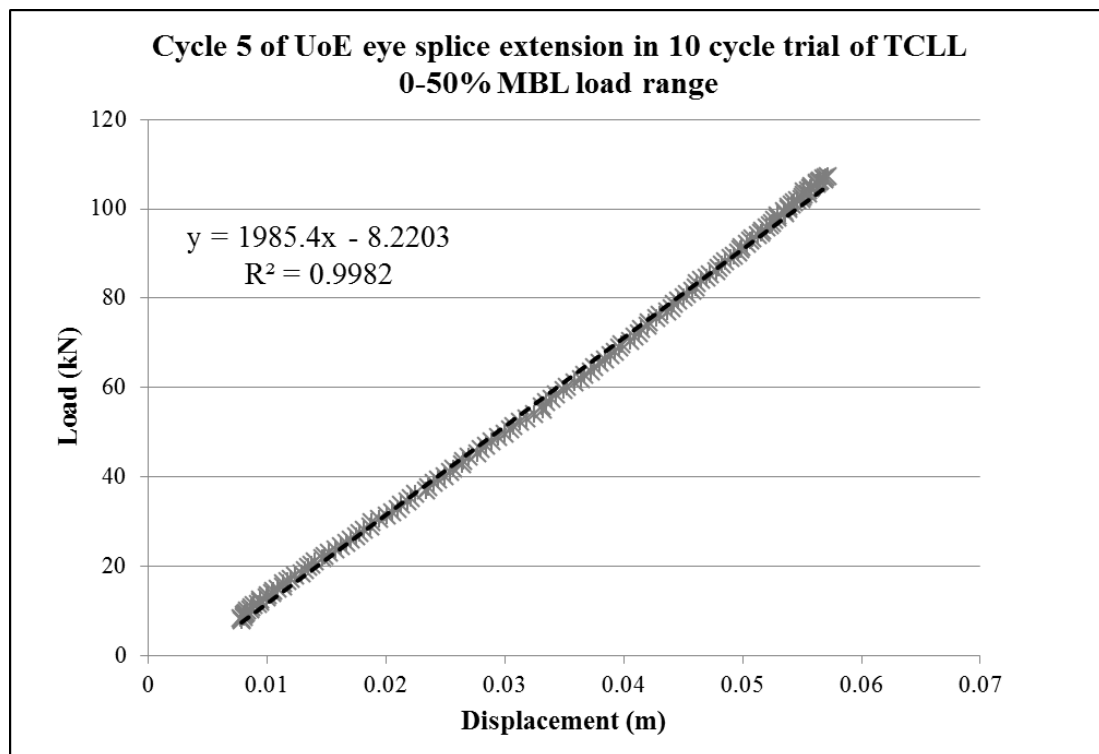
Figure 5.19: Cycle 5 data extracted from the load-displacement plot of UoE eye splice extension during a 10 cycle trial of TCLL in the 1-50% NWBS load range, plotted in grey crosses. The line of best fit is detailed by the dashed line and the equation is detailed along with the R^2 value calculated using the square of the Pearson product moment correlation coefficient.
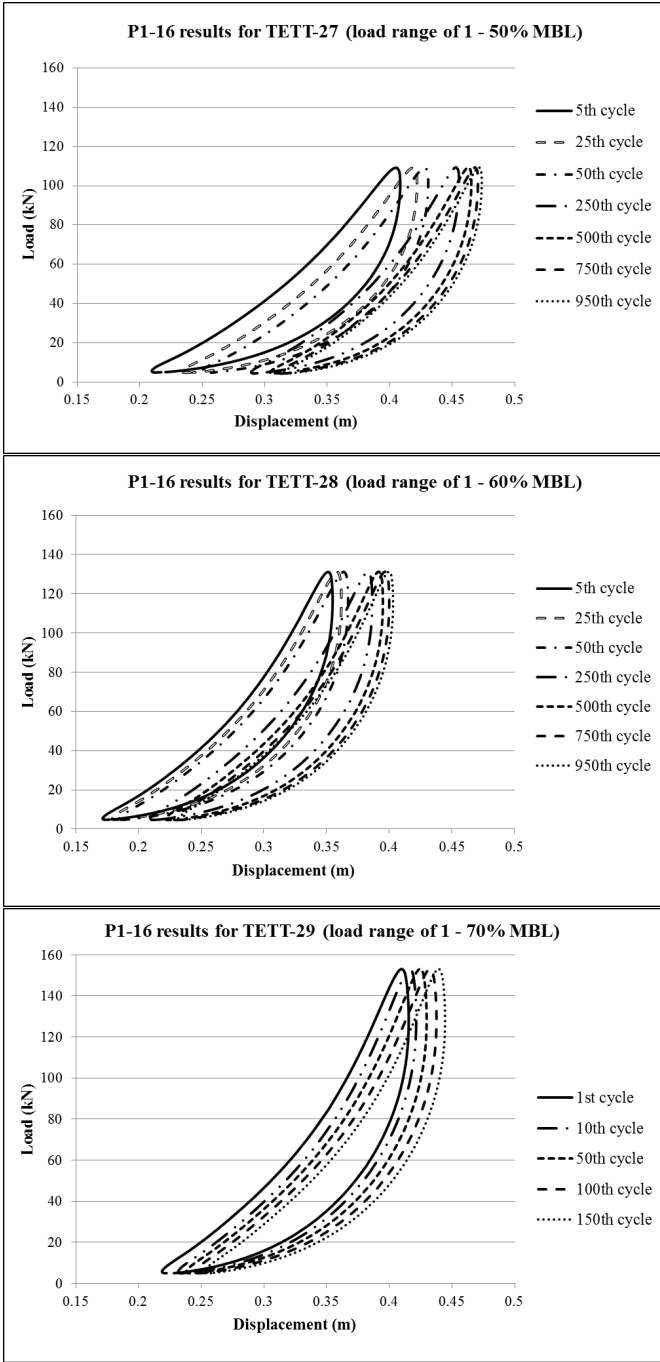
Figure 5.20: P1-16 TCLL results for a selection of cycle numbers across all TCLL ranges.

for the first load range (TETT-27) but is evident across all load ranges.

A further interesting observation from the graphs in Figure 5.20 is the step change in displacement between each test, which is particularly evident between tests TETT-27 and TETT-28. This step change is due to a unique feature of the Exeter Tether whereby following extension, the tether takes a temporary compression set due to the behaviour of the polymer core. When the last cycle of TETT-27 finished the load was held at 1 % NWBS (2.2kN). However, following completion of the test, the tether gradually recovered from the compression set, with the polymer core expanding radially and therefore trying to contract the length of the tether. As the tether was held in a fixed position this gradual recovery caused an increase in load. During the time between TETT-27 and TETT-28 the load increased from 2.2kN to 6.2kN. To fulfil the specification of the TCLL tests, TETT-28 had a starting load of 2.2kN so this extra load caused by the tether recovery had to be reduced by manually extending the DMaC linear actuator, to introduce further slack into the system and allow the tether to contract in length. This step change can be clearly observed between TETT-27 and 28 where the starting displacement decreases from 0.21m in TETT-27 to 0.17m in TETT-28.

To quantify the evolution of dynamic axial stiffness in the tether, data from each specified cycle was analysed and a secant was drawn between the loads of 20 - 90kN (as introduced in Section 5.3 and suggested by McKenna *et al.* (2000)). The strain at these loads was then calculated by interpolating the data to give the exact strain at each specified load. An example of the secant approach can be seen for the 250th cycle of TETT-27 in Figure 5.21.

Once the strain values were calculated for each cycle, the secant points were plotted and the equation of the line established. TETT 27 is again used as an example to demonstrate this method in Figure 5.22. The secant lines are plotted along with the equation for each line. The gradient of each secant line provides a value for dynamic axial stiffness at that particular cycle number. It should be noted that as the end terminations and rope structure are 'bedding in', the secant lines move to the right of the graph in Figure 5.22. Due to this bedding in process a greater strain can be achieved at a particular load. It is the slope of these graphs that is of interest however, which indicates the dynamic axial stiffness of the tether at each identified cycle.
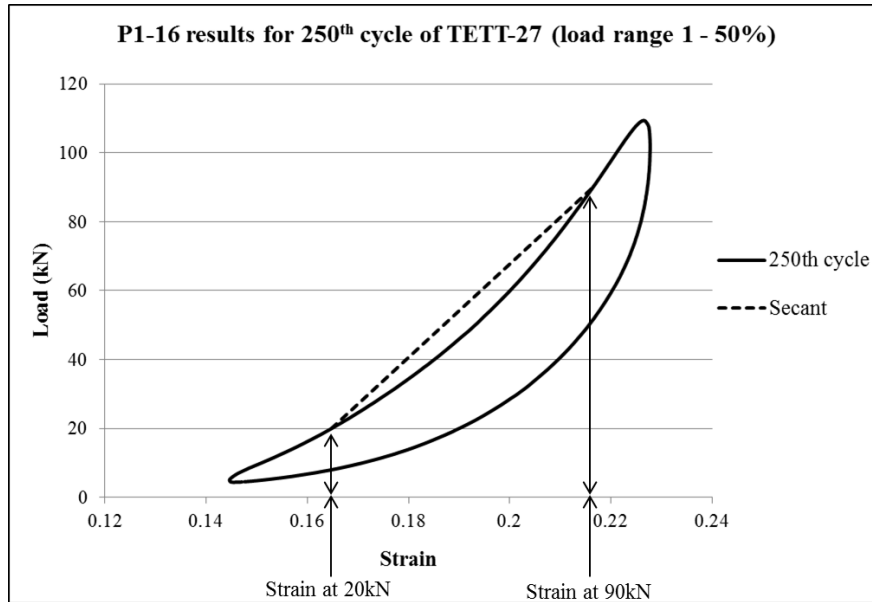
Figure 5.21: Example of the secant approach for quantifying dynamic axial stiffness of tether P1-16 using the 250th cycle of TETT-27 (a load range of 1 - 50%).

The dynamic axial stiffness value was then plotted against cycle number to observe how it evolved with increasing load cycles. Figure 5.23 details the evolving dynamic axial stiffness for each TCLL test conducted on P1-16. Discussing each graph in turn, it is clear from the first graph (TETT-27) that the stiffness increases with cycle number. Initially this increase is quite dramatic, with the stiffness increasing 23% between cycles 5 - 250. However over time the stiffness stabilises and from cycles 250 - 950 the stiffness only increases by a further 6% altogether, with the stiffness increasing by just 0.4% from cycles 750 - 950. The second graph (detailing TETT-28) shows signs of yield in the first 50 cycles. At this increased load level some component of the tether must have yielded to an extent, but not failed. This led to a decrease in stiffness over the first 50 cycles, but following this initial drop, a steady increase in stiffness is observed. Although the increase is clear, it is much less pronounced than during TETT-27, with a total increase over the whole range of just 4%. Again, the stiffness can be seen to stabilise, with the increase in stiffness between cycles 750-950 just 0.3%. Finally, the last graph (detailing TETT-29) shows the gradual reduction in tether stiffness as the tether yields further and approaches final failure.

Figure 5.24 brings all these graphs together to compare them on one plot. Here,

P1-16 secants plotted between 20 and 90kN for TETT 27 (load of 1 - 50% MBL)

$y = 1102x - 117.92$

$y = 1175.4x - 141.58$

$y = 1220.8x - 156.96$

$y = 1353.7x - 202.99$

$y = 1405.4x - 221.93$

$y = 1425.1x - 230.42$

$y = 1430.8x - 234.06$
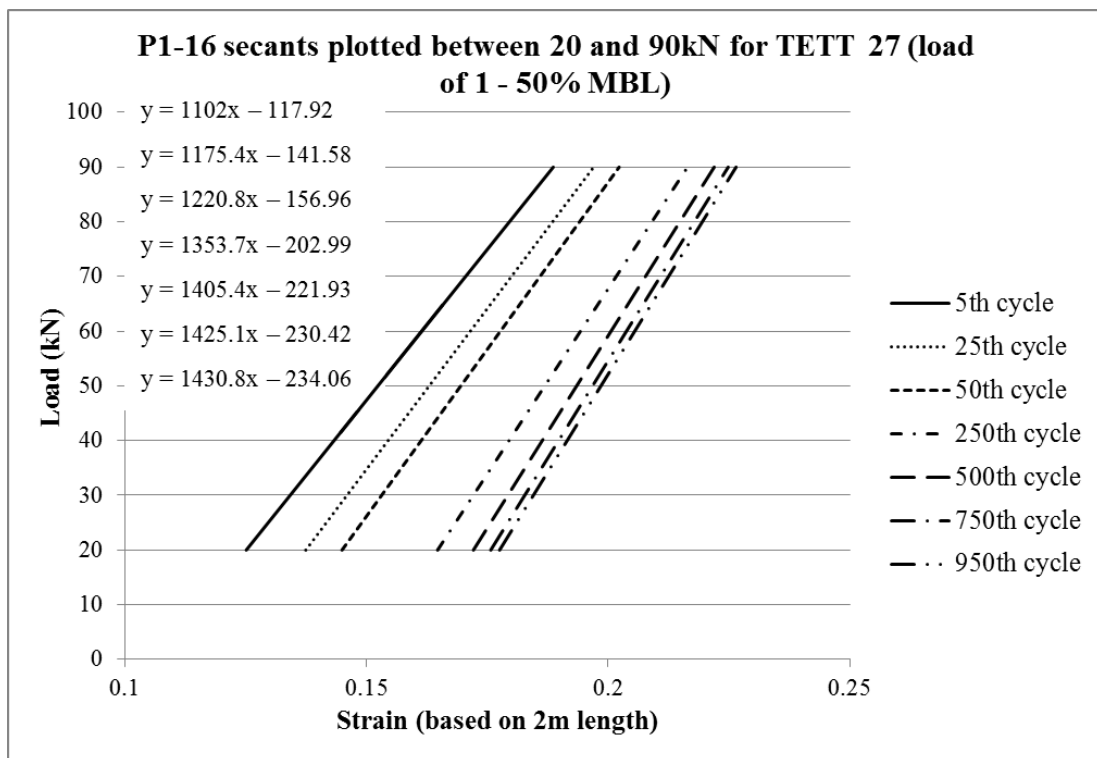
Figure 5.22: P1-16 secants plotted between 20 and 90kN for selected cycles of the TETT 27 test range (with a load of 1 - 50 %NWBS). Equation for each line is detailed to the left of the plot and is listed by increasing cycle number.
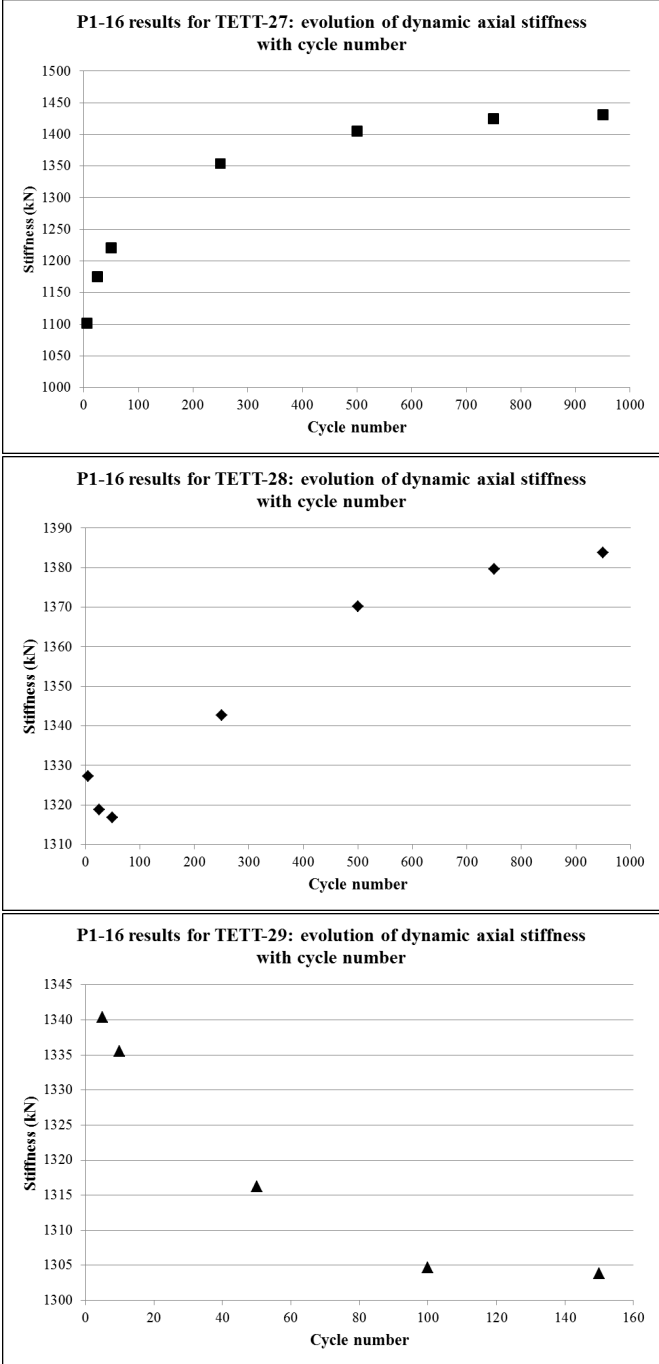
Figure 5.23: P1-16 dynamic axial stiffness evolution across all three TCLL tests. Note different axis between graphs.
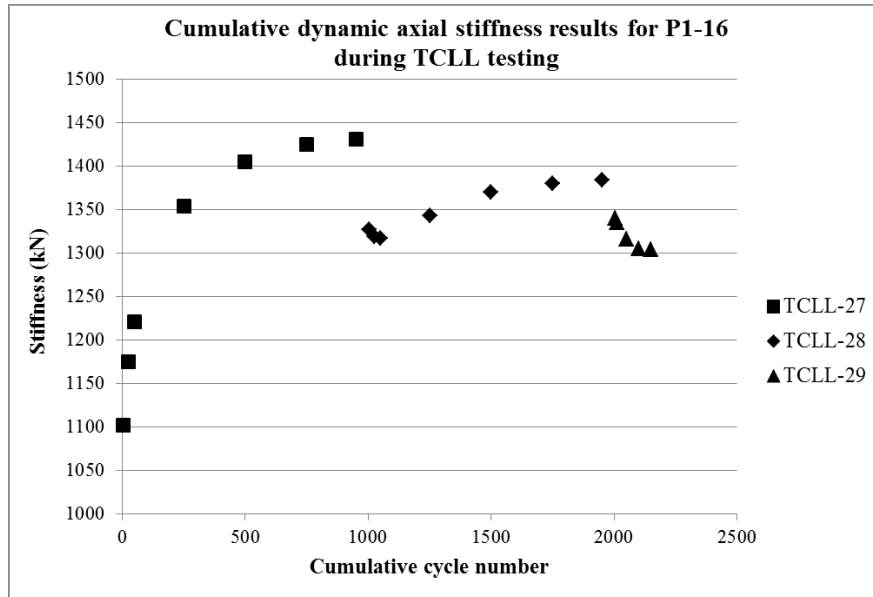
Figure 5.24: P1-16 cumulative dynamic axial stiffness evolution throughout the TCLL test series.

the effect of the test set-up adjustments between each load range (necessary to accommodate the recovery of the tether as previously discussed) is again evident, with an 11% drop in stiffness between TETT-27 cycle 950 and TETT-28 cycle 5 and a further 3% drop in stiffness between the equivalent cycles of TETT-28 and TETT-29. One would expect to see the stiffness evolution throughout TETT-28 to eventually increase beyond the maximum level of stiffness observed during the final cycles of TETT-27. The fact that it does not is further evidence of yielding within the tether construction during TETT-28.

Revised tether fatigue assessment - P1-20

One of the most important findings of the first TCLL test on P1-16 was the failure mode, which highlighted scope for improvement in subsequent tether iterations. In the original design, as the rope diameter increased to envelop the core bundle, the edge of the core bundle was clearly acting as a point of wear for the outer load carrying rope. As the tether was subjected to numerous cycles, the core bundle edge continued to wear the rope, eventually leading to a complete failure. Following this finding a new trial

tether was manufactured incorporating some adaptations to the end termination of the tether core. This tether combined aspects from both the seven strand core bundle tether and the articulated tether. The tether was adapted from P1-7 of the original P1 Series, manufactured from six Polymax Ø25mm EPDM 70 Shore A hardness cords with the seventh, central core made from Polymax Ø25mm EPDM foam, with 70 Shore A hardness. The existing P1-7 core was reduced in length to 1.3m and at each end of the core a small amount of material was removed from the edge of each cord to create a chamfer (Figure 5.25a). A female part of the articulated core was then fitted around the chamfered cords (Figure 5.25b) and held in place using PVC tape. A male double hemisphere part of the articulated core was then engaged into the female part (Figure 5.25c) and again held in place using PVC tape. Each of these articulated assemblies added 0.12m to the length of the core, so the final core length was 1.54m. Finally, the eye splices were re-made at either end of the tether by the UoE in line with the original splice design utilised by Lankhorst Ropes (Figure 5.25d). The major improvement of this tether iteration was that the male double hemisphere introduced a gradual slope to the end of the core bundle to avoid the wearing evident in the previous design.

Once the new tether was manufactured it was possible to repeat the TCLL test to ascertain any improvement in fatigue performance. As this was a brand new construction, the full suite of bedding in tests were conducted prior to the TCLL test set up. The repeat TCLL test, conducted on P1-20, was detailed alongside the original TCLL test procedure outlined in Section 5.3 in Table 5.3, Page 247.

Tether P1-20 survived the first 1000 cycles from 1% - 50% NWBS but unexpectedly failed during the eighth cycle of TETT-28, a much poorer performance than P1-16 with the original core design. Upon reviewing this failure, it was apparent that the eye splice construction at the actuator end of the DMaC was not evenly balanced. As discussed in Section 2.6.3.4 and detailed by Weller *et al.* (2013) if the eye splice is unbalanced then the proportion of load carried by one part of the eye splice will be increased, leading to a premature failure. Evidence of the un-even loading of the eye splice can be seen in Figure 5.26 which details two images of the failed tether. In both images two strands of the eye splice carrying the least load can be seen, having survived the tether failure. Following the failure of the other strands of the eye splice these surviving strands were put under higher load and 'pulled-through' the tether. This can be seen in Figure 5.26b

(a) (b)

(c) (d)
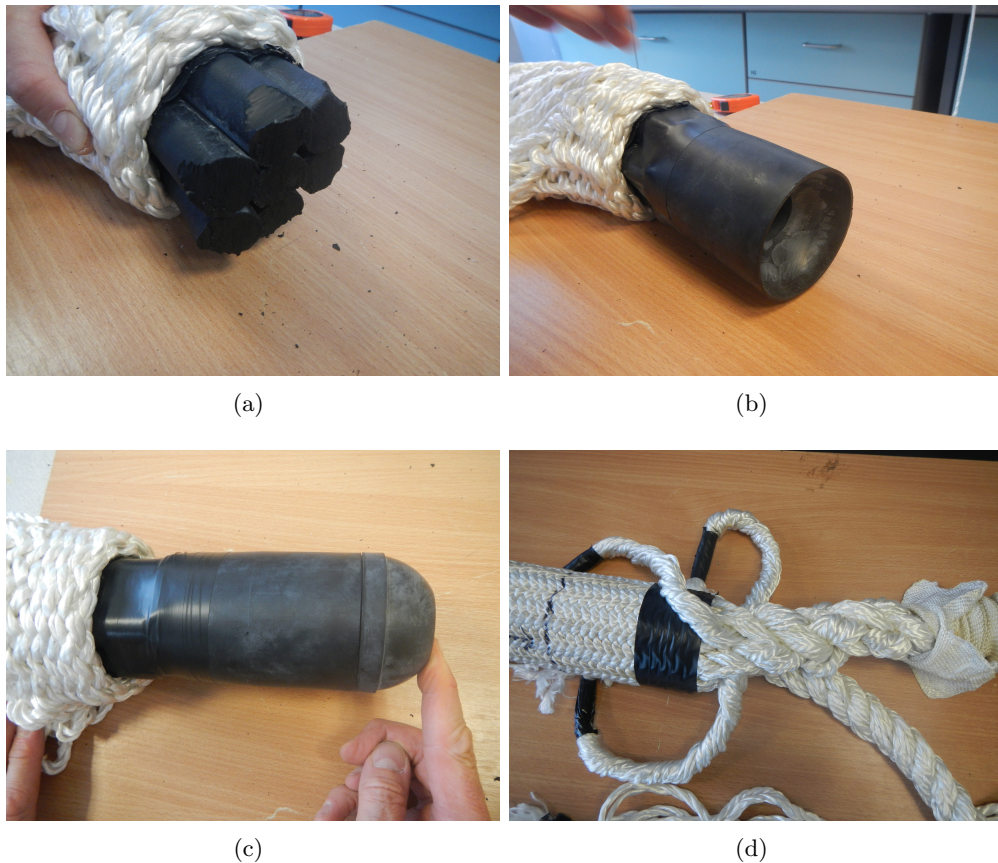
Figure 5.25: Revised tether termination. Key aspects of adaptation include: (a) chamfered ends to central cords; (b) female articulated component fitted around central cords; (c) male double hemisphere fitted into female component to provide a gradual radius to the end of the core bundle. The tether was completed with the same adaptation of the A3 Lankhorst Ropes eye splice as used in previous tethers.

(a)   (b)
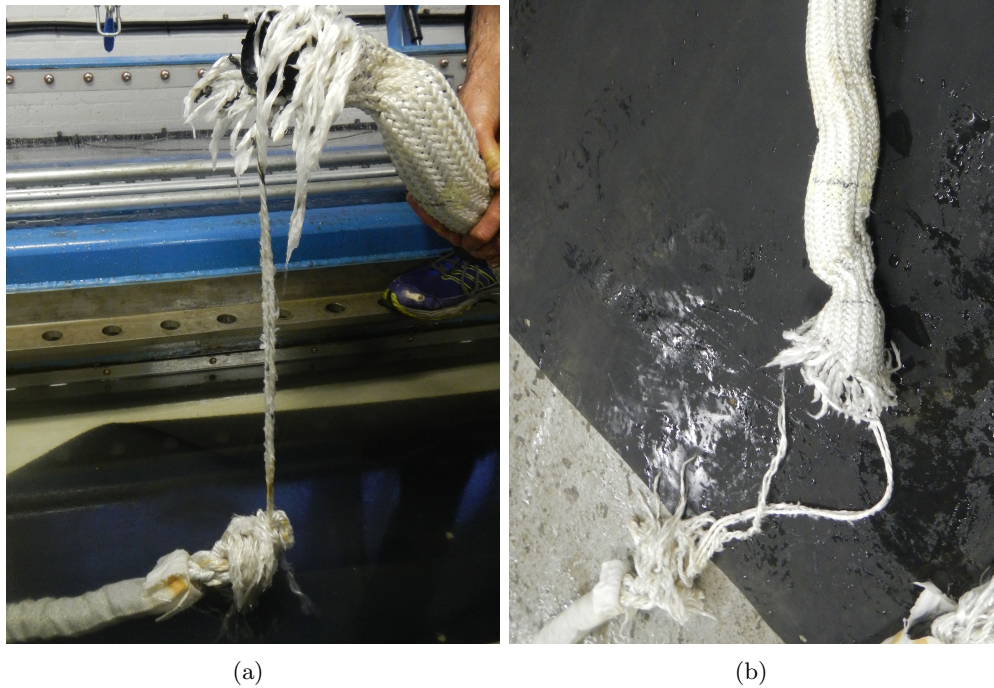
Figure 5.26: Images detailing failure mechanism of P1-20 during TCLL testing. The tether immediately following failure in DMaC is detailed in (a), where the two surviving strands can be seen. (b) details evidence of the surviving strands pulling through the rope jacket causing it to twist and deform.

where the rope jacket at the top of the image has been twisted and deformed due to the surviving strands pulling through the jacket assembly.

This premature eye splice failure means the design adaptations of P1-20 could not be evaluated. A visual inspection of the surviving end of the tether shows no evidence of fretting of the rope jacket (Figure 5.27). The articulated end component of the core has come away from the main core bundle, however smooth radii remain between the two and between the articulated component and the eye splice, with no indication of wear. Overall this end of the tether looks healthy.

Despite the premature failure, to complete the assessment of P1-20 tether testing the TCLL value for this tether should be calculated. Following the same methodology as for P1-16, the TCLL value for P1-20 was calculated as 50.26%.

As with P1-16, an assessment of the evolution of dynamic axial stiffness was also conducted for P1-20 test TETT-27, but was not possible for TETT-28 due to the low
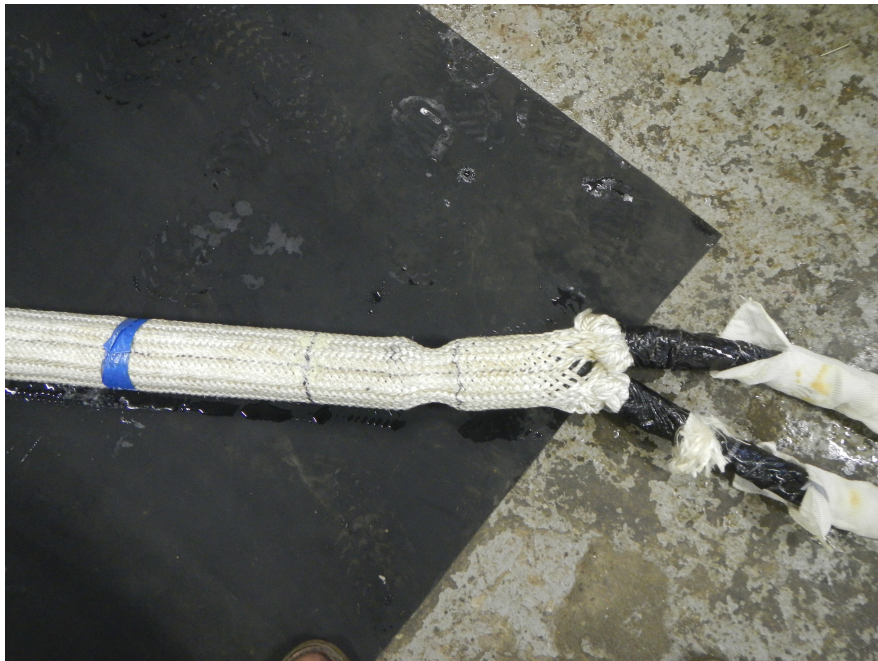
Figure 5.27: P1-20 surviving end following TCLL testing. The articulated component
has pulled away from the cord bundle but there are no signs of wear and this end of
the tether looks healthy.
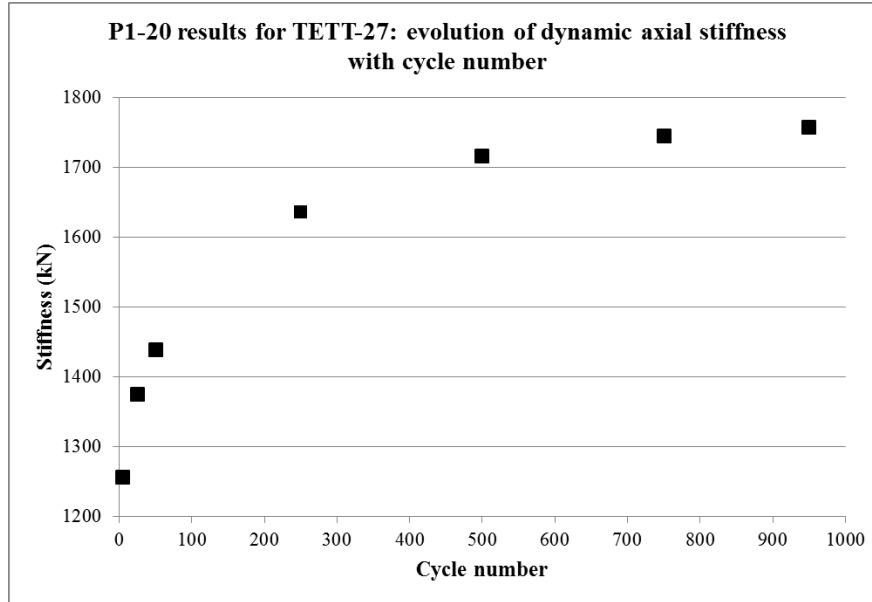
Figure 5.28: Tether P1-20 results for the evolution of dynamic axial stiffness with cycle number during test TETT-27 (a load range of 1% - 20% NWBS).

cycle number before failure (8 cycles). Following the same methodology the results of this assessment are detailed in Figure 5.28. The same pattern can be seen as documented for P1-16, with a large increase in stiffness during early cycle numbers (30% increase from cycle 5 - 250), and stiffness stabilising at higher cycle numbers with a further increase of 7% from cycle 250-950 and just 0.8% from cycle 750 - 950.

Due to the recovery of the tether as previously described, manual adjustments were made to the test set up between TETT-27 and TETT-28 which led to a decrease in stiffness at the start of TETT-28. Although not detailed in Figure 5.28, the secant stiffness calculated for cycle 5 of TETT-28 was 1627kN which was a 7% reduction on the stiffness measured at the 950th cycle of TETT-27.

5.4.1.2 Field assembly assessment - SWMTF

As detailed in Method Section 5.3.1.2, Page 250, four tethers were deployed on the SWMTF for a period approaching 6 months (4th June 2013 - 26th November 2013). Results from this deployment are presented below.

5. RELIABILITY ASSESSMENT OF A NOVEL MOORING COMPONENT: THE EXETER TETHER

Qualitative assessment

A detailed qualitative assessment was conducted on Tether P1-8 and findings from this investigation were reported by Gordelier *et al.* (2015). These findings are detailed below.

Significant marine growth developed on the upper tethers during the deployment as detailed in Figure 5.29a. This marine growth was removed using a bristle brush and fresh water. Following cleaning, there was no obvious evidence of external damage to the tethers, however there was a noticeable colour change to the rope as seen in Figure 5.29b. To investigate the penetration of the marine growth tether P1-8 was opened up and a visual inspection was conducted using microscopes to identify the extent of marine growth and any damage caused to the tether components.

Upon opening the tether, it was clear that the marine growth had fully penetrated all components of the tether. Figure 5.30 details this, with evidence of marine growth debris on the inside of the rope jacket, on the anti friction membrane and on the elastomeric core strands. Much of the marine growth was crushed by the action of the tether (Figure 5.31a) and further investigation using a microscope revealed byssal filaments on both the rope inner surface (Figure 5.31b) and on the anti friction membrane (Figure 5.31c). These byssal filaments are released by various species of bivalve mollusc (such as mussels) to enable attachment (Deming, 1999), and are evidence that the mollusc has fully infiltrated the rope and is attempting to attach to the inner rope and anti friction membrane. The main concern with marine growth (or bio-fouling) is that the debris from the marine growth will create high friction surfaces and promote wear on the yarns of the rope. Evidence of this fretting can be seen in Figure 5.31d and during longer term deployments further wear of this nature could ultimately lead to a premature failure of the load carrying rope.

In addition to investigating the extent of marine growth, the sea trial was also intended to investigate the durability of the anti-friction membrane and the elastomeric core. Figures 5.32a and 5.32b show the effect of the sea trial on the anti friction membrane which has been subjected to significant degradation. The edges of the membrane have started to fray and 'pressure tears' have developed in the membrane. Both the frayed edges and the pressure tears create high friction surfaces which again could promote wear of the load carrying rope. Indeed, Figure 5.33 details a region of rope yarns

Figure 5.29: (a) Upper tethers with significant marine growth following sea deployment; (b) tether P1-8 following cleaning with a bristle brush and fresh water

exhibiting signs of wear where red threads from the anti friction membrane are also present.

In terms of elastomeric core integrity, minor compression deformations were visible on the outer surface of the core strands, as detailed in Figure 5.34. These deformations are likely to have been caused by the high pressure exerted by the rope when extending during tether operation. As detailed by Gordelier *et al.* (2015) this is not likely to lead to a catastrophic failure of the tether. However, permanent damage of the core may affect the load-extension properties of the tether and therefore alter the designed operating parameters of the tether, potentially reducing the anticipated load mitigation of the tether.

Quantitative assessment

As outlined in Method Section 5.3.1.2, Page 250 the tether functionality test ETT-08 was used to quantify the alteration in functionality of the tether pre and post SWMTF deployment. As the full technique is detailed for the TCLL test results Section 5.4.1.1, only the final results are detailed here. It should be noted that test ETT-08 is a displacement driven test from a 1550N starting datum (in an operational tether such a datum would represent a mooring system pre-tension). Zero displacement is specified at the 1550N tension datum so all strain values are based on extension relative to this datum rather than absolute strain as detailed in the TCLL tests. These results were
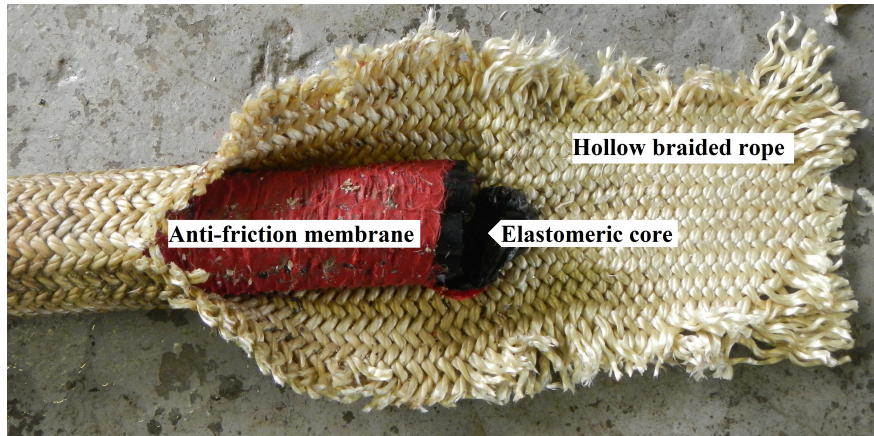
Figure 5.30: Internal view of P1-8 following sea trials. Marine growth and wear can be seen on the anti friction membrane.

not intended to be comparable to the TCLL tests but to provide information regarding the change in functionality of the tether following the SWMFT deployment.

Following the technique outlined in Section 5.4.1.1, an adjustment was made accounting for the extension of the eye splices to calculate the extension of the working portion of the tether from the results of ETT-08 for tethers P1-3 and P1-8. Strain values from a 1550N start datum where then calculated and the secant modulus was plotted between 10 and 35kN for ETT-08 test results recorded both before and after the SWMTF deployment. This graph can be seen in Figure 5.35.

The results show a shift from pre-deployment, where P1-3 and P1-8 displayed quite different dynamic axial stiffness behaviour, to post-deployment where the axial stiffness of both these tethers became more aligned; initially P1-3 was 19% stiffer than P1-8, however following the deployment the difference had dropped and P1-8 was just 6% stiffer. In addition to the greater agreement shown between the tethers in the post deployment data, both tethers also showed an increase in dynamic axial stiffness following deployment; this increased by 5% and 21% for tethers P1-3 and P1-8 respectively.

5.4.2 Elastomeric core durability assessment

This section of results focuses on the durability assessment of the elastomer core material, EPDM. A large suite of material testing was conducted on the EPDM polymer material to review the effect of exposure to the marine environment and exposure to
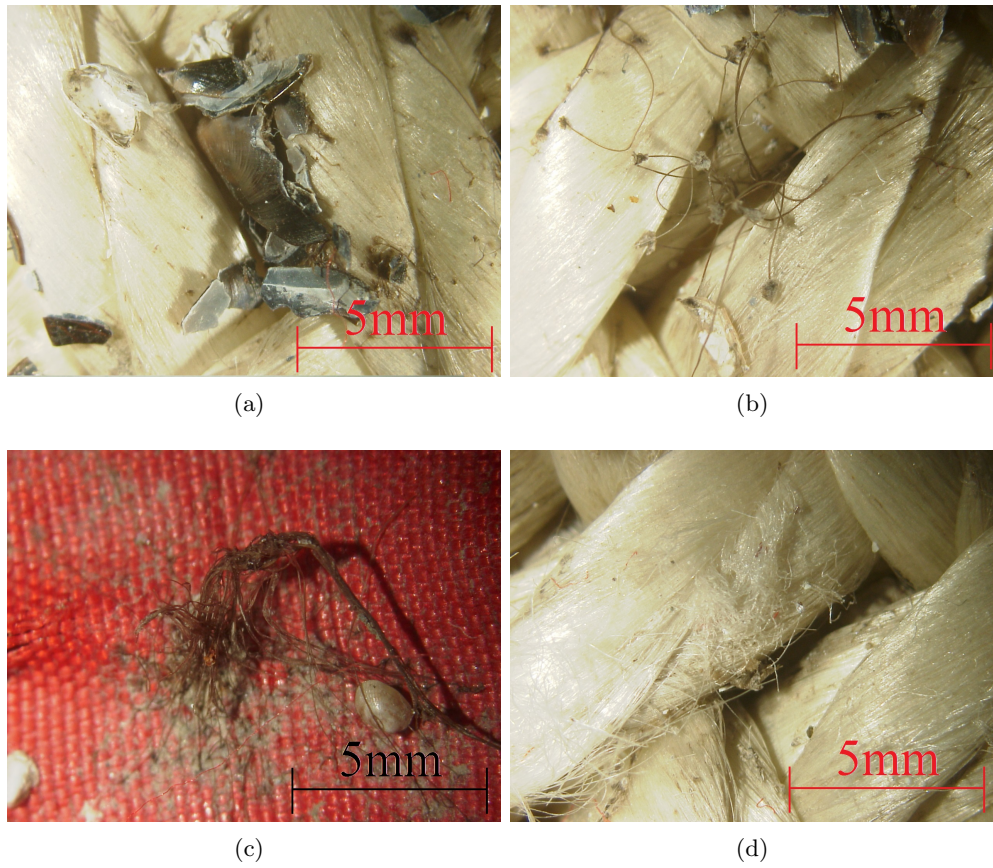
Figure 5.31: Microscope investigation of P1-8 following deployment:(a) Crushed mussel growth; (b) evidence of byssal filaments on the inner surface of the rope; (b) byssal filaments attached to the anti friction membrane; (d) worn rope yarns.

(a)

(b)

Figure 5.32: Anti-friction membrane following deployment:(a) Outer surface of membrane in-situ around the elastomer core; (b) inner surface of membrane, un-wound from the elastomer core.
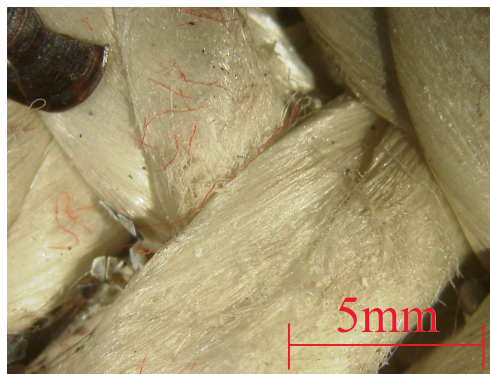
Figure 5.33: P1-8 yarns exhibiting signs of wear with red threads from anti friction membrane present.

Figure 5.34: Elastomer core following sea deployment showing minor compression deformations on the outer surface of the strands.
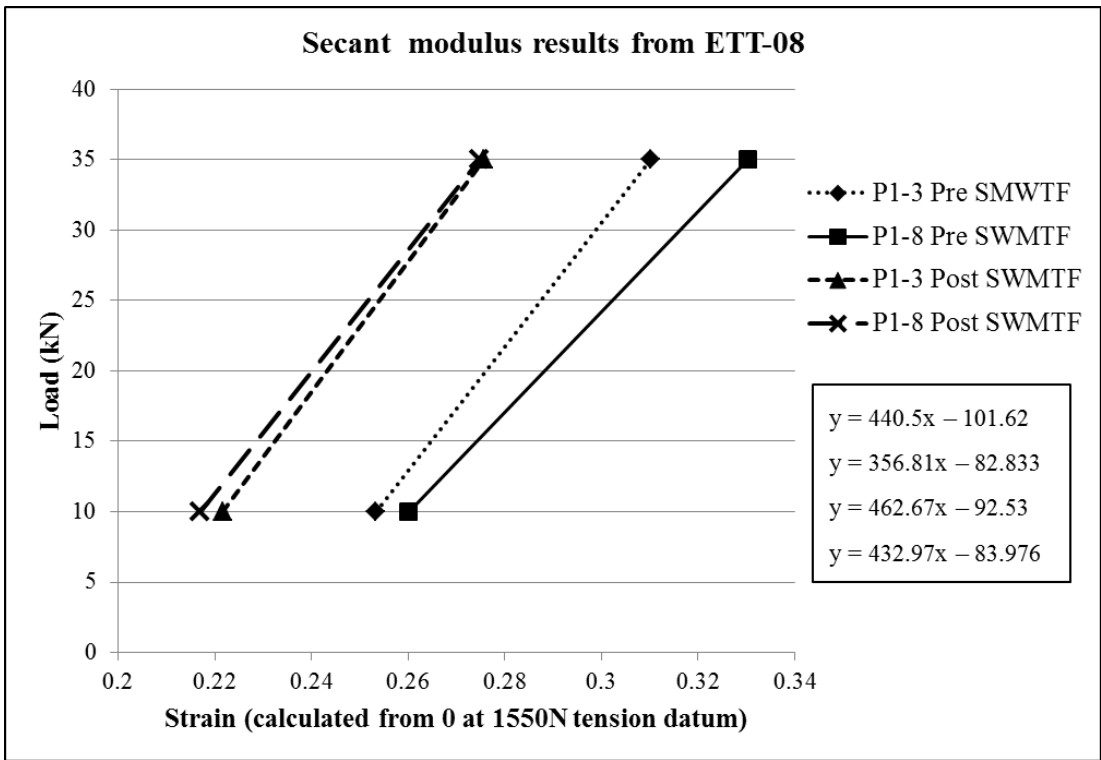
Figure 5.35: Secant modulus approach for defining the dynamic axial stiffness of tethers P1-3 and P1-8 both before and after SWMTF deployment. Note that strain is defined from a 0m start datum at 1550N. The equations of the secant are detailed in the bottom right of the figure, listed in the same order as the key.

the loading regimes anticipated through tether operation. The results from these tests are detailed below.

5.4.2.1 Ageing of polymer

As detailed in Method Section 5.3.2.1, Page 253, sheet and round samples of EPDM were immersed in tanks of sea water to encourage accelerated ageing. Following submersion in heated sea water for 1 month at 60°C the 2mm thick EPDM material was removed from the tank and prepared for tensile testing as described in Section 5.3.2.

Due to the larger dimensions of the Ø25mm round polymer samples, these sections immersed in the heated sea water tanks were not fully saturated after 1 month. To fully appreciate the effect of the sea water on the material properties of the polymer it was important that the water had fully penetrated the samples. The samples were therefore weighed and put back into the water tanks for further ageing. The samples were periodically removed from the heated sea water tanks and weighed. Figure 5.36 details the weight gain of the material samples over a period of 13 months. It was hoped that the weight gain would eventually level off, at which point it would be assumed the samples were fully saturated. The general trend in Figure 5.36 suggests that, had the samples been left for longer, further weight gain would have been observed. However, due to time limitations, the samples were removed at this point for testing. Although it does appear further weight gain would have occurred had the samples been left, the steady weight gain that occurred in the first 5 months of submersion had certainly slowed, and for the purposes of this test work, the samples were assumed saturated at this point. To observe the effect of this ageing process on the Ø25mm sections of polymer cord, compression testing was conducted, and results from this are reported in Section 5.4.2.4, Page 317.

5.4.2.2 Tensile tests

As described in Method Section 5.3.2.2, Page 255 all the tensile tests were conducted on 2mm sheet of EPDM, supplied by Ley Rubber Ltd, with a specified Shore A hardness of 70.
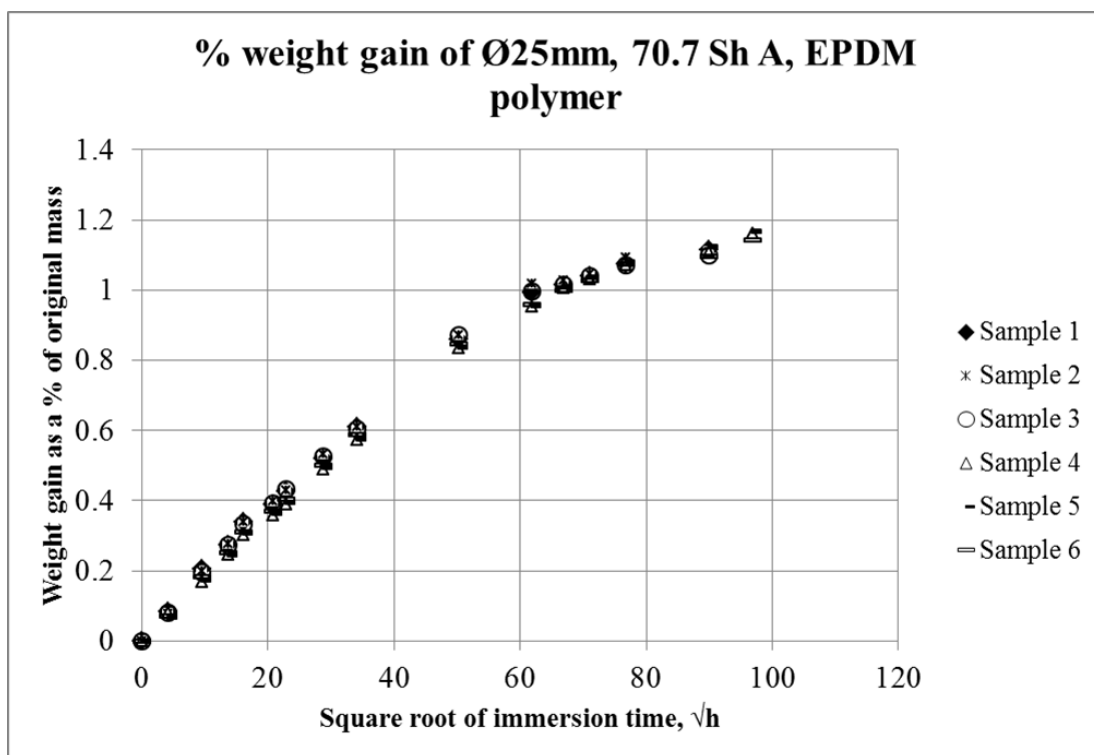
Figure 5.36: Weight gain of saturated Ø25mm, 70.7 Shore A hardness, EPDM polymer. Individual samples difficult to distinguish but general trend is apparent. Data recorded by team at IFREMER following the MARINET visit.

Figure 5.37: Example of a rejected sample for the ISO37 test procedure; the failure occurred too close to the end of the sample.

Table 5.8: ISO37 tests producing valid results

Speed of test	Repeats new sample	Repeats aged sample
10mm/min	4	2
100mm/min	4	5
500mm/min	5	3

ISO37: Determination of tensile stress-strain properties

As outlined in Method Section 5.3.2.2, Page 255 the ISO37 test procedure was followed to establish the tensile stress-strain properties of 2mm, 70 Shore A hardness samples of EPDM polymer.

The total number of valid results for the ISO37 procedure is detailed in Table 5.8. Certain results had to be rejected, for instance, if the failure occurred in the sample too near to a radii at either end (as detailed in Figure 5.37) the results had to be excluded. Results were also rejected if there were any errors with zeroing of the load cell. Unfortunately this leaves just 2 repeats for 10mm/min aged sample when the ISO37 standard specifies a minimum of 3. The two results show strong repeatability so will be assumed sufficient for the average results presented here.

It is not necessary to present every individual load-strain result for each ISO test conducted, but an example plot is provided in Figure 5.38 as a reference.

The key purpose of these tests is to observe the difference in material properties between the new and aged EPDM samples. Again, it is not necessary to plot every graph detailing the load-strain profiles comparing new and aged samples, but a typical plot is provided in Figure 5.39. This graph compares the load-strain profile of a new and
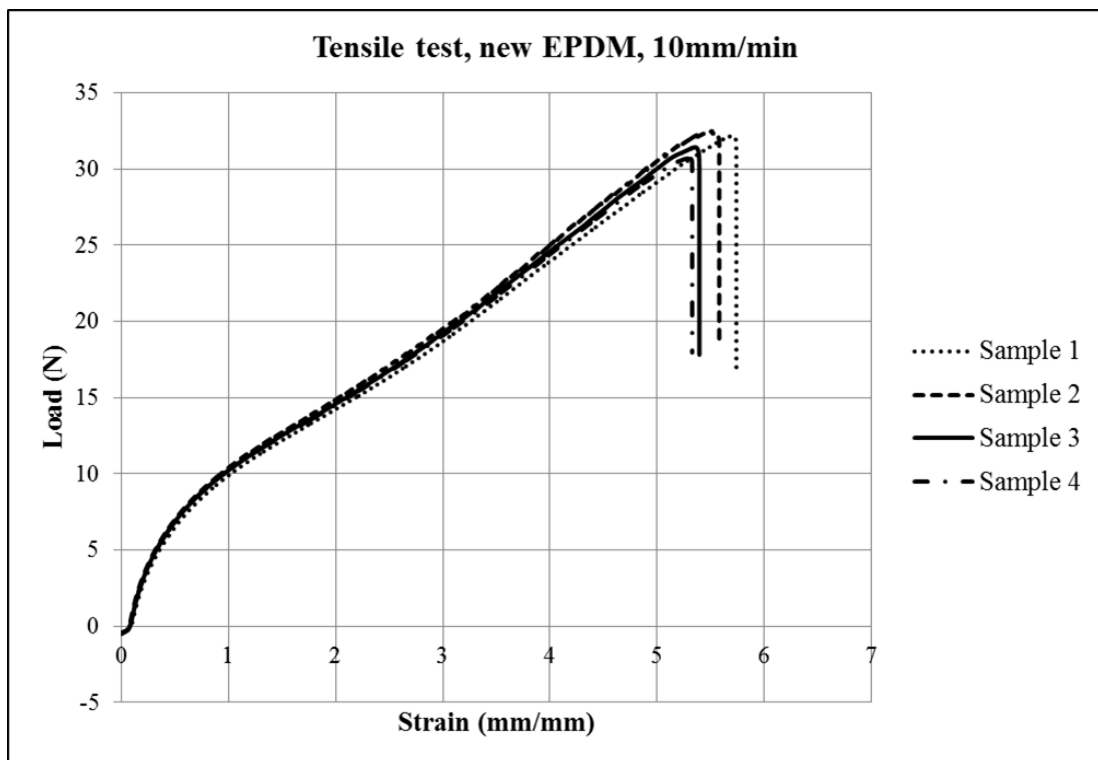
Figure 5.38: A typical load-strain plot example for ISO37. This plot shows the profile of new samples of EPDM, tested at a strain rate of 10mm/min. Although at lower strains it is difficult to differentiate between samples the failure points for each sample can be seen where the load drops off.
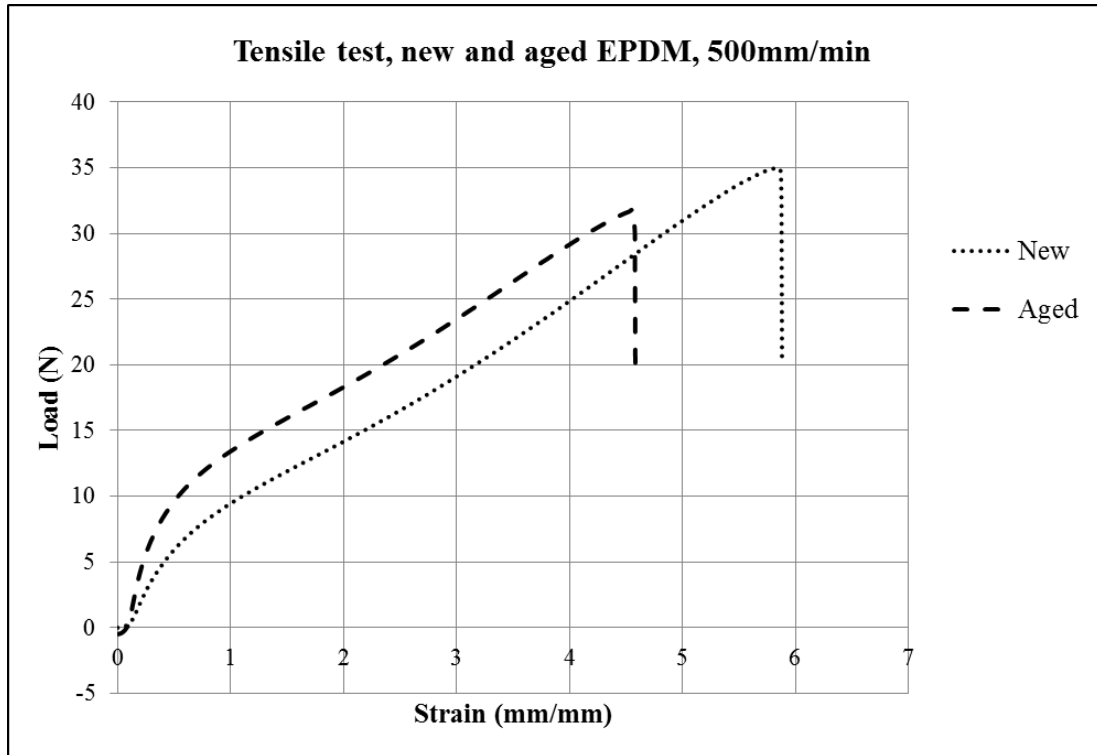
Figure 5.39: A typical new and aged load-strain plot example for ISO37. This plot shows the profile of 'Sample 5' for both new and aged samples of EPDM, tested at a strain rate of 500mm/min.

.

an aged sample of EPDM. The graph demonstrates two key points that were observed throughout the results comparing new and aged samples at all strain rates:

- The failure load is lower for the aged sample i.e. tensile strength of the aged sample is reduced.

- The strain at break is lower for the aged sample i.e. elongation at break of the aged sample is reduced.

To quantify these observations, the tensile strength and elongation at break of every sample was calculated according to the method detailed in Section 5.3.2.2, Page 255. The average was calculated for each condition and the results of all the valid samples are summarised in Figures 5.40 and 5.41. To account for the variance of each sample
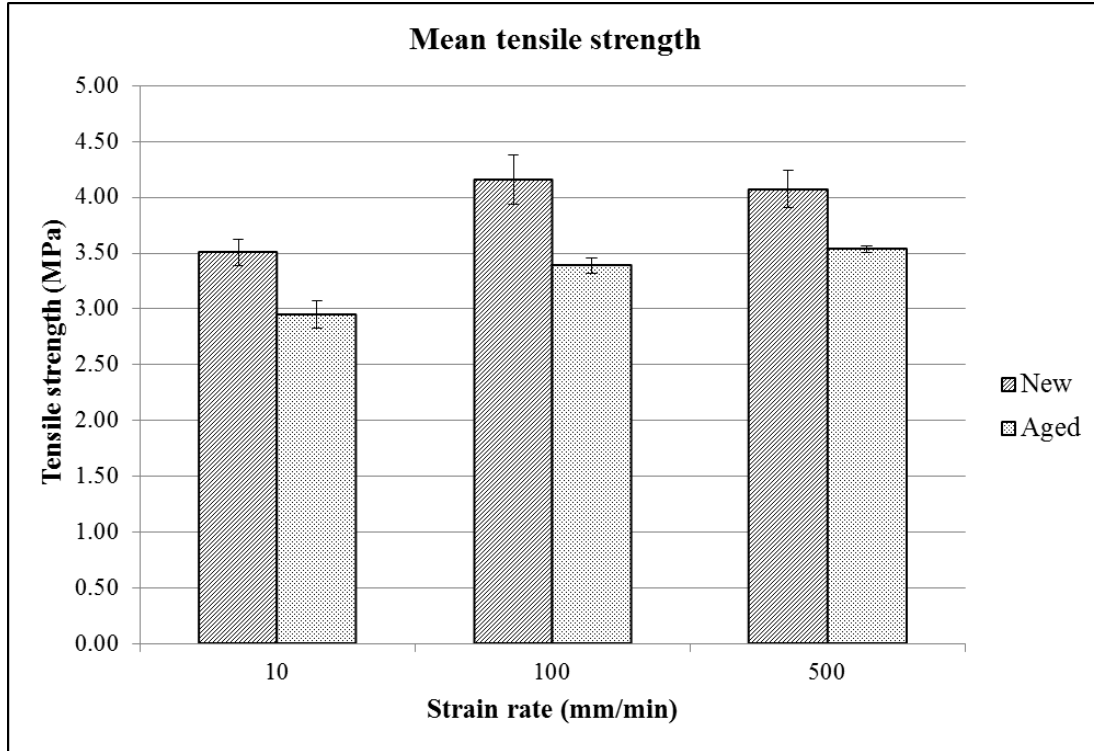
Figure 5.40: Tensile strength of new and aged 70.7 Shore A hardness EPDM samples. Error bars based on sample standard deviation.

.

from the calculated average, error bars have been plotted based on the sample standard deviation calculated for each condition. Sample standard deviation is calculated using:

$$SD = \sqrt{\frac{\Sigma(x - \bar{x})^2}{n - 1}} \tag{5.9}$$

Where:

SD = sample standard deviation

x = each value of the sample

$\bar{x}$ = mean of the sample values

n = number of samples

Reviewing Figure 5.40 which details the mean tensile strength of the samples, it is clear that ageing of the samples reduces the tensile strength. The tensile strength of the aged samples is reduced by 16%, 19% and 13% at strain rates of 10, 100 and
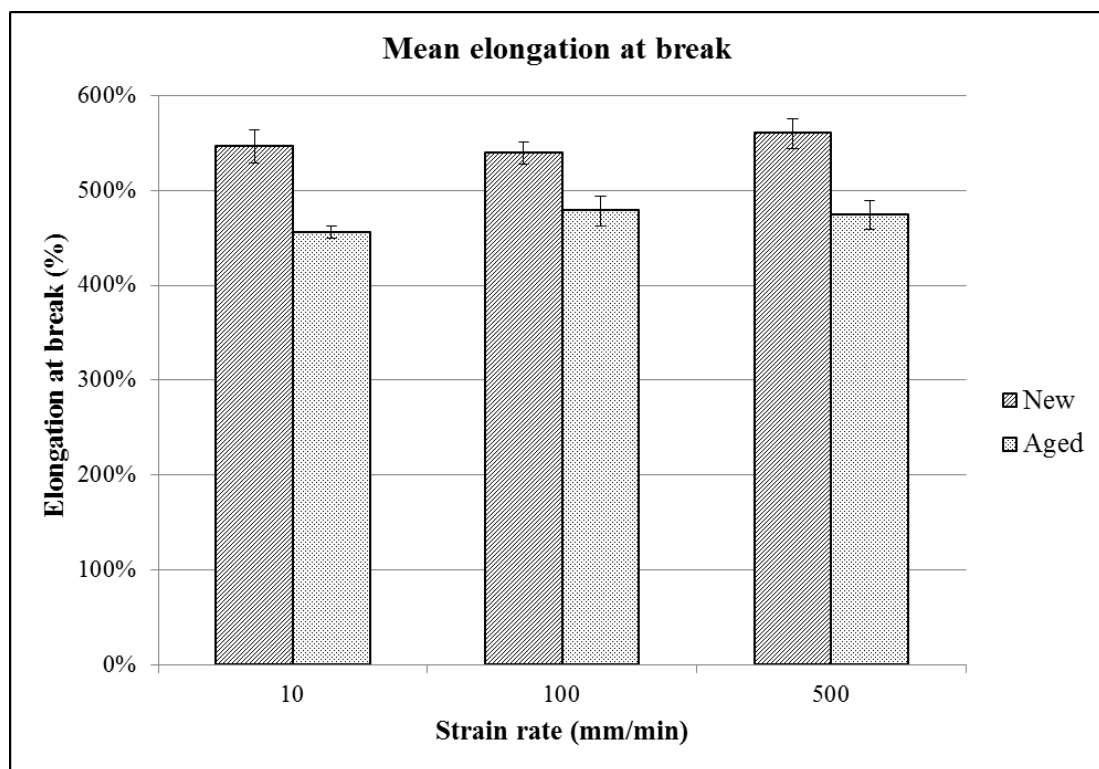
Figure 5.41: Elongation at break of new and aged 70.7 Shore A hardness EPDM samples. Error bars based on sample standard deviation.

.

500 mm/min respectively. This gives an average overall reduction in tensile strength of 16%.

The strain rate did appear to affect the tensile strength values. Reviewing new samples of EPDM, the lowest strain rate of 10mm/min resulted in 19% lower tensile strength than the equivalent test run with a strain rate of 100mm/min. In the aged samples, tensile strength was 15% lower when comparing strain rates of 10mm/min to 100mm/min. Despite this clear reduction in tensile strength when increasing the strain rate from 10mm/min to 100mmm/min, there is not an obvious difference between the results when further increasing the strain rate from 100 to 500 mm/min.

Regarding the results for mean elongation at break (Figure 5.41) again it is clear that the ageing process reduces the elongation at break of the samples. The elongation at break is reduced by 17%, 11% and 15% at strain rates of 10, 100 and 500 mm/min respectively. This gives an average overall reduction in elongation at break of 14%. The strain rate appears to have minimal affect on the elongation at break of the samples.

In addition to the above material properties, the affect of ageing on the Young's Modulus of EPDM can also be quantified. As previously mentioned, the Young's Modulus of a given polymer is not a static value and will vary with strain. To demonstrate how the Young's Modulus changes, Figure 5.42 details the Young's Modulus for new and aged EPDM at a strain rate of 500mm/min. The two samples detailed are Sample 5 from both the new and aged samples. Values of Young's Modulus below a strain of approximately 0.4 are not representative. At these low strains the sample is moving from a slack state to a taut state and the material properties are not being accurately measured so should be disregarded. The difference in Young's Modulus between new and aged samples is more pronounced at lower strains. Over a strain of 3 (or elongation of 300%) the Young's Modulus for both new and aged samples begins to stabilise at a value between 0.75-0.8MPa.

Average values for Young's Modulus were calculated at the three strain rates tested and at elongations of 100%, 200%, 300% and 400% for all tested samples. The data summarising these calculations is provided in Figure 5.43. Again, to demonstrate the spread within each data set the sample standard deviation was calculated and is shown in error bars on the chart.

Overall, ageing of the material seems to have a larger affect on Young's Modulus at lower strains. At an elongation of 100% aged samples have a 15% higher Young's
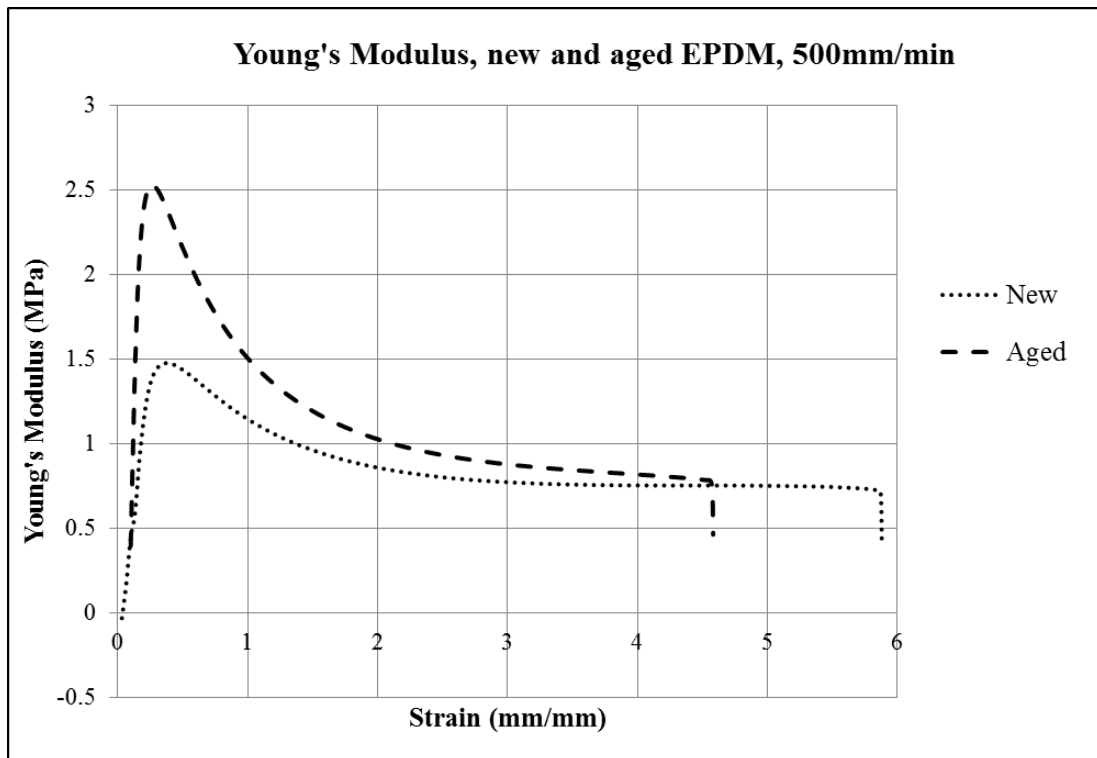
Figure 5.42: Young's Modulus for new and aged EPDM, tested at a strain rate of 500mm/min. Results detailed are from Sample 5 for both new and aged data sets. Values below a strain of 0.4 should be disregarded.

.
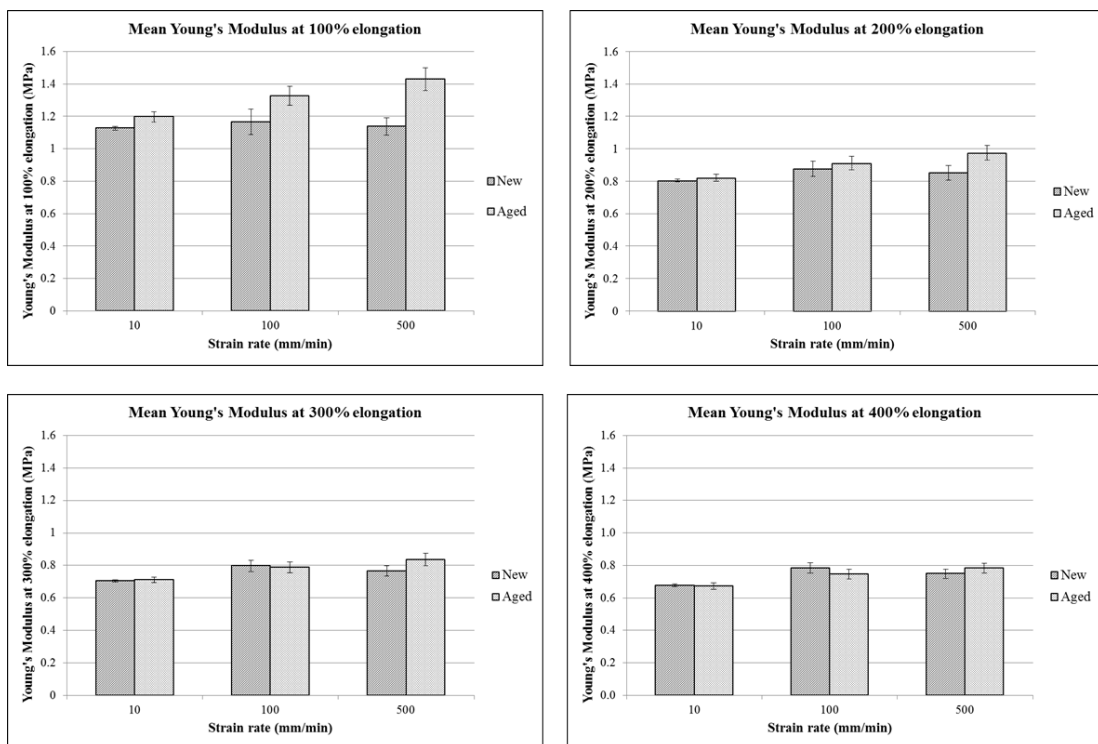
Figure 5.43: Average Young's Modulus for new and aged EPDM at different strain rates. Error bars are based on sample standard deviation.

Modulus than new EPDM. At an elongation of 200% the difference is less apparent
with aged samples having a 7% higher Young's Modulus on average. At elongations of
300% and 400% whether the material is new or aged appears to have little affect on
the value for Young's Modulus.

In addition, the strain rate appears to have a stronger affect on the aged EPDM,
with a higher strain rate producing a higher Young's Modulus value across all strains.
The strain rate however, does not appear to have an affect on the Young's Modulus
value calculated for the new samples. In addition, the increase in strain rate from
10mm/min to 100mm/min appears to increase the Young's Modulus calculated at all
strains for both new and aged polymers. However, a further increase in strain rate
from 100mm/min to 500mm/min appears to decrease the Young's Modulus in the new
samples and has a minimal increase in Young's Modulus for the aged samples.

Tensile fatigue tests

The next tensile tests to be presented aimed to review the tensile fatigue perfor-
mance of the 2mm sheet 70 Shore A EPDM polymer, as outlined in Method Section
5.3.2.2, Page 257.

To identify a suitable strain at which to conduct the full suite of tensile fatigue
tests, several trials were run with new EPDM samples subjected to fatigue cycles at
2Hz, whilst immersed in sea water. Initially a strain of 2.5 was trialled, but the samples
were found to fail too quickly at such a high strain. The strain was reduced to 2 and
then 1 in an attempt to obtain cycles to failure exceeding 10,000 to allow for valid
conclusions to be made. The results from these preliminary tests are detailed in Table
5.9.

Once it was established that fatigue testing at a strain of 1 (a displacement of 0-
25mm) provided a comprehensive set of results with the new samples of EPDM (95,291
cycles to failure on average) this test set up was repeated for aged EPDM. Again the
test was conducted at 2Hz and with the samples fully submerged in sea water. Table
5.10 details the results from this test, alongside the results for the new EPDM. The
sample standard deviation is also detailed in this table to demonstrate the spread of
results from the mean value.

Table 5.9: Fatigue cycles to failure, new 70 Shore A hardness EPDM, investigating different strains at 2Hz cycle frequency. (Sample position is location of failed sample counting from left to right, CTF = cycles to failure.)

Strain of 2.5 = 0-62.5mm		Strain of 2 = 0-50mm		Strain of 1 = 0-25mm	
Sample position	CTF	Sample position	CTF	Sample position	CTF
2	3225	5	4327	2	64300
7	3225	3	4870	1	73909
6	3405	1	5232	4	93430
5	3769	7	5414	7	95878
1	3950	2	5957	3	108543
4	4132	6	6682	6	108606
3	4312	4	7227	5	122370
Average	**3717**	**Average**	**5673**	**Average**	**95291**

It is immediately evident from Table 5.10 that the standard deviation of cycles to failure for the new EPDM samples is large in comparison to the aged samples. To aid visualisation of this data Figure 5.44 is included, which demonstrates the large distribution of failures for the new samples.

In addition to the large range observed for new samples, it is also clear from this figure that ageing in sea water significantly reduces the fatigue life of EPDM polymer. On average, the aged results survived just 18% of the cycles to failure achieved with the new EPDM samples.

5.4.2.3 Core bundle tests

As detailed in Section 5.3.2.3, Page 260 the intention of this section was to observe the localised deformation of polymer cords within the tether core bundle.

Results from tether assembly testing of P1-2* were used to measure the overall diametric compression of the tether before focusing on the scroll test which was used to measure the compression of individual cords. During assembly testing of tether P1-2*, at each increase in extension, six readings of tether diameter were taken, and the average result was calculated. Separate work by Parish measured the width of the rope wall under different loads and this was found to range from 6.6mm when unloaded to 1.7mm under a compressive load of 20kN. The average of these two values (4.15mm)

Table 5.10: Fatigue cycles to failure, new and aged EPDM, fatigue cycles at a strain of 1 and a frequency of 2Hz. (Sample position is location of failed sample counting from left to right, CTF = cycles to failure.)

New		Aged	
Sample position	**CTF**	**Sample position**	**CTF**
2	64300	7	13714
1	73909	4	14203
4	93430	5	14203
7	95878	6	14325
3	108543	3	17748
6	108606	1	21417
5	122370	2	22640
Average	**95291**	**Average**	**16893**
Standard deviation	**20444**	**Standard deviation**	**3773**
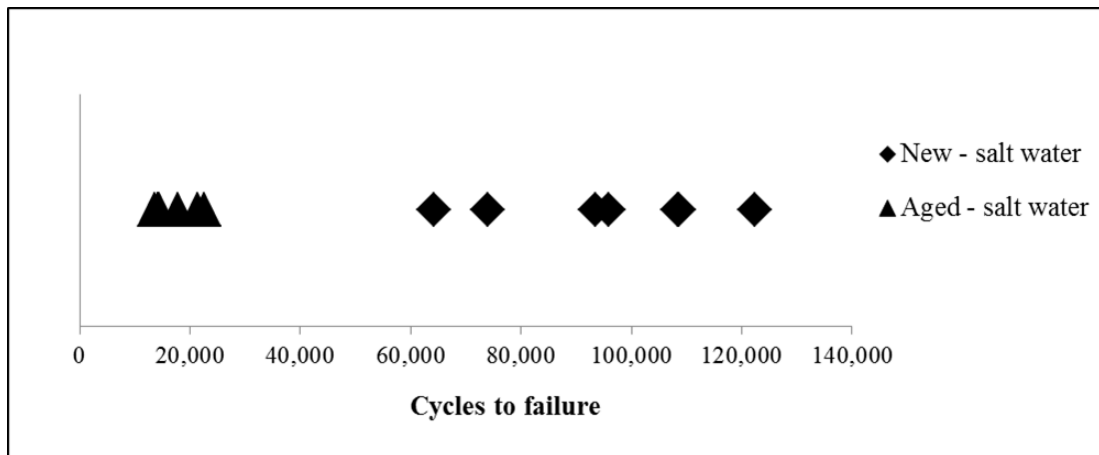
Figure 5.44: Cycles to failure for new and aged EPDM samples tested at a strain of 1 (0-25mm), 2Hz and fully submerged in sea water.
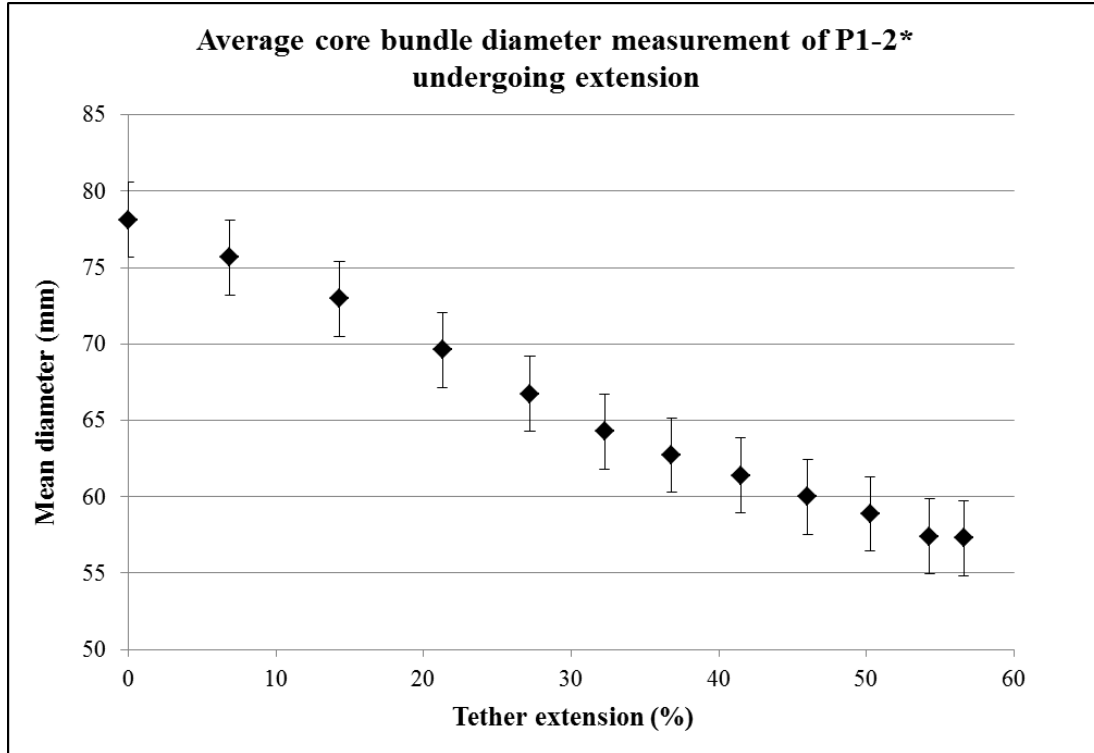
Figure 5.45: P1-2* core bundle diameter contraction whilst under extension. Result is average of 6 measurements and error bars indicate the range in rope wall thickness.

was deducted from the total diameter measurement and error bars have been used to account for the possible range in rope thickness. The final result is detailed in Figure 5.45.

During highly energetic wave conditions the tether could be assumed to operate with peak extensions of 30 - 40%. From results presented in Figure 5.45 a P1-2* tether extension of 36.8% has a corresponding core diametric compression of 20%. As discussed in Section 5.3, it could simply be assumed that this compression is evenly distributed across the core bundle, with each cord being subject to equal compressive strains of 0.2. However, this is likely to be a simplification and further analysis using the scroll test was required to investigate how this overall diametric strain is distributed within the core bundle.

A detailed analysis was conducted on the scroll test results for EPDM 54 Shore A hardness as this was the polymer used in tether P1-2* and as it is the softest polymer it exhibited the maximum strain in the load limited scroll test procedure. With reference
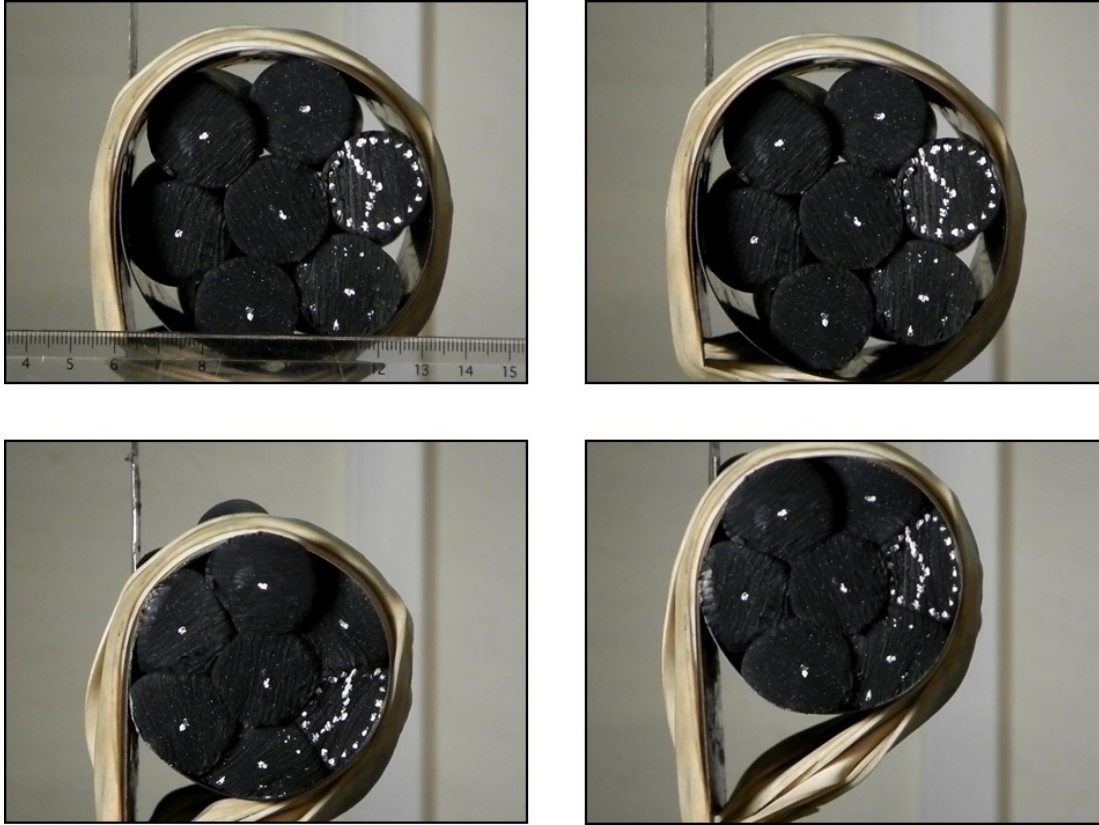
Figure 5.46: Images taken from Scroll Test 5_50_2 with the softest EPDM polymer, 54 Shore A hardness. Elastic bands used around the metal scroll to maintain tension in the system and hold the scroll in an optimum position. Clockwise from top left: Scale used to calibrate ImageJ software; un-loaded scroll; maximum load 4000N first cycle; maximum load 4000N fourth cycle.

to Table 5.6, Page 264, *Scroll test 5_50_2* achieved the highest load (4000N) and hence was used to quantify the deformation in the individual cords. Images taken from this test can be seen in Figure 5.46 which details four images from the test including the use of the scale to calibrate ImageJ software and images captured at different loading levels of Scroll Test 5_50_2.

To quantify the strain in each cord, a cord identifier was given to each cord in the bundle as detailed in Figure 5.47. For each test conducted the ImageJ software was calibrated using a scale such as the one detailed in the first image in Figure 5.46 (in this instance the calibration was 68.257 pixels = 10mm). Once the software had been
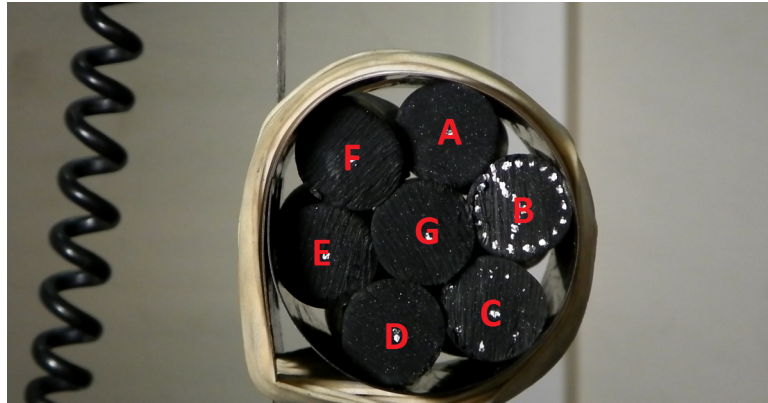
Figure 5.47: Identification of each cord in the core bundle for calculation of strain values.

calibrated, measurements were taken for the diameter of each cord in the bundle and for the total diameter of the bundle. For each distance required, 3 separate measurements were taken and an average calculated to maximise the accuracy of the final value. The diameter measurements for cords A-F were taken along the radius of the bundle, three separate distances of the central cord G diameter were measured, and the diameter of the complete core bundle was measured across A-D, B-E and C-F. Table 5.11 details the measurements taken .

In all cases except for cord F, the 4$^{\text{th}}$ cycle obtained the greatest compression of the cords, with the highest deformation recorded in cord B at 34%. These results clearly show that the strain value for the overall core bundle is not representative of what is happening to individual cords. Under the maximum 4000N load of cycle 4, the maximum overall core bundle compression was measured as 19% whilst at the same time, within that core bundle, the maximum individual cord compression was 34%. The individual cord strain is therefore up to 79% higher than the total core bundle strain.

Relating this data back to the tether assembly tests conducted in collaboration with Parish, we can see that at realistic working extensions of 30-40%, the tether core will see total diametric compression in excess of 20% (a strain of 0.2). Given the findings from the scroll test, it is likely that at these compression levels individual cords will be exceeding 35% compression (a compressive strain of 0.35). These findings are used to inform the compression tests.

Table 5.11: Measurements for Scroll Test 5_50_2, conducted with EPDM 54 Shore A at a peak load of 4000N.

Cord Identifier	Uncompressed				Compressed (cycle 1)					Compressed (cycle 4)				
	1	2	3	Mean	1	2	3	Mean	Strain	1	2	3	Mean	Strain
A	22.64	22.45	22.55	22.55	16.72	16.70	16.58	16.67	-0.26	16.29	16.44	16.70	16.48	-0.27
B	22.98	22.98	22.74	22.90	16.00	16.11	15.88	15.99	-0.30	15.10	15.21	15.27	15.19	-0.34
C	23.34	23.28	23.34	23.32	16.92	16.87	16.71	16.83	-0.28	15.61	15.90	15.92	15.81	-0.32
D	24.70	24.90	24.75	24.79	19.61	19.38	19.66	19.55	-0.21	18.89	19.13	19.10	19.04	-0.23
E	23.60	23.57	23.46	23.54	19.83	19.93	19.83	19.86	-0.16	19.75	19.84	19.72	19.77	-0.16
F	26.35	26.35	26.27	26.32	21.96	21.89	21.89	21.91	-0.17	22.96	22.80	22.87	22.87	-0.13
G (A-D)	23.83	23.52	23.76	23.70	23.04	22.94	22.89	22.96	-0.03	23.35	22.64	22.44	22.81	-0.04
G(B-E)	23.29	23.41	23.33	23.34	22.64	22.56	22.85	22.68	-0.03	22.52	22.36	22.41	22.43	-0.04
G (C-F)	23.26	23.26	23.15	23.22	20.57	20.56	20.43	20.52	-0.12	20.51	20.33	20.32	20.39	-0.12
Total core bundle diameters														
A-D	71.52	71.19	71.09	71.27	59.50	59.52	59.13	59.38	-0.17	58.88	58.92	58.63	58.81	-0.17
B-E	69.67	69.82	69.77	69.75	58.88	58.91	58.68	58.82	-0.16	57.53	57.80	57.75	57.70	-0.17
C-F	73.51	73.57	73.30	73.46	60.48	60.17	60.40	60.35	-0.18	59.35	59.84	59.35	59.51	-0.19

Table 5.12: ISO7743 valid results for calculation of compression modulus

Shore Hardness Value	Valid axial results	Valid radial results
54	1	2
59	2	2
70	3	2
70.7	3	2
80.7	3	2

5.4.2.4   Compression tests (25mm cord)

As described in the Methods Section 5.3.2.4, Page 262, the compression testing firstly established the compression stress-strain properties of the EPDM polymer core before assessing how these key properties are likely to evolve during tether operation. Results from this work are presented below.

ISO7743: Determination of compression stress-strain properties

As detailed in Section 5.3.2.4, Page 265, the ISO7743 procedure was repeated across the full range of polymers specified by Ley Rubber Ltd. As previously discussed, it should be emphasised that the tests conducted in the radial direction are not a standard material test and are affected by both the modulus and the geometry of the samples. These results are therefore not comparable to any other standard material test but are included here to understand how the behaviour of the polymer cord in this critical direction may change with ageing or compression cycles.

Three repeat tests were conducted for both the axial compression modulus and the radial compression modulus. In some cases there were difficulties with the test procedure and there are not three valid data sets for every sample. Table 5.12 details the number of valid test results for each polymer and test type.

The full test script for a typical ISO7743 test can be seen in Figure 5.48. The plot reveals the extent of the 'Mullins Effect' that is observed with this particular material. The Mullins Effect is observed in filled polymers and is characterised by the permanent softening of the stress-strain curve observed the first time a polymer is exposed to a compression or tension load (Cantournet *et al.*, 2009). This can be seen in Figure 5.48
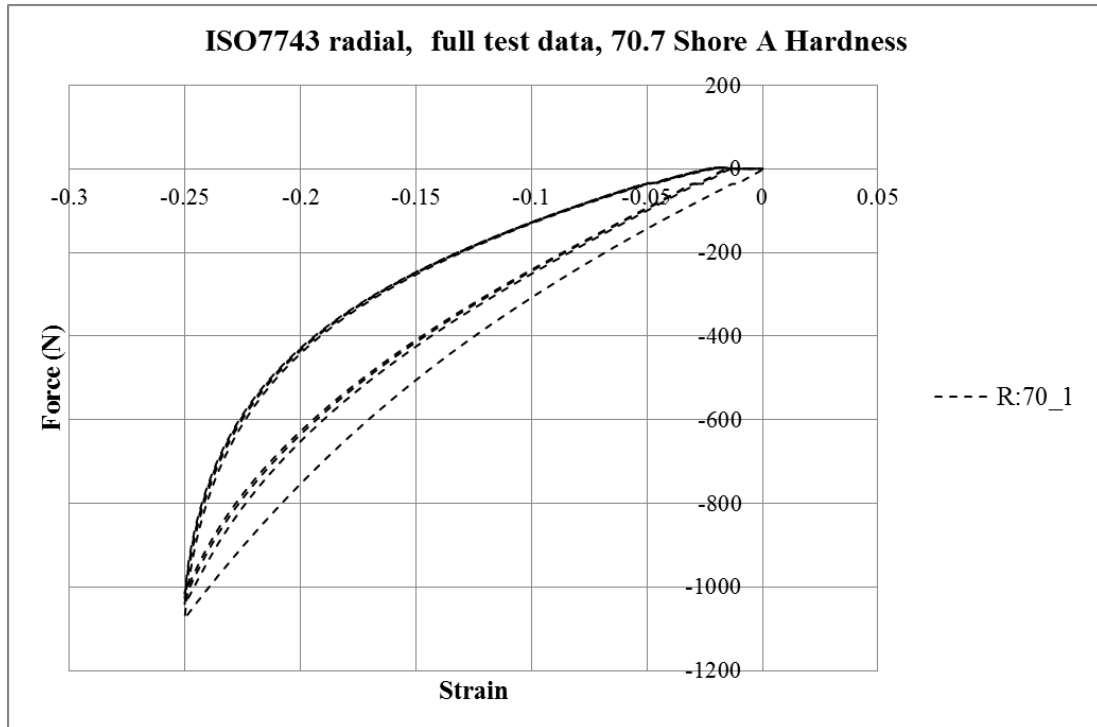
Figure 5.48: ISO7743 full data set for Sample 70_1 representing EPDM with 70.7 Shore A hardness, compressed radially.

where the first cycle to a strain of -0.25 requires greater loads than any subsequent cycles.

To calculate the compression modulus according to the guidance, the fourth cycle of each test script was extracted. Figure 5.49 details the fourth cycle for the two repeats of the ISO7743 radial tests for 70.7 Shore A hardness whilst Figure 5.50 details the fourth cycle for the three repeats of the axial tests. Good repeatability can be seen between the test repeats.

As discussed in Section 5.3 the compression modulus was calculated at both 0.1 and 0.2 strain using Equation 5.6, Page 265. The force at these strains was taken from the data (as detailed in Figure 5.51) and used to calculate compression modulus. It should also be noted that the strain was determined from the point at which the curve of the last cycle meets the strain axis (where Force = 0N) e.g. not absolute strain. In some cases it was difficult to determine the point at which the curve of the last cycle meets the strain axis as detailed in the Figure 5.52, Page 323 taken from the Radial 70_1 test.
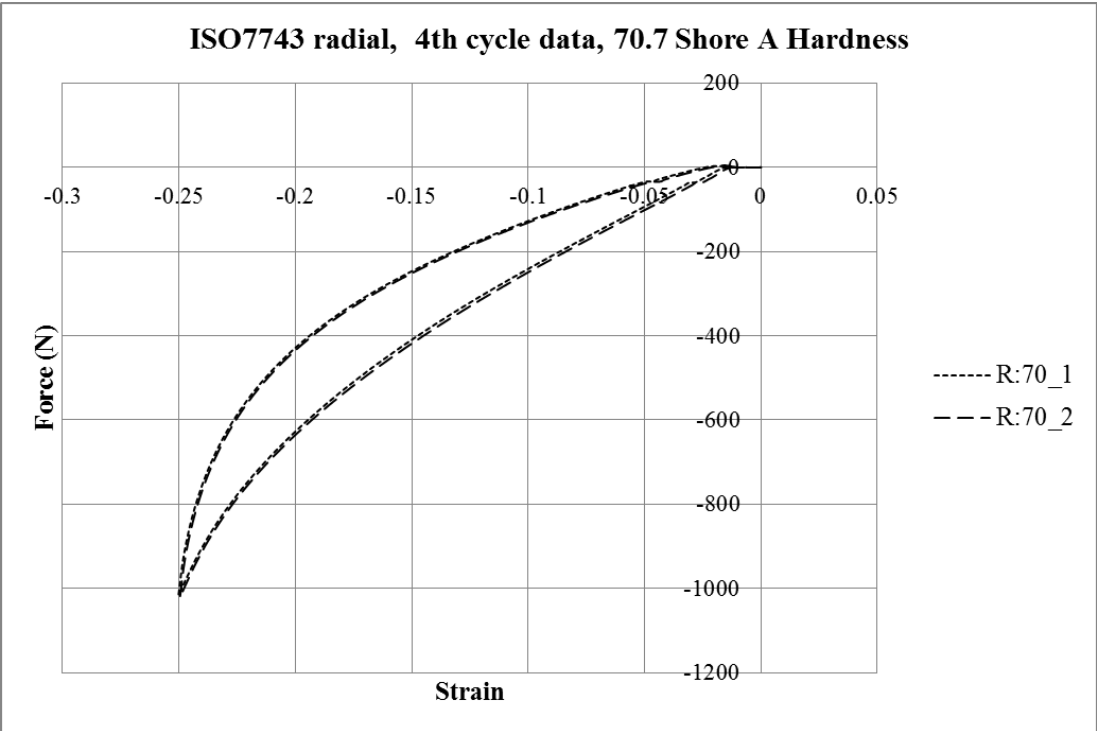
Figure 5.49: ISO7743 4th cycle extracted for Samples 70_1 and 70_2, representing EPDM with 70.7 Shore A hardness, compressed radially.
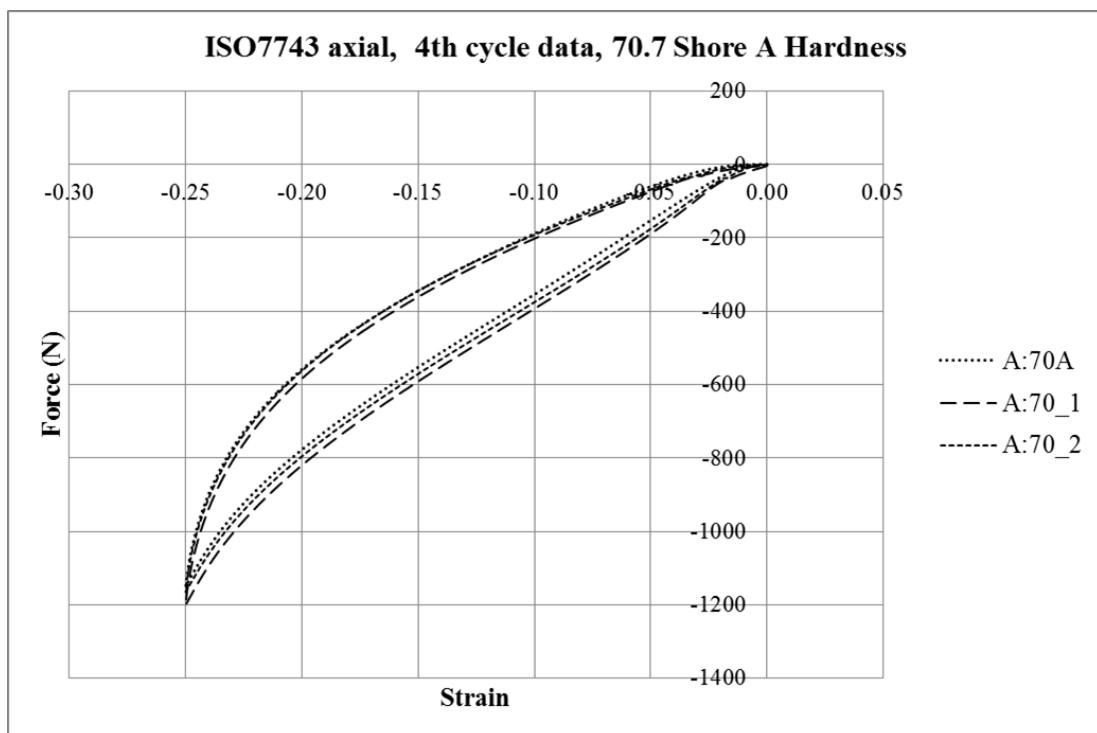
Figure 5.50: ISO7743 4$^{\text{th}}$ cycle extracted for Samples 70_A, 70_1 and 70_2, representing EPDM with 70.7 Shore A hardness, compressed axially.
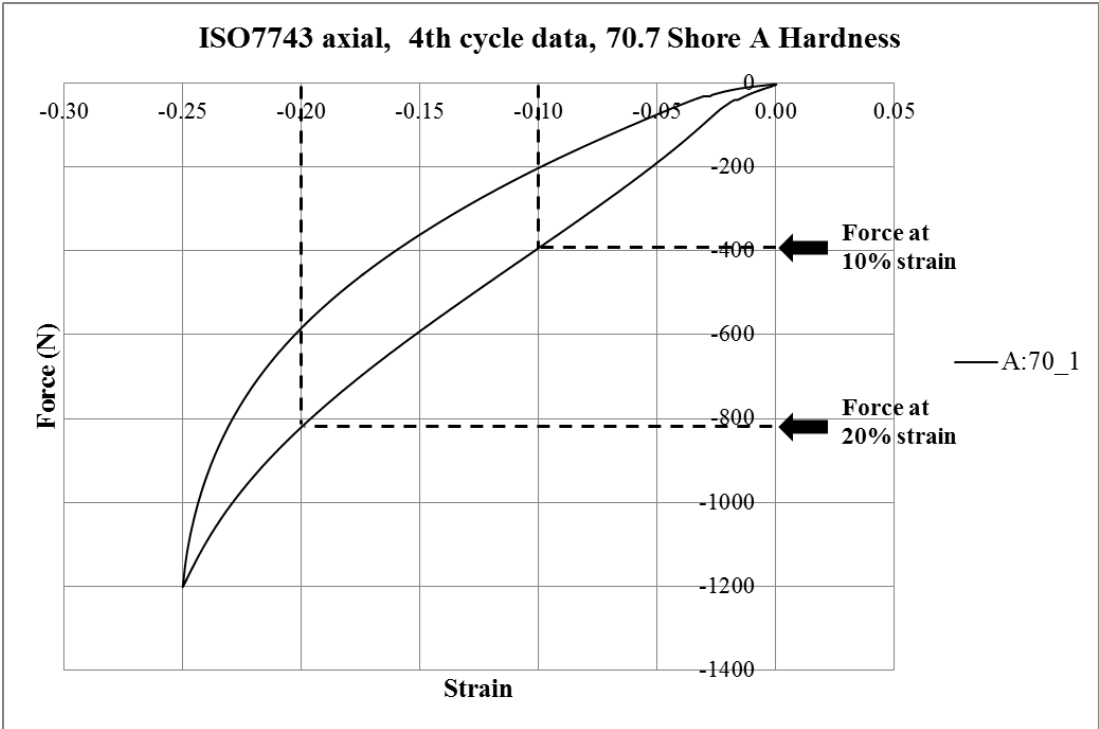
Figure 5.51: ISO7743 4$^{\text{th}}$ cycle extracted for Sample 70_1, representing EPDM with 70.7 Shore A hardness, compressed axially. Relative strains of 0.1 and 0.2 identified for use in calculation of Compression Modulus values.

The curve oscillates around the strain axis, going into positive and negative force. For consistency in all calculations, this relative 0 strain point was identified as the point following the last negative force value recorded. Where the figure oscillates just above the strain axis, the value was taken where the data starts a consistent climb, rather than continuing to float. Once the relative 0 strain point was established, 0.1 strain and 0.2 strain were identified as the relative 0 strain point plus 0.1 or 0.2 respectively. Linear interpolation was then used between the recorded values to calculate the force at the required strain value.

The calculation of compression modulus is detailed, continuing the example presented in Figure 5.52 from sample R:70_1. As this example is from a **radial** ISO7743 test, the calculated result is Radial Compression Modulus (RCM):

- Relative 0 strain (identified at $0N$) $= -0.014$

- Relative 0.1 strain (calculated by $-0.014 - 0.1$) $= -0.114$

- Linear interpolation used to calculate force at a strain of $-0.114 = -285.57N$

- RCM at 0.1 strain calculated using Equation 5.6: $E_{C,0.1} = \frac{\sigma_{0.1}}{\varepsilon_{0.1}} = \frac{Force_{0.1}}{\varepsilon_{0.1} \times A}$

- Original area calculated based on mean of three measurements taken for diameter and height of test cylinder $= 875.44mm^2$

- RCM at 0.1 strain therefore $= \frac{-285.57}{0.114 \times 875.44} = 2.858 MPa$

- The same approach was used to calculate the RCM at 0.2 strain giving $3.769 MPa$

The Axial Compression Modulus (ACM) was calculated from the axial ISO7743 tests in exactly the same way as the RCM except that the area calculation was updated to reflect the cross sectional area of the sample being perpendicular to the area used in the RCM calculation. The RCM and ACM were calculated for every sample, and where applicable, the mean and standard deviation of the samples from each EPDM specification was calculated. Tables 5.13 and 5.14 detail the results for ACM and RCM respectively. To visualise this data and the affect of the EPDM hardness on the compression modulus of the material Figure 5.53 is included.

As expected, this data confirms that the hardness value of the specified polymer has an effect on the Compression Modulus of the material, with a higher polymer hardness
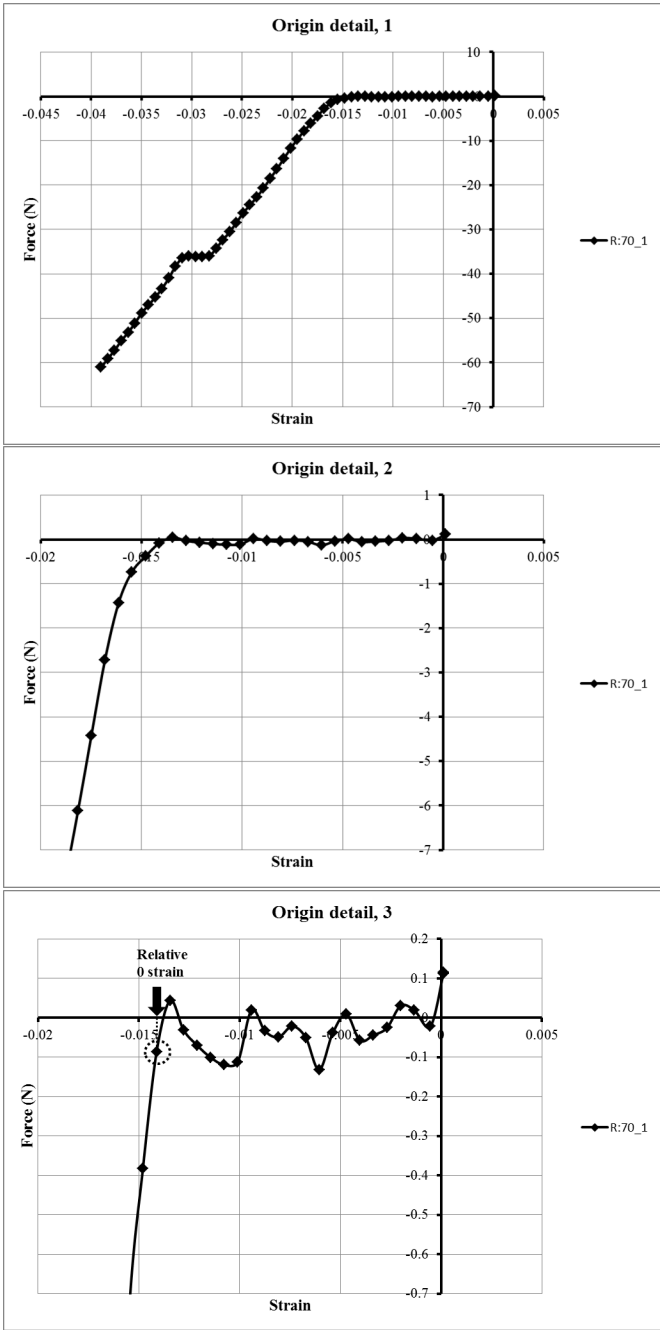
Figure 5.52: ISO7743 determination of relative 0 strain point using example data from R:70_1, representing EPDM with 70.7 Shore A hardness, compressed radially. Strain is oscillating about the x-axis, relative 0 strain point identified as the data point following the last negative force value recorded (as circled, representing an absolute strain of -0.0141 and a force of -0.0861N).

resulting in higher axial and compression modulus values. A higher compression modulus essentially means that the material demonstrates a higher resistance to compression. As the compression of the polymer core is key to the operation of the tether this range of compression modulus values is likely to be a dominant factor in the range of tether stiffness values observed in the Proof of Concept study (Presented in the Literature Review, Section 2.6.4, Page 122).

Once a baseline value for the compression modulus of each of the specified polymers was established, the main durability consideration was how this key material property may change during tether operation. The results of marine ageing and compression fatigue on the compression modulus of the polymer are presented in the following sections.

Aged polymer compression tests

The method for this work was detailed in Section 5.3.2.4, Page 268. Following ageing in renewed natural sea water, heated to a temperature of 60°C for a period approaching 13 months, samples of Ø25mm round section of 70.7 Shore A hardness EPDM were subject to ISO 7743 testing. The results of these tests were used to calculate the Axial and Radial Compression Modulus of the samples at strain values of 0.1 and 0.2.

Three results were taken for each sample type, and can be seen in Table 5.15. These results can be compared directly to the results conducted on the new samples of 70.7 Shore A hardness EPDM polymer. Figure 5.54 compares the average values for the new and aged polymer samples alongside one another. It is clear that the marine ageing of the polymer increases the compression modulus of the polymer with results from the axial and radial tests across both strain values 0.1 and 0.2 showing a marked increase. Taking the average across both strains, the Axial Compression Modulus is increased by 15% and the Radial Compression Modulus is increased by 22%. This effectively means that marine ageing increases the material's resistance to compression.

Compression fatigue

Cord samples of EPDM polymer 70.7 Shore A Hardness were exposed to repeated compression cycles as detailed in Method Section 5.3.2.4, Page 268. Due to the long

Table 5.13: Axial compression modulus results for the range of EPDM polymers tested. Strike through used to identify where a test was conducted but results were not valid and therefore not used in calculations.

	Specified hardness	Actual hardness	Test name	CM @ 0.1	CM @ 0.2
AXIAL COMPRESSION MODULUS	50	54	50_A axial (July)	2.6487	3.5308
			50_1 axial (Sep)		
			50_2 axial (Sep)		
			Average axial	*2.6487*	*3.5308*
			STDEV.S	*n/a*	*n/a*
	60	59	60_A axial (July)		
			60_1 axial (Sep)	4.1949	4.6373
			60_2 axial (Sep)	4.6078	4.9012
			Average axial	*4.4014*	*4.7692*
			STDEV.S	*0.2919*	*0.1866*
	70	70.7	70_A axial (July)	7.3401	8.0643
			70_1 axial (Sep)	8.1383	8.4944
			70_2 axial (Sep)	7.7377	8.2016
			Average axial	*7.7387*	*8.2534*
			STDEV.S	*0.3991*	*0.2197*
	80	70	80_A axial (July)	4.8111	5.6563
			80_1 axial (Sep)	5.8103	5.9674
			80_2 axial (Sep)	5.3685	5.7048
			Average axial	*5.3299*	*5.7762*
			STDEV.S	*0.5007*	*0.1673*
	90	80.7	90_A axial (July)	11.0776	11.6020
			90_1 axial (Sep)	11.1930	11.6847
			90_2 axial (Sep)	10.5418	11.2367
			Average axial	*10.9375*	*11.5078*
			STDEV.S	*0.3474*	*0.2384*

Table 5.14: Radial compression modulus results for the range of EPDM polymers tested. Strike through used to identify where a test was conducted but results were not valid and therefore not used in calculations.

	Specified hardness	Actual hardness	Test name	CM @ 0.1	CM @ 0.2
RADIAL COMPRESSION MODULUS	**50**	**54**	50_C radial (July)		
			50_1 radial (Sep)	1.3832	1.8191
			50_2 radial (Sep)	1.3450	1.7376
			Average radial	*1.3641*	*1.7783*
			STDEV.S	*0.0270*	*0.0576*
	60	**59**	60_C radial (July)		
			60_1 radial (Sep)	1.5472	1.9905
			60_2 radial (Sep)	1.5102	1.9623
			Average radial	*1.5287*	*1.9764*
			STDEV.S	*0.0262*	*0.0199*
	70	**70.7**	70_C radial (July)		
			70_1 radial (Sep)	2.8584	3.7691
			70_2 radial (Sep)	2.9916	3.8629
			Average radial	*2.9250*	*3.8160*
			STDEV.S	*0.0942*	*0.0663*
	80	**70**	80_C radial (July)		
			80_1 radial (Sep)	2.2561	2.9276
			80_2 radial (Sep)	2.1913	2.8462
			Average radial	*2.2237*	*2.8869*
			STDEV.S	*0.0458*	*0.0576*
	90	**80.7**	90_C radial (July)		
			90_1 radial (Sep)	4.3179	5.7299
			90_2 radial (Sep)	4.1601	5.5225
			Average radial	*4.2390*	*5.6262*
			STDEV.S	*0.1116*	*0.1467*
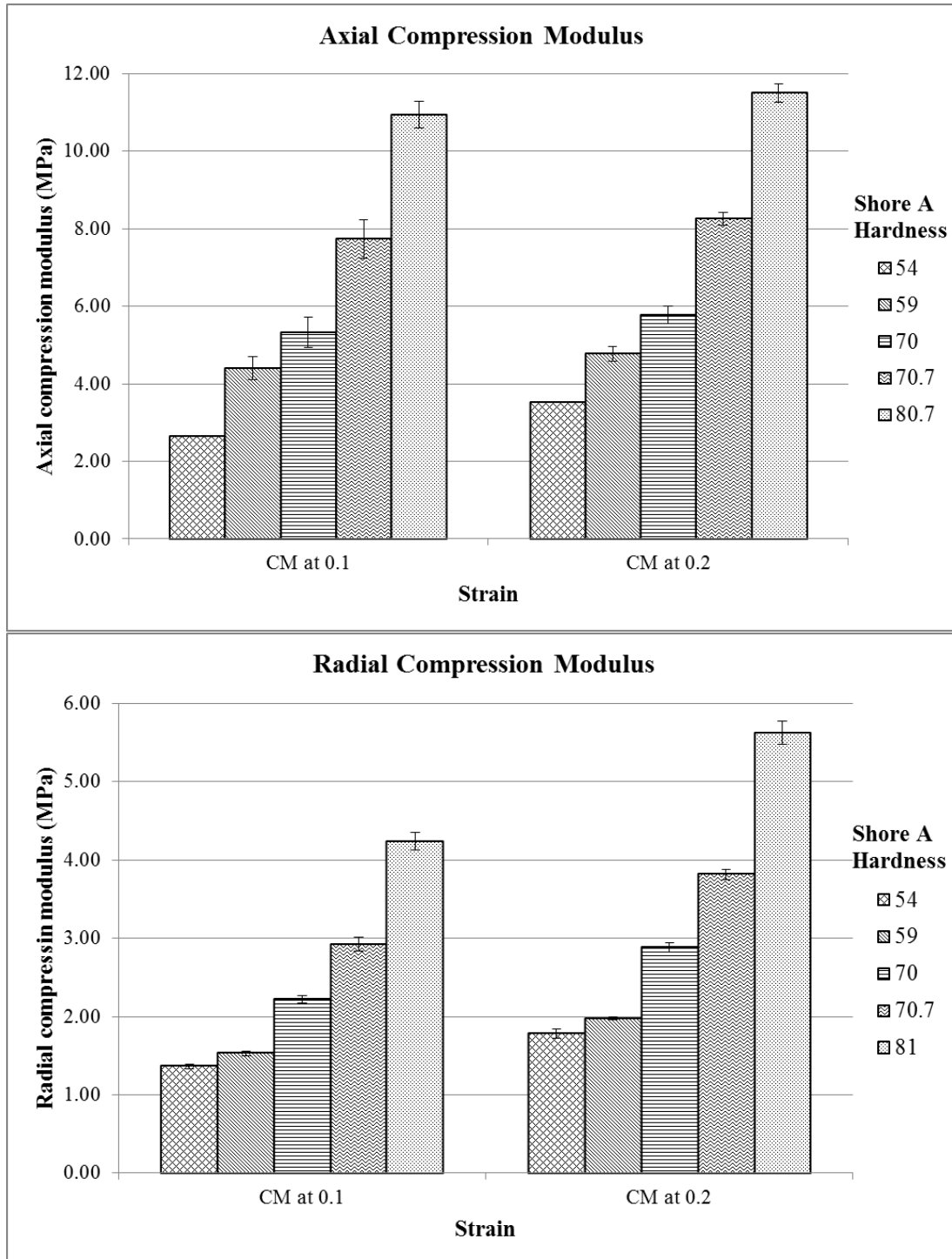
Figure 5.53: Compression Modulus of EPDM polymer, mean results plotted against Shore A hardness values. Error bars based on sample standard deviation.

Table 5.15: Compression Modulus results for EPDM 70.7 Shore A hardness polymer, aged in renewed natural sea water at 60°C for 9377.5 hours.

	Specified hardness	Actual hardness	Test name	CM @ 0.1	CM @ 0.2
COMPRESSION MODULUS AGED EPDM POLYMER	**70**	**70.7**	Axial 1	8.6076	9.3765
			Axial 2	9.0264	9.7393
			Axial 3	8.8185	9.6473
			Average axial	*8.8175*	*9.5877*
			STDEV.S	*0.2094*	*0.1886*
			Radial 2	3.7983	4.7867
			Radial 3	3.2439	4.4274
			Radial 4	3.6959	4.7425
			Average radial	*3.5793*	*4.6522*
			STDEV.S	*0.2950*	*0.1959*
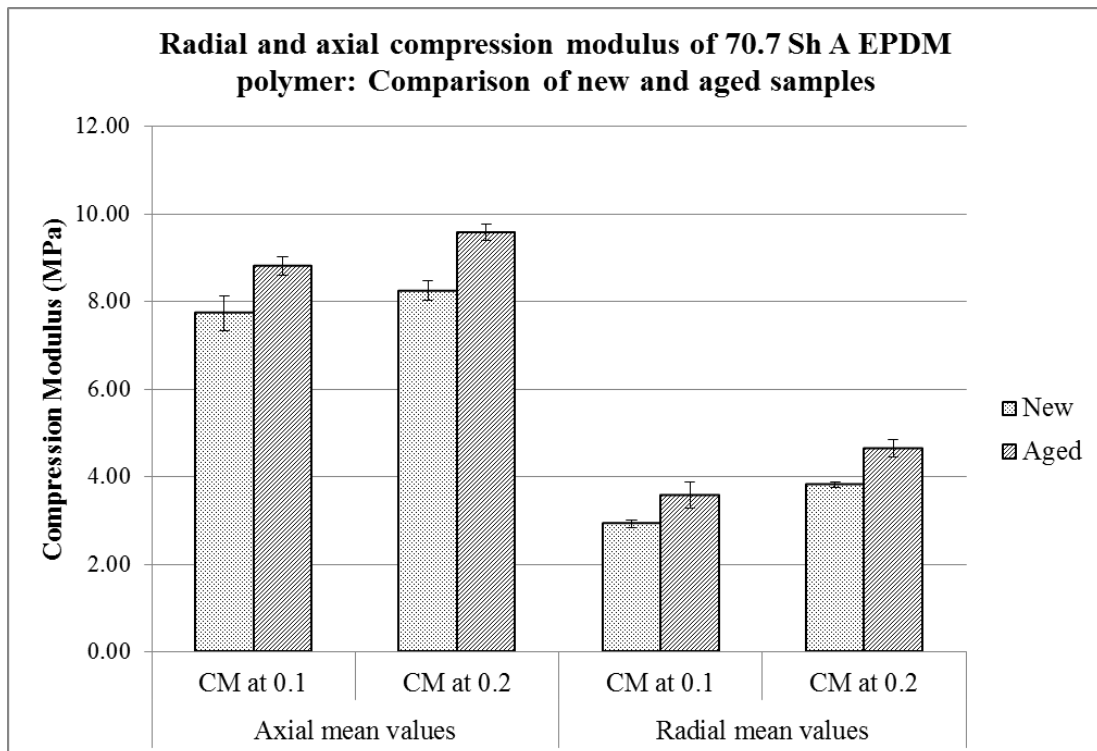
Figure 5.54: Average results for Compression Modulus of new and aged EPDM 70.7 Shore A hardness Polymer. Error bars are based on sample standard deviation.

Table 5.16: Compression fatigue testing of Ø25mm 70.7 Shore A hardness EPDM Polymer. *Indicates a machine fault during Radial_40_1 testing resulted in the polymer sample being held under compression for 1h20 in the middle of the testing period.

Test Name	Specified Strain	Cycle No.	Frequency	Notes
Radial_20_1	0.20	707,000	2Hz	ISO 7743 conducted at 0h12, 17h55, 42h20 and 66h20 following fatigue testing.
Radial_30_1	0.30	129,732	2Hz	ISO 7743 conducted at 0h12, following fatigue testing.
Radial_40_1	0.40	279,633	2Hz	ISO 7743 conducted at 0h12, 24h15 and 48h15 following fatigue testing.*
Radial_40_2	0.40	172,600	2Hz	ISO 7743 conducted at 0h12 and 23h45 following fatigue testing.

term nature of these tests, only limited data sets could be collected. Technical issues regarding the reliability of the test equipment resulted in limited control of the test length, which in some cases was terminated prematurely. In addition, some tests paused during a compression cycle for an extended period of time which limits the validity of the results.

These technical issues have led to a limited set of data, with no possibility of identically repeating tests; firm conclusions cannot be drawn from such a data set. The data can however provide an indication of potential patterns, and highlight any areas that require further investigation to progress the development of the Exeter Tether. Although not providing firm conclusions, this early analysis does add value to the project and is therefore reported here as a starting point for further investigation.

Table 5.16 indicates the tests completed as part of this investigation. Due to time limitations, the number of ISO 7743 tests conducted following the compression fatigue testing varies for each sample. The total number of ISO 7743 tests conducted and the time delay is detailed in the notes of the table.

Radial_20_1 stands out as having an extremely high cycle number, and the most comprehensive set of ISO 7743 test repeats. It is therefore the focus for analysis from this data set. Figure 5.55 details results from these tests, with the average of two control samples of new EPDM 70.7 Shore A hardness for comparison.
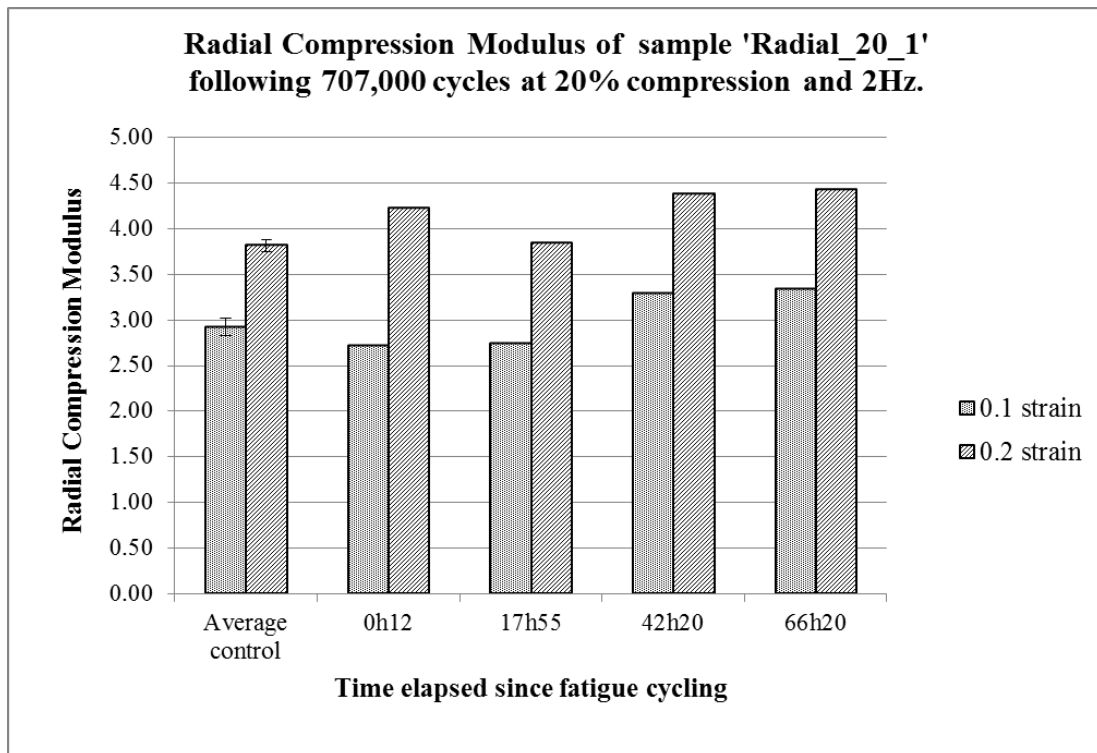
Figure 5.55: Radial Compression Modulus values calculated using ISO7743 at various intervals following compression fatigue cycling of a 70.7 Shore A hardness sample of EPDM for 707,000 cycles at 20% compression and a frequency of 2Hz. Error bars of control sample based on sample standard deviation.

It is clear from these results that the immediate Radial Compression Modulus (RCM) of the sample measured 12 minutes following the compression cycles, does not reflect the longer term RCM once the sample has had time to recover. At the 12 minute point, there does not seem to be a consistent change for the RCM measured at 0.1 and 0.2 strain; at a strain of 0.1 RCM is 7% less than the control sample, whilst at a strain of 0.2 it is 11% higher. Over time this difference levels out and at 42h20 after the compression cycling the RCM is 13% and 15% higher than the average control at strains of 0.1 and 0.2 respectively. ISO 7743 is finally repeated 66h20 after the compression cycling, and provides RCM values 14% and 16% higher than the average control at strains of 0.1 and 0.2 respectively.

The overall effect of repeated compression cycles of 0.2 strain and a frequency of 2Hz is to increase the RCM of the polymer, with an average long term increase of 15%. This means an increased material resistance to compression, and ultimately, a stiffer tether response.

The other data sets detailed in Table 5.16 are not as comprehensive as Radial_20_1 discussed above. Not only are the samples exposed to fewer compression cycles, but there are less ISO 7743 tests conducted following the compression testing to record any evolution in RCM as the material recovers. However an overview of the data sets will allow any patterns to be identified, Figure 5.56 details three graphs summarising the results from these tests.

The results for Radial_30_1 (0.3 strain for 129,732 cycles) show limited impact from the compression cycling, with RCM at a strain of 0.1 being 4% higher than the average control (and within the error bars of the control samples) and RCM at 0.2 strain virtually identical. This could be related to the relatively low cycle number at 129,732 cycles, which may have not been enough to induce any damage into the sample.

The results for Radial_40_1 should be treated with caution as during the compression cycles a machine error resulted in the sample being held in compression for 1h20, which could have a significant affect on the results. Due to this error, the absolute values should be regarded with caution, however it is interesting to note the change in RCM as the sample recovers reflects the change observed in the Radial_20_1 test. Immediately following the compression cycles the RCM is noticeably reduced by 15% and 13% in comparison to the control for strains of 0.1 and 0.2 respectively. The RCM increases with time and appears to be stable 24h after the compression tests. The final values at
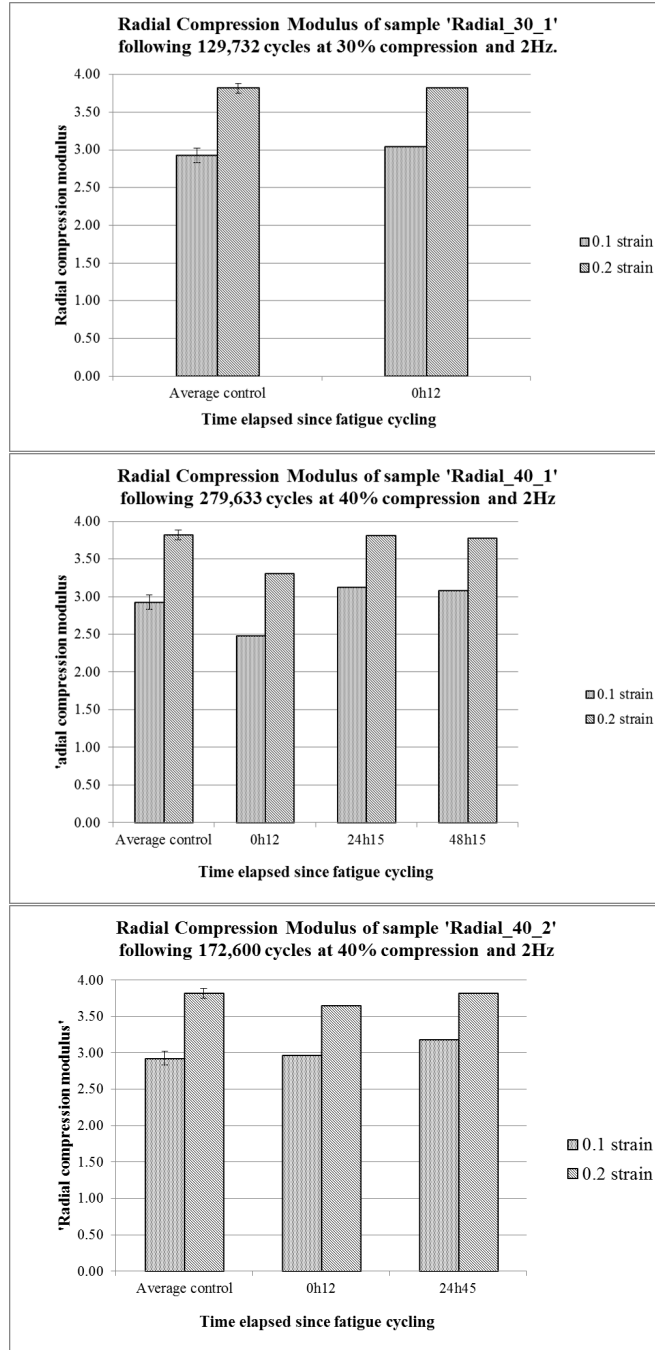
Figure 5.56: Radial Compression Modulus values calculated using ISO7743 at various intervals following compression fatigue cycling on 70.7 Shore A hardness EPDM polymer. Error bars of control sample detailed in each graph based on sample standard deviation.

48h show a RCM 5% higher than the control at a strain of 0.1 and virtually identical to the control at a strain of 0.2.

Finally, the results for Radial_40_2 show limited change in RCM immediately after the compression cycles (1% increase and 4% reduction in relation to the control at strains of 0.1 and 0.2 respectively). As has been documented before, when the sample recovers an increase in RCM is observed. This is particularly noticeable for the RCM measured at a strain of 0.1 which increases to 9% higher than the control over a 24h period. The RCM at a strain of 0.2 at this time has increased and is equal to the RCM of the control sample.

Although this data has limitations, a consistent observation throughout the analysis is the increase in RCM as the sample recovers from the fatigue testing. This is observed across the data sets for RCM calculated both at a strain of 0.1 and 0.2. The sample exposed to the highest cycle numbers (Radial_20_1) certainly suggests a long term increase in RCM at both strains. This finding is supported for RCM calculated at 0.1 strain for both Radial_40_1 and Radial_40_2, which show a long term increase of 5% and 9% respectively. The change in RCM at a strain of 0.2 is however less apparent in these samples.

Cord compression fatigue with thermal investigation

To review the heat generated from the EPDM cord samples during fatigue compression testing, thermal imaging was used to monitor a selection of compression tests as detailed in Method Section 5.3.2.4, Page 269. A series of tests at a fixed compression strain of 0.2 were conducted, gradually increasing the frequency of cycles through 0.01Hz, 0.1Hz, 0.5Hz, 1Hz, 2Hz, 3Hz and 5Hz. During this set of tests, the test machine was struggling to reach the full 20% compression when operating at the higher frequencies (3Hz and 5Hz). Example images taken with the thermal camera are detailed in Figure 5.57.

It should be noted at lower frequencies the platen exercising the sample had an elevated temperature which slightly heated the top of the polymer sample. This should not be confused with the sample heating up due to self heating, which is clear at higher frequencies and greater strains when the maximum heat occurs at the centre of the sample. The temperature reading was always taken at the centre of the sample
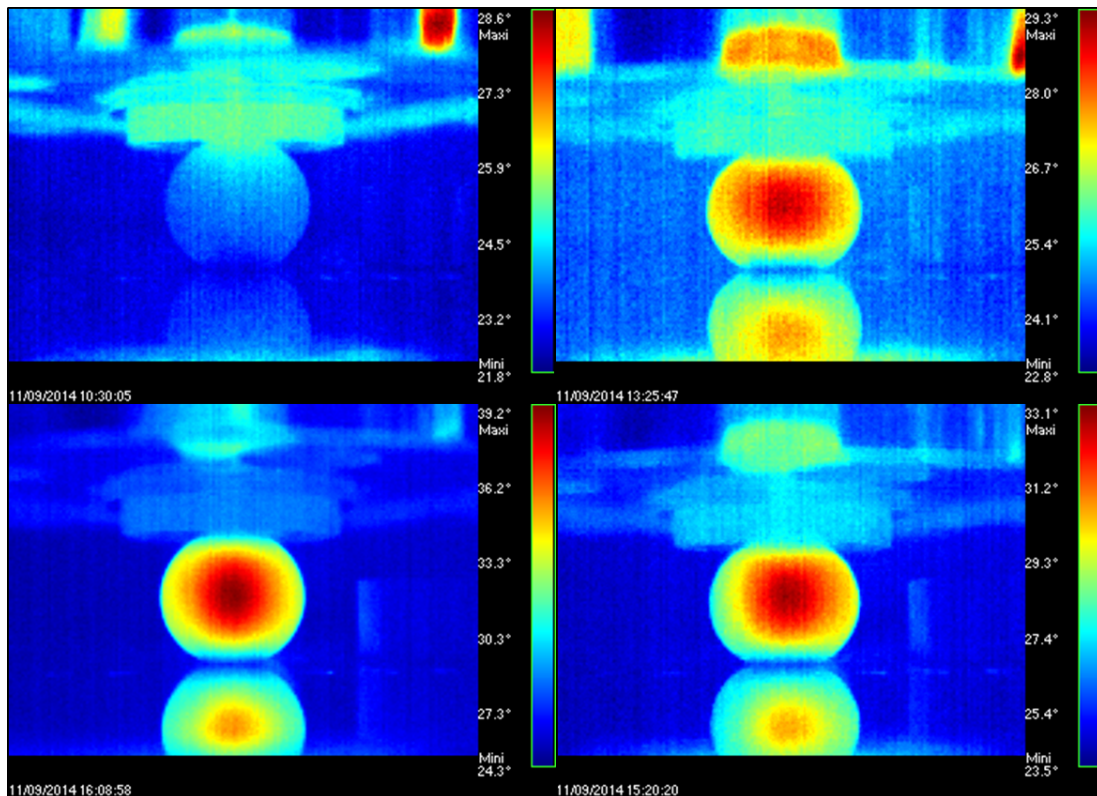
Figure 5.57: Thermal image stills from frequency investigation conducted on 70.7 Shore A hardness, EPDM polymer. Clockwise from top left: Start of test procedure at a frequency 0.1Hz; stabilised temperature at 1Hz; stabilised temperature at 2Hz; stabilised temperature at 5Hz.

**Effect of frequency on self heating of 70.7 Sh A EPDM Polymer
(Fixed compressive strain: 0.2)**
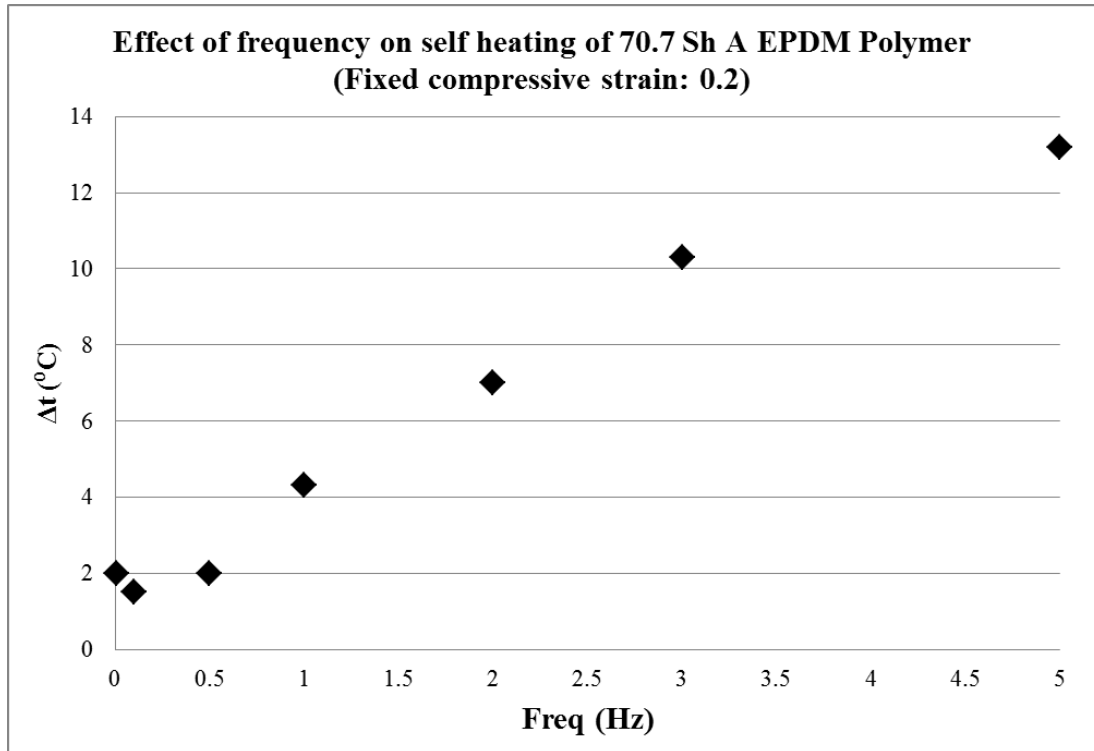
Figure 5.58: Temperature difference between test sample and control sample during compression testing of 70.7 Shore A hardness EPDM polymer at a fixed compressive strain of 0.2 with increasing frequency.

to ensure the heat from the platen did not affect the results. In addition, at higher frequencies the edge of the control sample can be seen to be heating slightly due to the heat generated from the test sample. Again in this case, the temperature measurement of the control sample was taken from the centre of the sample.

At each increase in cycle frequency the thermal images were reviewed and the maximum observed temperature difference between the control sample and the test sample was recorded. A graph detailing these results is included in Figure 5.58. Minimal self heating is observed at frequencies up to 0.5Hz. From a frequency of 1Hz and up self heating is evident, with a test frequency of 2Hz (as used for the Compression Fatigue testing) generating a temperature difference of approximately 7°C.

The second test series maintained a fixed testing frequency, whilst gradually increasing the compressive strain through 0.2, 0.3, 0.4 and 0.5. During this test range the test machine was not able to meet the full displacement stroke required for the

335
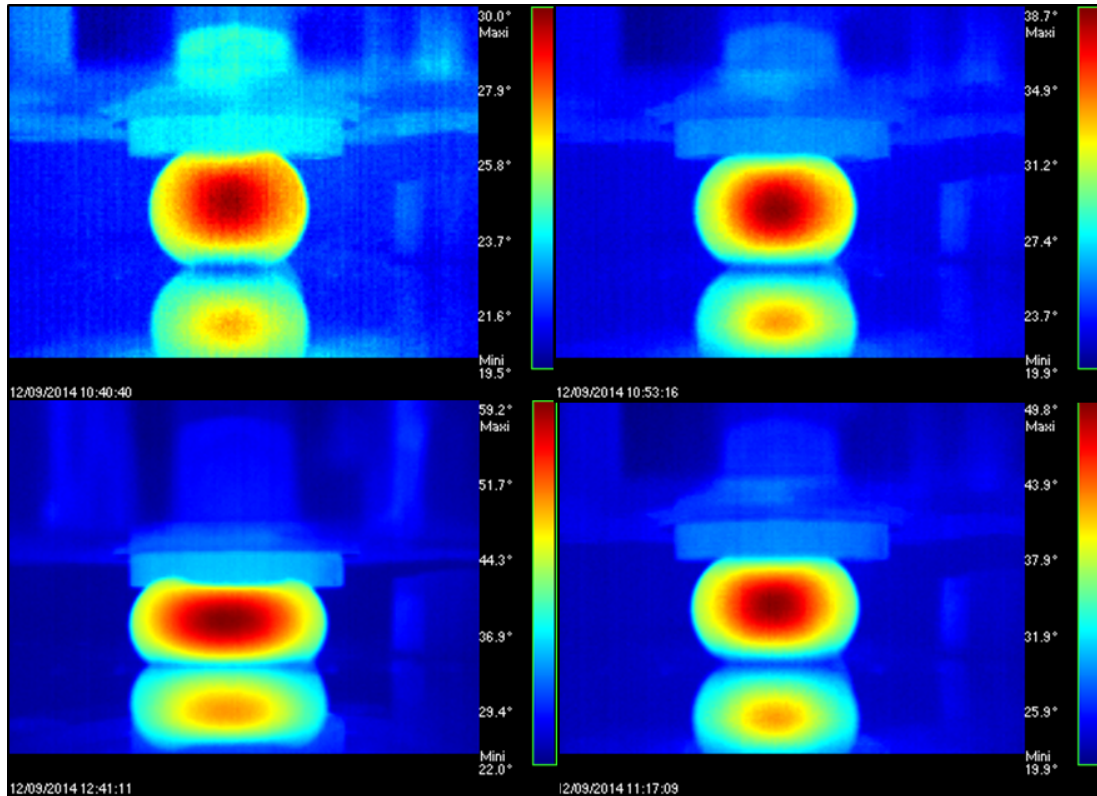
Figure 5.59: Thermal image stills from strain investigation conducted on 70.7 Shore hardness A, EPDM polymer at a fixed frequency of 2Hz. Clockwise from top left: Stabilised temperature at 0.2 compressive strain; stabilised temperature at 0.3 compressive strain; stabilised temperature at 0.4 compressive strain; stabilised temperature at 0.5 compressive strain.

0.5 strain test. At each increase in compressive strain, the temperature was permitted time to stabilise before further increases were made. Example images from this test range are detailed in Figure 5.59. The thermal images were reviewed and the maximum observed difference between the test sample and the control sample at each strain was recorded. Figure 5.60 details the results from these tests.

These results broadly correlate with the findings for the frequency controlled test with a measured temperature difference at 0.2 and 2Hz of approximately 8.5℃ (this compares to a result of 7℃ for the frequency controlled test). The temperature difference at higher strains dramatically increases, reaching a peak Δt of over 36℃ at a specified strain of 0.5.
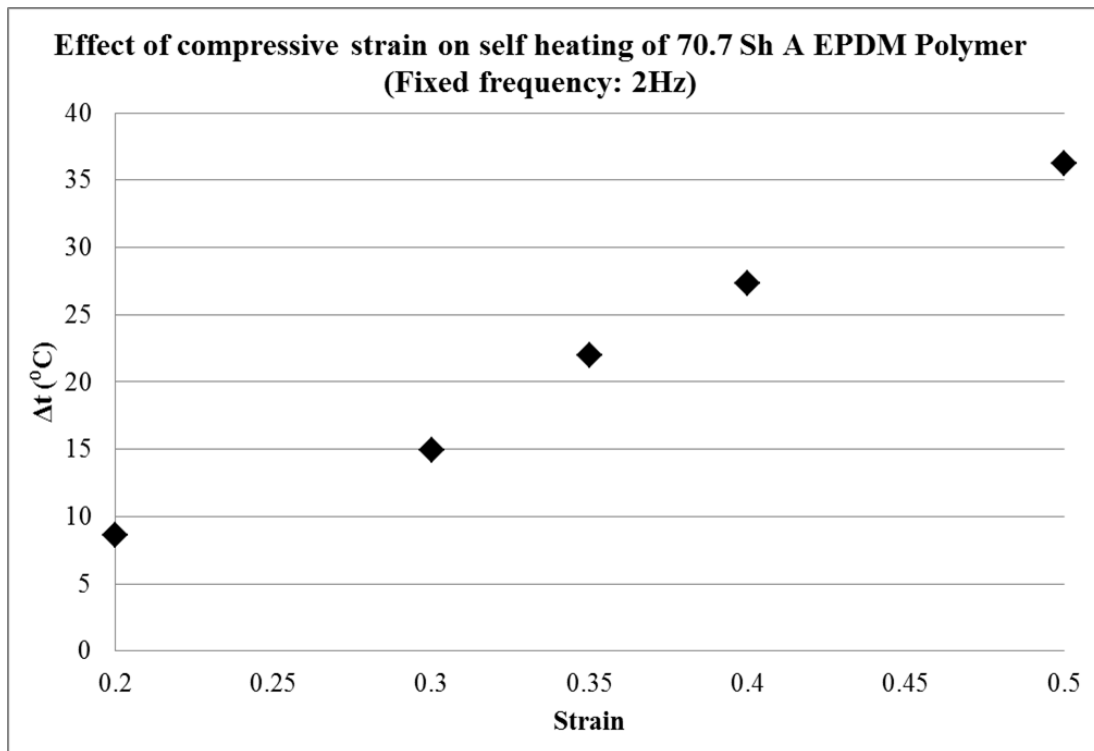
Figure 5.60: Temperature difference between test sample and control sample during compression testing of 70.7 Shore A hardness EPDM polymer at a fixed frequency of 2Hz with increasing compressive strain from 0.2 to 0.5. Note the different scale on the Y-axis in comparison to Figure 5.58

.

The impact of these results on the validity of the Compression Fatigue testing is explored in the Discussion (Section 5.5).

5.4.2.5 Dynamic Mechanical Analysis Tests (DMA)

Dynamic Mechanical Analysis of EPDM 70.7 Shore A Hardness material was conducted to observe the change in modulus with respect to temperature. The method for this work was outlined in Method Section 5.3.2.5, Page 270.

The key result of interest for the DMA tests is the effect of temperature on E' (the Storage Modulus). The first temperature sweep conducted failed as the sample vibrated itself out of the machine. This may have been due to the low temperature (the test started at -100°C) which is likely to have been well below the glass transition point of the polymer and will have made the sample extremely stiff.

The second temperature sweep was therefore conducted at a higher temperature range from -10°C to +100°C and successfully calculated the range of E' values observed over this temperature range. The results for this temperature sweep are detailed in Figure 5.61.

The results clearly show that an increase in temperature decreases the Storage Modulus. Although this value is not directly comparable to Young's Modulus, it does represent the elastic response of the material (PerkinElmer, 2008). It can therefore be assumed that an increase in temperature will have a similar affect on the Young's Modulus of the material. Figure 5.61 shows the scatter of calculated modulus values at a lower temperature is quite large and as the temperature increases, there is less scatter in the results.

The inherent scatter in results at the lower temperatures suggests that a temperature difference up to 10°C may not have a dramatic affect on the results in the likely operating temperatures of the tether and the room temperature at which the polymer test work was conducted. However temperature differences over 10°C may begin to affect the results by causing an excessive reduction in the Storage Modulus.

5.4.3 Anti-friction membrane investigation

Anti-friction membrane investigations were conducted to observe the durability of different material options under repeated extension cycles of the tether assembly. The methods applied for this work were outlined in Section 5.3.3, Page 272.
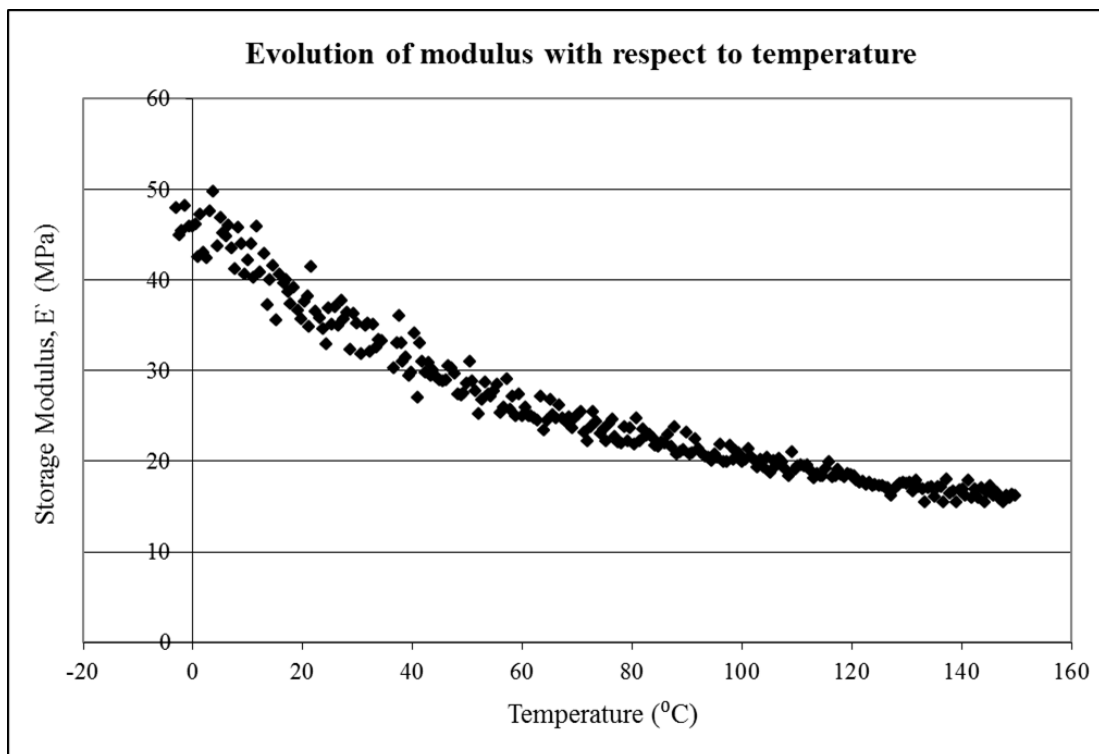
Figure 5.61: Dynamic Mechanical Analysis result calculating Storage Modulus of EPDM polymer, 70.7 Shore A hardness, over a temperature sweep from -10°C to 100°C.
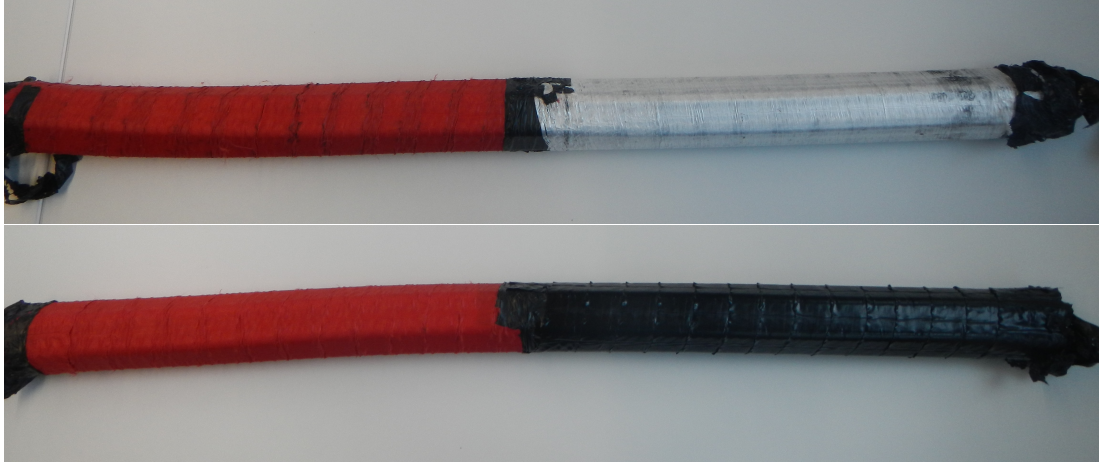
Figure 5.62: P1-16* and P1-17* anti friction membranes and core assembly following
DMaC testing involving 2000 cycles of 0.2m displacement at an 8s cycle period. Top
image: P1-16* (Left: 1 x layer of Dacron. Right: 2 x layers of Endumax tape TA23).
Bottom image: P1-17* (Left: 2 x layers of Dacron. Right: 2 x layers of Bell Plastics
Black UHMWPE)

Following initial bedding in, P1-16* and P1-17* were each subjected to 2000 cycles
of 0.2m displacement driven testing in DMaC, in order to review the performance of the
new anti friction membranes under trial. Following the displacement testing, the tethers
were de-constructed to review the effect of the cycling on the anti friction membranes.
Figure 5.62 details the tether core assemblies following testing. This can be directly
compared to the as-new membranes shown in the Method Section 5.3, Figure 5.13,
Page 274.

At this point in the development of the anti friction membrane a purely qualitative
review was conducted to assess the relative success of the different membranes trialled
and identify a suitable route for further development.

This additional testing was conducted as issues were observed following the tether
field testing regarding the durability of the original Dacron anti-friction membrane.
To compare the alternative materials on an even basis, Dacron was installed on half
of P1-16* and additionally two layers of Dacron were installed on half of P1-17* as
it was anticipated that slip would be promoted between the two layers reducing the
damage caused during operation. Figure 5.63 details both Dacron membranes following
the testing. Figure 5.63a shows the Dacron membrane installed on P1-16* with just

(a)   (b)
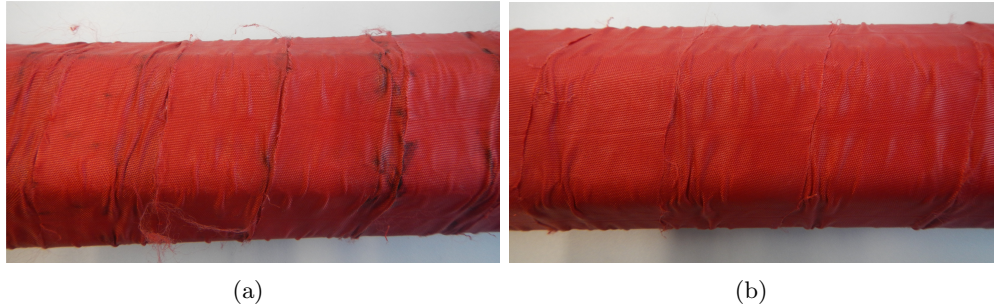
Figure 5.63: Dacron membranes condition following DMaC testing involving 2000 cycles of 0.2m displacement at an 8s cycle period. (a) One screen of Dacron installed; (b) two screens of Dacron installed.

one layer. Although the damage was not at the same level as observed following the field testing, significant damage had initiated. Pressure ripples had developed on the surface of the tape, the edges of the tape were frayed and areas where the tape has been pulled across the surface of the polymer were evident, highlighted by black marks. The two layers of Dacron installed on P1-17* (Figure 5.63b) showed a slightly improved performance. Although the pressure ripples and fraying did develop, they were not as extensive as seen with just one layer of Dacron. There were no black marks from the material being pulled across the surface of the polymer core, suggesting that (as intended) the two layers were slipping over one another and reducing the overall wear on the membrane.

A further material option investigated was Endumax TA23 UHMWPE that was applied in two layers and trialled on the remaining half of P1-16*; the membrane following testing is detailed in Figure 5.64a. This material was very thin (55 μm) and whilst having significant strength along the length of the tape, the strength across the width of the tape was limited; even before installing the core assembly small tears were present across the width of the tape. Following the trial the small tears in the width of the tape had multiplied and were evident across the whole length of the tether. However, they did not lead to any fraying or the development of any significant ripples or ridges. These small tears may indeed have afforded the material the movement it required during tether operation and therefore limited the overall damage encountered. The edges of the tape as originally applied were almost indistinguishable and the surface

(a)   (b)
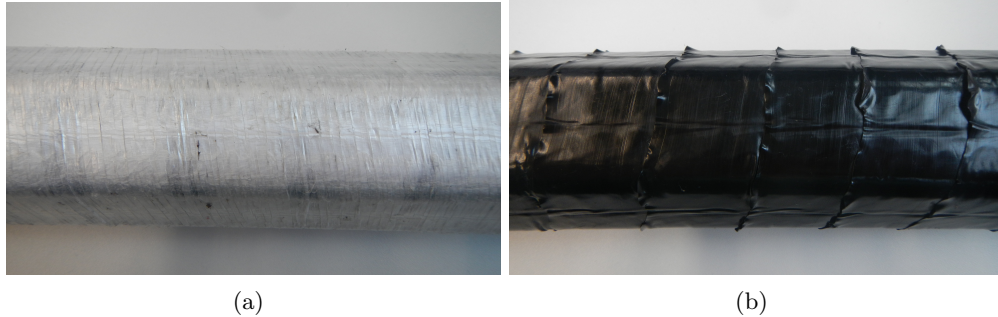
Figure 5.64: Alternative membrane material condition following DMaC testing involving 2000 cycles of 0.2m displacement at an 8s cycle period. (a) Endumax TA23 UHMWPE tape, two 55μm layers; (b) Bell Plastics' Black UHMWPE tape, two 200μm layers.

of the membrane appeared relatively smooth. Except for the presence of the small tears the membrane showed no further signs of damage.

Bell Plastics' Black UHMWPE was the final material trialled, installed in two layers on half of P1-17*. The membrane following testing is detailed in Figure 5.64b. This material, at 200μm thick, was much thicker than the TA23 tape and showed no signs of tearing as the previous tape did. There was also no fraying of the material and no pressure ridges developed during the trial. The surface of the tape itself was still extremely smooth, however, the edges of the tape as installed had lifted up along the length of the tether and created a very stiff ridge that ran helically along the length of the tether.

5.5 Discussion

The purpose of Chapter 5 was to provide an initial reliability assessment of a novel mooring component, the Exeter Tether. Before fully discussing the results, it should be noted that the P1-Series of tethers was manufactured to prove the working concept of the tether; durability was not one of the key considerations for this test series. The work identified in this Thesis therefore provides an early reliability assessment for the tether to highlight any areas requiring improvement and inform the next iteration of tether development.

This discussion section is structured to address the results in the order they were presented in the Results Section (Page 278 onwards). In addition to discussing the results for each section individually, the final section (Section 5.5.4) brings together results across the separate sections of work and discusses the overall implications for tether development.

5.5.1 Tether assembly durability assessment

The laboratory testing and the field testing of the tethers assessed the reliability of the entire tether assembly. The interaction of tether components during long term testing was of interest and additionally, the industry standard TCLL test was conducted to allow for comparison to alternative rope constructions. Field testing was also conducted to monitor the effects of bio fouling on the tether and document any change in tether performance by repeating functionality testing on DMaC before and after the field deployment. Findings from these investigations are discussed below, reflecting the order of the presented results.

During laboratory testing the first TCLL test conducted on P1-16 showed promising results with a TCLL value of 65.3%. It should be noted that some alterations were made to the standard test procedure, most notably a reduction in the test cycle period from the range of 20-60 seconds specified in the standard to a test time of 8 seconds used in the tether testing. However, increasing the frequency in this respect should make the testing more damaging and therefore reduce the TCLL value. The TCLL calculation for the tethers should therefore be regarded as conservative. The reason that the cycle period was reduced to 8 seconds for the tether testing was to make it more realistic to tether operating conditions. As the TCLL test was also used to assess the

343

Table 5.17: Comparison of TCLL values calculated for P1 tethers to other published industry figures. [1](Lankhorst Austraila, 2013); [2](Baaj, 2011); [3](Samson Rope, 2015).

Tether / rope construction	TCLL value achieved	Source
Exeter Tether: P1-16	65.3%	New result
Exeter Tether: P1-20	50.3%	New result
Monofilament nylon	55%	Lankhorst Ropes[1]
Monofilament polypropylene	52%	Lankhorst Ropes[1]
Euroflex®	79.6%	Lankhorst Ropes[1]
Eurofloat®	73.0%	Lankhorst Ropes[1]
Tipto®	70.7%	Lankhorst Ropes[1]
Lankoforce	100%	Lankhorst Ropes[2]
AmSteel®-Blue	100%	Samson Ropes[3]
Saturn-12	100%	Samson Ropes[3]

evolution of axial stiffness of the tether over time, conducting the testing at a realistic operating frequency was important as the stiffness of the tether is affected by the time-dependent visco-elastic properties of the polymer core. This approach is supported by Weller *et al.* (2013) who suggest rope characterisation should be conducted under *"appropriate conditions with respect to the final application."* It is of interest that a study into the effects of cycle frequency on the load-extension response of the tether by Parish (2015) confirmed that there was no significant alteration to the tether response within the range tested (a cycle period range from 6s - 14s).

Table 5.17 compares the calculated TCLL values from the tether series to published TCLL values and 65% is a very acceptable value for an early stage prototype. Lankhorst Austraila (2013) cites values of 55% and 52% for monofilament nylon and polypropylene ropes respectively in literature promoting Lankhorst's Euroflex®, Eurofloat® and Tipto®Eight ropes. More recently rope manufacturers have developed ropes that have completely survived the whole TCLL test series and achieved a TCLL value of 100%; this includes Lankhorst's LankoForce rope (Baaj, 2011) and Samson Rope's AmSteel®-Blue and Saturn-12 ropes (Samson Rope, 2015). 65% however, still remains a strong starting point for the P1-Series tethers, with clear areas for improvement identified that were incorporated into a revised tether design, P1-20.

P1-20 was tested to the same TCLL schedule as P1-16 and the University of Exeter

eye splice failed during the 60% NWBS test which resulted in a calculated TCLL value of 50.26%. This meant the new design alterations could not be fully tested (although a qualitative review of the surviving end showed promising results with no signs of deterioration following the TCLL test). Although this was clearly not the desired result, this finding does raise a key consideration regarding tether reliability. Currently the P1-Series is terminated with an eye splice which, despite being a standard method for rope termination, does have many limitations. It is widely accepted that the splice area of an assembly is weaker than the main body (ABSG Consulting Inc, 2015; Noble Denton Euorpe Limited, 2006) and it is even suggested by Ayres (2001) that partial damage to the main body of the rope will translate to an eye splice failure. Most sources suggest splicing reduces breaking load by approximately 10% (BEXCO, 2014; Oil Companies International Marine Forum, 2005) although a report by Noble Denton Euorpe Limited (2006) suggests a well spliced polyester rope can have a strength approaching 100% of the rope MBL. Interestingly, as part of a study into polyester rope damage in the offshore oil and gas industry, Ayres (2001) conducted a survey of rope manufacturers, consultants and oil and gas companies. This survey found that most operators have concerns regarding rope end splices. The study calls for more quality assurance for rope splicing, and better standards that acknowledge the different configurations of eye splice required depending on rope construction and fibre selection.

The type of failure observed in P1-20 showed clear signs that the load was unevenly distributed across the splice which will have led to the premature failure observed. As documented by McKenna *et al.* (2000) and Weller *et al.* (2013), manufacturing of eye splices is a highly skilled process requiring a high level of accuracy to ensure the load is evenly distributed. The early failure of P1-20 highlights the need for improved quality control as suggested by Ayres (2001) or alternative end termination techniques in further tether iterations.

Alternative termination techniques such as grips or potting are discussed by McKenna *et al.* (2000) and Noble Denton Euorpe Limited (2006), and a novel termination technique has been patented by Flory (1997). These alternative techniques however, are poorly documented in the wider literature with limited verification. Noble Denton Euorpe Limited (2006) also suggests various novel termination techniques which have been proposed such as splicing of sub-ropes individually and using these to create a number of eyes but again there is no data to validate these alternatives.

Given the scarcity of proven alternatives, the use of an eye splice in terminating the ends of the tether is still the best option in future iterations. Different splicing techniques should be trialled to investigate the load distribution afforded by each and improved quality control is suggested to ensure the load is evenly distributed across the eye splice.

In addition to the calculation of the TCLL values, the results from these tests were also analysed to assess the evolution of dynamic axial stiffness at this high level of loading. During the first loading level of the TCLL tests (0-50% NWBS), results from both P1-16 and P1-20 show a substantial evolution in stiffness over the first 250 cycles (23% and 30% increase respectively). This quickly levels out in both cases. During the first loading level from cycle 5 to cycle 950 the total observed increase in dynamic axial stiffness was 30% and 40% for tethers P1-16 and P1-20 respectively.

Further to the increase in individual cycle dynamic stiffness observed as the cycle numbers progress, an overall increase in strain is also observed throughout the testing (Figure 5.22, Page 286). This extension is observed in conventional fibre ropes and is well documented by Flory *et al.* (2004). It is due to the bedding in of the rope and end terminations (sometimes referred to as 'constructional stretch') in addition to the 'accumulated elastic stretch' which is temporarily accumulated during the tension cycles (Flory *et al.*, 2004). Whilst the constructional stretch is permanent, recovery of the accumulated elastic stretch is anticipated when the tension cycles stop for conventional fibre rope testing. This recovery is particularly pronounced during the TCLL testing of the tether due to the additional recovery of the polymer core which takes on a temporary compression set during cyclical loading (as observed from the step changes between TCLL test load levels in Figure 5.24, Page 288).

In contrast to the evolution of the tether stiffness profile, work presented by (Weller *et al.*, 2014a) assessing the performance of a conventional nylon rope (with a parallel stranded subrope construction), suggests that axial stiffness stabilises from 25 cycles. Referring to Figure 5.23, Page 287 and Figure 5.28, Page 293 the axial stiffness of the tether has clearly not stabilised by this point and extracting this data would not provide a representative operating profile for the tether. This suggests that, due to the novel construction and components of the tether, establishing a stabilised axial stiffness profile during cyclic loading may take longer than for conventional ropes. It

should be noted however, that the TCLL test loading requirements tested the tether to significantly higher loads than tests presented by Weller *et al.* (2014a).

Using the initial stiffness profile obtained from low cycle numbers will not provide a realistic profile for use in mooring system design with the Exeter Tether. The key recommendation from this finding is that the tether should be exposed to realistic operating loads (in controlled laboratory conditions) for cycles in the region of 1000 and the stiffness profiles reviewed for stabilisation. It is anticipated that by 750 cycles minimal further evolution will occur and a realistic operating stiffness profile for the tether can be established.

The sea deployment of the tethers formed the next section of this work and the qualitative assessment of tether P1-8 following nearly 6 months of sea deployment showed extensive marine growth (bio-fouling) had accumulated on the tether. Following cleaning, no external signs of damage were observed. However, upon opening the tether and conducting detailed microscope investigations, it became evident that the marine growth had fully penetrated the tether jacket and was attaching to the anti friction membrane. Sharp debris from hard shelled mollusc species was shown to have permanently damaged some of the rope yarns during the deployment of just six months, and the ingress of grit and other small debris is likely to accelerate fibre-on-fibre friction wear in the longer term as suggested by BEXCO (2014) and Weller *et al.* (2013, 2015a). The direct damage to the tether construction is not the only concern from bio-fouling, which will also significantly change the dynamics of the mooring system adding weight and drag to the mooring limbs (Bowie, 2012; Titah-Benbouzid & Benbouzid, 2015; Weller *et al.*, 2015a). A study by Tiron *et al.* (2015) discusses bio-fouling and WECs, and notes that attractive sites for development globally (i.e. with an energetic wave environment) will have *"significant biological activity"* due to the energetic sea state encouraging mixing, which results in good oxygen saturation and waste removal rates; both of which are very attractive for marine growth.

This problem is clearly not unique to the tether and bio-fouling of conventional rope constructions has led to the development of improved protective systems such as those used for DeepRope® polyester mooring lines, which now include an outer cover and a sand barrier (Figure 5.65) to protect the inner load bearing members (BEXCO,
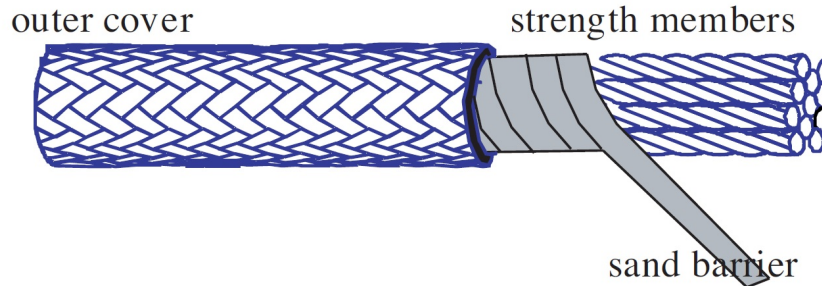
Figure 5.65: DeepRope® polyester mooring line construction, detailing a new sand barrier that filters particles down to 2μm. Replicated from (BEXCO, 2014)

2014). The new filter material being used for these moorings filters particles down to 2μm. Protection of this sort should be investigated for the tether.

Following field deployment DMaC was used to perform a quantitative assessment of the mooring tethers. Results from these tests showed a marked increase in axial stiffness of both tethers and a reduction in the difference in stiffness profiles originally observed between the two different tether designs (P1-3 manufactured from 59 Shore A hardness polymer cores supplied by Ley Rubber Ltd and P1-8 manufactured from 70 Shore A hardness polymer cores supplied by Polymax). The design concept of the P1 tether series utilises the different polymer specifications to achieve a variety of axial stiffness responses, however as the difference in response between polymer types appeared to diminish following sea trials this is an area that requires further investigation. Figure 5.66 details the load-extension profiles for the fifth cycle of the standard functionality test ETT-08. The change in profile from new to worked tether is evident. Additionally P1-2 and P1-6 have been added to this graph for comparison, as these two tethers represent the extremities of the range of tether responses achieved during the proof of concept study reported by Parish (2015) and Gordelier *et al.* (2015). Adding these two reference tethers to the plot show that, whilst before the SWMTF deployment tethers P1-3 and P1-8 were mid-range tethers with a load-extension profile somewhere between the two described extremities, following deployment the difference between the two tethers was significantly reduced and both tethers display a similar load-extension profile to P1-2, the softest polymer from the original series that displayed the stiffest
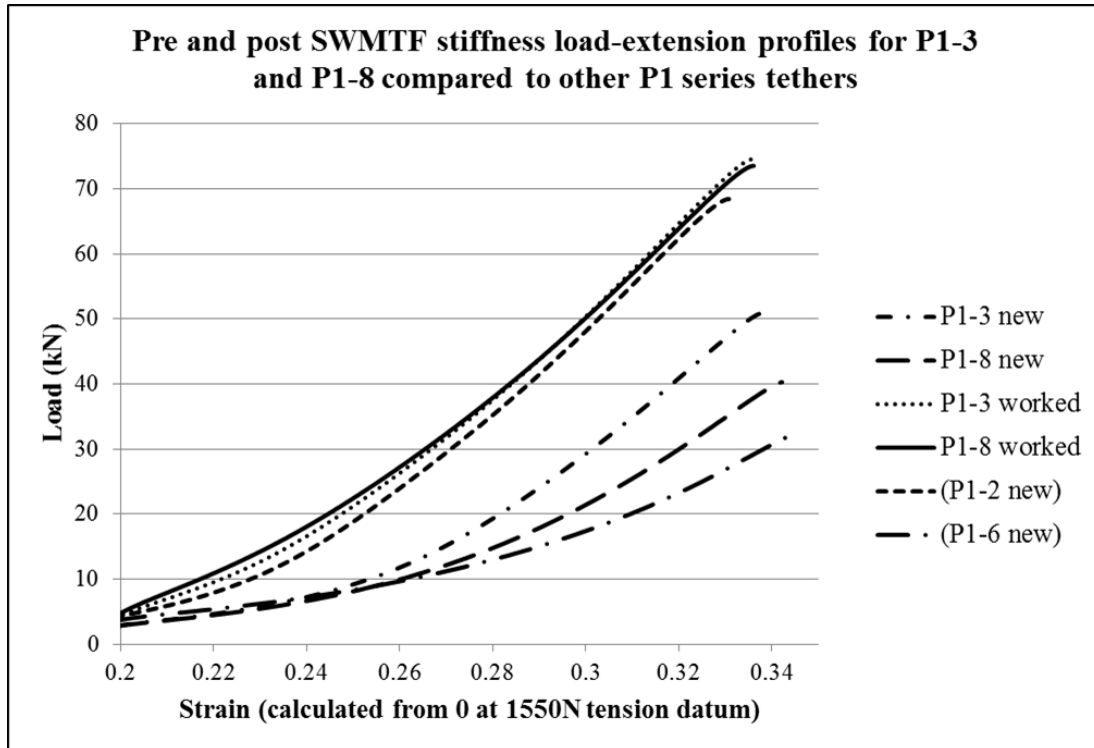
Figure 5.66: Load - Extension characteristics of worked tethers following SWMTF deployment in comparison to un-worked tethers and P1-2 and P1-6 representing the extremities of the original P1 Series (Gordelier *et al.*, 2015; Parish, 2015). Data extracted from the fifth cycle of test ETT-08, conducted from a 1550N start datum.

response (in the as-new state).

On comparing this to conventional fibre rope performance the literature is not conclusive. Although different methods have been applied, Weller *et al.* (2015a) review the performance of a nylon seven parallel-stranded rope and suggest a decrease in axial stiffness following an 18 month deployment at the SWMTF. This change in performance is attributed to mild damage occurring in the rope during the deployment. This is in contrast to results presented by Bitting (1980) who observes an increase in axial stiffness of both nylon and polyester ropes when exposed to the ocean environment for 4 to 5 years. Further to this, data published by rope manufacturers often suggests an increase in stiffness for worked ropes, with separate performance curves for 'new' and 'worked' ropes to account for this change in mooring system design. Figure 5.67 details a typical graph supplied by Bridon (2015a) to demonstrate the increase in stiffness observed for
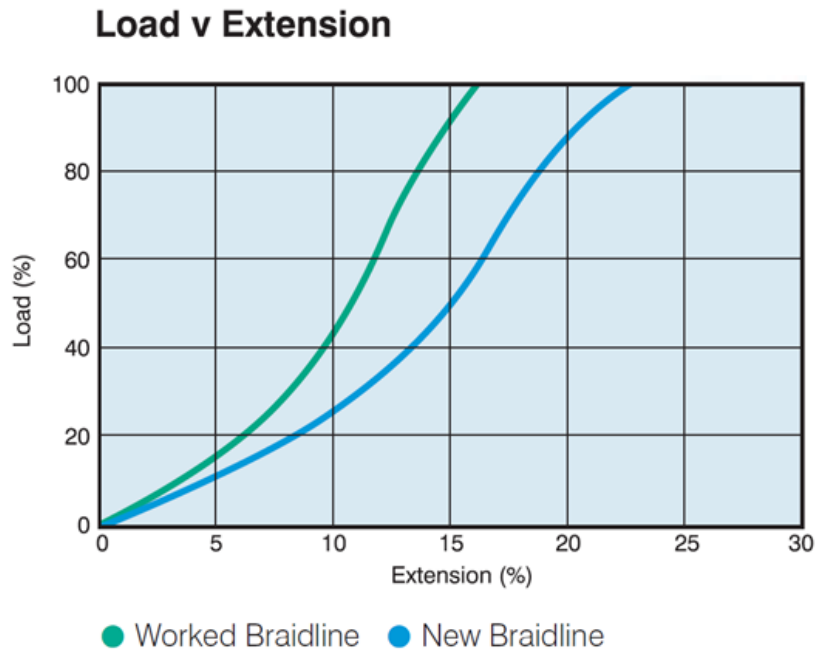
Figure 5.67: Load - extension plot for 'Viking Braidline' polyester rope in new and worked condition. Replicated from Bridon (2015a).

their 'Viking Braidline' polyester rope; on average the stiffness is increased by 25% in the worked rope.

The reduction in operating range of the post deployment tethers is clearly a concern. Due to the limited and varied nature of these results this area requires further attention. The Discussion at the end of this section (Section 5.5.4) brings together the complementary aspects of the tether reliability work and addresses this further.

The main limitations of the tether assembly work (including the TCLL work and SWMTF field testing) arise due to the limited number of samples available. With the high costs involved at the early stage of prototype development, the total number of tethers manufactured as part of the P1-Series was limited to 13. Although some of these tethers were re-conditioned for additional test work, the overall scope of work required to prove the tether concept meant it was not possible to conduct multiple repeats of tests. The calculation of the breaking strength of the tether (which was subsequently used to calculate loading levels for the TCLL tests) was based on only one tether and

only two tethers were used for the TCLL tests. Standards vary with the suggested number of samples required to ascertain MBL ranging from 3 (Bureau Veritas, 2007) to 5 (Det Norske Veritas, 2013a). However Banfield *et al.* (2005) suggest, with a well manufactured rope, a coefficient of variation of less than 3% on break strength can be achieved. The P1-Tethers utilised throughout this test work did have variations to the core geometry, the anti-friction membrane, and the splicing technique, however the load carrying rope manufacture for all tethers was identical. Given the limited samples available, using one break result to specify the TCLL tests was a necessary compromise for this work and should have limited implications given the findings from Banfield *et al.* (2005).

A further limitation of this work is the assumption that the extension of the eye splice at each end of the tether is identical. No two eye splices will be identically manufactured due to the skilled manual process required to make them (as discussed earlier in this section). The result of this is that there will be variation in the extension properties of each eye splice. As there was only one extensometer available for this work it was only possible to measure the extension of one eye splice per test. However, given the results for eye splice extension detailed in this Thesis correspond so closely to previous results presented in Gordelier *et al.* (2015), this limitation should not have a significant effect on the results.

The differences in the internal tether construction of the P1 series meant that results between tethers were not always directly comparable. Additionally, load history for each tether was not always identical, with minor alterations to bedding in regimes to suit each test. These differences were always at low load and low cycle number and will not have induced permanent damage, so are in-consequential in comparison to the high cycle numbers and high loads that the tethers were exposed to during TCLL and field testing. The TCLL test is regarded by some as excessively severe and not representative of realistic loading (McKenna *et al.*, 2000), however as it is widely used by rope manufacturers it was a useful exercise to enable benchmarking of the tether at this early stage.

It should also be noted that various methods exist for quantifying the axial stiffness of ropes. Various approaches are suggested by McKenna *et al.* (2000) and alternative approaches are applied by Davies *et al.* (2012); Flory *et al.* (2004) and Weller *et al.*

(2014c). In the work presented in this Chapter, the dynamic axial stiffness of the tether has been defined using the secant approach suggested by McKenna *et al.* (2000). This approach was adopted to allow the consistent quantification of axial stiffness between two load points (20 - 90kN) at the increasing load levels specified by the TCLL tests. For the tethers subjected to the sea trials the same approach was adopted, however the stiffness secant was obtained at lower loads of 10 - 35kN to match the loads of the ETT-08 test conducted. The purpose of this work was to observe how the stiffness profile of the tether evolves, due to either repeated loading cycles (as assessed in the TCLL tests) or when exposed to real sea conditions (as assessed in the SWMTF sea deployment). The critical point was therefore that a consistent approach was used to quantify the dynamic axial stiffness, that would allow for a valid assessment of the evolution of this stiffness. The method adopted in this Chapter allowed for this, and provided the data required to assess the evolution of the dynamic axial stiffness as required.

Despite the discussed limitations, the tether assembly assessments have provided a baseline reliability assessment of the tether assembly, with clear areas of improvement identified for further tether development. These recommendations are detailed in Chapter 7, Conclusions and Further Work.

5.5.2 Elastomeric core durability assessment

This section of work focused on the durability of the EPDM rubber used to manufacture the P1-Series tether cores. Prior to this work there was a large knowledge gap regarding the use of EPDM in a marine environment and when subject to compression fatigue cycles (which occur due to the operating action of the tether). Although the elastomer core is not a significant load bearing component of the tether (less than 10% of the total load is carried by the core (Parish, 2015)), it does control the load stiffness response of the tether, so it is important to understand how this may evolve during operation. Various test procedures were established to test the material response to a range of parameters designed to simulate processes the material is exposed to in an operational tether.

Before discussing the results of these tests a brief background to the choice of EPDM rubber is provided. As detailed by Parish (2015), Ethylene propylene diene monomer (EPDM) was the selected polymer for the tether core due to its very good ozone, ageing and weathering resistance properties (Rinnbauer, 2007), this is further

supported by Mark *et al.* (2013) and FTL Technology (2015). In addition, it is known to have 'excellent' water resistance properties (Elastomer Engineering Limited, 2009) which is a key requirement for tether operation. As well as having these desirable material properties, EPDM is a widely used polymer that is readily available from many suppliers which makes it an ideal material to manufacture multiple iterations of tether for the P1-Series tests.

The manufacturing process of EPDM is also of interest for this section as the addition of different compounds affects the finished material properties. A report by EPDM Roofing Association (2003) provides an overview of the key components of EPDM manufacture and highlights the variety of raw materials that are used including:

- EPDM polymer, the synthetic elastomer giving this material its name.

- Fillers, such as carbon black, that are used to reinforce the polymer.

- Softeners and plasticizers, such as paraffin, added to increase the plasticity of the material.

- Other ingredients to aid the vulcanization process (whereby the 'thermoplastic' is heated to achieve the final material a 'thermoset'). Sulphur is often used to initiate this process with additional accelerators sometimes added. Further additives may be included to enhance a particular property such as resistance to heat or flames.

Different manufacturers vary the percentages of each ingredient and employ different processing and curing techniques. Most manufacturers are not willing to provide detailed information on the specific content or process they have employed, so the same material properties cannot be assumed for two samples of 70 Shore A hardness polymer supplied from different manufacturers. The result of this variation in EPDM specification means that the results presented in this Chapter are only valid for the specific EPDM as supplied by the manufacturers detailed in Section 2.6.3. Although general conclusions can be drawn regarding potential changes to EPDM material properties, the specific details are only relevant to the EPDM tested throughout this work.

In addition to the variability in material properties, there is also very limited published data on some of the specific EPDM properties of interest, indeed there is no available data on the performance of EPDM in a marine environment for comparison

Table 5.18: Summary of results from material property tests conducted on EPDM
polymer aged in renewed natural sea water heated to a temperature of 60°C.

Polymer sample	Length of ageing	Material property	Average change following ageing
2mm sheet EPDM 70A Shore hardness (Ley Rubber)	1 month	Tensile strength	-16%
		Elongation at break	-14%
		Young's Modulus (100% elongation)	+15%
		Young's Modulus (200% elongation)	+7%
		Young's Modulus (300% elongation)	+3%
		Young's Modulus (400% elongation)	0%
		Fatigue cycles to failure (at 100% elongation and 2Hz)	-82%
Ø 25mm round EPDM 70.7A Shore hardness (Ley Rubber)	13 months	Axial compression modulus (0.1 strain)	+14%
		Axial compression moudlus (0.2 strain)	+16%
		Radial compression modulus (0.1 strain)	+22%
		Radial compression moudlus (0.2 strain)	+22%

to this work. The dearth of other literature in the area emphasises the importance of
this critical work for the development of a durable tether.

Finally, many of the tests established for this work are bespoke tests, developed
to replicate specific features of tether operation and understand the affect on material
properties (such as the fatigue compression tests). This again means that for some
aspects of this work there is no existing literature with which to draw comparisons.

5.5.2.1 Tensile tests

A standard test procedure (ISO37) was used to establish key tensile properties of the
2mm sheet EPDM 70 Shore A hardness polymer, supplied by Ley Rubber. This test
procedure was repeated for new polymer and polymer aged for 1 month in renewed
natural sea water heated to 60°C. A summary of the affects of marine ageing on key
material properties is provided in Table 5.18. The results from this test work found
that in the aged 2mm sheet samples, on average, the tensile strength was reduced by
16% and elongation at break was reduced by 14%. Young's Modulus was also affected
by ageing, and at a strain of 1 this was increased by 15%, but was less affected at higher
strains.

The ageing of the material also had a significant effect on fatigue life, with aged samples surviving on average just 18% of the cycles to failure survived by new samples (when tested at 2Hz and a strain of 1).

The marine ageing process clearly has a detrimental effect on the EPDM material tested, given there are no published results for EPDM to compare with these findings, data for other polymers was reviewed to see if this was in-line with expectations. Results published by Le Gac *et al.* (2012) review the effect of ageing at 60°C on another polymer, polychloroprene, and broadly the same effect is observed with a reduction in tensile strength of approximately 15% and a reduction in elongation at break of approximately 16% after 50 days ageing at 60°C. Results presented in this paper are superimposed with selected EPDM results in Figure 5.68. Polychloroprene is commonly known as neoprene which has very different material properties to EPDM, never-the-less a similar percentage reduction in tensile strength and elongation at break is observed when aged. Additionally, this research also concludes that the longer the ageing process the more significant the reductions observed, as detailed in Figure 5.68. Although it was not possible to age the EPDM for different lengths of time during this work, the research presented by Le Gac *et al.* (2012) certainly highlights this as an area for further investigation.

The results from the fatigue testing of EPDM are a significant concern. The fatigue tests presented were from samples cycled from 0 - 1 strain (0 - 100% elongation), which is clearly a much more severe regime than the tether would be exposed to in real operating conditions, with extensions of 30-40% anticipated. Interestingly, work presented by Alshuth *et al.* (2002) and Abraham *et al.* (2005) suggests that introducing a pre-tension into the testing (so increasing 'R' the ratio of minimum to maximum strain) improves the fatigue performance of filled EPDM. This effect is also apparent for natural rubber (Le Gac *et al.*, 2015a) and is thought to be caused by the strain induced crystallisation process of the rubber material. However, it is not fully understood why this effect is apparent with filled EPDM which is a non strain crystallising elastomer. Despite not being fully understood, the fatigue performance of filled EPDM can be improved by increasing the R ratio, even when this increases the maximum strain reached. The operating tether is likely to be installed in a mooring system with some pre-load, so
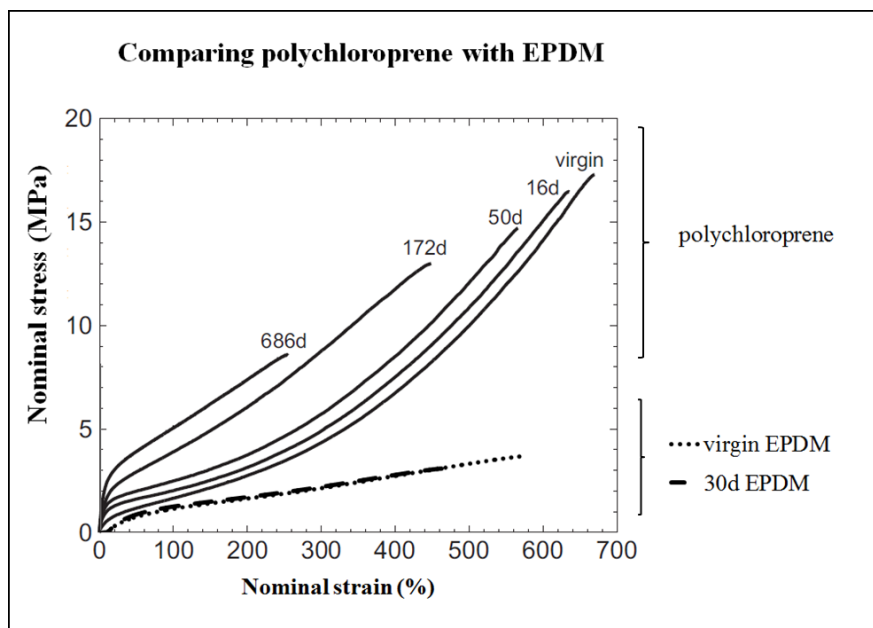
Figure 5.68: The affect of ageing at 60℃ for different time periods on polychloroprene in comparison to selected samples of EPDM. Data based on ISO37 tests, conducted at an extension rate of 10mm/min. Polychloroprene data replicated from Le Gac *et al.* (2012). d relates to number of days ageing.

further work should be conducted to quantify the potential improvements to the fatigue performance of the EPDM polymer given this. In addition to reviewing the effect of the R ratio, Le Gac *et al.* (2015a) also concludes that the fatigue life of natural rubber can be improved by increasing the level of stabilising additives in the rubber formulation. Further research should be conducted with a polymer specialist in order to improve the formulation of the EPDM material to afford better fatigue performance.

A full analysis of the physical material changes to the EPDM during the ageing process that caused the observed change in performance is beyond the scope of this Thesis. However a brief discussion of what may be driving these material changes is presented below.

Le Gac *et al.* (2015b) refer to the plasticization of polymers in sea water which causes mechanical changes in the polymer due to the presence of water within the material; this process is reversible. This paper also refers to chemical reactions occurring within the polymer (such as hydrolysis) due to the presence of water or oxygen; such chemical reactions are irreversible. A further paper reviewing the ageing of silica filled polychloroprene in a marine environment observes similar mechanical changes to those observed with the EPDM presented in this Thesis (Le Saux *et al.*, 2014). An increase in modulus is observed in addition to a reduction in stress and strain at break. This paper suggests *'hydrolytic degradation'* (hydrolysis) is predominantly responsible for this observed ageing in the polychloroprene. Fourier transform infrared spectroscopy (FTIR) can be used to detect hydrolysis in polymers as detailed in Le Gac *et al.* (2015b) and Le Gac *et al.* (2012) and would make an interesting extension to this work for a material scientist.

Limitations of this work revolve around the accuracy of the assumption that immersing samples in heated sea water will accurately accelerate the natural ageing process in line with Arrhenius behaviour. Although this technique is widely used (Celina *et al.*, 2005; Davies & Evrard, 2007; Le Gac *et al.*, 2012; Le Saux *et al.*, 2014; Scheirs, 2000; Wise *et al.*, 1995), it does have limitations, with critics concerned that using temperature to accelerate the ageing process may introduce failure mechanisms that would not have occurred through natural ageing at a more representative operational temperature (Davies & Evrard, 2007). Additionally the assumption that reaction rates calculated at higher temperatures can be linearly extrapolated to lower temperatures (as assumed by

the Arrhenius extrapolation using Equation 5.3.2.1, Page 253) is questioned by some (Wise *et al.*, 1995) with the suggestion that although an accurate relationship may be established for one particular material property e.g. elongation at break, the same assumption may not necessarily be valid for another material property e.g. tensile strength.

Given the serious implications of the presented results for the use of EPDM in the tether core, it is suggested that further work is done to verify the Arrhenius assumption for EPDM by reviewing the effect of a range of temperatures on key material properties and fully establishing the Arrhenius relationship. In addition, natural marine ageing of the material at a temperature representative of the operational envelope of the tether should be conducted. Due to the limited nature of the MARINET funding mechanism, this work was not possible within the scope of this Thesis, however the results presented offer a strong starting point for further investigation.

Although the test plan set out to achieve a minimum of 3 samples for each investigation, in reality due to sample failures and testing errors the final results presented here were not always based on 3 samples. This is the nature of testing in a limited time window and has been highlighted where applicable in the results section. Where relevant, the spread of results has been detailed for each investigation using the standard deviation. This highlighted the tensile fatigue tests of new samples as having an excessively large spread of results. Ideally this test would have been repeated to confirm the results obtained, but time did not allow for this.

5.5.2.2 Core bundle tests

The scroll test was used to investigate the deformation of individual cords within the core bundle and was conducted on the softest polymer with Shore A hardness of 54 to enable maximum deformation to be measured given the test was load limited. The main finding from this work was that the compressive strain for individual cords was up to 79% greater than that observed across the whole core bundle i.e. the strain was not evenly distributed across the bundle. To put this value into perspective, this was compared to tether assembly work conducted on tether P1-2* in collaboration with Parish which found that at likely tether operating extensions of 30 - 40% the diametric compression of the core bundle was in excess of 20%. Relating this to the

scroll test findings, maximum local material compression is likely to exceed 35% in these conditions.

The main limitation of this work is that the final measurements were only taken from one test that was not repeated. However the purpose of this work was to provide an indication of core bundle deformation, not a detailed measurement. By observing the deformation of multiple core bundles it was clearly established that some cord members were subject to greater compression than others. Quantifying this in detail for one test is adequate to enable the review of the further cord compression test work in a realistic, operating perspective.

5.5.2.3 Compression tests and Dynamic Mechanical Analysis

The standard ISO7743 compression test was used to bench line the axial and radial compression modulus (ACM/RCM) of the EPDM polymer cords supplied by Ley Rubber across the range of Shore A hardness values (from 54 to 81). It should be noted that although the calculation of ACM followed the standard test procedure with a scaled sample size, the calculation of the RCM is not a standard material test and the results for this are affected by both the material properties and the geometry of the sample. This test was created specifically for the tether work as the compression properties of the polymer cord diametrically are of great interest to the operation of the tether. Due to this, the result is not a standard material property that can be specified, however the ultimate purpose of the work is to understand how this key property changes when the material is subjected to realistic operating regimes.

Calculating the ACM and RCM across the range of Shore A hardness values confirmed the expectation that both axial and radial compression modulus increase with increasing Shore A hardness, with this key property likely to be a dominant factor controlling the range of tether stiffness values observed in the original 'Proof of Concept' tether work (Gordelier *et al.*, 2015; Parish, 2015). Once bench line values were established, the next step of this work was to expose the cord material to marine ageing and to compression fatigue cycles to observe any change in compression modulus. This work focused on the mid-range polymer with Shore A hardness of 70.7.

5. RELIABILITY ASSESSMENT OF A NOVEL MOORING COMPONENT: THE EXETER TETHER

Following immersion in renewed natural sea water heated to 60°C for a period of 13 months, it was assumed the samples had reached a condition close enough to full saturation. The standard ISO7743 was then repeated for these specimens and found that, following ageing, axial compression modulus increased on average by 15% and radial compression modulus increased by 22% resulting in greater resistance to compression. These results are also summarised in Table 5.18, Page 354. To put this into context within the range of polymer hardness values specified in the P1 Series, Figure 5.69 has been included. This figure shows that although the ACM and RCM have increased, the change has not been significant enough to alter the order of the specified polymers, with the aged 70.7 still having a ACM/RCM higher than for EPDM 70 and lower than EPDM 80.7.

The brief discussion presented in Section 5.5.2.1, Page 354, regarding physical changes to the EPDM material is also relevant here. This discussion covered some of the processes that may have caused the observed alteration to mechanical performance of EPDM following ageing in a marine environment and is also relevant to the observed change in compression modulus discussed here.

Again, as discussed for the tensile tests, the main limitations of this work revolve around the accuracy of the Arrhenius assumption that the elevated temperature of immersion will accurately speed up the natural ageing process. Further work should be done to confirm this assumption. Additionally the samples were assumed to be fully saturated after 13 months immersion, however as detailed in Section 5.4.2.1 the weight gain of the samples had not quite ceased at this point which suggests they may not have been fully saturated. Figure 5.36 on Page 301 details this, and it can be seen that the significant weight gain observed in the first five months of saturation ($\sqrt{h}$ equal to approximately 60) has considerably reduced and therefore the assumption of being fully saturated after 13 months should not dramatically affect the results.

In addition to investigating the affect of marine ageing on the compression properties of the polymer core, the affect of long term compression fatigue cycles was also investigated as during tether operation the polymer core is repeatedly compressed and extended with the movement of the floating body. Prior to discussing these results in detail, the results of the thermal investigation into the effect of the frequency and strain
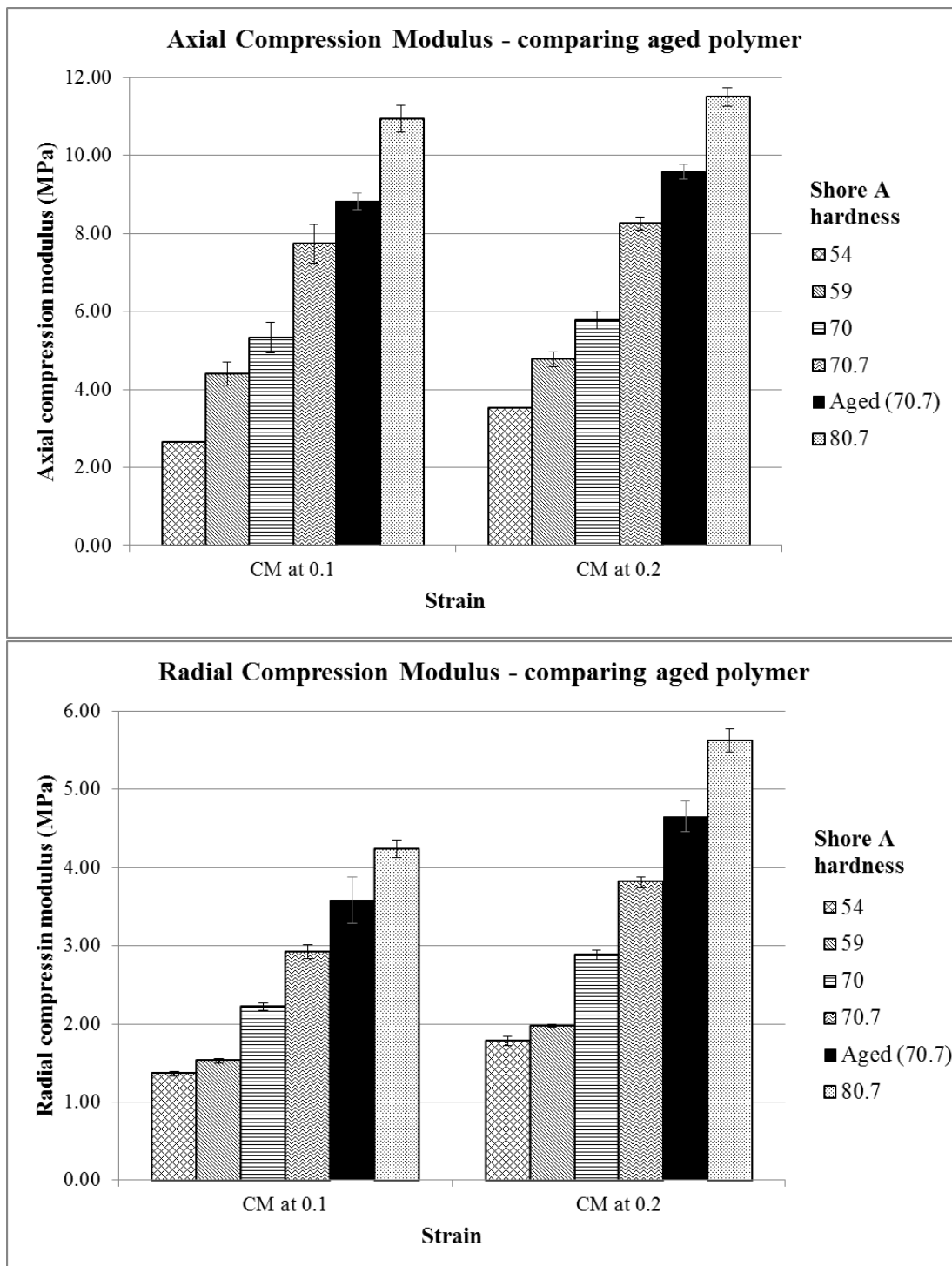
Figure 5.69: Comparing the mean compression modulus values of the aged polymer to the original values calculated for the range of Shore A hardness polymers supplied by Ley Rubber. The polymer was aged for 13 months in renewed natural sea water at a temperature of 60°C. Error bars are based on the sample standard deviation. Top: axial compression modulus. Bottom: radial compression modulus.

361

of fatigue cycles on the self heating of the polymer cords should be addressed. In conjunction with DMA results this thermal investigation informs the validity of the fatigue compression testing. The thermal investigations suggest that at a frequency of 2Hz and a strain of 0.2 the self heating of the polymer is limited with a temperature difference, Δt, between 7°C - 8°C. Based on the results from the DMA testing this change in temperature should not dramatically affect the modulus of the material, falling within the scatter of the results. However, once the strain of the fatigue cycles was increased to 0.3 the measured Δt increased to 15°C and continued to rise to over 35°C at a strain of 0.5. Based on the change to Storage Modulus observed from the DMA testing it is felt that a Δt of anything over 10°C may significantly affect the material properties. Therefore only results limited to a strain of 0.2 at a frequency of 2Hz are assumed valid for the fatigue compression investigation. The further testing conducted at strains of 0.3 and 0.4 is assumed to have generated a temperature rise that could have affected the material properties significantly and results from these samples are not considered representative.

Given the issues regarding self heating discussed above, the only long term fatigue cycling cord test with valid results was test Radial_20_1, conducted at a compressive strain of 0.2 and a frequency of 2Hz. This test certainly represents a realistic level of loading, in extreme conditions strains are likely to be much higher (over 0.35) so this test represents a conservative loading scenario. Although only subjecting the sample to a compressive strain of 0.2, this test does represent the highest number of fatigue cycles conducted, with the sample subjected to 707,000 compression cycles. This is a very realistic operational envelope and at a wave period of 8 seconds represents 65 days of operation. The long term affect of this test is an increase in radial compression modulus (RCM) with a 14% and 16% increase measured at strains of 0.1 and 0.2 respectively. This represents an increased resistance to compression. It is interesting to note that immediately after the testing, the RCM is lower but gradually increases to these final values. One reason for this could be due to the increased sample temperature immediately following the testing, (the DMA results confirmed that an increase in temperature decreases the material modulus). This affect does not fully explain the evolution of RCM over time, as after nearly 18 hours the RCM is still evolving and the temperature of the sample should have stabilised by this point. It is not clear what is
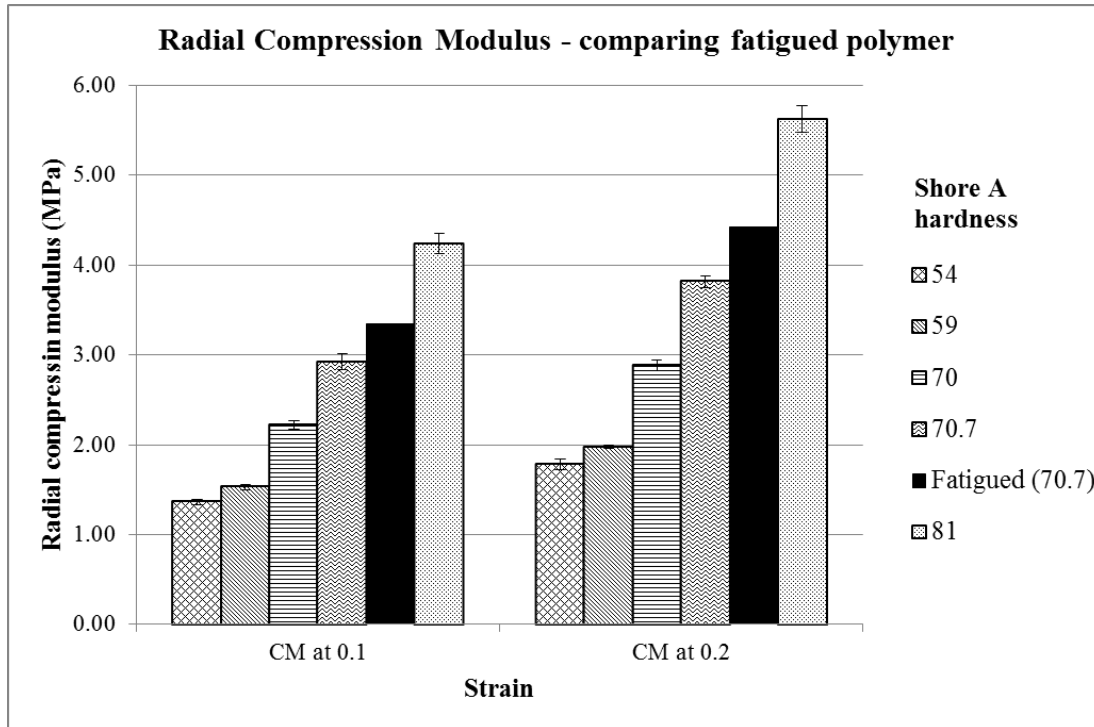
Figure 5.70: Comparing the mean compression modulus values of the fatigued polymer to the original values calculated for the range of Shore A hardness polymers supplied by Ley Rubber. The fatigued polymer was subjected to 707,000 cycles of 0.2 compression strain at a frequency of 2Hz. Results presented are based on the recovered sample 66h20 after the fatigue testing. Error bars are based on the sample standard deviation, no repeats were possible for the fatigued samples.

affecting the further change in RCM at this stage. To put this change of RCM into context within the range of specified polymer hardness values, Figure 5.70 has been included. This figure demonstrates that despite increasing the RCM of the material, the fatigued 70.7 polymer remains in consecutive order of increasing RCM with increasing Shore A hardness.

As detailed in Section 5.4.2.4 there are significant limitations with long term compression testing of the samples. Due to the long term nature of the testing and reliability issues with test equipment, it was not possible to conduct any repeat tests. Additionally, as this testing is completely novel it is not possible to compare this data to any previous work for validation. Given the findings from the self heating investigation,

results from samples at higher compression strains have been assumed invalid. The test parameters presented in Radial_20_1 reflect a very realistic operating regime, and it is unfortunate that a more extreme regime could not be fully tested (i.e. higher compression strains but at a lower frequency to limit the self heating of the sample). Although 707,000 is a high cycle number and represents 98 hours of continuous testing, it only represents approximately 65 days in an operational tether (assuming a wave period of 8 seconds). Further testing at much higher cycle numbers should be conducted to observe the impact on RCM in the likely operating lifetime of the tether (over 5 years).

Despite these limitations, the results from the data are very interesting and clearly indicate an increased RCM following the fatigue cycling which is of significant interest for tether development.

5.5.3 Anti-friction membrane investigation

Following the poor performance of the Dacron tape during the SWMTF field trials, alternative anti-friction membranes were investigated and subjected to 2,000 cycles of 0.2m extension at the DMaC test facility.

The use of two layers of Dacron was trialled as an improvement to the original design using one layer. Although using two layers of Dacron clearly improved the performance of the membrane, signs of damage remained evident (development of pressure ripples and fraying at the edges of the tape) and longer term testing would certainly amplify this damage. The ridges observed on both the one and two layer versions will certainly increase in size and are likely to cause significant wear to the load carrying rope, so in this format Dacron is not a viable anti-friction membrane.

Endumax TA21 UHMWPE tape was also trialled and the results for this material were promising, showing minimal damage and maintaining a smooth, low-friction surface following the testing. The presence of the numerous tears along the width of the material and how these may develop longer term is a concern, although it may be the case that these tears are providing the material the flexibility it needs to avoid further damage.

The final material trialled was Bell Plastics' Black UHMWPE. Although this material was very promising in terms of its durability, the presence of a very hard ridge

running along the edge of the installed tape makes this tape un-usable in this application. The sharp edge created by this ridge is very likely to lead to wear of the load carrying rope and promote an early tether failure.

Of all the alternative membrane options investigated the Endumax TA23 tape shows the most promising results, maintaining a smooth surface throughout the testing with minimal material damage. More extensive, longer term testing is suggested to further validate this material, however this initial trial has proven it to be better suited to this application than the original Dacron membrane.

The damage observed at the tape edge of both the Dacron and the Bell Plastics material suggest that a preferred option may be a woven sock that can fit over the core entirely. Given the findings from the Dacron trial, utilising two layers has a distinct advantage promoting slip between the two layers as the tether operates rather than slip occurring between the membrane and the polymer core or the load carrying rope. The Endumax TA23 Tape can be manufactured into flat material or rope construction (Teijin, 2014). Given the durability of this material in the weakest form as a 55μm tape, a woven sock could be expected to demonstrate further improved performance.

5.5.4 Tether implications

This section brings the different aspects of the tether work together, to consider whether results observed for individual tests complement one another to build up a larger picture of the long term reliability of the tether. The tether assembly test work observed an increase in dynamic axial stiffness of the tether operation; the laboratory based TCLL testing observed a maximum increase of 40% whilst functionality testing of the tether following the sea trials on SWMTF showed a maximum increase in stiffness of 21%. Although the literature is not conclusive, an increase in stiffness is a common observation for conventional worked ropes, with rope manufactures supplying performance curves for 'new' and 'worked' ropes to account for this as detailed in Figure 5.67, Page 350.

Does the effect seen in standard polyester ropes fully account for the change in stiffness observed in the tether or could there be any other processes affecting this? The polymer work suggests that ageing in a marine environment increases the stiffness of the polymer material (both in extension and compression) and additionally, the compression fatigue testing suggests that exposure to long term compression strain cycles

also increases the stiffness of the polymer in compression. The combination of these two effects in an operating tether will certainly lead to an increased polymer stiffness. Intuitively this increase in polymer stiffness would relate to an increase in tether stiffness (as referring back to the 'Operating principles' Section 2.6.2, Page 115, the axial extension of the tether is strongly governed by the diametric compressibility of the core bundle). This intuitive answer also supports the findings from the tether assembly testing, with all results indicating an increase in tether stiffness following marine ageing and operational loading.

Finally the key implications of this work should be highlighted. With the exception of the TCLL test to failure and the membrane testing, all other results presented in this Chapter relate to changes in the operating parameters of the tether, specifically, the change in dynamic axial stiffness of the tether (whether this was based on tether assembly testing or findings from the polymer testing, the implications are the same). The reason this is so critical relates to the whole design philosophy behind the Exeter Tether which is the ability to specify a mooring system with a specific axial stiffness, selected for a particular device in a particular operating climate, and hence reduce mooring loads. For the Exeter Tether to successfully reduce mooring loads as intended, it is critical to establish an understanding of how the stiffness profile of the tether may change over time (due to the marine environment or the loading exposure). Once this is established it can be accounted for within the system design, basing specifications on a 'worked' tether scenario as opposed to a new tether. Critically, key materials within the tether, such as the core, must be able to withstand the environment and loading scenario to which it is exposed, without changing significantly and altering the tether performance. Although a complete failure of the core will not lead directly to a catastrophic failure of the tether, it will negate any load reduction afforded by the tether design. This would lead to increased peak mooring loads, which could ultimately lead to a premature tether failure. Prior to this work there was no available literature regarding the use of EPDM in a marine environment or when subjected to long term fatigue compression cycles. The work presented here therefore provides a strong starting point, investigating the key implications of these parameters on the selected EPDM and the impacts of this on tether operation. The longer term durability assessment of the tether assembly complemented this polymer work by monitoring changes in dynamic

axial stiffness observed at the tether assembly level for comparison to the polymer work. In addition to this, the tether assembly durability trials also provided a bench line durability assessment of the tether and highlighted key areas of development to improve system durability. The issues raised regarding the durability of the Dacron membrane during these tether assembly trials led to the testing of a range of alternative options with recommendations made for future tether iterations.

A further overarching Discussion regarding the work presented in this Chapter is detailed in Chapter 6 and final Conclusions and further work are detailed in Chapter 7.

Chapter 6

Discussion

Contents

In the Introduction to this Thesis (Chapter 1), an overarching research question was set out: **How can reliable mooring solutions for wave energy devices be developed?** Four key research questions were set out in order to address this overarching question, and these are repeated below to set the scene for this discussion:

1. Is there industry consensus on priority areas for development to facilitate commercial wave energy generation?

2. Given the reduced consequence of a wave energy converter (WEC) mooring line failure, should the safety factors applied to mooring system design be reduced when using standard mooring components?

3. During the development of a novel mooring component how should reliability be assessed to ensure overall mooring system integrity is maintained?

4. What are the potential implications of novel mooring components on system reliability?

This Discussion section outlines how these research questions have been addressed through the work presented in this Thesis. Detailed discussions specific to the two reliability assessments presented can be found at the end of Chapters 4 and 5, along with a discussion of the research limitations. This final Discussion Chapter provides a summary discussion of the work presented in relation to the research questions identified.

6.1 Question 1 - Industry consensus on priority areas for development

A critical review of the literature relating to wave energy and reliability was reported in Chapter 2. Section 2.4 outlined the key sub-systems of a wave energy converter, before assessing several industry and government guidance documents outlining priority areas for sub-system development. In a unique contribution to the literature, these documents were reviewed within the context of device neutrality, to establish whether research for a particular sub-system would be beneficial to one particular device developer or beneficial to the broader industry.

This literature review clearly established industry consensus on priority sub-systems for development in the wave energy sector. All documents reviewed cited both power take off systems and mooring systems as areas for priority development. Additionally, electrical connectors were frequently cited as key areas for development, but did not appear in all reports. Following this review mooring systems were identified as a focus area for the work presented in this Thesis. Not only was this due to the unanimous recommendations from all reports but also due to the relatively device neutral nature of mooring systems and the potential for significant cost reduction through innovation (Low Carbon Innovation Coordination Group, 2012). Additionally the literature review established the majority of wave energy converter device types under development as floating devices with 53% point absorber types and 12% attenuator types (Thorpe, 2010); both these systems will be dependant on reliable, compliant mooring systems for successful operation.

This literature review supported the selection of mooring systems as the focus for the reliability assessments detailed in this Thesis.

The industry need for increased compliance in mooring systems was also established through the introduction of three novel mooring systems in Section 2.5.7, Page 107. The approaches applied for the reliability assessment of The Exeter Tether could equally be applied to the other novel mooring systems introduced in the Literature Review presented in Chapter 2. This includes identifying unique reliability challenges for each system and establishing a suitable test regime, using a combination of lab testing, field testing and sub-component testing.

6.2   Question 2 - Reduction of safety factors for standard mooring components given the reduced consequence of failure

The reliability assessment of a standard mooring shackle with regard to applied safety factors was presented in Chapter 4. This analysis is of significant interest as excessive safety factors lead to unnecessary costs. An optimum mooring system will be designed with adequate safety factors to survive the specified life time load spectrum without being over designed. As detailed in Chapter 2, Harris *et al.* (2004) clearly evidence the link between MBL and cost of mooring components (Figure 2.21, Page 91). This figure details the increase in £/m with MBL for a variety of typical mooring line materials. Comparable cost data for the shackles, purchased for the investigation presented in Chapter 4, is detailed in Figure 6.1. This details the increasing cost of shackles against WLL for standard D shackles supplied by CERTEX.

A trend line fitted to the data in Figure 6.1 shows that, in the range specified, the cost vs WLL is approaching an exponential relationship. At the lower loads a doubling of the specified WLL from 3 tonnes (29.4kN) to 6 tonnes (58.8kN) results in a cost increase of 141%.

It is interesting to relate the increase in shackle cost back to the findings for the shackle ultimate limit state tests in Section 4.4.2.1. When considering the embedded component safety factor of 4.5 present between the specified shackle WLL and the observed yield load of the shackle (note use of yield load rather than failure load) the 2.5 tonne shackle (24.5kN) could actually be used for loads up to 11.25 tonnes (110.3kN). Using the equation for the trend line calculated in Figure 6.1 the cost of these shackles
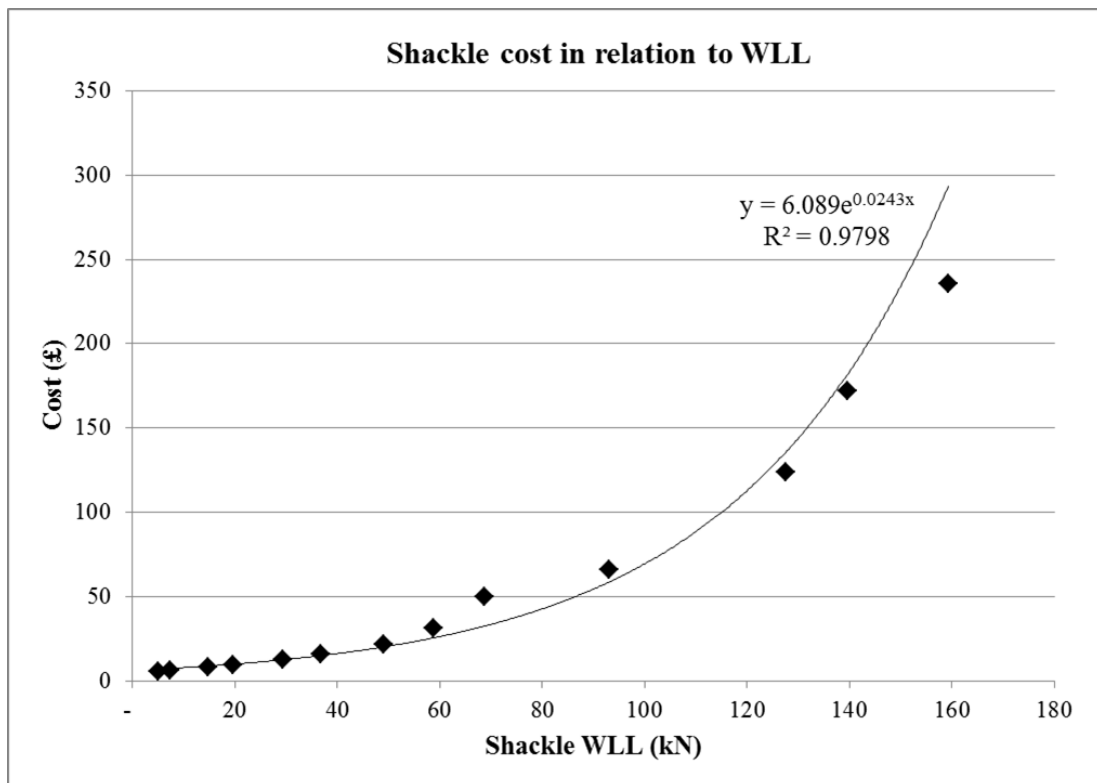
Figure 6.1: Cost Vs WLL of a standard large D shackle, type BS3032 with screw pin. Prices provided by Certex (Burtoft, 2015) and include VAT. Actual figures represented by black diamonds. Exponential trend line added to the data points for estimation purposes.

would be £11.05 and £88.89 for a 2.5 tonne and 11.25 tonne shackle respectively. Replacing one with the other represents a considerable cost saving. Clearly one would not design exactly to the yield load of a shackle and this exercise is purely for illustrative purposes, but it should be noted that this has only considered the embedded component safety factor before any additional mooring design safety factor has been added. Given that a standard mooring design would have added a further design safety factor of typically 1.7 (Det Norske Veritas, 2010a), the potential cost savings would be even greater. Considering the high numbers of shackles used per mooring line (as detailed in Chapter 3, Section 3.1.1 each SWMTF mooring limb uses 9 shackles) and the industry ambition to install arrays of multiple devices each with multiple mooring lines, the potential savings could quickly add up. As discussed previously, it is not only the reduced cost of the individual components that has benefits. The significantly reduced weight of down-rated components can have a knock on effect to the whole system, creating less weight on the mooring system which could lead to a reduced floater size. This downward spiral of weight and cost has potential benefits throughout the system.

Considering the static loads calculated through the ultimate limit state testing is however a simplification of the situation, and fatigue loading must also be considered. Any component deployed in a WEC device mooring limb will be subject to significant fatigue loading. Physical testing of the fatigue performance of the shackles was conducted at one load range, 10-90kN, and a large range of fatigue failures were observed with cycles to failure ranging from 19,952 - 101,526. Physical test results were compared to typical S-N curve predictions from DNV (Det Norske Veritas, 2011) and adjustments were made accounting for an appropriate stress concentration factor and the presence of a mean stress. These adjustments resulted in an S-N curve that provided a conservative prediction of fatigue life given the mean minus 2 standard deviations of the observed results (as specified by DNV guidance (Det Norske Veritas, 2011)).

Given the above adjustments the S-N curve was used to estimate the maximum load that could be applied for a deployment life of 10 years with an assumed cycle period of 8s. Given a pre-tension of 10,000N the maximum applied load calculated using the S-N curve was just 11,885N; less than half of the specified WLL (i.e. a FOS of 0.49) and just 10% of the specified MBL.

6. DISCUSSION

Assessing the shackle for fatigue loading in this way clearly shows the need for additional safety factors when designing a mooring system against fatigue. As detailed in the Literature Review, Section 2.5.5, the safety factor specified in DNV guidance (Det Norske Veritas, 2010a) applied to the mooring design for the fatigue limit state is detailed by Equation 2.11, Page 104 and can range from 5 - 8. This would give a resulting system factor of safety of 2.45 - 3.92, considerably less than calculated for the ultimate limit state. Although comparable literature regarding the fatigue performance of shackles is sparse, the dominance of fatigue failures in wave dominated environments has been raised as a concern by others (Grosenbaugh, 1995; Thies *et al.*, 2013a; Trask & Weller, 1995).

The work presented in Chapter 4 focused on the intrinsic variability in shackle manufacture which leads to the scatter observed in the fatigue results presented. This scatter leads to the design S-N curve being specified from collated test results minus two standard deviations and is part of the reason safety factors are required on mooring system designs. However, this component variability is not the only uncertainty in the design of mooring systems for WEC devices. Extrinsic factors, such as environmental parameters, are another source of uncertainty, further adding to the requirement for safety factors on component and system designs. There can be considerable annual variation in wave energy resource for a given location. As discussed by Tiron *et al.* (2015) mean wave power for a given location can vary significantly, as an example the West Coast of Ireland experiences an annual variation of up to 40%. For many device deployments however, wave estimates will be based on a limited period of monitoring of the wave climate, or based on numerical modelling using software such as SWAN. Neither of these routes however, can exactly predict the wave climate in the future. Physically monitoring a site using wave buoys is very informative, however will only measure the wave climates during a particular deployment and as such is unlikely to capture a 1 in 100 storm event. Although a numerical model can generate estimations over a longer period, there are still issues with accuracy in numerical modelling as discussed by Dodet *et al.* (2010), Thies *et al.* (2013a) and van Nieuwkoop *et al.* (2013). With van Nieuwkoop *et al.* (2013) stating that *"extreme significant wave heights are often underestimated by the wave model"*. Given design loads will generally be calculated by modelling a mooring system with anticipated wave climate data using software

such as Orcaflex® (as detailed in 2.3.2.7), and then applying appropriate safety factors for component specification, the quality of the data used for modelling can have a significant affect on these design loads. It is beyond the scope of this Thesis to fully investigate the limitations of the numerical modelling of wave climates but it is important to raise the point that this further adds to the uncertainties that lead to the requirement of safety factors on component and system designs in a WEC mooring system.

A further impact of the marine environment on the reliability of mooring system components is that of corrosion. Due to the limited time frame of the work presented in this Thesis it was not possible to subject the shackles investigated in Chapter 4 to corrosion, however given the proposed operating environment of the shackles, without adequate galvanic protection, corrosion will undoubtedly occur in the operating lifetime. The impact of corrosion on mooring chain is addressed by DNV in the guidance document DNV-OS-E301 relating to *Position mooring* (Det Norske Veritas, 2010a). This document suggests a corrosion allowance for chain ranging from 0.2 - 0.8mm/year, depending on the location within the mooring line, inspection and deployment location. Furthermore, due to the cyclical loading occurring in the mooring line, corrosion fatigue is likely to occur where-by cracks can initiate on surface areas of corrosion damage and crack growth rates are significantly increased by the corrosive environment, leading to a reduced component fatigue life (Schijve, 2009; Tomkins, 1979). A study presented by Palin-Luc *et al.* (2010) reviewing the effect of corrosion on low-alloy steel grade R5 (typically used for mooring chain manufacture) found that at 10^8 cycles the fatigue strength of pre-corroded specimens tested under artificial sea water flow was reduced by 74% in comparison to virgin specimens. The study additionally found that the scatter in fatigue strength of the pre-corroded specimens was greater than for virgin specimens. These findings were further supported by a study presented by Frendheim (2013) which found that the fatigue performance of R4 grade steel chain was significantly reduced following 10 years of operation on Asgard A FPSO. This reduction in strength caused by the effect of corrosion-fatigue is a further contributor to the requirement of safety factors when specifying mooring components based on as new MBL. A further threat to WECs highlighted by Tiron *et al.* (2015) is that of micro-fouling induced corrosion (MIC), whereby corrosion is exacerbated by the low pH conditions

created by bio-fouling organisms. This is an additional reliability consideration for mooring components.

The work presented in the shackle case study has shown that excessive margins are present in mooring component specification when assessed against ultimate limit state, these have the potential to lead to unnecessary costs. However, fatigue loading is a more complex issue and this work has shown that under a longer term fatigue loading regime, mooring components will fail below the specified WLL and as such, appropriate safety factors are required. Numerical modelling and analytical solutions, although providing some useful information, have not proved accurate enough to make load case design decisions without the support of physical testing. Given the additional unknowns relating to the measurement of wave climate (which is commonly used to predict peak and fatigue loads for a mooring system) and the potential degradation of the components due to corrosion, this work suggests that fatigue is the dominant concern with regard to shackle reliability, and current safety factors suggested for fatigue limit state are appropriate and should not be reduced. Given the findings from the shackle fatigue testing in conjunction with the uncertainties arising from the predicted load case and environmental effects, reliability would be compromised if safety factors were reduced.

6.3 Question 3 - Reliability assessment of a novel component

A novel mooring component, the Exeter Tether, under development by the University of Exeter was subjected to a reliability assessment, as reported in Chapter 5. A FMEA analysis was conducted on the tether (Section 5.2) and this was used to identify key reliability considerations that were novel to the P1 Tether Series of prototypes. Referencing the literature, Det Norske Veritas (2008), suggest that during early development phases a qualitative approach to reliability assessment may be more appropriate for novel technologies. Therefore, a range of physical test approaches were specified in order to further investigate the reliability considerations identified.

For much of this work, the term 'durability' was used. As outlined in the Literature Review (Chapter 2), the term durability encompasses both reliability and holding capacity, accounting for fatigue damage, wear, corrosion and other changes to material

properties (Weller *et al.*, 2014b). The term durability was felt more appropriate for much of this work which encompassed more aspects than the term reliability.

Initially, testing was conducted on the tether assembly to quantify the durability of the prototype as a whole. This testing was conducted both in a controlled laboratory environment at the DMaC test facility and also in the field through the deployment of four tethers on the SWMTF. The DMaC testing established a baseline TCLL value for the tether of 65%; this was compared to other ropes in the literature in Section 5.5.1, Table 5.17, Page 344 and for an early prototype 65% was established as a strong performance. The fatigue failure that occurred highlighted potential design improvements to the tether which were incorporated into tether P1-20, however due to un-even splice loading which led to an early failure these design alterations could not be validated.

The DMaC test facility was also used to establish a baseline tether performance to enable a comparison before and after a sea deployment at the SWMTF approaching 6 months. This benchmarking highlighted a marked increase in tether stiffness following deployment with the stiffness of tethers P1-3 and P1-8 increasing by 5% and 21% respectively. It was also noted that whilst the aim of the range of P1-Series tether designs was to provide a range of stiffness responses, following sea deployment the range of responses was reduced, with the performance of both tethers investigated becoming more aligned.

In addition to observing the functional change of the tether, the SWMTF field trial also allowed a qualitative investigation into the tether, reviewing the effects of bio-fouling and operational wear of sub-components. This investigation found that marine debris from bio-fouling had penetrated both the rope jacket and anti-friction membrane; evidence of fretting caused by this debris was identified. The field trial also confirmed the anti-friction membrane as an area of concern. Following the sea trial significant degradation of the membrane was observed and further work was identified to trial alternative membrane options.

Following the tether assembly testing, component testing was instigated. During the FMEA the polymer core was highlighted as a key reliability threat due to the unknown nature of the effects of both the marine environment and the repeated loading cycles on the EPDM material used to manufacture the polymer core. A series of polymer testing regimes were outlined to investigate these affects. EPDM was aged in sea water at elevated temperatures to speed up the ageing process. Key material property

alterations were detailed in Table 5.18, Page 354. Of note were the reduction in both tensile strength and elongation at break in tensile samples, in addition to an increased compression modulus (a stiffer response) for samples tested under compression. The validity of the Arrhenius extrapolation is discussed and establishing this relationship for the EPDM under investigation is highlighted as a key priority.

'Scroll tests' were used to observe the deformation of cords within the tether core bundle and found that strain for individual cords was up to 79% greater than the strain observed across the whole core bundle. This informed the fatigue compression testing of the cord material as it allowed the strains to be related to anticipated strains in an operational tether. Long term fatigue compression testing of EPDM cord observed an increase in radial and axial compression modulus which means greater resistance to compression.

Bringing these material elements together with the assembly testing a general trend was observed. Both the marine ageing and fatigue loading of EPDM material increased the stiffness of the samples. Complete tether assembly tests at the DMaC test facility observed an increase in tether dynamic axial stiffness when subjected to repeated cyclic loading during the TCLL tests. This was further supported by the comparison of tether performance before and after the SWMTF sea trial which also observed an increase in tether stiffness following field deployment. The results corroborate one another, all indicating an increased tether stiffness as a result of operating conditions. These findings are extremely important for further tether development as one of the principal aims of the tether is to specify stiffness for a particular device and location. These findings indicate that tether stiffness is likely to considerably evolve during use and it is critical that the mooring system design takes this into consideration. Further recommendations from this work will be detailed in Chapter 7, Section 7.2.2.

The final reliability work conducted on the novel tether design was an investigation into alternative anti-friction membrane materials following the poor performance of the Dacron sail cloth tape used during the SWMTF sea trials. Using a novel collet arrangement made specifically to facilitate this test work, four membrane options were exposed to 2,000 cycles of 0.2m travel at the DMaC test facility. This test work identified two layers of anti-friction membrane as having an advantage over one layer, due to the promotion of slip between the two layers. Additionally, Endumax TA23, which is a thin (55μm) UHMWPE tape, showed the most promising performance in this application,

with limited wear and a smooth surface following the displacement cycles. Further recommendations from this aspect of work will also be detailed in Section 7.2.2.

Referring to the original question, how should reliability be addressed, this case study has shown than any novel component will require a multi-faceted approach to reliability assessment. A FMECA as detailed in the literature (Det Norske Veritas, 2008) is an effective place to start and enables the identification of key reliability considerations for a novel system. Undoubtedly whole system testing is required (as conducted in this case study at DMaC and SWMTF) to establish overall system reliability and investigate component interactions that may affect long term reliability. Whole system testing also enables the identification of components requiring further investigation, such as the anti-friction membrane identified during tether assembly tests. Once specific areas have been highlighted as reliability concerns, bespoke component testing allows a thorough investigation of these critical areas, such as the work presented here on the polymer core and the membrane. Breaking down larger sub-systems in this way allows causal factors to be established, such as the observation in this work that both marine ageing and repeated compression cycles of EPDM lead to an increased stiffness of the tether as a whole. With this knowledge it is possible to quickly and effectively investigate alternative materials, without having to construct entire tether assemblies at great expense.

Given the early stage of reliability assessment conducted here, physical testing was utilised and a numerical modelling approach was not adopted for this case study. The critical reliability considerations for the tether could not be effectively modelled with available software packages and at this stage in development it was felt the key reliability considerations were most effectively addressed through physical testing. Although this was the right approach for this particular component, other novel components may be more readily modelled. As detailed in the Literature Review (Chapter 1) there are many benefits to computer modelling including reduced cost and reduced time enabling a quick investigation of multiple alternative designs.

6.4 Question 4 - Implications of novel mooring components on overall system reliability

In terms of the implications of novel mooring components on overall system reliability, the work conducted as part of this Thesis has shown that the long term performance of a novel component must be established before the full benefits on system reliability can be realised. For the mooring tether assessed, the FMEA conducted in Section 5.2.5 showed that catastrophic failure of the load carrying rope was unlikely as rope specification is a well known field in an established industry. However, the intended load mitigation introduced by the Exeter Tether, predominantly achieved through the material properties of the polymer core, and how this may evolve over time must be fully understood. The work presented in this Thesis has shown that the polymer core has the potential to become stiffer over time, due to both long term exposure to a marine environment (Section 5.4.2.1) and continuous compression cycles (Section 5.4.2.4). This increase in polymer stiffness is expected to lead to a stiffer tether response and therefore reduced peak load mitigation. This was observed in the presented tether assembly test results (Section 5.4.1.2). Although this change in performance may not lead directly to a catastrophic failure, if the peak load mitigation mechanism is not working, higher loads in the mooring system may eventually lead to a premature failure.

If the benefits of a reduction in the peak load are to be realised, which were estimated from numerical models as a peak tension reduction of a factor of three when replacing a nylon rope with the Exeter Tether (Parish, 2015), then this reduction must be permanent. As detailed in this Thesis, there is a significant correlation with cost of mooring components and specified MBL (Figures 2.21 page 91 and 6.1 page 372). One of the key aims of the Exeter Tether is to mitigate peak loads and lead to a downward design spiral of reducing loads and system costs. However, if the long term performance cannot be guaranteed, then the MBL of the other components in the mooring system cannot be down-rated and no reduction in system weight or cost will be observed. It is therefore critical to establish the long term performance of the Exeter Tether if overall system reliability is to be improved. The work presented in this Thesis has identified key areas that need further work to establish this.

The initial reliability assessment of the Exeter Tether reported in Chapter 5 highlighted some key design recommendations for future iterations of the Exeter Tether in

addition to several areas that require further work to fully establish the reliability implications. Both the design recommendations and areas of further work will be outlined in Section 7.2.2.

Chapter 7

Conclusions and further work

Contents

The previous Chapter discussed the work presented in this Thesis within the context of the overarching research question **'How can reliable mooring solutions for wave energy devices be developed?'** and the four research questions set out in order to address this question. This Chapter will summarise the main conclusions from the work presented, and outline key recommendations for further work.

7.1 Conclusions

To ascertain the focus for this Thesis, a thorough literature review of journal papers, industry and government guidance documents was conducted and presented in Chapter 2. This review firstly established wave energy generation as a potentially viable, low carbon form of energy generation, with economic and environmental advantages, particularly to the UK. Following a review of device development, a focused study on

wave energy converter sub-systems sought to establish whether there was any consensus on priority areas for further development to support the overall advancement of the marine energy sector. This study concluded that there is broad industry consensus on priority sub-systems for further development. The sub-systems identified as having the most benefit for further development were the mooring system and the power take off system.

In addition to establishing the mooring system as a key sub-system for development, the literature review also established reliability as a key issue for the marine energy sector, affecting investor confidence and proving a hindrance to sector development. The definition of reliability was established and discussed in the broader context of terms such as durability, survivability and maintainability. An overview of reliability techniques was conducted to inform the methods applied in this Thesis.

Through this review of the literature, mooring system reliability was selected as the focus for the work presented in this Thesis, and the specification of the overarching research question detailed above.

To investigate mooring system reliability, two research approaches were identified, one reviewing a standard mooring component and another reviewing a novel mooring component. The conclusions from each of these approaches is detailed in the following sections.

7.1.1 Standard mooring component conclusions

The first approach, presented in Chapter 4, assessed a standard mooring component, the shackle. Given much of the existing industry guidance is based on the oil and gas industries, where a mooring failure has severe consequences, a key focus for this case study was whether there was any scope in reducing safety factors due to the reduced consequence of a mooring line failure for a wave energy device, and hence the reduced risk associated with a failure[1]. This study used a combination of numerical modelling, experimental testing and analytical estimations to review whether current

---

[1]The overall risk of a failure is the result of the probability of the failure multiplied by the consequence of the failure (Hamedni & Bittencourt Ferreira, 2014) as detailed in Chapter 1. Additionally, specific *'Consequence Classes'* are used in the specification of the safety factor required for a given mooring system design, as detailed in Chapter 2, Section 2.5.5.2, Page 103.

safety factors applied to mooring designs are appropriate. Numerical modelling proved a useful tool for identifying potential failure modes however did not predict the failure modes observed in ultimate limit testing. A potential output from this work is utilising results from the numerical model to identify areas of weakness which could inform the inspections conducted on components, such as the dye penetrant testing utilised to identify fatigue cracks in Chapter 4. The results from the numerical models were conservative in predicting loads to failure and fatigue life of the shackles. The numerical models were used to identify stress concentration factors which were then used with published S-N curves to relate nominal tensile stress to peak tensile stress in the analytical estimations.

Physical testing of the shackles established large embedded component safety factors when testing in ultimate limit state (8.6 in relation to the specified WLL). When applying a typical mooring system design safety factor of 1.70 to this, the resulting safety factor of 14.6 was deemed excessive given the reduced consequence of a mooring line failure. However, when reviewing the shackles in relation to fatigue limit state, such a margin was not observed. Fatigue testing at one load range was conducted to compare with a typical S-N curve as published by DNV (Det Norske Veritas, 2011). By adjusting the curve to account for mean stress effects and stress concentration factors, the S-N curve was established as conservative. The S-N curve was then used to estimate the load at which a shackle could sustain a 10 year operating life with a typical cycle period of 8 seconds. The load was established as approximately half of the specified WLL of the shackle (an embedded component safety factor of 0.49). Given the suggested range of safety factors applied in a typical mooring design for fatigue, the total safety factor range was established as 2.45 - 3.92. A brief discussion regarding extrinsic uncertainties such as wave climate prediction for wave energy deployments and the impact of corrosion on mooring system component reliability concluded that this total safety factor is not excessive and there is limited scope to reduce it.

This work has shown that fatigue failures are the dominant concern for the reliability of wave energy mooring systems. It has also highlighted the complexity of the stress distribution within a shackle, and further consideration of shear dominated failures is required. Although the focus of the work has been on wave energy converters, the findings are just as applicable to other marine energy fields that require floating

platforms in dynamic sea states, such as floating wind. Further work identified to develop these findings is suggested in Section 7.2.1.

7.1.2 Novel mooring component conclusions

The second approach conducted a reliability assessment of a novel mooring component, The Exeter Tether. The P1-Series of tether prototypes was manufactured to prove the working concept of the Exeter Tether. Reliability was not a key consideration in this original design so the research presented in this Chapter provides an initial reliability assessment of the P1-Series in order to inform future design iterations. Work presented focused on reliability aspects unique to the tether, including tether assembly interactions, the use of EPDM in the polymer core (which had no known data regarding use in a marine environment or fatigue compression testing), and a review of the anti-friction membrane in this completely novel application.

Tether assembly durability testing showed promising results, with a maximum TCLL value of 65% achieved and clear areas for improvement highlighted. The tether successfully survived 6 months of sea trials. The impact of bio-fouling and marine debris accumulation were highlighted as areas of concern, and further tether design improvements following this work were identified. In the case of the anti friction membrane (also identified as an area of concern following sea trials), a bespoke testing regime was instigated to trial alternative membrane solutions. An increase in tether dynamic axial stiffness was observed following assembly trials in the laboratory and at sea. This must be accounted for during tether design stage ensuring the correct 'worked tether' properties are designed for. Further recommendations following these durability assessments will be detailed in Further Work, Section 7.2.2.

Detailed testing of the polymer material used for the tether core construction was conducted. This work raised concerns regarding the impact of accelerated marine ageing on key material properties including 16% reduction in tensile strength, 14% reduction in elongation at break and considerably reduced fatigue performance. With regard to tether operation, the most significant finding was an average 22% increase in radial compression modulus, observed following marine ageing. This material property is key to tether operation therefore the observation of such a significant alteration requires some attention. Further work is required, assessing the data produced from ageing

the polymer at different temperatures and for different lengths of time, to confirm the validity of the accelerated ageing regime.

In addition to the marine ageing, durability tests exposing the polymer material to realistic operational compression loads were conducted. These also led to an increase in radial compression modulus of the material (15% on average), despite an equivalent operational time of just 65 days. The observed changes in material property are intuitively expected to result in a stiffer tether response, which agrees with the observed tether assembly tests.

A qualitative investigation was conducted on the anti-friction membrane assessing different material options and varying the number of layers installed. The optimum result was achieved using two layers of Endumax TA23, a 55μm thick UHMWPE tape.

To realise the full benefits of the novel mooring tether in a complete mooring system, the long term performance must be proven. The work presented in this Thesis suggests that the dynamic axial stiffness of the tether has the potential to increase over time (due to ageing in the marine environment and repeated compression). This increased stiffness directly opposes the design intention of the tether which is to reduce stiffness leading to reduced mooring system loads and hence allow the specification of lower rated components and reduce the overall weight and cost of the mooring system. In addition these reductions should lead to further benefits in the overall system design (such as a reduced floater size). If a mooring system design was specified based on the anticipated load mitigation of the tether, but over time the load mitigation diminished, then the reliability of the overall system would be severely compromised. This should therefore be a key focus for further development of the tether.

Relating this work back to the Certification Approach outlined by DNV in Det Norske Veritas (2008) and presented in Chapter 2 (Figure 2.24, Page 101), the Tether reliability assessment presented in Chapter 5 has addressed many of the requirements necessary for a 'New technology' to become classed as a 'Proven technology'. This system of certification, outlined by DNV, was used to inform the approach applied for the assessment of the Exeter Tether. However, to become formally certified a 'Qualification Basis' would have to be specified, listing specific criteria against which to assess the tether.

Further work on the Exeter Tether needs to be addressed before reaching this Qualification Stage, and the next steps to progress this are presented in the last section of this Chapter; Further Work, Section 7.2.1.

7.2 Further work

The work presented in this Thesis has been based on two case studies and the further work will be described for each study individually.

7.2.1 Standard mooring component further work

The reliability case study conducted on a standard shackle established that, given the embedded component safety factors of the shackle under investigation, further safety factors typically applied for mooring system design (Det Norske Veritas, 2010a) are excessive for the ultimate limit state but more appropriate for the fatigue limit state. This work was based on a limited number of load cases, with fixed amplitude and fixed frequency of load cycles. This is clearly a simplification of a real sea state and an interesting extension to this work would be to utilise actual mooring load data from a wave energy deployment and review the safety factors in relation to the relative dominance of ultimate limit state or fatigue limit state. It should be noted that the relative contribution of each will be dependant on the specific load spectrum assessed. In the absence of mooring data a collaboration with an oceanographer to establish a realistic wave spectrum for a given deployment could be used for modelling purposes. Through global modelling using software such as Orcaflex® a typical floating device could be modelled to provide a load spectrum for the mooring system given the wave climate. This could be used to conduct an assessment of the relative contribution of fatigue loads and peak loads to the reliability of a typical shackle within the mooring system, relating this to design safety factors suggested by guidance documents.

As discussed in Section 6.2, due to the relatively short term nature of this work, the effects of corrosion have not been considered. Corrosion can have a significant effect on component reliability and a further extension to this work would be to conduct some longer term investigations into the impacts of corrosion on fatigue life on a standard shackle. As well as physical testing, numerical modelling could be utilised, removing material to represent the loss of material due to corrosion, and observing the impacts

on ultimate and fatigue limit of the shackle.

As described in Chapter 2 there is very limited information on mooring system reliability within the marine energy sector. This is in part due to the fledging nature of the industry but also due to the commercial advantage perceived by such knowledge. The highly dynamic nature of wave energy devices in particular does introduce new challenges for mooring system design not accounted for by existing guidance, predominantly developed for the oil and gas industry, with relatively static deployments. Improved industry collaboration, sharing data on mooring loads measured and failures observed would be beneficial in moving towards reliable but not excessively designed mooring systems. As detailed in Chapter 2, the OREDA database (OREDA, 2015) is already effectively sharing information on offshore reliability for the oil and gas industries, and the SPARTA initiative has started collating similar data for the offshore wind industry (The Crown Estate, 2015). An equivalent for the marine energy sector would be hugely beneficial. Other examples of successful data sharing from the oil and gas industry include the joint industry project *Floating production systems - mooring integrity* (Noble Denton Euorpe Limited, 2006). Similar sharing of data for the marine energy sector would further progress the optimisation of mooring systems for marine energy deployments.

Due to the limited availability of specific fatigue data for off-the-shelf mooring components, the analytical fatigue analysis presented in Chapter 4 utilised S-N curve data published by DNV (Det Norske Veritas, 2010a). In the absence of suppliers providing this information, some suggestions are made to improve the usefulness of the generic S-N curves provided by DNV:

- Given the strong influence of the stress concentration factor on the fatigue results, a useful addition to the DNV guidance would be the publication of appropriate stress concentration factors for use with the published S-N curve. DNV's *Position Mooring* guidance (Det Norske Veritas, 2010a) currently states that for estimations of the fatigue performance of shackles in mooring systems, the B1 S-N curve detailed in the *Fatigue design of offshore steel structures* guidance (Det Norske Veritas, 2011) should be use with *"appropriate stress concentration factors obtained by a finite element method"*. Given the complexities in developing a

finite element model of the shackle, as demonstrated in this Thesis, an extremely helpful addition to this guidance would be the additional publication of stress concentration factors for use with this curve. It would be necessary to calculate these factors for different shackles such as bow shackles, dee shackles, safety shackles with a bolt etc. A common reference for this would certainly improve the ease and accuracy with which fatigue life estimations could be conducted for the design of mooring systems.

- The published S-N curves used in this work (Det Norske Veritas, 2011) are based on tensile-tensile loading and through the experimental aspects of this work it has been shown that many fatigue failures occur under shear loading (Mode II). Further discussion of shear dominated failures within the guidance would be useful, and the publication of generic shear S-N curves to assist mooring developers in designing against shear fatigue failures would also be a welcome addition to the guidance.

- This work has also shown that the literature widely acknowledges that the presence of a mean stress has an affect on fatigue life. Given that many marine energy mooring system deployments will have a mean stress, guidance from DNV on the most appropriate mean stress adjustment method would also be helpful. Following a review of the literature in this Thesis, the Smith, Watson and Topper approach was established as the most appropriate. If a standard mean stress adjustment approach could be advised within the DNV guidance, it would ensure a consistent approach to mooring system design across the sector.

7.2.2 Novel mooring component further work

Chapter 5 focused on the key reliability considerations of the novel mooring component the Exeter Tether. From this work several recommendations for further tether development have been highlighted. These are detailed below:

- Improved termination of the polymer core assembly within the rope jacket is required. As trialled in P1-20, it is suggested that a more gradual decrease in radius of the core bundle is required to avoid promoting a rope failure at this interface. Further TCLL testing of such a prototype is required to quantify any

improvements. The P1-20 trial used articulated core components to round the end of the core bundle, however this was observed to pull away from the main bundle during testing. A method for moulding a rounded end onto the original bundle to avoid this would be advantageous.

- Improved quality control of rope splicing to ensure even distribution of load across eye splice is required given the limited alternative termination options.

- To obtain realistic load-extension profiles for mooring system design, new tethers should be subjected to realistic load levels and frequencies to approximately 1000 cycles. Initial profiles obtained from 5 - 10 cycles are not representative of longer term performance. Accuracy would be further improved by fully quantifying the worked vs new tether profile through sea trials.

- Use of a protective jacket around the tether to reduce the ingress of bio-fouling detritus as observed during sea trials is recommended.

In addition to these design recommendations, several areas of work have been identified that have potentially serious durability implications, and should be progressed from this initial reliability assessment. These are listed below:

- Research into the durability of the EPDM polymer currently used for the tether core highlighted concerns regarding potential degradation from marine ageing. Further work is required at a range of temperatures and over a range of time periods to establish the Arrhenius relationship and confirm the accuracy of the accelerated testing regime. Some EPDM samples have been subjected to further accelerated ageing at different temperatures at the IFRMER laboratories, and assessment of data from this work should be considered a priority. Material testing of naturally aged polymer is also suggested for complete validation.

- Relating to the above item, tension fatigue testing in particular showed dramatic deterioration following ageing. Once the above item is established, further work should be conducted representing more realistic tension fatigue conditions. The benefit of increasing the 'R' ratio of minimum to maximum strain to improve fatigue performance should also be investigated in addition to collaborating with

a polymer specialist to optimise the EPDM formula for improved fatigue performance.

- Fatigue compression testing of the EPDM polymer at low strains and (relatively) low cycle numbers raised concerns regarding the increase in radial compression modulus. An extended testing regime is recommend, exposing the polymer to higher compressive strains and for longer cycle numbers. Work presented here regarding self-heating of the polymer should be referred to ensuring that an appropriate frequency of cycling is selected to maintain a minimal temperature increase in the test samples.

- Following the above investigations if the properties of EPDM are found to be unsuitable for the tether application, alternative materials should be investigated. Natural rubber is a potential alternative with some information regarding fatigue performance available (Le Gac *et al.*, 2015a).

- Further research into an appropriate anti friction membrane between the tether rope and polymer core is required. Alternative materials trialled during research presented in this Thesis showed promising results but further improvements are required. The use of UHMWPE manufactured into a two layered sock system is suggested and should be further developed.

To realise the full potential of the load mitigation offered by the Exeter Tether, understanding long term performance is necessary to avoid compromising whole system reliability. Bringing together many of the aspects suggested above, clearly defining how the operating profile of the tether will evolve over time is necessary to enable the anticipated load mitigation and cost reductions to be achieved, and should be considered a priority in future tether development.

7.2.3 Ongoing work

A further project already in progress, with the potential to answer some of these questions for both component case studies, is the Open Sea Operating Experience to Reduce Wave Energy (OPERA) project (Ruiz-Minguela, 2016). Funded through the European Commission's Horizon 2020 programme, this project will see the deployment of

MARMOK, an offshore oscillating water column wave energy converter, using a network mooring system. The project will involve two deployments, each lasting a year: The first deployment will utilise a network mooring system with conventional polyester catenary mooring lines; the second deployment will see the installation of the Exeter Tether to replace the polyester catenary lines on the two mooring lines facing the dominant wave front. Condition monitoring of the mooring system throughout both deployments is intended to provide thorough mooring system load profiles in addition to quantifying the load mitigation offered by the Exeter Tether. Further to this, environmental monitoring will allow bench-lining of the mooring loads in relation to sea states and an assessment of whether the load mitigation offered by the Exeter Tether is maintained throughout the deployment, or whether this is compromised by a change in operating profile of the tether. Mooring load data captured from this project could also be used to develop the shackle case study through conducting a further assessment based on actual operating data as suggested in Section 7.2.1.

Key outcomes from this Thesis that will be adopted in the design of the full scale tethers for deployment in the second phase of the OPERA project include:

- The use of the aged operating profile of the Exeter Tether (ascertained following sea trials in Section 5.4.1.2) in the design process, to ensure reduced load mitigation is accounted for in the mooring design.

- Manufacturing the polymer core bundle to have tapered ends, moulded to the main body of the core to avoid the rope failure observed in the TCLL tests (Section 5.4.1.1).

- Improved inspection procedures for the eye splices will be set out to ensure quality control for the eye splices used to terminate the load carrying rope.

- An outer protective jacket will be manufactured around the load carrying rope to reduce bio-fouling ingress into the core of the tether as observed in Section 5.4.1.2.

- Finally, following results observed in the anti-friction membrane trials (Section 5.4.3), a UHMWPE material will be used as an alternative to the Dacron and PVC used in the P1-Series of tether prototypes.

7. CONCLUSIONS AND FURTHER WORK

Due to the time restrictions on this project there was not a large enough window to fully investigate an alternative polymer to use in the tether core. Given the data that has been collected on EPDM through this Thesis it was concluded that the informed use of EPDM for the polymer core was in preference to an alternative polymer with limited or no operational data. The restricted length of the deployment at one year also reduced the concerns regarding the change in operating profile, as this Thesis has already established the operating profile following a 6 month deployment (Section 5.4.1.2).

The OPERA project runs to May 2019 and a key deliverable is an operational analysis of the mooring system and quantification of the load mitigation offered by the Exeter Tether. In addition, mooring data from this project will be made available for further projects, such as a continuation of the shackle case study.

References

ABRAHAM, F., ALSHUTH, T. & JERRAMS, S. (2005). The effect of minimum stress and stress amplitude on the fatigue life of non strain crystallising elastomers. *Materials & design*, **26**, 239–245. 355

ABSG CONSULTING INC (2015). Study on mooring system integrity management for floating structures. Tech. rep., The Bureau of Safety and Environmental Enforcement (BSEE). 345

ADZIEV, G., SEDMAK, A., ADZIEV, T. & SEDMAK, S. (2004). Structural mechanics applied to mooring components design. In *European Conference of Fracture 15, Stockolm 2004*. 219

ALLAN, G., GILMARTIN, M., McGREGOR, P. & SWALES, K. (2011). Levelised costs of wave and tidal energy in the uk: Cost competitiveness and the importance of banded renewables obligation certificates. *Energy Policy*, **39**, 23–39. 47, 48

ALSHUTH, T., ABRAHAM, F. & JERRAMS, S. (2002). Parameter dependence and prediction of fatigue properties of elastomer products. *Rubber Chemistry and Technology*, **75**, 635–642. 355

AMERICAN PETROLEUM INSTITUE (2005). Recommended practice 2SK. design and analysis of stationkeeping system for floating structures. 99, 100

ANDERSON, T.L. & ANDERSON, T. (2005). *Fracture mechanics: fundamentals and applications*. CRC press. 167, 168

ANDREASSEN, R. (2012). Offshore mooring chain - quality fabrication revisited. Presentation, Det Norske Veritas. 98

REFERENCES

ANSYS (2013). Mechanical user's guide (release 15.0). 161, 164, 168, 169

AQUAMARINE POWER (2013). Technology - how oyster wave power works. Online; accessed 25/04/2016, http://www.aquamarinepower.com/technology/how-oyster-wave-power-works.aspx. 44

ARNOLD, A. (2010). Port kembla wave generator on sea floor. Online news article Illawarra Mercury; accessed: 29/11/2015., http://www.illawarramercury.com.au/story/628562/port-kembla-wave-generator-on-sea-floor/. 95

AYRES, R. (2001). Characterizing polyester rope mooring installation damage. Tech. rep., Stress Engineering Services report to Minerals Management Service. 345

BAAJ, H.P. (2011). Maritime ropes briefing 1/2011. Tech. rep., Lankhorst Ropes. 344

BANFIELD, S., CASEY, N. & NATARAJA, R. (2005). Durability of polyester deepwater mooring rope. In *Offshore Technology Conference, 2 - 5 May, Houston, Texas.*, vol. 17510. 351

BANFIELD, S.J., FLORY, J.F., HEARLE, J.W. & OVERINGTON, M.S. (1999). Comparison of fatigue data for polyester and wire ropes relevant to deepwater moorings. In *18th International Conference on Offshore Mechanics and Arctic Engineering Proceedings*. 107

BANFIELD, S.J., HEARLE, J.W.S., LEECH, C.M., TEBAY, R. & LAWRENCE, C.A. (2001). Fibre rope modeller (frm): a cad program for the performance and prediction of advanced cords and ropes under complex loading environments. *Techtextil, Germany*. 71

BASTID, P. & SMITH, S.D. (2013). Numerical analysis of contact stresses between mooring chain links and potential consequences for fatigue damage. In *ASME 2013 32nd International Conference on Ocean, Offshore and Arctic Engineering*, V02BT02A037–V02BT02A037, American Society of Mechanical Engineers. 220, 221

BAYAR, T. (2013). Testing times for european marine energy. *Power Engineering International*, 11–15. 57

BBC (2014a). Jobs go after no buyer found for pelamis wave business. Online; accessed 22/01/2016, http://www.bbc.co.uk/news/uk-scotland-scotland-business-30560980. 43

BBC (2014b). Jobs threat as aquamarine power 'downsizes'. Online; accessed 22/01/2016, http://www.bbc.co.uk/news/uk-scotland-scotland-business-30313111. 44

BBC (2014c). Wave power firm pelamis calls in administrators. Online; accessed 22/01/2016, http://www.bbc.co.uk/news/uk-scotland-scotland-business-30151276. 43

BBC (2015a). Aquamarine power boosted by european union grant. Online; accessed 22/01/2016, http://www.bbc.co.uk/news/uk-scotland-scotland-business-34250777. 44

BBC (2015b). Aquamarine power calls in administrators. Online; accessed 22/01/2016, http://www.bbc.co.uk/news/uk-scotland-scotland-business-34659324. 44

BBC (2015). Jobs lost as wave energy firm aquamarine power folds. Online; accessed 22/01/2016, http://www.bbc.co.uk/news/uk-scotland-scotland-business-34901133. 22

BELLOWS, R.S., MUJU, S. & NICHOLAS, T. (1999). Validation of the step test method for generating haigh diagrams for ti-6al-4v. *International journal of fatigue*, **21**, 687–697. 154

BENGTSSON, N. & EKSTRM, V. (2010). Seaflex. the buoy mooring system: Increase life cycle and decrease cost for navigation buoys. Tech. rep., Navigations Teknik. 109

BEXCO (2014). *Deeprope; polyester and dyneema mooring ropes manual*. 345, 347, 348

BITTENCOURT, C. (2007). DNV OSS-312 Standardisation in the renewable marine energy sector. In *2nd International Seminar on Ocean Energy*, paper 64. 59

BITTING, K.R. (1980). The dynamic behavior of nylon and polyester line. Tech. rep., DTIC Document. 349

REFERENCES

BOAKE, C.B., WHITTAKER, T.J., FOLLEY, M. & ELLEN, H. (2002). Overview and initial operational experience of the limpet wave energy plant. In *The Twentieth International Offshore Polar Engineering Conference, 26-31 May 2002, Kitakyushu, Japan.*, 586–594. 74, 76

BOUD, R. (2002). Status and research and development priorities 2003. wave and marine current energy. Tech. rep., UK Department of Trade & Industry. 38, 39, 55, 72, 80, 87, 88

BOUD, R.C.T. (2012). Carbon trust: UK wave energy resource. Tech. rep., AMEC Envrionment & Intrastructure UK Ltd on behalf of the Carbon Trust. 22, 33, 34

BOWIE, A. (2012). *Flexible Moorings for Tidal Current Turbines*. Ph.D. thesis, University of Strathclyde. 347

BOYCE, B. & RITCHIE, R. (2001). Effect of load ratio and maximum stress intensity on the fatigue threshold in Ti-6Al-4V. *Engineering Fracture Mechanics*, **68**, 129–147. 170

BRIDON (2015a). Fibre rope catalogue. Online; accessed 11/01/2016, http://www.bridon.com/china/x/downloads/fibre/Fibre.pdf. 251, 349, 350

BRIDON (2015b). Technical information. Online; accessed 08/12/2015, http://www.bridon.com/russia/x/downloads/fibre/technical.pdf. 114

BROWN, A. (2009). *Towards reliable and survivable ocean wave energy converters*. Ph.D. thesis, Oregon State University. 50, 52, 59, 60, 63

BSI (1989). BS 6349-6: Maritime structures: Design of inshore mooring and floating structures. 98

BSI (2011). ISO 7743:2011. Rubber, vulcanized or thermoplastic - determination of compression stress-strain properties. 262, 265

BUGG, D., VICKERS, D., DORCHAK, C. *et al.* (2004). Mad dog project: Regulatory approval process for the new technology of synthetic (polyester) moorings in the gulf of mexico. In *Offshore Technology Conference, Houston, Texas, USA.*, Offshore Technology Conference. 107

BUREAU OF OCEAN ENERGY MANAGEMENT (2011). Catastrophic failures in mooring systems possibly put floating structures at risk. Tech. rep., U.S. Department of the Interior. 95

BUREAU VERITAS (2007). Certification of firbre ropes for deepwater offshore services. 351

BUREAU VERITAS (2015). Classification of mooring systems for permanent offshore units. *NR 493DTR03E*. 99

BURTOFT, C. (2015). BS3032 shackles "a" - type screw pins. Personal communication - email 02/02/2015. 372

CANTOURNET, S., DESMORAT, R. & BESSON, J. (2009). Mullins effect and cyclic stress softening of filled elastomers by internal sliding and friction thermodynamics model. *International Journal of Solids and Structures*, **46**, 2255–2264. 317

CARBON TRUST (2005). Guidelines on the design and operation of wave energy converters. 52, 59, 60, 63, 67, 70, 75, 99

CARBON TRUST (2007). Key marine energy component technologies for cost reduction r&d. Black & Veatch for the Carbon Trust. 45, 46, 80, 81, 87, 88

CARBON TRUST (2011). Accelerating marine energy: The potential for cost reduction - insights from the carbon trust marine energy accelerator. Tech. rep. 33, 47, 54

CELINA, M., GILLEN, K. & ASSINK, R. (2005). Accelerated aging and lifetime prediction: review of non-arrhenius behaviour due to two competing processes. *Polymer Degradation and Stability*, **90**, 395–404. 253, 254, 357

CHENG, X., ZHANG, H., LI, H. & SHEN, H. (2015). Effect of tempering temperature on the microstructure and mechanical properties in mooring chain steel. *Materials Science and Engineering: A*, **636**, 164–171. 98

CHOI, K. & HAMMOUDEH, S. (2010). Volatility behavior of oil, industrial commodity and stock markets in a regime-switching environment. *Energy Policy*, **38**, 4388–4399. 22

REFERENCES

CHOI, Y.J., GILBERT, R.B., DING, Y. & ZHANG, J. (2006). Reliability of mooring systems for floating production systems. Tech. rep., Offshore Technology Research Center, Texas A&M University. 95

CHRISTENSEN, L., FRIIS-MADSEN, E. & KOFOED, J. (2005). The wave energy challenge: the wave dragon case. In *POWER-EN 2005 Europe Conference*. 94

CHRISTIANSEN, N.H., VOIE, P.E.T., HGSBERG, J. & SDAHL, N. (2013). Efficient mooring line fatigue analysis using a hybrid method time domain simulation scheme. In *ASME 2013 32nd International Conference on Ocean, Offshore and Arctic Engineering*, American Society of Mechanical Engineers. 217

CLÉMENT, A., MCCULLEN, P., FALCÃO, A., FIORENTINO, A., GARDNER, F., HAMMARLUND, K., LEMONIS, G., LEWIS, T., NIELSEN, K., PETRONCINI, S. *et al.* (2002). Wave energy in europe: current status and perspectives. *Renewable and sustainable energy reviews*, **6**, 405–431. 34, 55

CORDAGE INSTITUE (2015). *International Standard CI-1500A Test Methods for fiber rope physical properties*. Cordage Institue. 246

CORSATEA, T. & MAGAGNA, D. (2013). Overview of european innovation activities in marine energy technology. Tech. rep., Publications Office of the European Union, Luxembourg, (doi:10.2790/99213). 47

CUI, W. (2002). A state-of-the-art review on fatigue life prediction methods for metal structures. *Journal of marine science and technology*, **7**, 43–56. 217

DANKO, P. (2014). Pioneering pelamis falters, but scotland looks to drive wave energy tech convergence. Breaking Energy Online; accessed 24/11/2014, http://breakingenergy.com/2014/11/24/pioneering-pelamis-falters-but-scotland-looks-to-drive-wave-energy-tech-convergence/. 22, 57, 210

DAVIES, P. & EVRARD, G. (2007). Accelerated ageing of polyurethanes for marine applications. *Polymer Degradation and Stability*, **92**, 1455–1464. 357

DAVIES, P., WELLER, I.S. & JOHANNING, I.L. (2012). Testing of synthetic fibre ropes. Tech. rep., MERiFIC. 351

DAVIES, P., JOHANNING, L., WELLER, S. & BANFIELD, S. (2014). A reveiw of sythetic fibre moorings for marine energy applications. In *International Conference on Ocean Energy, Halifax.*. 107, 108

DAY, A., BABARIT, A., FONTAINE, A., HE, Y.P., KRASKOWSKI, M., MURAI, M., PENESIS, I., SALVATORE, F. & SHIN, H.K. (2015). Hydrodynamic modelling of marine renewable energy devices: A state of the art review. *Ocean Engineering*, **108**, 46–69. 35

DEMING, T.J. (1999). Mussel byssus and biomolecular materials. *Current opinion in chemical biology*, **3**, 100–105. 294

DENGEL, D. & HARIG, H. (1980). Estimation of the fatigue limit by progressively increasing load tests. *Fatigue & Fracture of Engineering Materials & Structures*, **3**, 113–128. 154

DEPARTMENT FOR BUSINESS ENTERPRISE AND REGULATORY REFORM (2008). Atlas of UK marine renwable energy resources - a strategic environmental assessment report. Tech. rep., Crown Copyright. 33

DEPARTMENT OF ENERGY AND CLIMATE CHANGE, UK (2010). Marine energy action plan: Executive summary and recommendations. Tech. rep. 53, 83, 87, 88

DEPARTMENT OF ENERGY AND CLIMATE CHANGE, UK (2011). Renewable energy roadmap. 54

DEPARTMENT OF ENERGY AND CLIMATE CHANGE, UK (2015a). Dukes 2015 chapter 5: Electricity. Tech. rep., Department of Energy and Climate Change. 22, 34

DEPARTMENT OF ENERGY AND CLIMATE CHANGE, UK (2015b). Dukes 2015 chapter 6: Renewable sources of energy. Tech. rep., Department of Energy and Climate Change. 34

DET NORSKE VERITAS (2008). DNV-OSS-312 Certification of tidal and wave energy converters. *Offshore ServiceSpecification DNV-OSS-312*. 71, 99, 100, 101, 102, 128, 132, 134, 376, 379, 387

REFERENCES

DET NORSKE VERITAS (2010a). DNV-OS-E301: Position mooring. 22, 67, 98, 99, 100, 101, 105, 130, 154, 175, 213, 214, 216, 221, 229, 373, 374, 375, 388, 389

DET NORSKE VERITAS (2010b). Fatigue assessment of ship structures - classification notes no.30.7. Tech. rep., Det Norske Veritas. 69

DET NORSKE VERITAS (2011). DNV-RP-C203: Fatigue design of offshore steel structures. 22, 67, 69, 98, 154, 155, 156, 175, 187, 194, 203, 204, 210, 213, 214, 217, 218, 221, 230, 231, 373, 385, 389, 390

DET NORSKE VERITAS (2013a). DNV-OS-E303: Offshore fibre ropes. 351

DET NORSKE VERITAS (2013b). DNV-OS-J103: Design of floating wind turbine structures. 99

DET NORSKE VERITAS (2015). DNVGL-SE-0163: Service Specification - Certification of tidal turbines and arrays. 59, 61, 100, 238

DIETER, G. (1997). *ASM Handbook Volume 20 Materials Selection and Design*. ASME Handbook. 50

DIMATTEO, A., LOVICU, G., DESANCTIS, M., VALENTINI, R., D'AIUTO, F. & SALVATI, M. (2011). Influence of galvanizing process on fatigue resistance of microalloyed steels. In *Conference IGF XXI Cassino 2011*. 216

DODET, G., BERTIN, X. & TABORDA, R. (2010). Wave climate variability in the north-east atlantic ocean over the last six decades. *Ocean modelling*, **31**, 120–131. 374

DONALD, C. (2013). Oyster will offer a pearl after gritty wave energy tests. Herald Scotland Online; accessed 15/04/2013, http://www.heraldscotland.com/business/13100131. 57

DOWLING, N. (2004). Mean stress effects in stress-life and strain-life fatigue. In *2nd SAE Brasil International Conference on Fatigue, Sao Paulo*, 78. 222, 224, 225, 227

DOWLING, N., CALHOUN, C. & ARCARI, A. (2009). Mean stress effects in stress-life fatigue and the walker equation. *Fatigue & Fracture of Engineering Materials & Structures*, **32**, 163–179, 93. 222, 223, 224, 225, 227

Dragon, W. (2005). Wave dragon. 42

Drew, B., Plummer, A. & Sahinkaya, M.N. (2009). A review of wave energy converter technology. *Proceedings of the Institution of Mechanical Engineers, Part A: Journal of Power and Energy*, **223**, 887–902. 35

DTI and OVE ARUP (2002). DTI technology road-map: Wave energy. Tech. rep., Department of Trade and Industry. 79

DTI and Ove Arup (2002). Sustainable energy technology route maps: Wave energy. Tech. rep., Departmenet of Trade and Industry. 87, 88

Elastomer Engineering Limited (2009). Rubber material properties. 353

EPDM Roofing Association (2003). Epdm membrane production: materials and manufacturing processes. 353

ETI and UKERC (2010). Eti/ukerc marine energy technology roadmap october 2010. Tech. rep. 82

European Commission (2015). Horizon 2020 work programme 2016 - 2017 10. 'secure, clean and efficient energy'. Tech. rep., European Comission. 55, 72

Eurpoean Marine Energy Centre (2013). Emec website. Online; accessed 18/06/2013, http://www.emec.org.uk/. 76

Eurpoean Marine Energy Centre (2015). Wave developers. Online; accessed 10/07/2016, http://www.emec.org.uk/marine-energy/wave-developers/. 35

Falcao, A. (2010). Wave energy utilization: A review of the technologies. *Renewable and sustainable energy reviews*, **14**, 899–918. 35

Ferrario, S., King, D. & Gould, J. (2004). The technical challenges in designing, building and installing a moored wave energy device at port kembla, new south wales. Tech. rep. 222

Flory, J.F. (1997). Patent No. 5611636 A: Tension member termination with segmented potting socket and cetnral passage. 345

REFERENCES

Flory, J.F., Banfield, S.P., Petruska, D.J. *et al.* (2004). Defining, measuring, and calculating the properties of fiber rope deepwater mooring lines. In *Offshore Technology Conference*, Offshore Technology Conference. 346, 351

Fraunhofer (2015). Wind energy information data pool. Tech. rep., Fraunjofer IWES. 58

Frendheim, S.H.L.L.H., S.; Reinholdsten (2013). Corrosion fatigue testing of used, studless, offshore mooring chain. 375

Friedlingstein, P., Andrew, R., Rogelj, J., Peters, G., Canadell, J., Knutti, R., Luderer, G., Raupach, M., Schaeffer, M., van Vuuren, D. *et al.* (2014). Persistent growth of co2 emissions and implications for reaching climate targets. *Nature geoscience*, **7**, 709–715. 21

FTL Technology (2015). Technical information - mechanical properties of rubber. Tech. rep. 353

Gadgets, H. (2009). Hacked gadgets forum - wave energy converter. Onlline; accessed 10/07/2016, http://hackedgadgets.com/2009/07/17/hydro-electric-wave-energy-converter/. 45

Gallagher, D. & Ku, A. (2013). Assessment and mitigation of low-toughness forged mooring components for floating structures. In *Offshore Technology Conference Brasil*, Offshore Technology Conference. 95

Gillen, K.T., Bernstein, R. & Derzon, D.K. (2005). Evidence of non-arrhenius behaviour from laboratory aging and 24-year field aging of polychloroprene rubber materials. *Polymer Degradation and Stability*, **87**, 57–67. 253

Gordelier, T., Johanning, L. & Thies, P. (2013). Reliability verification of mooring components for floating marine energy converters. In *SHF Marine Renewable Energy Conference. October 9-11, 2013. Brest, France*. 246

Gordelier, T., Parish, D., Thies, P.R. & Johanning, L. (2015). A novel mooring tether for highly-dynamic offshore applications; mitigating peak and fatigue loads via selectable axial stiffness. *Journal of Marine Science and Engineering*, **3**, 1287–1310.

29, 106, 109, 110, 115, 116, 117, 119, 120, 122, 123, 124, 125, 130, 242, 248, 294, 295, 348, 349, 351, 359

GROSENBAUGH, M.A. (1995). Designing oceanographic surface moorings to withstand fatigue. Tech. Rep. 5. 374

GUNN, K. & STOCK-WILLIAMS, C. (2012). Quantifying the global wave power resource. *Renewable energy*, **44**, 296–304. 34

GUOYANG, J. & TORGEIR, M. (1992). Reliability-based fatigue and fracture design criteria for welded offshore structures. *Engineering Fracture Mechanics*, **41**, 271–282, paper 56. 67

HALLIWELL, A. & HARRIS, R. (1988). A parametric experimental study of low-frequency motions of single point mooring systems in waves. *Applied Ocean Research*, **10**, 74–86. 73

HAMEDNI, B. & BITTENCOURT FERREIRA, C. (2014). Generic wec risk ranking and failure mode analysis (deliverable d5.2 of the structural design of eave energy devices). Tech. rep., DNV-GL. 22, 384

HARNOIS, V. (2014). *Analysis of highly dynamic mooring systems: peak mooring loads in realistic sea conditions.*. Ph.D. thesis. 139, 153, 167, 217

HARNOIS, V., JOHANNING, L. & THIES, P. (2013). Wave conditions inducing extreme mooring loads on a dynamically responding moored structure. EWTEC, Aalborg, Denmark. 173

HARNOIS, V., WELLER, S., JOHANNING, L., THIES, P.R., LE BOULLUEC, M., LE ROUX, D., SOUL, V. & OHANA, J. (2015). Numerical model validation for mooring systems: Method and application for wave energy converters. *Renewable energy*, **75**, 869–887. 69

HARRIS, R., JOHANNING, L. & WOLFRAM, J. (2004). Mooring systems for wave energy converters: A review of design issues and choices. *3rd International Conference on Marine Renewable Energy, 6th - 9th July, Blyth, UK.*. 36, 37, 38, 89, 90, 91, 106, 371

REFERENCES

HENDERSON, R. (2006). Design, simulation, and testing of a novel hydraulic power take-off system for the pelamis wave energy converter. *Renewable energy*, **31**, 271–283, paper 60. 70, 73

HOLPUCH, A. (2015). Long-suffering california can blame drought on global warming, experts say. Online news article, http://www.theguardian.com/us-news/2015/aug/20/california-drought-blame-global-warming Accessed: 29/11/2015. 21

HOUSE OF COMMONS (2012). The future of marine renewables in the UK volume 1. Tech. rep., The Energy and Climate Change Committee. 54

HUDSON, J., PHILLIPS, D. & WILKINS, N. (1980). Materials aspects of wave energy converters. *Journal of Materials Science*, **15**, 1337–1363, paper 107. 77, 90, 94

INTERNATIONAL ELECTROCHEMICAL COMMISION (2015). Iect ts 62600-10:2015 marine energy - wave, tidal and other water current converters - part 10: Assessment of mooring system for marine energy converters (mecs). Tech. rep. 99

INTERNATIONAL ENERGY AGENCY (2014). 2014 key world energy statistics. Tech. rep. 22

ISO (2005). ISO 37:2005 Rubber, vulcanized or thermoplastic - Determination of tensile stress-strain properties. 255

JING, F., ZHANG, L. & YANG, Z. (2012). Fatigue life prediction of mooring chains for a floating tidal current power station. *Journal of Marine Science and Application*, **11**, 216–221. 67, 68, 217

JOHANNING, L. & SMITH, G. (2009). Deliverable d7.3.2 consideration of the cost implications for mooring mec devices. Tech. rep., EquiMar. 94

JOHANNING, L., THIES, P. & SMITH, G. (2010). Component test facilities for marine renewable energy converters. In *Marine Renwable & Offshore Wind Energy Conference, 21-23 April 2010, London, UK.*, paper 4. 63, 68, 73, 139

JOHANNING, L., THIES, P.R., PARISH, D. & SMITH, G.H. (2011). Offshore reliability approach for floating renewable energy devices. In *ASME 2011 30th international*

conference on Ocean, offshore and Arctic engineering, 579–588, American Society of Mechanical Engineers. 136, 138

KOFOED, J.P., FRIGAARD, P., FRIIS-MADSEN, E. & SRENSEN, H.C. (2006). Prototype testing of the wave energy converter wave dragon. *Renewable energy*, **31**, 181–189. 75

KOH, R., S.K.; STEPHENS (1991). Mean stress effects on low cycle fatigue for a high strength steel. *Fatigue Fracture Engineering Materials and Structures*, **14**, 413–428, 77. 187, 222, 225

KROHN, D., WOODS, M., ADAMS, J., VALPY, B., JONES, F. & GARDNER, P. (2013). Wave and tidal energy in the uk: conquering challenges, generating growth. Tech. rep., renewableUK. 47, 48

KVITRUD, A. (2014). Anchor line failures - norwegian continental shelf 2010-2014. Tech. rep. 95, 96, 97

LANKHORST AUSTRAILA (2013). What is tcll? Lankhorst online; accessed 10/12/2015, http://www.leaustralia.com.au/what-is-tcll/. 242, 344

LE GAC, P.Y., LE SAUX, V., PARIS, M. & MARCO, Y. (2012). Ageing mechanism and mechanical degradation behaviour of polychloroprene rubber in a marine environment: Comparison of accelerated ageing and long term exposure. *Polymer Degradation and Stability*, **97**, 288–296. 253, 254, 355, 356, 357

LE GAC, P.Y., ARHANT, M., DAVIES, P. & MUHR, A. (2015a). Fatigue behavior of natural rubber in marine environment: Comparison between air and sea water. *Materials & Design*, **65**, 462–467. 254, 258, 259, 355, 357, 392

LE GAC, P.Y., DAVIES, P. & CHOQUEUSE, D. (2015b). Evaluation of long term behaviour of polymers for offshore oil and gas applications. *Oil & Gas Science and Technology–Revue dIFP Energies nouvelles*, **70**, 279–289. 357

LE SAUX, V., LE GAC, P.Y., MARCO, Y. & CALLOCH, S. (2014). Limits in the validity of arrhenius predictions for field ageing of a silica filled polychloroprene in a marine environment. *Polymer Degradation and Stability*, **99**, 254–261. 253, 357

REFERENCES

LOW, Y. & CHEUNG, S. (2012). On the long-term fatigue assessment of mooring and riser systems. *Ocean Engineering*, **53**, 60–71, paper 73. 95

LOW CARBON INNOVATION COORDINATION GROUP (2012). Technology innovation needs assessment (tina) marine energy summary report. Tech. rep., Low Carbon Innovation Coordination Group. 22, 45, 46, 47, 83, 87, 88, 370

MA, K.t., SHU, H., SMEDLEY, P., L'HOSTIS, D., DUGGAL, A. *et al.* (2013). A historical review on integrity issues of permanent mooring systems. In *Offshore Technology Conference*, Offshore Technology Conference. 95, 96, 97

MACDONALD, J. (2014). *Providing Scope for Reducing the Carbon Footprint of an Offshore Oil Rig*. Ph.D. thesis, University of Strathclyde. 42

MACGILLIVRAY, A., JEFFREY, H., HANMER, C., MAGAGNA, D., RAVENTOS, A. & BADCOCK-BROE, A. (2013). Ocean energy technology: gaps and barriers. Tech. rep., SI Ocean. 85

MACGILLIVRAY, A., JEFFREY, H. & WALLACE, R. (2015). The importance of iteration and deployment in technology development: A study of the impact on wave and tidal stream energy research, development and innovation. *Energy Policy*, **87**, 542–552. 76

MAGAGNA, D. & UIHLEIN, A. (2015). Ocean energy development in europe: Current status and future perspectives. *International Journal of marine energy*, **11**, 84–104. 35, 41, 47

MARINET (2013). Marine renewables infrastructure network for emerging energy technologies. Online; accessed 03/04/2014, http://www.fp7-marinet.eu/. 72, 73

MARK, J.E., ERMAN, B. & ROLAND, M. (2013). *The science and technology of rubber*. Academic press. 353

MASCIOLA, M., ROBERTSON, A., JONKMAN, J. & DRISCOLL, F. (2011). *Investigation of a FAST-OrcaFlex Coupling Module for Integrating Turbine and Mooring Dynamics of Offshore Floating Wind Turbines: Preprint.*. Citeseer. 68

MCCABE, A., BRADSHAW, A., MEADOWCROFT, J. & AGGIDIS, G. (2006). Developments in the design of the ps frog mk 5 wave energy converter. *Renewable energy*, **31**, 141–151. 74

MCEVOY, P. (2012). Combined elastomeric and thermoplastic mooring tethers. In *4th Int. Conf. on Ocean Energy, Dublin, Ireland.*. 109, 111

MCKENNA, H., HEARLE, J.W.S. & O'HEAR, N. (2000). *Handbook of fibre rope technology*. Woodhead Publishing in Textiles, Cambridge, UK. 246, 250, 284, 345, 351, 352

MENARD, K.P. (2008). *Dynamic mechanical analysis: a practical introduction*. CRC press. 270

MUELLER, M. & JEFFREY, H. (2008). UKERC Marine (wave and tidal current) renewable energy technology roadmap. Tech. rep. 87, 88

MUELLER, M. & WALLACE, R. (2008). Enabling science and technology for marine renewable energy. *Energy Policy*, **36**, 4376–4382. 71, 74

NANDHA, M. & FAFF, R. (2008). Does oil move equity prices? a global view. *Energy Economics*, **30**, 986–997. 22

NASH, W.A. (1992). *Statics and mechanics of materials*. McGraw-Hill International. 169

NOBLE DENTON EUORPE LIMITED (2006). Floating production system: JIP FPS mooring integrity. 70, 95, 96, 98, 211, 345, 389

OBERG, E., JONES, F.D., HORTON, H.L., RYFFEL, H.H. & GERONIMO, J.H. (1984). *Machinery's handbook 22nd Addition*, vol. 200. Industrial Press New York. 162

OCEAN ENERGY (2013). OE Technology. Online; accessed 13/06/2013, http://www.oceanenergy.ie/oe-technology/platform.html. 42

OCEAN POWER TECHNOLOGIES (2013). Utility scale systems. Online; accessed 13/06/2016, http://www.oceanpowertechnologies.com/products.html. 43, 44

REFERENCES

OIL COMPANIES INTERNATIONAL MARINE FORUM (2000). *Guidelines for the purchasing and testing of SPM hawsers*. Witherby's Publishing, Livingston, UK. 242, 245, 246

OIL COMPANIES INTERNATIONAL MARINE FORUM (2005). *Effective Mooring: Your guide to mooring equipment and operations*. Witherby's Publishing, Livingston, UK, 2nd edn. 345

OREDA (2015). Offshore and onshore reliablity data (OREDA). Online: accessed 16/04/2016, https://www.oreda.com/about-us/. 389

OVE ARUP ENERGY (2002). Wave energy: Technology transfer options and r&d requirements. Tech. rep., Department of Trade and Industry. 53

OYSU, C. (2007). Finite element and boundary element contact stress analysis with remeshing technique. *Applied Mathematical Modelling*, **31**, 2744–2753. 159

PACHAURI, R.K., ALLEN, M., BARROS, V., BROOME, J., CRAMER, W., CHRIST, R., CHURCH, J., CLARKE, L., DAHE, Q., DASGUPTA, P. *et al.* (2014). Climate change 2014: Synthesis report. contribution of working groups i, ii and iii to the fifth assessment report of the intergovernmental panel on climate change. 21

PACHECO, P., KENEDI, P.P., JORGE, J.C.F., GAMA, H., SAVI, M.A. & PAIVA, A. (2003). Modeling residual stresses in offshore chain links using finite element method. In *COBEM-2003, 17th International Congress of Mechanical Engineering, São Paulo*. 210

PALIN-LUC, T., PREZ-MORA, R., BATHIAS, C., DOMNGUEZ, G., PARIS, P.C. & ARANA, J.L. (2010). Fatigue crack initiation and growth on a steel in the very high cycle regime with sea water corrosion. *Engineering Fracture Mechanics*, **77**, 1953–1962. 375

PAREDES, G.M., BERGDAHL, L., PALM, J., ESKILSSON, C. & PINTO, F.T. (2013). Station keeping design for floating wave energy devices compared to floating offshore oil and gas platforms. In *10th European Wave and Tidal Energy Conference, Aalborg, Denmark.*. 98, 99, 100

PARISH, D. (2011). UK Patent Application GB 2476986 A Mooring Limb. 113

PARISH, D. (2015). *A novel mooring tether for highly dynamic offshore applications.* Ph.D. thesis. 107, 111, 113, 115, 116, 117, 119, 122, 130, 132, 134, 136, 137, 139, 142, 146, 235, 237, 238, 248, 344, 348, 349, 352, 359, 380

PARISH, D. & JOHANNING, L. (2011). International Patent Application Publication Number: WO 2011/089545 A1. Mooring Limb. 113

PARISH, D. & JOHANNING, L. (2014). US Patent No.US 8,807,060 B2. Mooring Limb. 113

PARSONS, T. (2013). Wave power. 43

PASCUAL, F.G. & MEEKER, W.Q. (1999). Estimating fatigue curves with the random fatigue-limit model. *Technometrics*, **41**, 277–289. 154

PELAMIS WAVE POWER (2013). Pelamis wave power. 43

PERKINELMER (2008). *Dynamic Mechanical Analysis (DMA): A Beginner's Guide.* PerkinElmer Inc. 270, 338

PETRECCA, G. (2014). World energy demand. In *Energy Conversion and Management*, 25–29, Springer. 21

PILKEY, W.D. (2005). *Formulas for stress, strain, and structural matrices.* John Wiley & Sons New Jersey. 165

POLINDER, H., DAMEN, M. & GARDNER, F. (2005). Design, modelling and test results of the AWS PM linear generator. *European transactions on electrical power*, **15**, 245–256. 76

RENEWABLE ENERGY RESEARCH GROUP - UNIVERSITY OF EXETER (2013a). Dynamic Marine Component Test Facility (DMaC). Online; accessed: 07/05/2013, http://emps.exeter.ac.uk/renewable-energy/research/research-interests/offshore/reliability/facilities/dynamicmarinecomponenttestfacilitydmac/. 139

RENEWABLE ENERGY RESEARCH GROUP - UNIVERSITY OF EXETER (2013b). FaB - Falmouth Bay Test Site. Online; accessed

REFERENCES

11/06/2013, http://emps.exeter.ac.uk/renewable-energy/research/research-interests/offshore/reliability/facilities/falmouthbaytestsitefabtest/. 76

RENEWABLE ENERGY RESEARCH GROUP - UNIVERSITY OF EXETER (2013c). South West Mooring Test Facility (SWMTF). Online; accessed 11/06/2013., http://emps.exeter.ac.uk/renewable-energy/research/research-interests/offshore/reliability/facilities/southwestmooringtestfacilityswmtf/. 136

RENEWABLEUK (2010). Channelling the energy - a way forward for the UK wave and tidal industry towards 2020. Tech. rep. 22, 33

RENEWABLEUK (2011). Wave and tidal energy in the UK: State of the industry report. Tech. rep. 35

RHINEFRANK, K., AGAMLOH, E., VON JOUANNE, A., WALLACE, A., PRUDELL, J., KIMBLE, K., AILLS, J., SCHMIDT, E., CHAN, P. & SWEENY, B. (2006). Novel ocean energy permanent magnet linear generator buoy. *Renewable energy*, **31**, 1279–1298. 70, 73, 75

RIDGE, I., BANFIELD, S. & MACKAY, J. (2010). Nylon fibre rope moorings for wave energy converters. In *OCEANS 2010*, 1–10, IEEE. 108

RINNBAUER, M. (2007). *Technical Elastomers*. SV corporate medioa GmbH. 238, 352

RUIZ-MINGUELA, P. (2016). Opera: Open sea operating experience to reduce wave energy cost. Online; accessed 04/07/2016, http://opera-h2020.eu/. 392

SALTER, S. (2003a). Proposals for a component and sub-assembly test platform to collect statistical reliability data for wave energy. In *Fourth European Wave Energy Conference, Cork.*, paper 59. 74

SALTER, S. (2003b). Research requirements for fourth generation wave energy devices. Tech. rep., paper 58. 72, 74, 75

SAMSON ROPE (2015). Samson technical bulletin: Tension fatigue testing. Online; Accessed 07/01/2016, http://www.samsonrope.com/Documents/Technical 246, 344

SANTHAMMA, K., RAJAGOPALAN, S. & GHOSE, M. (1988). Reliability testing and demonstration. *Reliability Engineering & System Safety*, **23**, 207–217, paper 63. 72

SCHEIRS, J. (2000). *Compositional and failure analysis of polymers: a practical approach*. John Wiley & Sons. 253, 357

SCHIJVE, J. (2003). Fatigue of structures and materials in the 20th century and the state of the art. *International journal of fatigue*, **25**, 679–702. 67, 154

SCHIJVE, J. (2009). *Fatigue of Structures and Materials*, vol. Second Edition with CD-ROM. Springer. 67, 216, 375

SI OCEAN (2013). Ocean energy: cost of energy and cost reduction opportunities. Tech. rep., Strategic Initiative for ocean energy. 45, 46, 47

SINCLAIR, J. (1998). *Collins English Dictionary*. Millenium Addition, Harper Collins Publishers. 49

SKJONG, R. & TORHAUG, R. (1991). Rational methods for fatigue design and inspection planning of offshore structures. *Marine Structures*, **4**, 381–406. 64, 67

SMITH, K., TOPPER, T. & WATSON, P. (1970). A stress-strain function for the fatigue of metals(stress-strain function for metal fatigue including mean stress effect). *Journal of Materials*, **5**, 767–778. 224

STANDARD NORGE (2009). Norwegian standard ns 9415. e: 2009 marine fish farmsrequirements for site survey, risk analyses, design, dimensioning, production, installation and operation. *Standard Norge, Lysaker*. 100

STARLING, M. (2009). Guidelines on reliability, maintainability and survivability of marine energy conversion systems. *London: European Marine Energy Centre (EMEC)*. 51, 52, 56, 59, 75

SUNDARAVADIVELU, R., HARIKRISHNA BABU, M. & MURUGAGANESH, R. (1991). Experimental investigation on a single point buoy mooring system. *Ocean Engineering*, **18**, 405–417. 73

SYVERTSEN, K. (1997). Fatigue reliability and life-cycle cost analysis of mooring chains. *International Journal of Offshore and Polar Engineering*, **7**. 95

TEIJIN (2014). Endumax - an ultra-strong thin tape with a high modulus. Tech. rep. 365

REFERENCES

THE CROWN ESTATE (2015). Pioneering sparta system for offshore wind farms goes live. Online; accessed 22/10/2015, http://www.thecrownestate.co.uk/news-and-media/news/2015/pioneering-sparta-system-for-offshore-wind-farms-goes-live/. 58, 389

THE UNIVERSITY OF EDINBURGH (2013). Flowave tt. Online; accessed 18/06/2013, http://www.flowavett.co.uk/. 75

THIES, P. & JOHANNING, L. (2010). Development of a marine component testing facility for marine energy converters. In *3rd International Conference on Ocean Energy, 6 - 8 October 2010, Bilbao, Spain.*, paper 1. 57, 60, 73, 139

THIES, P., FLINN, J. & SMITH, G. (2009). Is it a showstopper? Reliability assessment and criticality analysis for wave energy converters. 57, 60, 62, 63

THIES, P., JOHANNING, L. & SMITH, G. (2012a). Assessing mechanical loading regimes and fatigue life of marine power cables in marine energy applications. *Proceedings of the Institution of Mechanical Engineers, Part O: Journal of Risk and Reliability*, **226**, 18–32, paper 5. 69, 73

THIES, P., JOHANNING, L. & SMITH, G. (2012b). Lifecycle fatigue load spectrum estimation for mooring lines of a floating marine energy converter. Paper 2. 67

THIES, P., SMITH, G. & JOHANNING, L. (2012c). Addressing failure rate uncertainties of marine energy converters. *Renewable energy*, 360–370. 60, 64

THIES, P., JOHANNING, L., HARNOIS, V., SMITH, H. & PARISH, D. (2013a). Mooring line fatigue damage evaluation for floating marine energy converters: Field measruements and prediction (draft). *Renewable Energy.*. 217, 222, 374

THIES, P., JOHANNING, L., BASHIR, I., TUK, T., TUK, M., MARA, M. & MULLER-SCHUETZE, M. (2014a). Accelerated reliability testing of articulated cable bend restrictor for offshore wind applications. *International Journal of Marine Energy*, 65–82. 141

THIES, P., JOHANNING, L. & MCEVOY, P. (2014b). A novel mooring tether for peak load mitigation: Performance and service simulation testing. *International Journal of Marine Energy*, **7**, 43–56. 109, 110, 141

THIES, P., CROWLEY, S., JOHANNING, L., MICKLETHWAITE, W., YE, H., TANG, D., CUI, L. & LI, X. (2015). Novel mooring design options for high-intensity typhoon conditions - an investigation for wave energy in china. In *Structural Load & Fatigue on Floating Structures conference, London UK, 25 February 2015*. 109, 134

THIES, P.R., JOHANNING, L. & GORDELIER, T. (2013b). Component reliability testing for wave energy converters: Rationale and implementation. In *Tenth European Eave and Tidal Energy Conference, Aalborg, Denmark, 2-5 September, 20013.*, European Wave and Tidal Energy Conference. 94, 95

THOMPSON, D. & BEASLEY, D.J. (2012). SP-2209-OCN Handbook for marine geotechnical engineering. Tech. rep. 99

THORPE, T. (2010). 2010 survey of energy resources. Tech. rep., World Energy Council. 22, 34, 35, 36, 39, 42, 55, 370

THORPE, T.W. (1999). *A brief review of wave energy*. Harwell Laboratory, Energy Technology Support Unit. 33, 38

TIRON, R., MALLON, F., DIAS, F. & REYNAUD, E.G. (2015). The challenging life of wave energy devices at sea: A few points to consider. *Renewable and Sustainable Energy Reviews*, **43**, 1263–1272. 347, 374, 375

TITAH-BENBOUZID, H. & BENBOUZID, M. (2015). Marine renewable energy converters and biofouling: A review on impacts and prevention. In *Eleventh European Wave and Tidal Energy Conference Series, Nantes, France. 6-11 September, 2015.*, Paper–09P1. 347

TOMKINS, B. (1979). Role of mechanics in corrosion fatigue. *Metal Science*, **13**, 387–395. 375

TRASK, R.P. & WELLER, R.A. (1995). Cyclic fatigue testing of surface mooring hardware for the arabian sea mixed layer dynamics experiment. Tech. rep., Woods Hole Oceanographic Institution. 216, 374

TTI (2015). Fibre rope modeller (frm) pc based modelling software for rope design and performance prediction. Online, accessed: 09/11/2015 URL: https://www.tensiontech.com/software/fibre-rope-modeller. 71

REFERENCES

UNIVERSITY OF WISCONSIN-MADISON (2015). Image J. Online; accessed 10/11/2015, http://imagej.net/Welcome. 262

US DEPARTMENT OF ENERGY (2013). Energy efficiency and renewable energy - water power program. 35, 38, 40

VAN BEEST (2006). Green pin super shackles product brochure. Online; accessed 15/04/2016, http://www.vanbeest.com/getattachment/Products/Product-Brochures/GP_Super_Shackles_EN.pdf. 216

VAN BUSSEL, G. & ZAAIJER, M. (2001). Reliability, availability and maintenance aspects of large-scale offshore wind farms, a concepts study. In *Proceedings of MAREC*, 119–126. 50

VAN NIEUWKOOP, J.C., SMITH, H.C., SMITH, G.H. & JOHANNING, L. (2013). Wave resource assessment along the cornish coast (uk) from a 23-year hindcast dataset validated against buoy measurements. *Renewable energy*, **58**, 1–14. 374

VICENTE, P.C., FALCÃO, A.F. & JUSTINO, P.A. (2011). Optimization of mooring configuration parameters of floating wave energy converters. In *ASME 2011 30th International Conference on Ocean, Offshore and Arctic Engineering*, 759–765, American Society of Mechanical Engineers. 93

WALKER, K. (1970). The effect of stress ratio during crack propagation and fatigue for 2024-T3 and 7075-T6 aluminum. *Effects of Environment and Complex Load History on Fatigue Life, ASTM STP*, **462**, 1–14. 224

WASHINGTON, D., FONTAINE, E., MA, K.t., CARRA, C., KILNER, A., PHADKE, A., KUSINSKI, G. & LASKOWSKI, D. (2014). Industry survey of past failures pre-emptive replacements and reported degradations for mooring systems of floating production units. In *Offshore Technology Conference*, Offshore Technology Conference. 95

WASHIO, Y., OSAWA, H., NAGATA, Y., FUJII, F., FURUYAMA, H. & FUJITA, T. (2000). The offshore floating type wave power device "mighty whale": open sea tests. In *Proceedings of the Tenth International Offshore and Polar Engineering Conference, Seattle, USA, 28 May - 2 June, 2000*, vol. 1, 373–80. 75, 76

WAVE ENERGY CENTRE (2006). OWC Pico Power Plant - Technology. Online; accessed 13/06/2013, http://www.pico-owc.net/cms.php?page=542&wnsid=dbb177dd9668f08318207830330904df. 41

WAVE HUB (2013a). Marine licence apporved for first wave hub deployment. Wave Hub online; accessed 17/06/2013, http://www.wavehub.co.uk/news/press-releases/marine-licence-approved-for-first-wave-hub-deployment/. 76

WAVE HUB (2013b). Wave hub. Wave Hub online; accessed 18/06/2013, http://www.wavehub.co.uk/. 42

WAVE HUB (2015). Wave hub attracts new customer. Wave Hub online; accessed 20/10/2015, http://www.wavehub.co.uk/latest-news/wave-hub-attracts-new-customer. 42

WEHNER, T. & FATEMI, A. (1991). Effects of mean stress on fatigue behaviour of a hardened carbon steel. *International journal of fatigue*, **13**, 241–248, 80. 222, 225

WELLER, S., DAVIES, P., JOHANNING, I.L. & BANFIELD, S. (2013). Deliverable 3.5.2 from merific project: Guidance on the use of synthetic fibre ropes for marine energy devices. 119, 236, 289, 344, 345, 347

WELLER, S., DAVIES, P., VICKERS, A. & JOHANNING, L. (2014a). Synthetic rope responses in the context of load history: Operational performance. *Ocean Engineering*, **83**, 111–124. 346, 347

WELLER, S., HARDWICK, J., JOHANNING, L., KARIMIRAD, M., TEILLANT, B., RAVENTOS, A., BANFIELD, S., DELANEY, M., YEATS, B. & SHENG, W. (2014b). Deliverable 4.1: A comprehensive assessment of the applicability of available and proposed offshore mooring and foundation technologies and design tools for array applications. Tech. rep., DTOcean Deliverable. 52, 89, 90, 92, 93, 100, 107, 132, 377

WELLER, S., JOHANNING, L., DAVIES, P. & BANFIELD, S. (2014c). Synthetic mooring ropes for marine renewable energy applications. *Renewable Energy*, 1268–1278. 351

WELLER, S., DAVIES, P., VICKERS, A. & JOHANNING, L. (2015a). Synthetic rope responses in the context of load history: The influence of aging. *Ocean Engineering*, **96**, 192–204. 347, 349

REFERENCES

WELLER, S.D., THIES, P.R., GORDELIER, T. & JOHANNING, L. (2015b). Reducing reliability uncertainties for marine renewable energy. *Journal of Marine Science and Engineering*, **3**, 1349–1361. 23, 141

WISE, J., GILLEN, K. & CLOUGH, R. (1995). An ultrasensitive technique for testing the arrhenius extrapolation assumption for thermally aged elastomers. *Polymer Degradation and Stability*, **49**, 403–418. 253, 357, 358

WOLFRAM, J. (2006). On assessing the reliability and availability of marine energy converters: the problems of a new technology. *Proceedings of the Institution of Mechanical Engineers, Part O: Journal of Risk and Reliability*, **220**, 55–68. 35, 59, 63

XIA, Z., KUJAWSKI, D. & ELLYIN, F. (1996). Effect of mean stress and ratcheting strain on fatigue life of steel. *International journal of fatigue*, **18**, 335–341. 222, 225

XU, T.J., ZHAO, Y.P., DONG, G.H. & BI, C.W. (2013). Fatigue analysis of mooring system for net cage under random loads. *Aquacultural Engineering*. 217

YEMM, R. (2003). Pelamis wec - intermediate scale demonstration. Tech. rep., Ocean Power Deliery Ltd. 74

YOUNG, W.C. & BUDYNAS, R.G. (2002). *Roark's formulas for stress and strain*, vol. 7. McGraw-Hill New York. 93, 165, 166, 231

Appendix A

Reference load cell calibration certificate

A. REFERENCE LOAD CELL CALIBRATION CERTIFICATE

Load cell used for the calibration of the DMaC tailstock load cell on 02/12/2015 as detailed in Chapter 3, Section 3.2.2.1, Page 142.

CALIBRATION CERTIFICATE

Calibration of Transducer

APPLIED MEASUREMENTS LIMITED

3 MERCURY HOUSE
CALLEVA PARK
ALDERMASTON
BERKSHIRE
RG7 8PN
UK
Tel: (+44) 0118 981 7339
Fax: (+44) 0118 981 9121
e-mail: info@appmeas.co.uk
internet: www.appmeas.co.uk

Customer:
University of Exeter
Northcote House
Exeter
Devon
EX4 4QJ

Date: 23rd October 2015

Customer Ref: SHC/5290

AML Order Ref: 103944

Calibration Results:

Transducer Type:	DBBSM-10,000kg-003-000
Serial No:	50137
Load Rating:	10,000kg
Proof Rating:	15,000kg
Zero Output:	- 0.050mV @ 10Vdc
Sensitivity:	2.4004mV/V
Non-Linearity:	± 0.021% FS
Hysteresis:	0.031% FS
Supply Voltage:	10.0000Vdc
Insulation Resistance:	> 20 Gohms at 100Vdc

Electrical Connections:

3m Cable
Red   +ve Exc
Blue   -ve Exc
Green   +ve Sig (Tension)
Yellow -ve Sig

Applied Measurements Limited hereby certifies that the above items have been inspected, tested and calibrated – using UKAS traceable test equipment - in all respects with the requirements of the customer's order.

Directors:
PETER LEWIS
ROBERT DAVIES
OLIVER MORCOM
DARREN SKIPP

Reg. No. 2583968

Visit our website at: www.appmeas.co.uk

Appendix B

List of Publications

- **Gordelier, T.**, Johanning, L. & Thies, P. (2013). Reliability verification of mooring components for floating marine energy converters. SHF Marine Renewable Energy Conference. October 9-10, 2013. Brest, France.

- Thies, P.R., Johanning, L. & **Gordelier, T.** (2013). Component reliability testing for wave energy converters: Rationale and implementation. 10th European Wave and Tidal Energy Conference. September 2-5, 2013. Aalborg, Denmark.

- Thies, P.R., Johanning, L. and **Gordelier, T.**, and Vickers, A., and Weller, S. (2013). Physical Component Testing to Simulate Dynamic Marine Load Condition. ASME 2013 32nd International Conference on Ocean, Offshore and Arctic Engineering, June 9-14, 2013, Nantes, France.

- Weller, S.D., Thies, P.R., **Gordelier, T.**, Parish, D., Harnois, V., & Johanning, L. (2014). Navigating the valley of death: Reducing reliability uncertainties for marine renewable energy. ASRANet International Conference on Offshore Renewable Energy, September 15-17, 2014, Glasgow, UK.

- **Gordelier, T.**, Parish, D., Thies, P.R. & Johanning, L. (2015). A novel mooring tether for highly dynamic offshore applications; mitigating peak and fatigue loads via selectable axial stiffness. Journal of Marine Science and Engineering, Vol 3, Issue 4, pg 1287-1310.

- Weller, S.D., Thies, P.R., **Gordelier, T.** & Johanning, L. (2015b). Reducing reliability uncertainties for marine renewable energy. Journal of Marine Science and Engineering, Vol 3, Issue 4, pg 1349-1361.

- Weller, S.D., Thies, P.R., **Gordelier, T.**, Davies, P. & Johanning, L. (2015). The Role of Accelerated Testing in Reliability Prediction. 11th European Wave and Tidal Energy Conference 2015. September 6-11, 2015, Nantes, France.

Appendix C

Accolades

- Yoshio Masuda Memorial Award for Best Young Researcher. 10th European Wave and Tidal Energy Conference. September 2-5, 2013. Aalborg, Denmark.

- Awarded MARINET funding through the EU's FP7 framework. This provided financial support to enable 2 weeks of test work at the IFREMER Materials in a Marine Environment Laboratory.

- Best Poster Prize. SuperGen UKCMER Annual Assembly. November 28, 2014. Edinburgh, UK.

- 3rd Prize for Oral Presentation. Postgraduate Research Conference. March 21, 2014. Cornwall, UK.

- (Co-author) Best Poster Prize. SuperGen UKCMER Annual Assembly. November 27, 2015. Edinburgh, UK.

C. ACCOLADES